Histone, chromatin structure and their role in DNA repair during carcinogenesis

By

Ajit Kumar Sharma

[LIFE09200704009]

Tata Memorial Centre

Mumbai

A thesis submitted to the
Board of Studies in Life Sciences
In partial fulfillment of requirements
for the Degree of

DOCTOR OF PHILOSOPHY
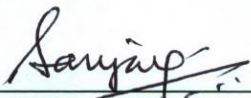
Of

HOMI BHABHA NATIONAL INSTITUTE

June, 2014

Homi Bhabha National Institute

Recommendations of the Viva Voce Committee

As members of the Viva Voce Committee, we certify that we have read the dissertation prepared by Ajit Kumar Sharma entitled "Histone, chromatin structure and their role in DNA repair during carcinogenesis" and recommend that it may be accepted as fulfilling the thesis requirement for the award of Degree of Doctor of Philosophy.
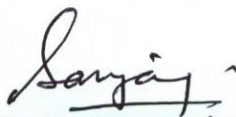
Director & Acting Chairperson - Dr. S.V.Chiplunkar   Date: 13/6/14

ABSENT DUE TO ILLNESS

Chairperson - Dr. Rita Mulherkar   Date:

Convener - Dr. Sanjay Gupta   Date: 13/6/2014

External Examiner - Dr. Tapas K. Kundu   Date: 13/6/14

Member 1 - Dr. Sorab Dalal   Date: 13/6/2014

Member 2 - Dr. Ashok Varma   Date: 13/6/14

Final approval and acceptance of this thesis is contingent upon the candidate's submission of the final copies of the thesis to HBNI.

I hereby certify that I have read this thesis prepared under my direction and recommend that it may be accepted as fulfilling the thesis requirement.

Date: 13/6/2014

Place: ACTREC, Kharghar

Dr. Sanjay Gupta

Guide
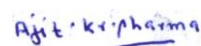
STATEMENT BY AUTHOR

This dissertation has been submitted in partial fulfillment of requirements for an advanced degree at Homi Bhabha National Institute (HBNI) and is deposited in the Library to be made available to borrowers under rules of the HBNI.

Brief quotations from this dissertation are allowable without special permission, provided that accurate acknowledgement of source is made. Requests for permission for extended quotation from or reproduction of this manuscript in whole or in part may be granted by the Competent Authority of HBNI when in his or her judgment the proposed use of the material is in the interests of scholarship. In all other instances, however, permission must be obtained from the author.

Navi Mumbai,
Date: 13.6.14

Ajit Kumar Sharma

DECLARATION

I, hereby declare that the investigation presented in the thesis has been carried out by me. This work is original and has not been submitted earlier as a whole or in part for a degree / diploma at this or any other Institution / University.

Navi Mumbai,   Ajit Kumar Sharma

Date: 13.6.14

List of Publications arising from the thesis

Journal

1. "Molecular modeling of differentially phosphorylated Serine 10 and acetylated lysine 9/14 of histone H3 regulates their interactions with 14-3-3ζ, MSK1 and MKP1", **Ajit K Sharma**, Abhilasha Mansukh, Ashok Varma, Nikhil Gadewal and Sanjay Gupta, Bioinformatics and Biology Insights, **2013**, 7., 271–288.

Conferences (Abstract Published)

1. "Histone H3 Serine 10 phosphorylation associates with DNA damage response," **Ajit K Sharma**, S.A. Khan, S. Bhattacharya, B.S. Khade, Sanjay Gupta, Journal of Cancer Research and Therapeutics-Supplement1, **January 2012**, 8., OA15, S13.

2. "A Dynamics of G1-phase specific loss of H3-Serine10 phosphorylation in response to IR induced DNA damage in human cells," **Ajit K Sharma**, Tejkiran Sagwekar, Shafqat A Khan, Bharat Khade and Sanjay Gupta, Journal of Cancer Research and Therapeutics, **July-September 2012**, 8., Abstract no 166, pp 491

Navi Mumbai,   Ajit Kumar Sharma

June, 2014

Dedicated to
My Beloved Parents

ACKNOWLEDGEMENTS

CONTENTS

Synopsis

Homi Bhabha National Institute

Ph.D. PROGRAMME

1. **Name of the Student:** Ajit Kumar Sharma

2. **Name of the Constituent Institution:** TMC-ACTREC, Mumbai

3. **Enrolment No :** LIFE09200704009

4. **Title of the Thesis:** Histone, chromatin structure and their role in DNA repair during carcinogenesis.

5. **Board of Studies:** Life Sciences

SYNOPSIS

1. Introduction

Previous studies in different models from yeast to human cells imply that chromatin structure serves as a barrier for repair at DNA damage sites. The complex array of histone modifications/variants alter the overall charge and conformation of chromatin which helps in recruitment of factors at damage site to facilitate repair, and thus in maintaining genomic integrity in response to DNA damaging agents (1,2). DNA damage response (DDR) process requires multiple steps: (i) 'prime' phase - initial sensing of the break, (ii) 'repair' phase - the admittance of repair factors to the chromatin, and (iii) 'recovery' phase - the reinstatement of native chromatin state (3). This reflects a range of different signals embedded in chromatin itself, each helping to orchestrate the repair and checkpoint events depending on the DNA damaging agents and cell cycle stage (4,5).

Role of histone modifications in regulation of transcription are well studied (6), but recent studies are unraveling the role of histone marks in the DDR (7). The first histone mark in response to DNA damage is phosphorylation of H2AX at the γ position in its C-terminal tail (γH2AX) along chromatin tracks flanking DSBs which is mediated through ATM and DNA-PK (8-10). DNA damage produced by irradiation, radiomimetic drugs, cisplatin, etoposide, mitomycin C, oxidative stress, psoralen plus UV etc can also induce γH2AX suggesting its universal nature for potent DNA damage responsive histone mark and indicator of cellular sensitivity after radiotherapy and chemotherapy (11-13). In addition H2BSer14 is rapidly phosphorylated at sites of DNA double-strand break and accumulated in to irradiation-induced foci (14). In contrary to this PKCδ mediates H2BSer14 phosphorylation and subsequent chromatin condensation during apoptosis (14). H4Lys16Ac and H2A ubiquitylation have also been shown to increase after ionizing radiation (7). The global reductions of H3Lys9Ac and H3Lys56Ac during the DNA damage response have been reported (15). Further reports appear with ambiguous observation regarding differential pattern of alteration of H3Lys9Ac and H3Lys56Ac in response to DNA damage mediated by genotoxic agents like MMS, CPT, H_2O_2, UV and ionization irradiation (4).

Histone modifications/variants not only undergo dynamic alteration in context of DNA damage but also, are known to be altered during cell cycle facilitating distinct chromatin states (4,16). This might lead to differential radio-sensitivity in different phases of cell cycle. Earlier study suggests that in response to DNA damage, cells in late S-phase are more radio-resistant whereas G2/M-phase cells are less radio-resistant as compare to G1-phase cells (17). The different repair pathways are predominantly active during different cell cycle stages.

Like, homologous recombination (HR) is predominant in late S-phase and G2/M phase and non-homologous end-joining (NHEJ) is predominant in G1-phase (1). The different repair pathways might associate with specific histone marks and distinct chromatin states in different phase of cell cycle. We hypothesize that in addition to the chromatin-modifying machinery being regulated in a cell-cycle-specific manner, the 'marks' that induce at the sites of a DSBs could be read differently by repair machinery depending on the stage of the cell cycle. Therefore, the cell cycle phase specific histone marks may be key determinants for their differential response to ionizing radiation.

2. Aims and objectives

2.1. Whether any alterations in histone modifications/variants is associated with specific cell cycle stage that alter chromatin structure for DNA repair in response to double strand DNA damage?

2.2. What are the interacting protein partners of altered histone(s) in response to double strand DNA damage?

3. Materials and Methods:

Objective 1. To investigate whether any alteration in histone modifications/histone variants is associated with specific cell cycle stage that alters chromatin structure for DNA repair in response to DNA damage.

3.1. Cell lines and Synchronization

WRL68 and HepG2 cells were cultured in MEM and RPMI1640 media (Invitrogen) whereas MCF7, U87, A549, A2780, U2OS were maintained in DMEM media respectively at $37^{\circ}C$ with 5% CO2 supplemented with 10% FBS, 100U/ml penicillin, 100mg/ml streptomycin and 2mM L-glutamine (Sigma). Cells were enriched in early G1-phase by serum starvation (0.01% of FBS) for 72 hrs. To arrests cells in S-phase and pro-metaphase phase, cells were incubated twice in the presence of 4mM thymidine (sigma) for 15 h, with

12 h in thymidine free complete medium in between double thymidine exposures. S phase cells were obtained 4 h after the release from double thymidine block. For Pro-metaphase arrest, cells were incubated for 18 h with complete medium containing 200ng/ml of nocodazole (Sigma) after double thymidine block. Cells were washed with media and released with 10% FBS before irradiation. After irradiation, cells were processed for histone isolation, comet assay, cell cycle analysis and IF-studies.

3.2. Antibodies and inhibitors: Antibodies toward γH2AX (05-636) and H4 (07-108) and MSK1 inhibitor, H89 (19-141) were obtained from Millipore and against H3Ser10P (ab5176), H3Lys14Ac (ab52946), H3Lys56Ac (ab76307), H3Lys9Ac (ab4441), and p-MSK1S376 (ab32190) were procured from Abcam, UK. Antibodies towards H3 (97155), anti-rabbit-HRP IgG Secondary (7074) were from Cell signaling, USA and MKP1 (Sc370) from Santa Cruz, USA. Anti-β-actin (A5316), secondary anti-mouse IgG (A-4416), and sanguinarine (S5890) were obtained from Sigma, USA. Micrococcal nuclease (P/N 70196Y) was obtained from USB.

3.3. Gamma ionizing irradiation and treatment with DNA damaging agents:

Cells enriched in different phases of cell cycle were either exposed to 2.5Gy (clinically relevant dose) or 15Gy (high dose) of ionization radiation with Co-60 as IR source. In parallel, cells were treated with other DNA damaging agents like cisplatin (sigma, 2μg/ml, 4h), etoposide (100μM, 4hs), H_2O_2 (500μM, 30min), Adriamycin (10μg/ml) and UV treatment at 10 J/m^2 followed by recovery for 1hr. Subsequently, cells were incubated to allow post-IR repair and recovery before harvesting at the indicated time.

3.4. Fluorescence-activated cell sorting analysis for cell cycle analysis

Ethanol fixed cells were washed twice with PBS and suspended in 500μl of PBS with 0.1% Triton X-100 and 100μg/ml of RNaseA followed by incubation at 37°C for 30mins. After incubation, propidium iodide (25μg/ml) was added followed with incubation at 37°C for

30mins. DNA content analysis was carried out in a FACSCalibur flow cytometer (BD Biosciences, USA). Cell cycle analysis was performed using the mod-fit software from BD Biosciences.

3.5. Immunofluorescence microscopy

The adherent cells grown on coverslips were washed twice with PBS and fixed with 4% paraformaldehyde for 20 minutes. Cells were permeabilized in 0.5% Triton X-100 for 20mins and blocked with 5% BSA containing 0.1% NP-40 in PBS (PBS-N) for 1hr. Cells were incubated with primary antibodies for 1hr in 5% BSA containing PBS-N, further washing with PBS-N and followed by incubation in the dark with Alexa-conjugated secondary antibodies.. Cells were washed and mounted on slides in Vecta-shield mounting medium (Vector laboratories) and counter stained with DAPI (Sigma, 0.5μg/ml). Cells were imaged with Ziess 510 META confocal laser scanning microscope with 63X magnification objective lens and numerical aperture 1.4 (Zeiss, Jena, Germany). Routinely, 0.72μm thick focal planes were processed using the Ziess software (LSM 510 Meta).

3.6. Comet assay: Alkaline comet assay was performed as described by Singh et al (18).

3.7. Histone isolation and immunoblot analysis:

Histones were extracted and purified as described by Bonenfant et al (19) with slight modifications. Purified histone was suspended in 0.1% β-mercaptoethanol in H_2O and stored at $-20^{\circ}C$. Histones resolved on 18% SDS-polyacrylamide gel were transferred to PVDF membrane, probed with site-specific modified histones antibodies and signals were detected by using ECL plus detection kit (Millipore; Catalog no.WBKLS0500)

3.8. MNase digestion assay

Purified nuclei from irradiated and non-irradiated G1 enriched WRL68 cells followed by post-IR incubation were subjected to MNase digestion to analyse chromatin structure (20). Nuclei containing 2mM $CaCl_2$ were incubated for 0, 2.5 and 5mins with 5U MNase/mg of

DNA at 37°C in digestion buffer. MNase digested samples were extracted and ethanol precipitated at -20°C. The precipitated DNA was dissolved in 50µl of TE buffer, estimated at A260/A280 absorbance and resolved on 1.8% 1XTAE agarose gel electrophoresis with 0.5µg/ml ethidium bromide.

3.9. Purification of mononucleosomes and Coimmunoprecipitation

MNase-digested (as mentioned above) samples were layered on glycerol-gradient (10 to 40%) and centrifuged for 16hrs at 27,500 rpm at 4°C in a Beckman SW28 rotor. The mono-nucleosomal ring was collected and quality was confirmed on 1.8% TAE-agarose gel. The pre-treated protein-G beads were incubated overnight at 4°C either with 3µg anti-γH2AX or anti-H3Ser10P antibody. Mono-nucleosomes (25µg) from control and irradiated cells were incubated overnight at 4°C with bead bound antibodies. The separated, bound and unbound immunoprecipitated fractions were analyzed by immunoblotting with either γH2AX or H3S10P antibodies respectively.

3.10. Western blotting analysis of H3 variants specific modification

H3 variants were resolved on AUT-PAGE gels followed by either silver staining or transfer to PVDF membrane (21,22). Primary anti-H3Ser10P was used to analyze H3Ser10P in different H3 variants in response to IR in G1 and pro-M phase rich population of WRL 68 cells.

Objective 2. To investigate what are the interacting protein partners of altered histone(s) in response to double strand DNA damage?

3.11. Homology modelling of MKP1 and MSK1 structures:

The model of active C-terminus phosphatase domain of MKP1 (172-314aa) was constructed using PDB ID: 3EZZ as template due to unavailability of crystallographic structure. The N-terminal crystal structure of MSK1 is available but to model the phosphorylated Ser376 residue of flexible loop near the active site, PDB ID: 3A8X was

used as a template for homology modelling of MSK1 with amino acid residues from 42-380. Modelling studies were performed using Swiss Model. The modelled structure of MKP1 and MSK1 were cross validated using multiple tools like Procheck, Verify_3D and Errat using SAVEs server (http://nihserver.mbi.ucla.edu/SAVES/).

3.12. Molecular association of MSK1 and MKP1 with histone H3 and its PTM modified structure

The modelled structure of MSK1 was docked with native and three PTM modified structure of full length (1-21aa) loop structure of histone H3 [Lys9, Lys14, Lys9-Lys14] using Haddock server. The active site residues (Lys85, Ile88, Val89, Thr95, Arg102, Gln122, and Leu127) of MSK1 and (Lys9, Ser10 and Lys14) of histone H3 was provided as input parameters for targeted docking.

The full length (1-21aa) loop structure of histone H3 (PDB ID: 1KX5) was used for generation of site specific acetylation and phosphorylation resulting in seven PTM modified structure of histone H3 [Lys9, Ser10, Lys14, Lys9-Ser10, Lys9-Lys14, Ser10-Lys14, and Lys9-Ser10-Lys14]. The modelled structure of MKP1 was docked with native and seven PTM modified structure of histone H3 using Haddock server. The active site residues (His257, Cys258, Gln259, Ala260, Gly261, Ile262, Ser263 and Arg264) of MKP1 and modified (Lys9, Ser10 and Lys14) of histone H3 was provided as input parameters for docking. The molecular interactions of the docked complexes were analysed by Ligplot for hydrophobic interactions. Discovery studio visualizer 3.5 was used for identification of residue involved in hydrogen bonding between two proteins and for the diagrammatic illustration of the residues involved in the hydrogen bond formation in docked complex.

3.13. Isolation of total extract and chromatin-bound histones

G1-enriched human cells treated with or without IR and with or without specific inhibitors of MSK1/MKP1 (H89/Sanguinarine) were lysed in MKK lysis buffer for 30mins at 4°C.

Following hypotonic lysis, cells were centrifuged at 12,500rpm for 20mins at 4°C to separate non-chromatin supernatant and chromatin pellet fraction. The supernatant, total lysate without chromatin were resolved on 10% SDS-PAGE and transferred on PVDF membrane which were then probed with antibodies specific for downstream proteins of MAP kinase pathway. The histones extracted from chromatin pellet were resolved on 18% SDS-PAGE gels and probed with specific antibodies.

4. Results

4.1. Decrease in phosphorylation of H3Ser10 and its restoration in response to IR induced DNA damage in G1 enriched cells

Phosphorylation of H3Ser10 in G1 phase correlates with chromatin relaxation and gene expression whereas it also correlates with chromosome condensation in mitosis (23). The phosphorylation status of H3Ser10 in response to DNA damage in mammalian system in specific phase of cell cycle is poorly studied. To understand role of H3Ser10P in G1-enriched cells after DNA damage we determined time interval for repair and restoration phase of DNA damage response. Time dependent post-IR analysis of γH2AX foci formation, comet tail moment and cell cycle analysis were studied following clinically relevant and high dose ionization radiation (IR) on G1 enriched transformed (HepG2) and normal immortalized embryonic liver cells (WRL68). The γH2AX foci formation and comet tail moment suggest that the initiation of DNA damage response, 'repair phase' ranges from 0min (immediately after irradiation) to 8h with an overlapping 'recovery phase' from 8h time point. At recovery phase i.e. from 8h of post-IR nuclei restore circular structure without any comet tail moment in both the cell lines irradiated at 2.5Gy and 15Gy. To delineate H3Ser10P in association with G1-phase of cell cycle and DNA damage phase-specific alteration we performed post-IR time-dependent western blot analysis against H3Ser10P and γH2AX. The data shows a gradual decrease in H3Ser10P level in both the

cell lines from 0min to 6h that coincides with the 'repair' phase of DDR. The restoration of phosphorylation starts at 8h with a complete recovery at 24h of post-IR. The level of H3Ser10 phosphorylation after 24hr post-IR is comparable to that of the non-irradiated WRL68 and HepG2 cells. Interestingly, the phosphorylation of H3Ser10 shows an inverse correlation with γH2AX in G1-enriched cells. Immunofluorescence staining of G1-enriched irradiated cells confirms the loss of nuclear H3Ser10P and gain of γH2AX in comparison to non-irradiated cells. The reversible reduction of H3Ser10P after IR is concomitant with DNA damage response and not associated with cell cycle progression, serum starved G1-enriched WRL68 were released in normal cell cycle progression with 10% serum. Western blot analysis shows H3Ser10P status as per the phase of cell cycle at respective time points but no decrease or restoration as observed during DDR in G1-enriched cells. Further to elucidate change in phosphorylation of H3Ser10 is cell cycle phase specific, normal immortalized embryonic liver WRL68 cells were arrested in three distinct phases. Western blot analysis reveals that H3Ser10 phosphorylation decreases in G1 phase cells whereas S-phase and pro-M phase arrested cells doesn't show any change during repair time points after ionization irradiation. Also, decrease in H3Ser10 phosphorylation with increase of γH2AX in WRL68 cells in response to various DNA-damaging agents (Adriamycin, etoposide, UV, H_2O_2 and cisplatin) and multiple cell lines arrested in early G1-phase (U87, U2OS, MCF7, A2780 and A549) of different tissue origin in response to IR establises the loss of H3Ser10P as a universal phenomenon in DDR.

4.2. Decrease of H3Ser10 phosphorylation is specific to G1 phase of cell cycle and is from H3.3 variant

In mammals, H3Ser10 residue is highly conserved in H3 variants (H3.1, H3.2 and H3.3) and is shown to be phosphorylated with dual functions in G1 and G2/M phases. The decrease in phosphorylation at H3.3Ser10 is prominent in G1-enriched cells. However,

cells enriched in pro-M phase shows higher level of phosphorylation at H3.1Ser10 without detectable change in phosphorylation status in irradiated cells in comparison to non-irradiated cells. Collectively our data suggests that decrease of phosphorylation is predominately from H3.3Ser10 is a G1-specific DNA damage responsive histone mark.

4.3. Decrease in H3Ser10 phosphorylation in G1 cells is associated with de-acetylation of histone marks Lys9, Lys14 and Lys56 on H3 in response to increasing IR dose

During G1-phase of cell cycle, H3Ser10P along with H3Lys9Ac and H3Lys14Ac is important for transcriptional activation mediated through 14-3-3 class of proteins (23). To determine whether decrease in level of H3Ser10P is associated with change in acetylation status of H3Lys9, Lys14 and Lys56, G1-enriched WRL68 cells irradiated with increasing dose of IR. The dose-dependent increase in DNA damage was confirmed by comet tail moment and analysis of H3Lys9, Lys14 and Lys56 acetylation status reveals a continuous steady decrease in these H3-acetylation marks along with decrease in H3Ser10P and increase in γH2AX.

4.4. Phosphorylation of H2AX and de-phosphorylation of H3Ser10 are marks on a same mono-nucleosome in response to DNA damage

The previous data raises a query whether loss of H3Ser10P and gain of γH2AX may occur from the same mono-nucleosomes. To address this, we isolated mononucleosomes from G1-enriched WRL68 nuclei before and after 4hr post-IR. The mononucleosomes (MN) were co-immunoprecipitated with either anti-H3Ser10P or anti-γH2AX followed by western blotting against H3Ser10P and γH2AX to confirm co-localization of these marks on same nucleosome. Collectively, the western blot with MN-Co-IP histones in bound and unbound fractions confirms that γH2AX is present on mononucleosomes purified from irradiated cells which do not have phosphorylated H3Ser10, whereas, mononucleosomes from non-irradiated cells bearing H3Ser10P do not contain γH2AX. γH2AX-IP with non-

irradiated cells shows the presence of γH2AX in bead-bound fraction but not in the input. This demonstrate the 'negative cross talk' of the histone marks, 'loss' of H3Ser10P and 'gain' of γH2AX from the same mono-nucleosome at DSB site during DDR in G1 phase.

4.5. Condensation and decondensation of chromatin in 'repair' and 'recovery' phase of DDR in G1-enriched cells

Histone modifications alteration in response to DNA damage may alter chromatin organization. The alteration of global chromatin structure is studied by MNase accessibility assay. The data suggests moderate global chromatin compaction at 0 and 4hrs ('repair' phase) post-IR as evident from decrease in intensity of nucleosomes and increase in high MW DNA at 2.5mins digestion in comparison to non-irradiated and 24hr post-IR recovered cells. The restoration of native chromatin organization coincides with 'recovery phase' of DDR.

4.6. In *silico* studies for prediction of modifying enzymes of H3Ser10 phosphorylation:

The phosphorylation of histone H3Ser10 is known to facilitate acetylation of Lys9 and Lys14. So far our studies demonstrate H3Ser10P and its neighbouring residues like Lys9Ac and Lys14Ac decreases in response to DNA damage. Here, we have carried out *in silico* studies to predict (a) interacting domain on regulatory proteins, MKP1 and MSK1 for different combination of site-specific histone H3 modifications on Lys9, Ser10 and Lys14, and (b) the acetylation of H3Lys9 and H3Lys14 is the prerequisite conditions for interaction of MKP1and MSK1 with H3Ser10P.

4.6.1. Docking of native MKP1 with histone H3 and its PTM modified structure

In silico studies were carried out to predict the interacting domain on MKP1 for interaction with H3Ser10P and its neighbouring acetylated marks on H3Lys9 and H3Lys14 of H3.

The homology model structure of C-terminal phosphatase domain of MKP1 (172-314aa) was used for docking with the loop crystal structure of H3 peptide (1-21aa) using Haddock

server. The active site amino acid, Cys258 and nearby residue for formation of active site (His257, Cys258, Gln259, Ala260, Gly261, Ile262, Ser263 and Arg264) for MKP1 were obtained from UniProt ID: P28562. These residues were used for targeted docking with native and modified histone H3 peptides. Haddock scores from all eight complexes suggest that complex between MKP1 and H3Lys9AcSer10PLys14Ac shows best binding as compared to complex with native histone H3 and MKP1. The binding affinity of histone H3 increases i.e. -61.8 to -90.3 with MKP1 when H3Ser10 is phosphorylated. But when either Lys9 or Lys14 acetylation is added with Ser10P the Haddock score rises from -90.3 to around -122. The residues that are involved in the interaction with phosphorylated Ser10 are mostly from active site (Gln259, Ala260, Gly261, Ile262, Ser263, Arg264) of MKP1 seen in all the complexes. Interestingly H3S10P forms hydrogen bond with Cys258 active side residues of MKP1 which mediate dephosphorylation of H3Ser10P. Our studies suggest that modification of H3 at all the three places (Lys9, Ser10, and Lys14) increase the hydrophobic interactions leading to form a stable and high affinity interaction with MKP1.

4.6.2. Docking of native MSK1 with histone H3 and its PTM modified structure

MSK1 belongs to a family of protein kinases that contain two active domains in one polypeptide chain. In the dual domain protein kinase MSK1, the N-terminal kinase has been shown to be phosphorylated by exogenous substrates, while the C-terminal kinase and the linker region act to regulate activity of the N-terminal kinase (24).

The modelled structure of N-terminal domain of MSK1 (42-380aa) was docked with native and acetylated histone H3 at Lys9 or Lys14 independently or together. The active site residues (Lys85, Ile88, Val89, Thr95, Arg102, Gln122, and Leu127) of MSK1 were obtained from literature (25). The haddock score of native histone H3 scored best when compared to the acetylated Lys9 and Lys14. This suggests that acetylation is not the prerequisite for phosphorylation of H3Ser10P by MSK1.

4.7. Phosphorylation status of H3Ser10 in G1 phase cells is correlated with phosphorylation of MAP kinases and their de-phosphorylation by MKP1 in response to irradiation

To elucidate association of MAP kinase pathway in G1 phase cells with reversible alteration of H3Ser10P during IR induced DDR, we assessed the levels of phospho (ERK, JNK, p38, MSK1) and MKP1 in soluble fractions of cells, and H3Ser10P and γH2AX level in chromatin fraction after IR treatment. Western blot analysis with specific antibodies shows significant decrease in phosphorylation of p38, ERK1/2, JNK and MSK1 whereas increase in MKP1 is at protein level immediately (0min) after IR doses i.e. 2.5 and 15Gy. The increased level of p-p38, p-JNK, p-ERK and p-MSK1 are restores to its basal level in 'repair' phase (4 and 24hr post-IR treatment). In chromatin fraction, H3Ser10P decreases with increase in γH2AX after 0 and 4hr IR treatment and there levels are restored during 'recovery' phase. MKP-1 is known to be induced by γ-radiation and repressed radiation induced pro-apoptotic status. These observations regarding increase of MKP1 level in response to different stress inducing agents raises the possibility of MKP-1 as a phosphatase mediating decrease of phospho-MAP kinases and H3Ser10P in response to IR induce DNA damage. To test above possibility G1 enriched WRL68 cells are treated with MKP1 inhibitor, sanguinarine (10μM) for 1hr before IR. Western blot analysis with anti-phospho-MAP kinases immediately after irradiation (0min) suggests that the loss of phospho-MAP kinases (p-p38, p-JNK, p-ERK1/2 and p-MSK1) are inhibited in sanguinarine and IR-treated cells as compare to only irradiated cells. The total proteins of MAP kinases remain unaltered whereas MKP1 protein increases in dose-dependent manner in response to IR irrespective of sanguinarine treatment. Thus overall data reveals that dephosphorylation of MAP kinases is mediated through phosphatase, MKP-1 immediately after IR induce DNA damage in G1-phase cells. This raises the possibility of MKP-1 as a

phosphatase for de-phosphorylation of H3Ser10P and inhibition of MAP kinases responsible for phosphorylation of H3Ser10. The delay in dephosphorylation of H3Ser10 in relation to MAP kinase strongly implies role of downstream effectors of MAP kinase pathway in dynamic regulation of H3Ser10P in response to DNA damage.

4.8. Reversible reduction of phosphorylation of H3Ser10 during DNA damage response mediated through dynamic balance between MKP1 and MSK1 activity in G1 phase

To investigate reversible reduction of H3Ser10P after irradiation is mediated through dynamic balance between MKP1 and MSK1 activity. G1-enriched cells are treated with potent MKP1 inhibitor, sanguinarine (10μM) and specific MSK1 inhibitor, H89 for 1hr before irradiation. Collectively western blot and immunofluorescence analysis against H3Ser10P demonstrates MKP1 as a phosphatase for dephosphorylation of H3Ser10P during repair phase whereas MSK1 as downstream kinase for phosphorylation of H3Ser10 during recovery phase of DNA damage response in G1-phase of cell cycle.

5. Discussion

The covalent histone modifications undergo dynamic alterations throughout the cell cycle and regulate chromatin structure and functions (16, 26). Phosphorylation of H3Ser10 is a chromatin condensation mark in mitosis whereas in interphase favors chromatin relaxation and gene transcription (23). Previous studies have shown ambiguous result of increase or decrease of H3Ser10P in response to DNA damage (4) which may be due to the use of different (a) doses of radiation, (b) time for histone marks analysis after damage and (c) phase of the cell cycle. Therefore damage-induced alterations in histone mark, H3Ser10P and its regulation need scientific clarity. In this study we have demonstrated that in G1-phase cells dephosphorylation of H3Ser10 is mediated through MKP1 and chromatin condensation in 'repair phase' whereas restoration of phosphorylation is favored by MSK1

with chromatin relaxation in 'recovery phase' of DDR in response to clinically-relevant and high dose of IR. The specific loss of serine10 phosphorylation is predominantly from H3.3 variant after DNA damage in G1-enriched cells but the cells arrested in pro-M phase show predominant presence of Ser10P at H3.1 which remain unaltered in response to DNA damage. Earlier study has suggested decrease in H3Ser10P is due to change in mitotic population of cells, a cell cycle phase where this PTM is most abundant (15). Our studies of serine 10 on H3 variant profiling in cell cycle phases, G1 and pro-M phase clearly shows presence of cell cycle specific H3 variants in both the phases and specific loss of serine 10 phosphorylation occur only from H3.3. Histone, H3.3 variant is reported to be predominantly present in transcriptionally active chromatin in G1-phase of cell cycle. This confirms that reduction of H3Ser10P level is specific to G1 phase cells in response to DNA damage and not due to reduction in proportion of mitotic cells after post-irradiation.

The histone phosphorylation that is known to increase at and around flanking region of DSBs is the γH2AX. Our studies have revealed for the first time de-phosphorylation of H3Ser10P occur at the same mono-nucleosomes bearing γH2AX signifying the alteration of cell cycle specific histone marks during DDR. Also, this establishes that reversible reduction of H3Ser10P in 'repair and recovery phase' are associated within the flanking region of DSBs and supports our notion that H3Ser10P is an integral component for maintaining genomic stability in G1 phase cells.

Histone PTMs are known to regulate the DDR by the dynamic cross-talk with other modifications, recruitment of proteins at sites of DNA damage and alteration in chromatin structure. The pre-existence of H3Ser10P and acetylated neighboring lysine (Lys9, Lys14 and Lys56) residues induce repulsive force between intra- and inter-nucleosomal interactions on chromatin fiber and favoring relaxed chromatin state thus facilitating active transcription. The reduction of phosphorylation from H3Ser10 with induction of γH2AX

along with hypoacetylation of H3 at Lys9, Lys14 and Lys56 will minimizes the repulsive force on nucleosomes and may induce compact chromatin state in 'repair phase' of DDR in G1 phase of the cell cycle as demonstrated by MNase digestion assay. The compact chromatin could influence DNA repair efficiency by upsurge of repair proteins in the surrounding area of the DSB, favoring tethering of damage DNA molecule and decreases the chances of aberrant DNA repair. The similar mode of chromatin organization has also been proposed for increase in γH2AX which modulates NHEJ and protects genomic integrity. Also, the inhibition or delay in transcription due to de-phosphorylation of H3Ser10 will prevent transcription from interfering with DNA repair process. Therefore, we propose initial remodeling of chromatin in 'repair phase' may be essential for maintaining the condensed state of chromatin for efficient repair of DNA damage. After DNA damage gets repaired, the decrease of γH2AX phosphorylation, increase of H3Ser10P favor open chromatin organization in 'recovery phase' and may facilitate active transcription in G1 phase of cell cycle.

The contribution of H3Ser10P to chromatin dynamics and defining the precise functions during DDR cannot be easily determined by genetic manipulation. The multiple copies of histone H3 genes and their homomorphous variants makes it difficult to study effect of different modifications individually or in combination by generating mutants. In silico studies suggested that the active site residues of MSK1 and MKP1 are interacting with highest binding affinity to H3Lys9AcSer10PLys14Ac and native H3, respectively. Our western data show that the MAP kinases (ERK1/2, JNK, p38 and MSK1) phosphorylation status decreases with increase in the level of MKP1 immediately after IR. Also, MKP-1 is known to be induced by γ-radiation and repressed radiation-induced pro-apoptotic status. Ataxia Telangiectasia Mutated (ATM) down-regulates phospho-ERK1/2 via activation of MKP1 in response to radiation whereas induction of MKP-1 by H_2O_2 correlates with

inactivation of JNK and p38 activity. Overexpression of MKP-1 increases cell resistance to H_2O_2-induced death. In agreement with earlier reports and our data also suggest that MKP1 is highly inducible by IR-radiation and the immediate increase in level of MKP1 is not due to transcriptional activation of gene but proposed mechanism is due to stability of protein mediated by post-translational modifications. The specific inhibitor of MKP1 or MSK1 alters the dynamic phosphorylation of H3Ser10 with accumulation of γH2AX after IR-induced DNA damage in G1-enriched cells. It is tempting to speculate in consent with our results that the incomplete restoration of H3Ser10P affects the restoration of native chromatin state. Our result suggests that γH2AX foci accumulated in sanguinarine-treated irradiated cells in 'repair phase' and H89-treated irradiated cells in 'recovery phase' of DDR as compare to untreated irradiated cells which may be due to reactivation of ATM mediated through altered chromatin organization. These observations suggest that DNA strand breaks causes change in nucleosomal organization mediated through histone marks in 'prime and repair' phase if not restored in 'recovery' phase will affect the repair mechanism and genomic surveillance.

6. Conclusion:

The present study suggests that reversible reduction of histone mark, H3Ser10 phosphorylation is a universal phenomenon and associated with G1-phase of cell cycle after irradiation. The alteration in histone modification profile, acetylation and phosphorylation in response to DNA damage may play a critical role in chromatin organization and thereby contributing in differential sensitivity against radiation. Thus, the study raises the possibility of combinatorial modulation of H3Ser10P and neighboring histone acetylation(s) with specific inhibitors to target the cancer cells in G1-phase and may serve as promising targets for cancer therapy.

G1-phase cells

Damage

Gain of γH2AX and loss of H3S10P from same mono-nucleosome with chromatin condensation

Repair

Gain of H3S10P and loss of γH2AX with chromatin restoration

Restoration

H3S10P

MKP1

Pi

MSK1

Pi

H3I0P

Nucleosome with γH2AX

Nucleosome with H3S10P
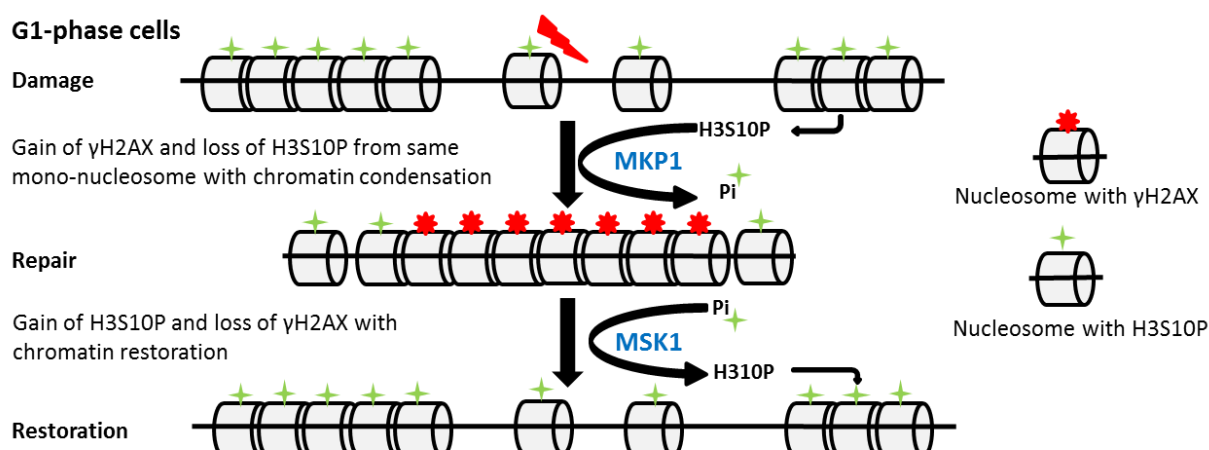
7. References:

1. Downs, J.A., Nussenzweig, M.C. and Nussenzweig, A. (2007) Chromatin dynamics and the preservation of genetic information. *Nature*, **447**, 951-958.

2. Takahashi, K. and Kaneko, I. (1985) Changes in nuclease sensitivity of mammalian cells after irradiation with 60Co gamma-rays. *International journal of radiation biology and related studies in physics, chemistry, and medicine*, **48**, 389-395.

3. Soria, G., Polo, S.E. and Almouzni, G. (2012) Prime, repair, restore: the active role of chromatin in the DNA damage response. *Molecular cell*, **46**, 722-734.

4. Corpet, A. and Almouzni, G. (2009) A histone code for the DNA damage response in mammalian cells? *The EMBO journal*, **28**, 1828-1830.

5. Jackson, S.P. and Bartek, J. (2009) The DNA-damage response in human biology and disease. *Nature*, **461**, 1071-1078.

6. Berger, S.L. (2007) The complex language of chromatin regulation during transcription. *Nature*, **447**, 407-412.

7. Rossetto, D., Truman, A.W., Kron, S.J. and Cote, J. (2010) Epigenetic modifications in double-strand break DNA damage signaling and repair. *Clinical cancer research : an official journal of the American Association for Cancer Research*, **16**, 4543-4552.

8. Rogakou, E.P., Pilch, D.R., Orr, A.H., Ivanova, V.S. and Bonner, W.M. (1998) DNA double-stranded breaks induce histone H2AX phosphorylation on serine 139. *The Journal of biological chemistry*, **273**, 5858-5868.

9. Rogakou, E.P., Boon, C., Redon, C. and Bonner, W.M. (1999) Megabase chromatin domains involved in DNA double-strand breaks in vivo. *The Journal of cell biology*, **146**, 905-916.

10. Stiff, T., O'Driscoll, M., Rief, N., Iwabuchi, K., Lobrich, M. and Jeggo, P.A. (2004) ATM and DNA-PK function redundantly to phosphorylate H2AX after exposure to ionizing radiation. *Cancer research*, **64**, 2390-2396.

11. Olive, P.L. and Banath, J.P. (2004) Phosphorylation of histone H2AX as a measure of radiosensitivity. *International journal of radiation oncology, biology, physics*, **58**, 331-335.

12. Clingen, P.H., Wu, J.Y., Miller, J., Mistry, N., Chin, F., Wynne, P., Prise, K.M. and Hartley, J.A. (2008) Histone H2AX phosphorylation as a molecular pharmacological marker for DNA interstrand crosslink cancer chemotherapy. *Biochemical pharmacology*, **76**, 19-27.

13. Huang, X., Okafuji, M., Traganos, F., Luther, E., Holden, E. and Darzynkiewicz, Z. (2004) Assessment of histone H2AX phosphorylation induced by DNA topoisomerase I and II inhibitors topotecan and mitoxantrone and by the DNA cross-linking agent cisplatin. *Cytometry. Part A : the journal of the International Society for Analytical Cytology*, **58**, 99-110.

14. van Attikum, H. and Gasser, S.M. (2005) The histone code at DNA breaks: a guide to repair? *Nature reviews. Molecular cell biology*, **6**, 757-765.

15. Tjeertes, J.V., Miller, K.M. and Jackson, S.P. (2009) Screen for DNA-damage-responsive histone modifications identifies H3K9Ac and H3K56Ac in human cells. *The EMBO journal*, **28**, 1878-1889.

16. Bonenfant, D., Towbin, H., Coulot, M., Schindler, P., Mueller, D.R. and van Oostrum, J. (2007) Analysis of dynamic changes in post-translational modifications of human histones during cell cycle by mass spectrometry. *Molecular & cellular proteomics : MCP*, **6**, 1917-1932.

17. Terzoudi, G.I., Hatzi, V.I., Donta-Bakoyianni, C. and Pantelias, G.E. (2011) Chromatin dynamics during cell cycle mediate conversion of DNA damage into chromatid breaks and affect formation of chromosomal aberrations: biological and clinical significance. *Mutation research*, **711**, 174-186.

18. Singh, N.P., McCoy, M.T., Tice, R.R. and Schneider, E.L. (1988) A simple technique for quantitation of low levels of DNA damage in individual cells. *Experimental cell research*, **175**, 184-191.

19. Bonenfant, D., Coulot, M., Towbin, H., Schindler, P. and van Oostrum, J. (2006) Characterization of histone H2A and H2B variants and their post-translational modifications by mass spectrometry. *Molecular & cellular proteomics : MCP*, **5**, 541-552.

20. Carey, M. and Smale, S.T. (2007) Micrococcal Nuclease-Southern Blot Assay: I. MNase and Restriction Digestions. *CSH protocols*, **2007**, pdb prot4890.

21. Pramod, K.S., Bharat, K. and Sanjay, G. (2009) Mass spectrometry-compatible silver staining of histones resolved on acetic acid-urea-Triton PAGE. *Proteomics*, **9**, 2589-2592.

22. Delcuve, G.P. and Davie, J.R. (1992) Western blotting and immunochemical detection of histones electrophoretically resolved on acid-urea-triton- and sodium dodecyl sulfate-polyacrylamide gels. *Analytical biochemistry*, **200**, 339-341.

23. Sawicka, A. and Seiser, C. (2012) Histone H3 phosphorylation - a versatile chromatin modification for different occasions. *Biochimie*, **94**, 2193-2201.

24. McCoy, C.E., Campbell, D.G., Deak, M., Bloomberg, G.B. and Arthur, J.S. (2005) MSK1 activity is controlled by multiple phosphorylation sites. *The Biochemical journal*, **387**, 507-517.

25. Smith, K.J., Carter, P.S., Bridges, A., Horrocks, P., Lewis, C., Pettman, G., Clarke, A., Brown, M., Hughes, J., Wilkinson, M. *et al.* (2004) The structure of MSK1 reveals a novel autoinhibitory conformation for a dual kinase protein. *Structure*, **12**, 1067-1077.

26. Kouzarides, T. (2007) Chromatin modifications and their function. *Cell*, **128**, 693-705.

Publication from the Thesis:

a. <u>Accepted:</u> **Ajit K Sharma**, Abhilasha Mansukh, Ashok Varma, Nikhil Gadewal and Sanjay Gupta Molecular modeling of differentially phosphorylated Serine 10 and acetylated lysine 9/14 of histone H3 regulates their interactions with 14-3-3ζ, MSK1 and MKP1. *Bioinformatics and Biology Insights (In press)*

b. <u>Communicated:</u> **Ajit K Sharma**, Shafqat A Khan, Tejkiran Sagwekar, Saikat Bhattacharya, Sanjay Gupta. Dynamics of G1-phase specific loss of H3-Serine 10 phosphorylation in response to IR induced DNA damage in human cells. *(Under revision)*

c. <u>Manuscript under preparation:</u> Ajit Kumar Sharma, Shafqat A Khan, Sanjay Gupta Reversible decrease in phosphorylation of H3S10 is universal phenomenon in response to DNA damage.
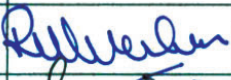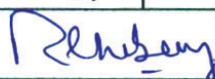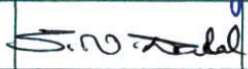
Other Publications:

a. Khare SP, **Sharma A K**, Deodhar KK, Gupta S .Overexpression of histone variant H2A.1 and cellular transformation is related in N-nitrosodiethylamine-induced sequential hepatocarcinogenesis. *Exp Biol Med* (Maywood), 2011; 236(1):30-5.

d. Rhea Mohan, **Ajit K. Sharma**, Sanjay Gupta, C. S. Ramaa. Design, synthesis, and biological evaluation of novel 2, 4-thiazolidinedione derivatives as histone deacetylase inhibitors targeting liver cancer cell line. *Med. Chem. Research*, March 2011, pp, 1-10.

Signature of Student: Ajit·k·pharma   **Date:** 22.7.13

Doctoral Committee:

S. No.	Name	Designation	Signature	Date
1	Dr. Rita Mulherkar	Chairperson		22.7.13.
2	Dr. Sanjay Gupta	Convener		22/7/2013
3	Dr. R. C. Chaubey	Member		22/7/2013
4	Dr. Sorab Dalal	Member		22/7/2013

Forwarded through

Dr. S.V. Chiplunkar
Chairperson
Academics and Training Programme
ACTREC

Dr. S.V.Chiplunkar
Dy. Director
CRI-ACTREC

Dr. R. Sarin
Director
ACTREC

Dr. K.S. Sharma
Director Academics,
Tata Memorial Centre
Mumbai

Prof. K.S. Sharma
DIRECTOR - ACADEMICS, TMC
Mumbai - 400 012

LIST OF ABBREVIATIONS

ADP	Adenosine diphosphate
AraC	Cytosine Arabinoside
ATP	Adenosine triphosphate
ATM	Ataxia-Telangiectasia
AP site	Abasic site
ATR	Ataxia-Telangiectasia-and RAD3-related
AUT	Acetic acid Urea Triton
BSA	Bovine Serum Albumin
CHZ1	Nuclear Chaperon for H2A.Z
CENP-A	Centromeric Protein A
CAF-1	Chromatin Assembly Factor-1
CHK	Checkpoint Kinase
CPT	Camptothecin
DNA-PK	DNA-dependent Protein Kinase
DSBs	Double Strand Breaks
DDR	DNA Damage Response
DMEM	Dulbecco's Modified Eagle Medium
DTT	DL-Dithio Threitol
FBS	Fetal Bovine Serum
HFD	Histone Fold Domain
HAT	Histone Acetyl-Transferases
HDAC	Histone Deacetylase
HIRA	Histone Regulation A
HMT	Histone methyltransferases
HP1	Heterochromatin Protein 1
H3S10P	Histone H3 Serine10 phosphorylation
H3Lys (9,14,56) Ac	Histone H3Lysine (9,14,56) Acetylation
H3K9me1,2,3	Histone H3 Lysine 9 methylation-mono, di,tri
H4K20me1,2,3	Histone H4 Lysine 20 methylation-mono,di,tri

H4K16Ac or H4Lys16Ac	Histone H4 Lysine 16 Acetylation
H3K4me1,2,3	Histone H3 Lysine methylation-mono,di,tri
JmjC	Jumonji Demethylases
JAK-2	Janus Kinase-2
LSD1	Lysine-Specific Demethylase 1
MBT	Malignant Brain Tumour
MARTs	Mono-ADP-Ribosyltransferase
MEM	Minimum Essential Medium
MMS	Methyl Methane Sulfonate
NAD	Nicotinamide Adenine Dinucleotide
NHEJ	Non-Homologous End-Joining
PTM	Post-Translational Modification
PHD	Plant Hetero Domain
PRMT	Protein Arginine Methyl Transferases
PARPs	Poly-ADP-Ribose Polymerase
PIK	Phospho-Inositide Kinase
PBS	Phosphate Buffer Saline
PVDF	Poly Vinyliene Di-Fluoride
RPMI	Roswell Park Memorial Institute medium
SAM	S-Adenosyl Methionine
SSB	Single Strand Breaks
SDS-PAGE	Sodium-Dodecyl-Sulphate –Poly-Acrylamide Gel Electrophoresis
TSS	Transcriptional Start Site
Tip60	Tat Interacting Protein-60

LIST OF TABLES

Table Title

LIST OF FIGURES

Figure Title

Chapter 1

Introduction

1.1. Definition of Epigenetics

Historically, the term epigenetics was used to describe various biological phenomena that could not be explained by genetic principles. Conrad Waddington (1942) originally coined the term '*epigenetics*' to describe '*how genes of a genotype bring about a phenotype*'. In 1987, Holliday applied the term epigenetics to situations in which 'changes in DNA methylation result in changes in gene activity'.[1] Few years later, Holliday redefined epigenetics as (i) the study of the changes in gene expression, which occur in organisms with differentiated cells and (ii) the mitotic inheritance of given patterns of gene expression which is not based on differences in DNA sequence.[2] The epigenetic modification plays a critical role in the regulation of all DNA-based processes, such as transcription, DNA repair and replication etc. Epigenetic regulations include DNA methylation, histone modification, nucleosome remodeling and RNA interferences [Figure 1.1].[3]

Figure 1.1: Schematic representation of mechanisms of epigenetic regulation. DNA methylation, histone modifications and RNA-mediated gene silencing constitute three distinct mechanisms of epigenetic regulation.[3]
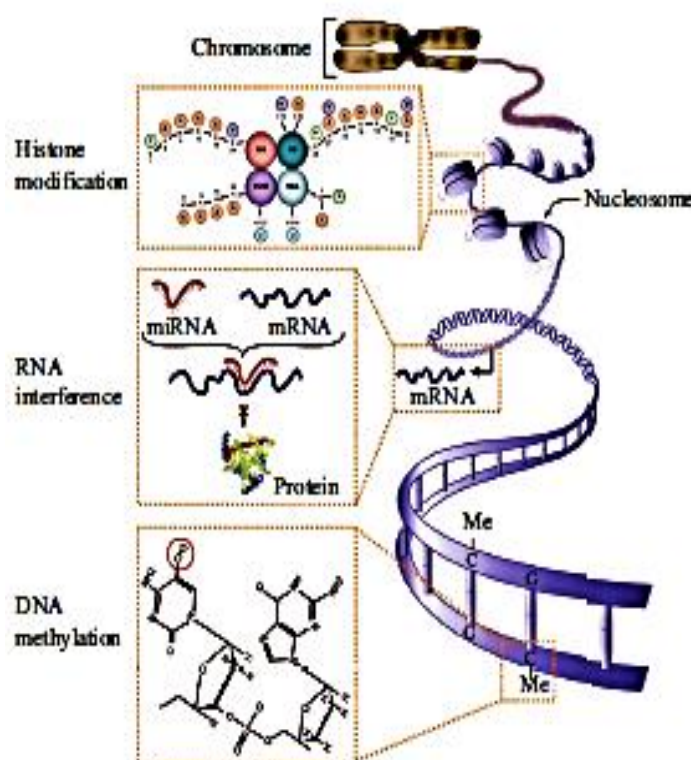
Epigenetics in today's modern terms can be mechanistically defined as '*the sum of the alterations to the chromatin template that collectively establish and propagate different patterns of gene expression (transcription) and silencing from the same genome*'.[4] James Watson, while revisiting the Central Dogma in the 50th anniversary of the double helix, stated, '*The major problem, I think, is chromatin.... you can inherit something beyond the DNA sequence. That's where the real excitement of genetics is now*'.[5]

1.2. Basic Unit of Chromatin Template

Chromatin is the macromolecular complex of DNA, histone proteins and non-histone proteins, which provides the scaffold for the packaging of genome. Human nuclear DNA is condensed into nucleosomes, which consist of 146 base pairs of DNA wrapped twice around an octamer core of histones (two molecules each of histones H2A, H2B, H3 and H4). The core histones are predominantly globular except for their N-terminal 'tails', which are unstructured. In between core nucleosomes, the linker histone H1 attaches and facilitates further compaction. All histones, except histone H4, are known to have multiple subtypes called 'variants' that are coded by non-allelic genes and that can take part in octamer formation leading to large variety of nucleosomes. Each nucleosome core particle represents the basic repeating unit in chromatin and exists in the form of arrays that forms basis for higher-order chromatin structure.[6] Nucleosomes are connected by a linker DNA of variable length (10-80 base pairs) that forms a 10-nm, beads-on-a-string array. The positioning of histones along the DNA is mediated by ATP-dependent nucleosome-remodeling complexes to non-covalently reposition histone octamer and thereby generate nucleosome free or dense chromatin.

The basic structure of the nucleosome core particle was resolved by X-ray crystallography and showed a disc shaped structure with the flat 1.65 left-handed super

helical DNA structure, corresponding to 145-147 base-pair stretch of DNA [Figureure1.2].[7]

Figure 1.2: Nucleosome core particle. Ribbon represent 146-bp DNA phosphodiester backbones (brown and turquoise) and eight histone protein main chains (blue: H3; green: H4; yellow: H2A; red: H2B.[7]
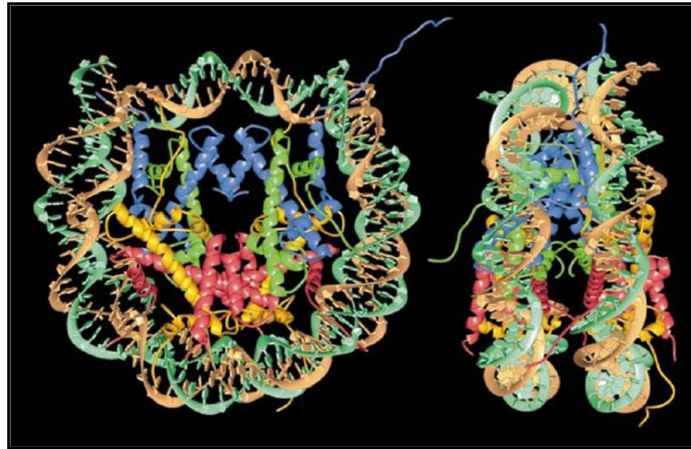
Each of the four core histones and their variants share the common and highly conserved structure domain known as histone fold domain (HFD) which consists of three α-helixes linked by two short loops (L1 and L2). The HFDs fold together in anti-parallel pairs like '*hand and shake*' arrangement between H2A and H2B and H3 and H4 [Figure1.3]. This dimeric structure of core histones is the building block of tetramer and octamer required for nucleosome formation.
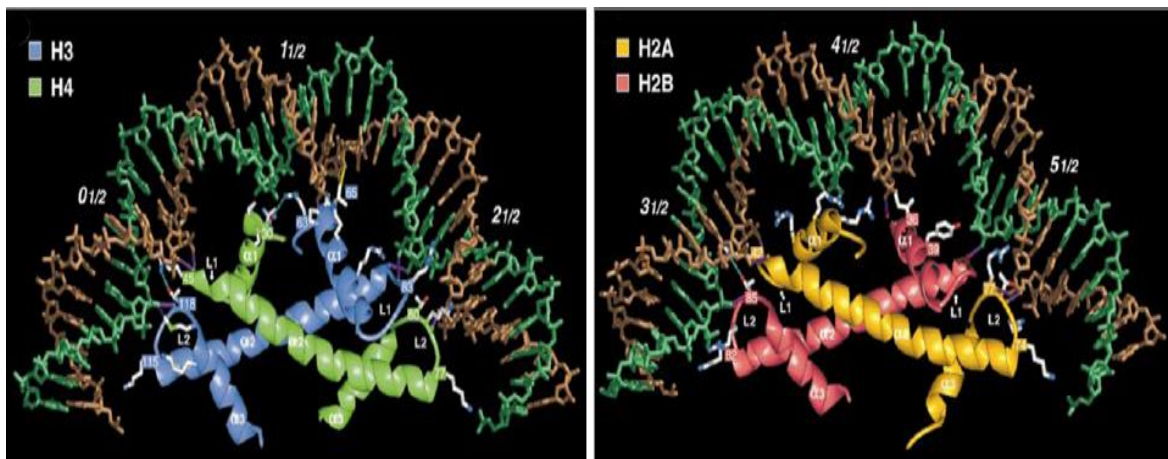
Figure 1.3: The α1-L1-α2-L2-α3 structure and ribbon traces of the H3-H4 and H2A-H2B histone-fold pairs.[7]

The N-terminal tails of all the core histones protrude out from nucleosomes and serve as sites for epigenetic signature. The affinity of histones for DNA and DNA-associated

proteins is modulated by site-specific post-translational modification specifically on N-terminals tails of histone. The modification and positioning of histones, in turn, organize the genome into open and condensed chromatin thereby governs transcriptional activity, and the availability of DNA for recombination, replication and repair.

1.3. Histone Post-translational Modifications

Vincent Allfrey's pioneering studies suggested histones can undergo variety of post-translational modifications (PTM) and reported histone acetylation in 1964.[8] Today, modifications of histones are central in the regulation of chromatin dynamics and are the target for variety of covalent modifications at specific amino-acid residue (Table 1.1). Reported histone modifications include acetylation, methylation, phosphorylation, ubiquitylation, glycosylation, ADP-ribosylation, carbonylation and SUMOylation. The lysine residues of histones may be acetylated, methylated or coupled to ubiquitin; arginine residues may be methylated; and serine or threonine residues can be phosphorylated.

Figure 1.4: Histone Modifications on the nucleosome core particle.[9] The nucleosome core particle shows 6 out of 8 core histone N-terminal tail domains. The epigenetic signals, the post-translational modifications are indicated by color symbols.
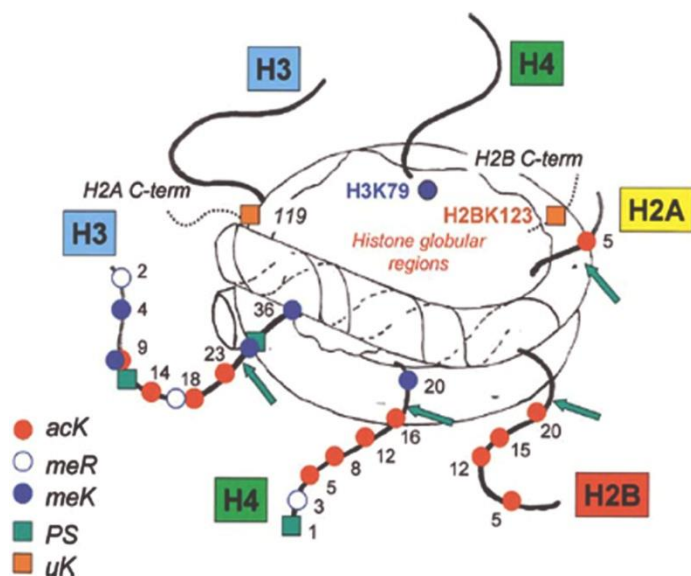
Table 1.1: Different classes of histone modifications and their functions[10]

Modifications	Nomenclature	Writers	Chromatin reader motif	Eraser	Attributed function
Acetylation	K-ac	HAT	Bromodomain	HDAC	Transcription, repair, replication and condensation
Methylation (K)	K-me1, K-me2, K-me3	HMT	Chromo, MBT and PHD domains	LSD1	Transcription and repair
Methylation (R)	R-me1, R-me2s, R-me2a	PRMT 1, 4, 5 and 6	Tudor domain	JMJD6	Transcription
Phosphorylation (S and T)	S-ph, T-ph	Kinase	14-3-3, BRCT	Phosphatase	Transcription, repair and condensation
Phosphorylation (Y)	Y-ph	Kinase	SH2	Phosphatase	Transcription and repair
Ubiquitylation	K-ub	E1, E2 and E3 enzymes	UIM, IUIM	Isopeptidases	Transcription and repair
Sumoylation	K-su	E1, E2 and E3 enzymes	SIM	----	Transcription and repair
ADP-ribosylation	E-ar	PARP1	Macro domain, PBZ domain	poly-ADP-ribose-glycohydrolase	Transcription and repair
O-GlcNAcylation (S and T)	S-GlcNAc, and T-GlcNAc	O-GlcNAc transferase	Unknown	β-N-acetyl glucosaminidase	Transcription

Histone modifications are written by specific histone modifying enzymes known as 'writers', recognized by specific proteins called 'readers' and are removed by 'erasers'. Histone methylation is a post-translational modification which takes place on the side chains of both lysine (K) and arginine (R) residues. Histone methylation is reversible process, catalyzed by histone methyl transferases (HMT), such as PRMT1 or Suv39H whereas histone demethylation is catalyzed by histone demethylases, such as LSD1 or Jumanji domain-containing proteins. The consequence of histone methylation on transcriptional state of a gene depends on the methylated residue and degree of methylation. The modulation of chromatin condensation can also be achieved via reversible acetylation on the lysine residues of histone tails. The acetylation reaction consists in the transfer of an acetyl group from acetyl coenzyme A (acetyl-coA) on the ε-amino group of the lysine residue, neutralizing the positive charge. This process results from a balance between the activities of two families of antagonistic enzymes, histone deacetylases (HDACs) and histone acetyl transferases (HATs), respectively removing or adding acetyl groups from/into core histone. Histone phosphorylation occurs on serine and threonine residues and influences transcription, chromosome organization, DNA repair and apoptosis.

Most of these modifications target the protruding amino or carboxy-terminal tails of the core histones; however, more recently some modifications have also been described in the globular domain.[11] A different kind of modification, *'tail clipping'* has also been detected in histones, a process associated with removal of a part of histone N-terminal tail. [12] These modifications alter higher order chromatin state by affecting interaction of histone with DNA or inter- and intra-nucleosomes interaction in order to unravel chromatin, and also facilitate recruitment of non-histone regulatory proteins on chromatin. The timing of induction of different modification on different histones

depends on the signaling and physiological condition within and surrounding the cell. The major question in the field of chromatin biology is 'how diverse PTMs interact to each other and required to perform a specific function?' One possible answer is that multiple independent modifications enable combinatorial complexity resulting in a large variety of functionally distinct nucleosomes. Many of the modifications can affect the others, collectively constituting the '**histone code**'.[13, 14] Today, 'Histone code' hypothesis states that:

- *Distinct modifications* on core and tails region of histone generate *docking sites* for a large number of non-histone chromatin associated proteins.

- Modifications on the same or different histone tails may be inter-dependent, generate various combinations and '*cross-talk*' within themselves to perform different functions.

- Distinct regions of *higher order chromatin*, such as euchromatic or heterochromatic domains, are largely depend on the local concentration and combination of differentially modified nucleosomes.

- '*Binary switches*' represent the differential readout of distinct combinations of marks on two neighboring residues, where one modification influence the binding of an effector protein onto another modifications on an adjacent or nearby residue.

- '*Modification cassettes*' signifies combinations of modifications on adjacent sites within these short clusters lead to distinct biological readouts.

1.4. Histone Variants

Chromatin structure is dynamic and a canonical histone can be exchanged for a variant within its own class. Variants differ from canonical histones in their primary sequence and are encoded by non-allelic genes and their incorporation has structural

consequences on the biophysical properties of the nucleosome core particle, altering accessibility of DNA to transcription factors and chromatin remodelers. Although a large number of histone variants exist, very few have been studied and well characterized. Except histone H4, all histones have multiple histone variants. Histone H2A has the largest number of identified variants. For example, histone H2A.Z (H2AZ, H2AFZ) is a histone H2A variant, a protein similar to canonical histone H2A but with different molecular identity and unique functions. H2A.Z is highly conserved during evolution. It plays an important role in basic cellular mechanisms such as gene activation, chromosome segregation, heterochromatic silencing and progression through the cell cycle.[15, 16] Histone H2A.X (H2AX, histone family member X) replaces conventional histone H2A in a subset of nucleosomes. Histone H2AX is required for checkpoint-mediated arrest of cell cycle progression in response to DNA damaging agents and for efficient repair of DNA double-strand breaks (DSBs), specifically when modified by C-terminal phosphorylation.[17] Histone macroH2A (mH2A) has a unique C-terminal domain [the macro domain, also called the non-histone domain (NHD)] in addition to the histone-like region. mH2A associates with condensed chromatin, including the inactive mammalian female X chromosome, senescence-associated heterochromatin foci, imprinted genetic loci and regions of chromatin that are CpG methylated.[18, 19] There are some well-studied histone H3 variants also. The number of histone H3 variants varies among species but in mammals it comprise of four members. H3.1 and H3.2 are the replicative histones expressed during S-phases, whereas H3.3 is the replacement histones expressed throughout the cell cycle and centromeric protein A (CENP-A) is specifically present at centromeres.[20] It has been proposed that the modification patterns of each H3 histone variants, H3.1, H3.2 and H3.3 can act as a signature to create different active and repressive chromatin regions in different phases of cell cycle.
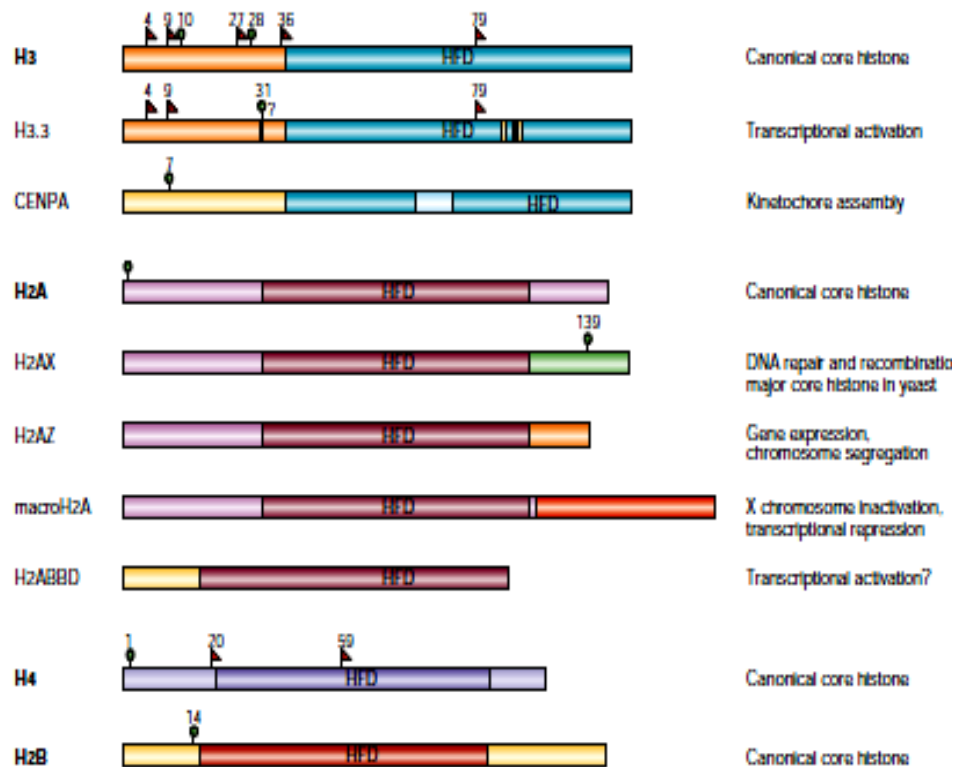
Figure 1.5: Canonical core histones and their variants.[21]

1.5. Chromatin Structure: Natural Barrier for DNA-mediated functions

Chromatin act as a natural barrier for most of the DNA based cellular processes and the eukaryotic cells has developed mechanisms to "open" or modulate conformation of chromatin to overcome the hindrance and make it accessible to cellular machineries to perform specific functions. The conformation of chromatin can be modulated by incorporation of histone variants in place of canonical histones and site-specific post-translational modification of histones. These modifications affect the chromatin structure by altering interactions within and between nucleosomes, and serving as docking sites for specific proteins with unique domains to perform specific functions.

1.6. Chromatin and Genome integrity

In order to survive and populate, every living organism must pass on accurately their genetic material to the next generation. The integrity of DNA is constantly subjected to alterations by cellular metabolites and exogenous DNA-damaging agents. These genetic lesions can block genome replication and transcription, if they are not repaired or are repaired incorrectly, they lead to accumulation of mutation or genomic aberration that drive cells towards cell death and if survived lead to progression of cancer .[22] To counter this threats posed by DNA damage, cells have evolved molecular circuitry known as 'DNA damage response' that detect DNA lesions, signal and promote their repair.[23] The various forms of DNA damage that cells encounter can trigger a variety of responses based on the nature of the damage and usually occur through common programs as represented in Figure 1.6.
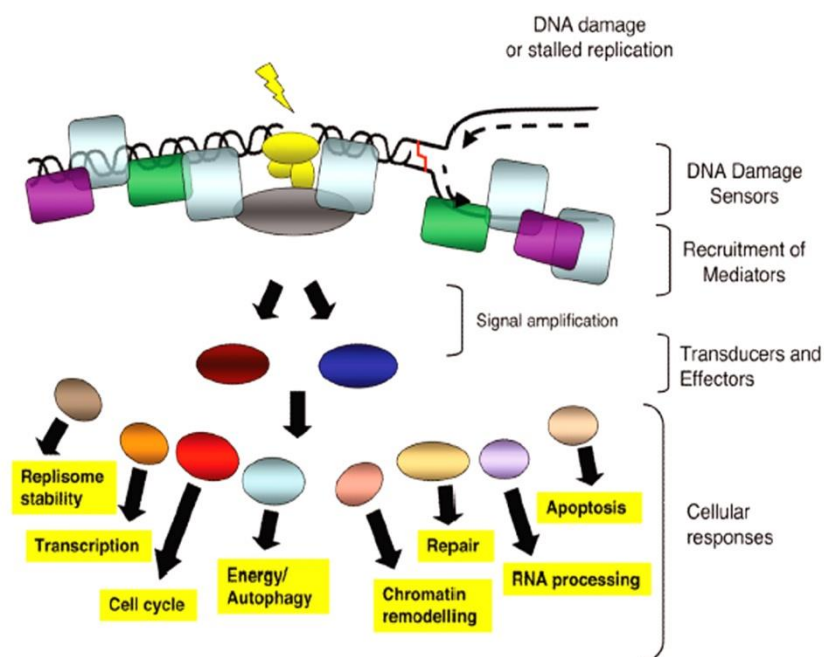
Figure 1.6: Schematic representation of model for the DDR: The presence of a lesion in the DNA, which can lead to replication stalling, is recognized by various sensor proteins. These sensors initiate signaling pathways that have an impact on a wide variety of cellular processes.[24]

Chromatin acts as a natural barrier in the detection, repair and recovery of DNA damage. The complexity and heterogeneous nature of chromatin organization present a series of challenges to the DSB-repair machinery. The impact of chromatin structure on DNA repair was first described in the proposed "*access-repair-restore*" model.[25] The model describes basic aspects of chromatin reorganization after DNA damage: damaged chromatin first becomes more accessible, altered chromatin organization facilitate DNA repair, followed by restoration of native chromatin state after completion of DNA repair.[26, 27] Almouzni *et al* proposed a refined model for the DDR in chromatin i.e. '*Prime-Repair-Restore*" model.[28]
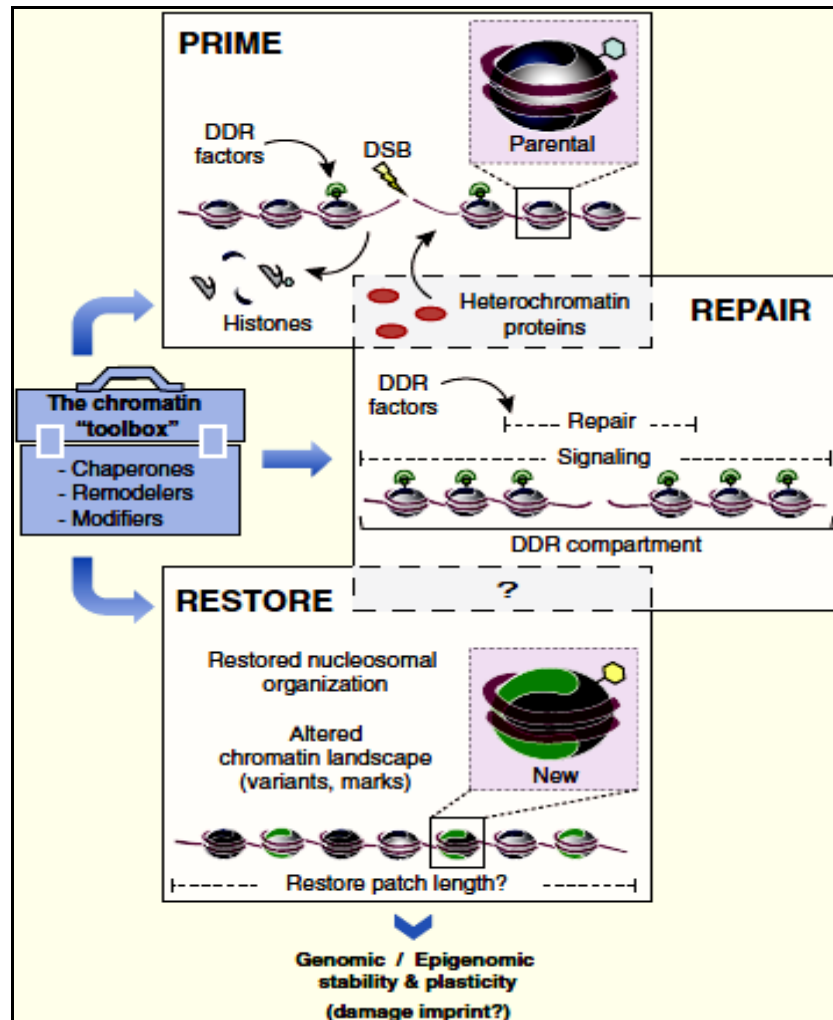
Figure 1.7: A Prime-Repair-Restore Model of DDR in context to chromatin.[28]

The earlier model '*access*' step is replaced by '*prime*' step to account both for positive and negative contribution of chromatin components which facilitates alteration in chromatin structure and recruitment of DDR factors at damage sites during early steps of the DDR. The efficacy of '*prime*' step depend on the parameter like cell cycle phase, site of damage location i.e. euchromatin or heterochromatin, and type of DNA damage which also determine the choice of a specific DNA repair pathway.

In the repair step, the signaling pathways integrate with chromatin dynamics. The degree of overlap exists between '*prime*' and '*repair*' phase and therefore, these steps cannot be regarded as sequential. The 'chromatin toolbox' comprising of histone chaperones, chromatin remodelers and chromatin modifiers are required to remodel the local chromatin architecture to provide access to DNA repair machinery to the site of damage and further reorganize the nucleosome-DNA template for processing and repair of the damage. In the '*restore*' step, cell restore native chromatin state after DNA repair is complete. The '*restore*' step overlap with '*repair*', since histone eviction mediated by histone chaperones could be accompanied with deposition in areas surrounding the damage before completion of DNA repair. The restoration of chromatin organization, not only involves recycling of parental histones, but also incorporation of new histones. The incorporation of new histones bearing typical histone modifications pattern and distinct variants may alter functional properties of restored DNA damage site. Further, restoration of chromatin state may leave a 'damage imprint' to react faster or differently upon re-exposure of cell to DNA damage.

1.7. DNA damage response

The cellular DNA damage response maintains genome integrity by repair of damaged DNA or inducing cell death.[29] The proteins involved in the DDR can be classified as sensors, transducers and effectors. The DDR is primarily activated by members of the

PIK-related kinase proteins, which include sensors such as ataxia-telangiectasia mutated (ATM), DNA-dependent protein kinases (DNA-PK) and ataxia-telangiectasia- and RAD3-related (ATR).[30, 31] Damage leads to activation of kinases affecting the downstream pathways and associated changes in chromatin conformation. Upon activation, PIK-related kinase phosphorylate and activate the transducer kinases, Chk1 and Chk2, where ATM primarily activates Chk2 and ATR primarily activates Chk1.[32] Further, Chk1 and Chk2 together with ATM and ATR, decreases cyclin-dependent kinase (CDK) activity that are either mediated through activation of p53 transcription factor or other proposed mechanisms.[30, 33, 34] Inhibitions of CDKs slows down or arrest the cell cycle progression at the G1-S, intra-S and G2-M check-points, which is thought to increase the DNA repair time before replication or mitosis. If cell fail to repair damaged DNA, DDR signaling induces cell death or senescence in order to avoid any pathological events.

1.8. Chromatin Structure and Modifications in DNA DSB Repair

It is now evident that induction of DSB results in change in chromatin organization at the local as well as global level, an essential requirement for activation of the DNA damage response (DDR) and subsequent DSB repair. The altered chromatin organization in response to DNA damage alters the sensitivity of chromatin to micrococcal nuclease digestion. [25, 35] Furthermore, recent reports suggest that DSBs induce a local decrease in the density of the chromatin fiber, increase in accessibility to MNase digestion alteration in the position of the nucleosomes and the eviction of the histone octamer.[36-38] The chromatin containing DSBs has been shown by energy-filtering transmission electron microscopy to exhibit limited mobility but undergoes an energy-dependent local expansion immediately after DNA damage.[37] KAP-1 phosphorylation (pKAP-1) by

ataxia-telangiectasia mutated (ATM) at S824 in response to DSBs has been associated with dynamic and localized increase in MNase accessibility during DSB repair.[39-41] DSB formation has been reported to lead to a localized disruption of nucleosomes, a process that depends on NBS1 and ATM.[42] These alterations in chromatin structure help in recruitment and maintenance of DDR proteins close to the site of the primary lesion and in this way contribute to more downstream aspects of the DDR.

In addition to histones, non-histone proteins are also involved in developing special chromatin structures. The histone modifications reported to induce following ionizing radiation exposure are phosphorylation, acetylation, methylation and ubiquitination. Except for ubiquitination, all these modifications alter histone/DNA electrostatic interactions and ultimately change chromatin dynamics and function by altering access of the cellular factors involved in DDR.

Figure 1.8: Major types of histone modification of specific histone residues linked with the DNA damage response (DDR) and DSB repair.[54]
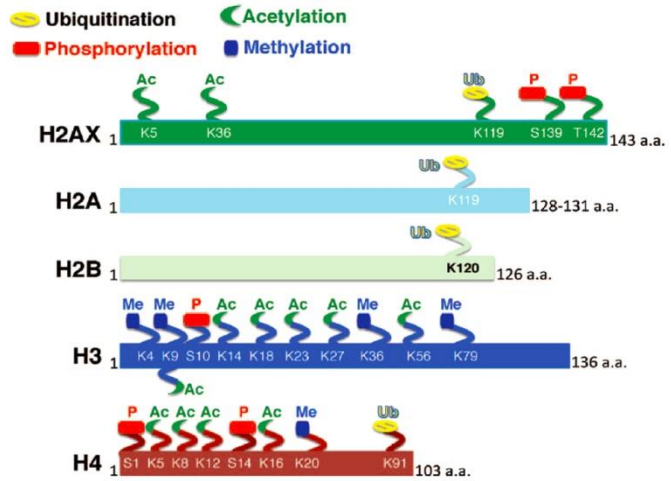
Among these major chromatin modifications, post-damage-induced histone phosphorylation has been the most thoroughly studied. Recent studies have provided evidence that histone acetylation of lysine is also critical for the DDR. Post-translational modifications (PTMs) of histone proteins are critical for cellular recognition of DNA damage and subsequent recruitment of repair protein complexes to the damage sites.

Moreover, evidence is emerging suggesting that pre-existing chromatin modifications also play an important role in the DDR.

1.9. Histone Modifications in DNA DSB Repair

1.9.1. Histone phosphorylation

H2A phosphorylation has been extensively studied in response to DNA damaging agents. The phosphorylation of a subset of histone H2A, H2AX at the Ser139 (γ position in its C-terminal tail)[43] gets amplified in megabase pair (Mbp) of DNA along chromatin tracks flanking DSBs.[44] The phosphorylation is carried out by members of the phosphatidylinositol-3 kinase-like family of kinases (PIKK) including ATM and DNA-dependent protein kinase (DNA–PK) within minutes of IR induced breaks[17] and ATR (ATM and Rad3-related) following DNA replication stress.[45] γH2AX is a key step in DNA damage response (DDR) signaling which facilitates recruitment of sensor, mediator and effector protein of DDR at damaged sites. H2AX phosphorylation mediated by ATM occurs in all phases of cell cycle and thus required for both DSB repair pathways.[46] γH2AX has been shown to interact with NBS1, 53BP1, MDC1/NFBD1 and MRN complexes and deficiency of H2AX results in enhanced genomic instability, radio sensitivity further supporting the role of γH2AX in DDR.[46, 47] The binding of repair proteins like MDC1 to γH2AX is modulated by hMOF (males absent on the first) dependent H4K16 acetylation. In coherence, H2AX phosphorylation has also been shown to facilitate the recruitment of ATP-dependent chromatin remodeling complexes like SW1/SNF, RSC and helicases. The H2X is reported to be phosphorylated at Tyr142 (Y142) by WSTF (Williams Beuren syndrome transcription factor enzyme) but gets dephosphorylated by the EYA (Eyes absent homologue) phosphatase after exposure of cells to DNA damaging agents.[48, 49] The dephosphorylation at Tyr142 (Y142) acts as a switch for the cell to repair the DNA damage, if remains phosphorylated cells undergoes

apoptosis. Further, other histones have also been reported to undergo phosphorylation in addition to H2AX during DDR e.g. phosphorylation of H2B at Ser14 is mediated by sterile 20 kinase[50] and N-terminal phosphorylation of H4 by casein kinase 2.[51-53]

Table 1.2: Histone phosphorylation in response to DNA damage[55]

Modification	Modifier	Histone	Role in DNA repair
pS139	ATM, ATR, DNA-PKcs	H2AX	Recruits and accumulates DDR proteins (MDC1) to the repair lesion and promotes histone acetylation
pT142	WSTF	H2AX	Recruits activated ATM and MDC1
pT14	CK2	H4	Promotes NHEJ by 53BP1 recruitment and methylation of H4K20
pS1	CK2	H4	Role in DDR

1.9.2. Histone acetylation

Histone acetylation plays a key role in both DDR signaling and DNA repair by altering the chromatin fiber intra- and inter-nucleosomal interactions to alter chromatin structure for access of repair machinery to site of DNA damage. Table 1.3 summarizes the histone acetylation enzymes with known connections to the DDR and their specific histone substrates. The histone acetylation is regulated by the balance between HATs and HDACs. Acetylation has been detected at four lysine residues (K5, K8, K12 and K16) in the N-terminal tail of the H4 histone. Histone H4Lys16 is acetylated by NuA4-TIP60 which facilitates accumulation of DDR proteins, 53BP1, BRCA1 and RAD51 and facilitates DSB repair.[56] Acetylation of histone H4 at lysine 16 is also mediated by hMOF and has been implicated in the proper compaction of chromatin 30nm fibers.[57] More importantly, lack of hMOF also influences ATM activation and result in delayed appearance of IR induced γH2AX foci.[58] Thus, H4Lys16Ac plays an important role in

maintenance of genomic stability and has also been implicated in tumorigenesis.[59] The N-terminus of H3 at Lys56 (K56) has been reported to play a key role in genomic stability and DNA repair. The conflicting reports for pattern of alteration and its regulatory enzymes in response to DNA damage have been reported. Das *et al* found that the level of H3Lys56Ac on chromatin increases in response to various types of DNA damage and mediated through CBP/p300.[60] Whereas, Tjeertes *et al* demonstrated reversible reduction of H3Lys9Ac (H3K9Ac) and H3Lys56Ac (H3K56Ac) in response to DNA damage[61] and the reduction of H3Lys56Ac and H4Lys16Ac is mediated by the localization of HDAC1 and HDAC2 to DNA breaks.[62] The restoration of H3Lys56Ac to its native level after repair of damaged DNA is part of a signal to switch-off the DNA damage checkpoint and enable the cells to enter normal cell cycle progression.[63] Interestingly, increased levels of H3Lys56 acetylation were found in tumor sample, suggesting a link between this mark and cancer development.[60]

Table 1.3: Histone acetylation in response to DNA damage[55]

Modification	Modifier	Histone	Role in DNA repair
K5Ac	TIP60	H2AX	Helps in K119ub of H2AX and removal of H2AX from chromatin
K36Ac	CBP/p300	H2AX	Recruits Ku during NHEJ
K9Ac, K14Ac, K23Ac K27Ac	GCN5,CBP/p300	H3	Recruits SW1/SNF complex, promotesspreading of γ-H2AX domain and regulates ATM activity
K18Ac	GCN5,CBP/p300, RTT109	H3	Regulates Ku protein recruitment during DSB repair
K5Ac, K8Ac,	MOF, TIP60-TRRAP;	H3	Depletes after IR to promote NHEJ, enriches K56ac after HR and UV repair
	CBP/p300	H3	Recruits DDR and repair proteins and recruits SW1/SNF nucleosome remodeling complex

1.9.3. Histone methylation

Histone dimethyl Lys79 promote accumulation of DDR-mediator protein, 53BP1 through Tudor domain at DNA damaged sites immediately after DNA damage.[64] H3Lys79me2 does not seem to increase globally, but the hidden site of modification is exposed after DNA damage and thus facilitating interaction with 53BP1. The interaction of 53BP1 to the DNA damage site is further stabilized by another modification, dimethyl Lys20 of H4. (H4K20me2).[65] H4Lys20me2 is mediated by the histone methyl transferase MMSET (also known as NSD2 or WHSC1) in mammals, also not increases globally after DNA damage, but does increase in the vicinity of DSBs. The depletion of MMSET significantly decreases H4Lys20 methylation and the subsequent accumulation of 53BP1 highlighting its importance in DDR.[66] Based on these observations, it is likely that a pathway involving γH2AX–MDC1–MMSET regulates the induction of H4Lys20 methylation on histones around DSBs, which, in turn, facilitates 53BP1 recruitment.

H3Lys9me3 has been associated with heterochromatin and transcription repression. Oncogene-induced DNA replication stress induces a global increase of H3Lys9me3 which raises the possibility of its role in DDR activation. Although, globally H3Lys9me3 remains unchanged in exogenously damaged cells but localization of Tip60 to DNA damaged sites is dependent on this modification.[67, 68] Further, Tip60 can activate ATM through specific histone acetylation.[68] Overall these results suggests that H3Lys9me3 regulates the DDR by recruiting Tip60 at DSBs site in order to activate ATM and thus H3Lys9me3 play key role in early sensing of the damage DNAs. Some of the recent reported histone methylated marks linked to DDR are summarized in **Table 1.4.**

Table 1.4: Histone methylation in response to DNA damage[55]

Modification	Modifier	Histone	Role in DNA repair
K4me3	SET1	H3	Stimulates V(D) J recombination via recombination activating gene (RAG) complex
K9me3	Suv3-9H1/Suv3-9H2	H3	Interacts with HP1β, phosphorylates damage-induced HP1β and activates TIP60
K36me2	Metnase/SETMAR	H3	Accumulates NBS1 and Ku to stimulate NHEJ
K79me3	DOT1	H3	Recruits RAD9 in budding yeast
K20me2	Suv4-20H1/Suv4-20H2; MMSET	H3	Recruits DDR and repair proteins

1.9.4. Histone Ubiquitylation

Ubiquitylation plays a key role in the recruitment of DDR factors that are involved in enhancing DDR activation. Ubiquitylation of H2AX on Lys119 (K119) and Lys120 by UBC13, RNF8 and RNF168 favors local accumulation of 53BP1 and BRCA1.[69, 70] Human histone H2A has been found to be mono-ubiquitinated at Lys119 in the vicinity of UV-induced DNA lesions.[71] Further, H2AX phosphorylation is part of a cross talk that also involves histone ubiquitylation which suggests that cooperation between histone marks has functional role during DNA damage. γH2AX is ubiquitylated by ring finger protein 2 (RNF2), which causes the recruitment of BMI1 to sites of DNA lesions. BMI1 recruitment to damaged DNA and assists proper localization 53BP1, BRCA1 and RAP80 and further it facilitates DNA repair by HR.[72] In addition to H2A, Ubiquitylation of H2B at Lys120 (K120) mediated by RNF20/40 involved in DDR signaling and thus promotes DNA repair by both HR and NHEJ.[73] The major histone sites of ubiquitination, the

enzymes required and the role of the modification in the DDR are summarized in Table1.5.

Table 1.5: Histone ubiquitination in response to DNA damage[55]

Modification	Modifier	Histone	Role in DNA repair
K119ub/K119ub2, K119poly-ub	RNF8, RNF168	H2A	Accumulates BRAC1 and 53BP1 for DNA repair
K119ub/K119ub2, K119poly-ub	RNF8, RNF168, TIP60–UBC13	H2AX	Recruits DDR proteins to the repair lesion
K120ub	RNF20–RNF40	H2B	Recruits XRCC4 and Ku for NHEJ and BRCA1 and RAD51 for HR
K91ub	BBAP	H4	Induces H4K20me modification and recruits 53BP1 to promote NHEJ

1.10. Double Strand and Break (DSBs) repair

Double strand breaks (DSBs) in the DNA are most deleterious genetic lesions induced directly by IR and radiomimetic drugs. Indirectly, through impediment of replication fork progression by damaging agents like CPT, Ara-C and DNA cross-linking agents like cisplatin are also known to DSBs.[74] DSBs are recognized by DNA damage sensor proteins within chromatin and activate the recruitment of DNA repair proteins at the sites of damage. The DSB repair follows two principal mechanisms: (1) Non-homologous end-joining (NHEJ) and (2) homologous recombination (HR).[75]

1.10.1. Chromatin Modifications during Non-Homologous End Joining Repair

In mammalian cells, the majority of DSBs are repaired by NHEJ throughout the cell cycle.[76] There are two types of NHEJ repair: (1) Canonical end joining pathway (C-NHEJ) and the (2) Alternative NHEJ (A-NHEJ) pathway, the latter being a minor DSB repair pathway that operates at telomeres in telomerase deficient cells or in the absence of

Ku. In C-NHEJ, DSBs are recognized by the heterodimer, Ku70/Ku80 protein, which forms a ring like structure around each end of the broken DNA molecule, binds, activates the protein kinase, DNA-PKcs, leading to recruitment and activation of end-processing enzymes, polymerases and DNA ligase IV.[77] Prior to loading of the repair proteins, histone modifications occur which facilitate the recruitment of repair proteins at the damage site. Ligation is mediated by the donation of an AMP on to the exposed 5' phosphate by the DNA ligase-adenylate complex. The A-NHEJ uses a region of micro-homology to align the broken DNA strand and before joining and is independent of Ku and XRCC4 but dependent on PARP and CtIP. The A-NHEJ pathway is relatively poorly characterized; certain features of A-NHEJ are well characterized such as a slower kinetics of DSB repair than in C-NHEJ and competitive repression of A-NHEJ by Ku under normal conditions. Whether C-NHEJ and A-NHEJ require any pathway specific chromatin modifications is not yet known.

The chromatin modification that occurs immediately after cellular exposure to IR is phosphorylation of histone H2AX on Ser139 (γH2AX) which functions to recruit repair proteins. Besides γH2AX, other modifications reported in the NHEJ are dimethylation of histone H3 residue Lys36 (H3K36me2) by Metnase,[78] whereas H3Lys4me3, carried out by Set1p methyl transferase has been found at DSBs and the absence of this modification has been linked to poor DNA DSB repair.[79] The induction of H4K16Ac in response to DNA DSB influences repair as cells with decreased levels of H4K16Ac have reduced efficiency of DNA DSB repair by NHEJ.[58] It is interesting to note that at DSBs, RSC complex recruits MRE11, which is followed by ATPase remodeling to facilitate access to the site by proteins required for NHEJ-mediated repair.[36] Furthermore, acetylation of H3 and H4 by CBP and p300 cooperate with the SW1/SNF complex to facilitate recruitment of Ku70/80.[80]

1.10.2. Chromatin Modifications during Homologous Recombination Repair

During the DNA DSB repair by HR, nucleotide sequences are exchanged between two similar or identical molecules of DNA, allowing the cells to accurately repair DNA. HR type repair is predominant during meiosis and in the S- and G2-phases of the cell cycle because sister-chromatid sequences are required as the template to mediate accurate repair.[75] DSB is recognized by Mre11/Rad50/Nbs1 (MRN) complex, which promotes activation of ATM.[81] MRE11 has endo- as well as exo-nuclease activities for resection of DNA ends, an essential step for initiation of HR repair. Further, recruitment of RPA, RAD51 and RAD52 to the single strand and tail searches for a homologous region and initiates pairing, which is facilitated by RAD54. DNA synthesis occurs from the invading end of the damaged DNA, extending the repair region and forming the Holliday junction. This junction translocates along the DNA by a branch migration complex and is cleaved by a resolvase enzyme. The DNA ends are rejoined to yield intact duplex products. HR repair is a complex process and all steps require major changes in the chromatin structure in order to allow repair proteins access to damaged DNA. The acetylation of H3 and H4 by histone acetyl transferases, GCN5, NuA4 and HAT1 are implicated in DSB repair.[56, 82] GCN5 has also been reported to interact with BRCA1 suggesting its possible role in HR repair of DNA DSBs.[83] Furthermore, at the completion of HR repair chromatin structure must be restored to the pre-damage state, a process that starts with dephosphorylation of γ-H2AX by protein phosphatase PP4C and deacetylation marks occurs by HDACs in mammals.[84] Besides histones, a non-histone protein, HP1β has been reported to play both negative as well as positive role in maintaining genomic stability in mammalian cells.[27, 41, 85, 86] The decrease in phosphorylation of HP1β leads to its transient displacement from H3Lys9me3 and increase in the level of ATM for efficient repair in heterochromatic regions at DNA damage sites.[67]

1.11. Pre-existing histone modifications and their role in DDR

Histone modifications in response to DNA damage play an important role in marking the site of a DNA break to facilitate the recruitment of DNA repair proteins and altering the chromatin architecture for access of repair proteins to the damaged DNA site.[87] But, pre-existing histone modifications, H3Lys79 (H3K79) and H4Lys20 (H4K20) are reported not to increase globally after DNA damage, but are critical for 53BP1, Crb2 (*S. pombe*, Crb2) and Rad9 (*S. cerevisiae,*Rad9) recruitment to double-strand breaks for foci formation at damage sites.[60, 64, 65, 88] H3Lys56Ac (H3K56Ac) has been reported recently to decrease in response to DNA damage in human cells.[61] The pre-existing modifications are also known to influence DNA damage response at the level of cell signaling. The depletion of MOF in human cells reduces H4Lys16Ac (H4K16Ac) levels that results in decrease of ATM activation as well as defective appearance of γH2AX foci after irradiation.[89] Furthermore, Sharma *et al* demonstrated a direct relationship of decrease in H4Lys16Ac levels and γH2AX foci per cell after irradiation in differentiated HL60 cells.[58] Thus, emerging evidences are suggesting that pre-existing chromatin modifications at the histone level can directly affect the initial DDR and subsequent pathway preference of DNA repair.

1.12. Dynamics of histone modifications during cell cycle

The cell cycle constitutes a series of interrelated processes that includes accurate duplication of DNA in the chromosome and segregation of the copies into two genetically identical daughter cells. These events define the two major phases of the cell cycle: DNA replication, which occurs during synthesis S-phase and chromosome segregation followed by cell division, which take place during mitosis, M-phase. The two gap phases, G1 and G2, before S and M phases, allow cells to grow. Pederson *et al* demonstrated that the

pancreatic DNase1 digest chromatin from different phases of the cell cycle in the decreasing order, G1 and G2/M.[90] Thus, the differential pattern of chromatin digestion suggests that particular set of histone marks are associated with specific phase of cell cycle. The histone modifications and their level changes throughout the cell cycle to maintain specific chromatin organization for phase-specific functions like transcription, replication and segregation.[91] Cells enriched in G1, S and G2 shows mostly identical pattern of core histone marks in the G1 and S phase, whereas M-phase marks are drastically different from G1 and S phase marks.[92] Histone H1 is phosphorylated in a cell cycle-dependent manner, levels are usually lowest in the G1 phase, rises continuously during S and G2 and in the M phase, where chromatin is highly condensed, shows the maximum number of phosphorylated sites.[93, 94] Phosphorylation of histone proteins is involved in the transition from interphase to mitotic chromatin. However, definitive roles of phosphorylation in this process have not yet been elucidated. An increase in histone H3Ser10 phosphorylation is a well-known hallmark for mitosis and meiosis in various eukaryotic organisms. However, H3Ser10 phosphorylation is a highly dynamic and its level alter throughout the cell cycle. H3Ser10P plays a dual role (i) maintaining relaxed chromatin for active transcription in interphase, and (ii) condensed chromatin state in mitosis. Recent reports have shown that H3 is also phosphorylated at Ser 28, Thr 11, Thr 3 and H3.3 Ser 31 during mitosis.[95] Histones H4 is hyperphosphorylated at Ser1 residues during mitosis in mammalian cells, where as phosphorylation status of H2AS1 remains unchanged during different phases of cell cycle. [92] The pattern of of cell cycle dependent methylation is more complex and appears to have multiple effects on chromatin function. The H3Lys27 and Lys36 are known to decrease, whereas H4Lys20 increases in G2/M phase of cell cycle. The increase in histone H4Lys20 is consistent with increase of its methyl transferase, PR-set7 activity during G2/M phase. For histone acetylation, it is now

generally accepted that hyper acetylated histones are mostly associated with activated genomic regions, whereas deacetylation mainly results in repression and gene silencing. The level of site-specific acetylation on core histones decreases in G2/M phase at H2ALys5, H2BLys12, H2BLys15, H2BLys20, H3Lys18, H3Lys23, H4Lys5, H4Lys8, H4Lys12, H4Lys16. The increase in H4Lys16Ac has been reported to inhibit the formation of the 30nm chromatin fiber and prevents the formation of higher order chromatin states in G1 phase.[96] H3Lys56 is acetylated preferentially during S-phase and gets deacetylated, as soon as cells enter into the later stages of cell cycle. H3Lys56Ac has been reported to favour the increase in DNA breathing on the nucleosomes that may help in efficient replication of DNA in S-phase of cell cycle.[97, 98] The reversible histone modifications during cell cycle affect the charge density of the flexible N- and C-terminal domains and have considerable potential to modulate histone/DNA interactions in chromatin. Histone modifications are also able to affect binding interactions with other proteins that may, in turn, alter higher order structure of chromatin.

1.13. Paradox: Histone Modifications, Cell Cycle and DNA damage

DNA damage occurs continuously as a result of various factors-intracellular metabolism, replication and exposure to genotoxic agents, such as ionizing radiation, UV, chemicals and chemotherapeutic drugs. Endogenous sources of DNA damage are by-product of a variety of metabolic processes which can react with macromolecules such as lipids, proteins or nucleic acids. Endogenous DNA damage is typically caused by three classes of chemical reactions: (1) oxidation, (2) alkylation and (3) hydrolysis.

Earlier literature has suggested that 'Access-Repair-Restore' steps to repair the damaged DNA is a complex phenomenon and require the combinatorial effect of type of DNA

damaging agent, type of DNA damage, phase of cell cycle and chromatin state to decide

the alteration and importance of marks in DDR.
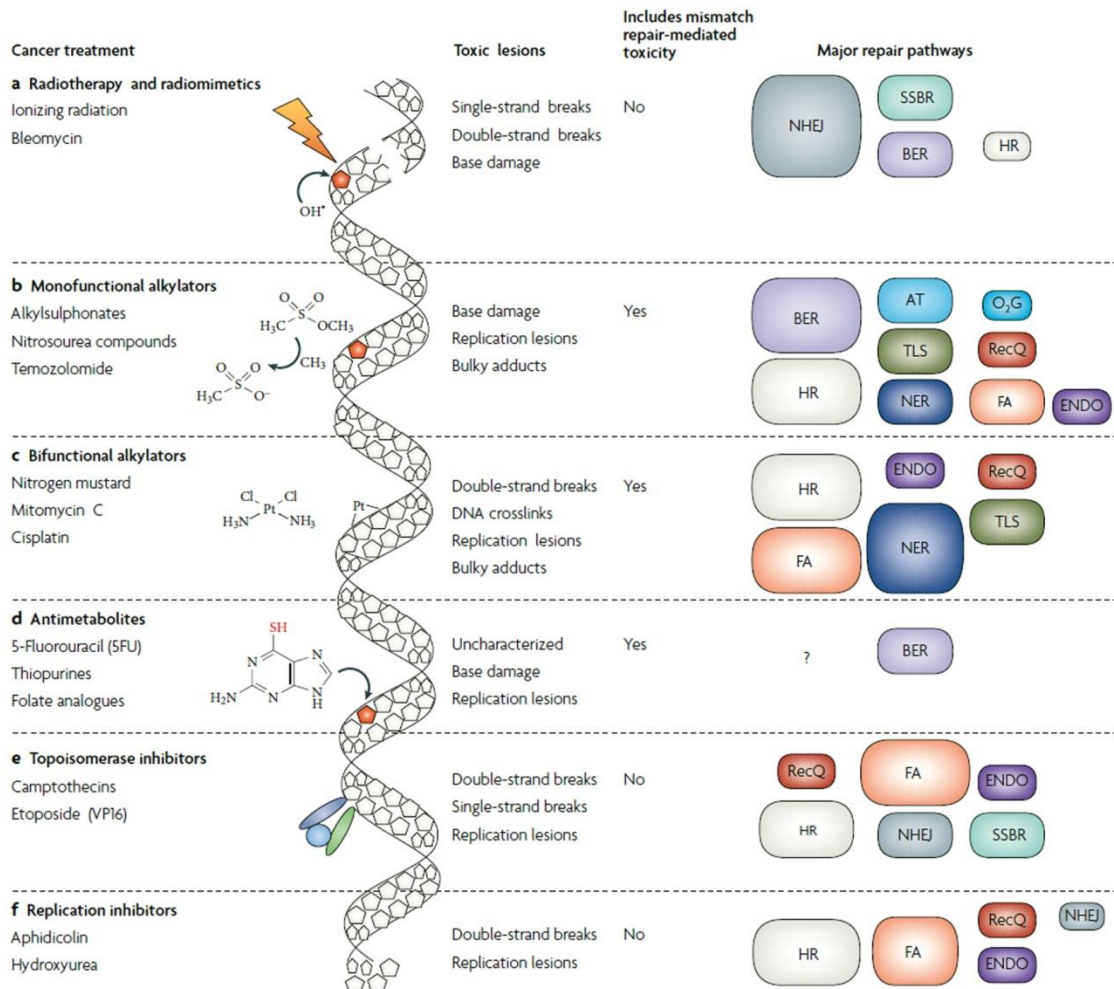
Figure 1.9: Overview of DNA repair pathways involved in repairing toxic DNA lesions formed by cancer treatments.[99]

Recent reports regarding pattern of DNA damage responsive histone marks appear with

ambiguous observation. The ultraviolet (UV) rays induced DNA damage, recruits GCN5

to sites of DNA damage and increases H3Lys9 acetylation (H3K9Ac) to facilitate

efficient nucleotide excision repair.[100] In contrary, Tjeertes *et al* demonstrated that

H3Lys9Ac decreases in response to DNA damage.[61] H3Lys56Ac (H3K56Ac) is reported

to be conserved in human cells and appears to be regulated in a DNA damage-dependent

manner with conflicting reports.[60, 61, 101-103] DNA damaging agents, MMS and CPT,

induces DNA damage in S-phase and are associated with increase of H3K56Ac [60, 101, 102]

whereas, Tjeertes *et al* demonstrated that H3Lys9 and H3Lys56 acetylation decreases in response to genotoxic stress and their level are restored after DNA repair. In addition, Battu *et al* reported reversible reduction of H3Lys56Ac in response to UV induced DNA damage. The HAT, CBP/p300 in human cells has been reported for acetylation of H3Lys56, whereas another report suggests that the localization of HDAC1 and HDAC2 to DSBs after DNA damage is responsible for reduction of H3Lys56Ac.[62] Thus, the status of H3Lys56Ac in DDR is still a matter of debate in mammals.

Table 1.6: Paradox in DNA damage responsive histone marks.

Histone marks	Pattern of alteration	Enzymes	Damaging agents	Cell cycle phase	Ref
H3K9Ac	Increases	GCN5	UV-rays	Asynchronous	[100]
H3K9Ac	Decreases	HDAC1, HDAC2	IR-rays, MMS, CPT, Phleomycin, H_2O_2,UV rays	Asynchronous	[61, 103]
H3K56Ac	Increases	CBP/p300, p300	IR, MMS, UV,CPT	Asynchronous	[60, 102]
H3K56Ac	Decreases	HDAC1, HDAC2	IR-rays, MMS, CPT, Phleomycin, H_2O_2, UV rays	Asynchronous	[61, 103]
H4K16Ac	Decreases	HDAC1, HDAC2	IR, Phleomycin	Asynchronous	[62]
H4K16Ac	Increases	hMOF	IR	Asynchronous	[89]
H3S10P	Decreases	Inhibition of aurora B kinase, PP1, ATM	H_2O_2, UV,IR	Asynchronous	[105-107]
H3S10P	Increases	ERK, p38 kinase, PKCδ, MSK1	UV, IR, Cisplatin	Asynchronous	[108, 109]

Additionally, H4Lys16Ac (H4K16Ac) and H2A ubiquitylation have been shown to increase after ionizing radiation.[89, 104] In contrary, Jackson *et al* demonstrated that

decreases of H4Lys16Ac is mediated through recruitment of HDAC1 and HDAC2 at DNA damage sites.[62] Additionally, decrease as well as increase in H3Ser10 phosphorylation has been reported in response to DNA damage.[105-109] Also, phosphorylation of H3Ser10 is reported to increase during apoptosis and is mediated through pro-apoptotic kinase, protein kinase Cδ.[110]

Recently, Almounzni *et al* proposed in order to comprehend how histone marks behave during the DNA damage response, a careful comparison of cell lines, passage number, cellular physiological condition, source of antibodies, method of extract preparation and damage treatment is required.[111]

1.14. H3Ser10 phosphorylation: Dual role in Interphase and Mitosis

The serine at the tenth position of the histone H3 amino acid sequence (H3Ser10) is phosphorylated in association with gene transcription, meiosis and mitosis. The level of H3Ser10P undergoes dynamic alteration throughout the cell cycle to facilitate distinct cellular functions in specific phase of cell cycle.[92] It is crucial for chromosomes condensation and cell-cycle progression during mitosis and meiosis, whereas enables activation of transcription in interphase or G1 phase of cell cycle.[93]
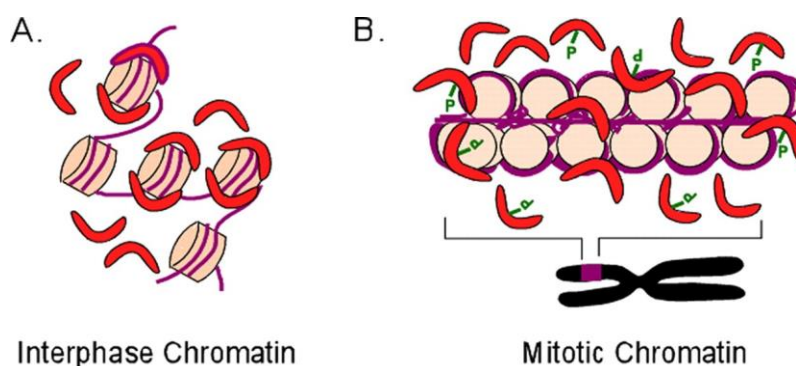
Figure 1.10: Schematic representation of Interphase and Mitotic Chromatin

1.14.1. H3Ser10 phosphorylation during Interphase

Phosphorylation of H3Ser10 in interphase or G1-phase cells is associated with small fraction of chromatin that is actively involved in gene transcription. The phosphorylation of H3Ser10 is inter-dependent on post-translational modification status of neighboring residues, Lys9 and Lys14. The phosphorylation of H3Ser10 on the promoter of immediate early genes in response to epidermal growth factor (EGF) is mediated through mitogen- and stress-activated kinase1 (MSK1), whereas dephosphorylation of H3Ser10P occurs by mitogen-activated protein kinase phosphatase 1 (MKP1) in response to vascular endothelial growth factor (VEGF).[112, 113] Earlier reports have shown that H3Ser10P enhances the recruitment of GCN5, which acetylates Lys14 on the same histone tail.[114, 115] Also, H3Ser10 phosphorylation is reported to be dependent on the methylation status of H3Lys9.[116] An increase in phosphorylation of H3Ser10 is observed in methyl transferase-deficient cells whereas it is reduced after dimethylation of Lys9. Previous reports have shown that other than transcriptional activation, H3Ser10 phosphorylation also alters during oxidative and UV induced DNA damage that is mediated through MAP kinase pathway. But, recent reports have shown ambiguous result of increase or decrease of H3Ser10P in response to DNA damage in context with MAP kinase pathway.[105, 108]

1.14.2. H3Ser10 phosphorylation during Mitosis

H3Ser10P is closely associated with condensation of chromatin to chromosomes in mammalian cells during mitosis or G2/M phase of cell cycle. In mammalian cells, phosphorylation of H3Ser10 is first evident in peri-centromeric heterochromatin region in late G2-phase and spreads along the chromosomes at prophase with maximum level at the metaphase.[117] Aurora B kinase phosphorylates H3Ser10 in mitotic phase of cell cycle.[118] In addition, vaccinia-related kinase (VRK1) is also reported for H3Ser10 phosphorylation

in mammalian cells during mitosis. The activity of these kinases is balanced by the activity of type-1 phosphatase (PP1). The functional role of H3Ser10P is established by abnormal chromosome segregation and extensive chromosomes loss during mitosis and meiosis in H3Ser10A mutant strain in mammalian cells.[119]

Such contrasting reports about pattern of alteration DNA damage responsive marks may be due to different (i) origin of cell line, (ii) DNA damaging agents, (iii) doses, (iv) time of exposure and (v) phase of cell cycle used for the analyzing the importance of specific histone marks in DDR. The pattern of alteration of H3Ser10P in response to DNA damage and its regulatory pathway have not yet been well understood and require better scientific clarity under control conditions.

Chapter 2

Aims & Objectives

2.1. Statement of the problem:

Earlier reports have shown ambiguous alteration of histone marks in response to DNA damage in asynchronized population of cells. These histone marks not only undergo dynamic alteration in context of DNA damage but are also known to alter during cell cycle in order to maintain phase specific chromatin states. This might lead to differential radio-sensitivity in different phases of cell cycle. Previous studies suggest that in response to DNA damage, cells in late S-phase are more radio-resistant whereas G2/M-phase cells are less radio-resistant compared to G1-phase cells. The different repair pathways are predominantly active during specific cell cycle stages. Like, homologous recombination (HR) is predominant in late S-phase and G2/M phase and non-homologous end-joining (NHEJ) is predominant in G1-phase. The specific histone marks might associate with repair pathways and distinct chromatin states in response to DNA damage in different phase of cell cycle.

2.2. Hypothesis

We hypothesize that the 'histone marks' that are induced at the site of DNA damage could be different and are associated with specific phase of the cell cycle and repair machinery. Therefore, the cell cycle phase specific histone marks may be the key determinants for phase specific differential response to ionizing radiation.

The aim of the present study is to investigate cell cycle phase specific alteration of histone marks and chromatin structure in response to ionization irradiation and to delineate the proteins associated with histone modifications.

Accordingly, the objectives of the present research work are:

2.3. Objectives

2.3.1. Whether any alterations in histone modifications/variants is associated with specific cell cycle stage that alter chromatin structure for DNA repair in response to double strand DNA damage?

2.3.2. What are the interacting protein partners of altered histone(s) in response to double strand DNA damage?

The following experiments were conducted on cultured human cells as a model system in order to address the objectives:

2.4. Whether any alterations in histone modifications/variants is associated with specific cell cycle stage that alter chromatin structure for DNA repair in response to double strand DNA damage?

- Time dependent cell cycle profiling after irradiation of G1 enriched cell lines (WRL68 and HepG2) by flow cytometry.

- Time dependent immunofluorescence staining of γH2AX in G1 enriched cell lines (WRL68 and HepG2) after irradiation in order to understand prime, repair and restoration phase of DNA damage response.

- Time dependent alteration of histone marks profiling in G1 enriched cell lines (WRL68 and HepG2) after irradiation by western blotting.

- Dual immunofluorescence staining of different histone marks after irradiation in order to understand co-localization with γH2AX (DNA damage mark).

- Synchronization of cells in different phases of cell cycle in order to validate altered histone marks and its association with specific phase of cell cycle.

- Induction of different type of DNA damage in order to validate universal nature of altered histone marks in G1 phase of cell cycle.

- Enrichment of cells in G1 phase of different tissue origin in order to demonstrate altered histone marks in response to DNA damage is independent of tissue origin and universal in nature.

- MNase sensitivity assay to demonstrate global changes in chromatin organization at the nucleosomal level in response to IR induced DNA damage in G1 phase of cell cycle.

- Mononucleosomal immunoprecipitation experiment to demonstrate alteration of DNA damage responsive histone marks on same γH2AX bearing mononucleosomes in response to IR induced DNA damage in G1 phase of cell cycle.

2.5 What are the interacting protein partners of altered histone(s) in response to double strand DNA damage?

- Protein expression profile of downstream effectors of MAP Kinase pathway by western blotting in order to establish its association with altered histone marks after irradiation.

- *In-silico* docking studies to demonstrate interaction between effector enzymes with its respective altered histone marks.

- Biochemical fractionation studies to demonstrate localization of effector enzymes to altered chromatin structure in response to DNA damage in G1 phase of cell cycle.

- Mononucleosomal immunoprecipitation to demonstrate direct interaction of effector enzymes with γH2AX bearing mononucleosomes in response to DNA damage in G1 phase of cell cycle.

- Inhibitor-based approaches for mechanistic studies of alteration of histone marks in response to DNA damage.

- Functional studies such as colony formation assay for survival, cell viability by trypan blue staining and DNA damage repair by comet assay to demonstrate significance of effector enzymes and altered histone marks in DNA damage response.

Chapter 3

Materials & Methods

Antibodies and histones used in the study

S. No.	Antibody name	Company	Cat.no.
1	Alexa Fluor-488 (anti-rabbit)	Invitrogen	A-11029
2	Alexa Fluor-568 (anti-mouse)	Invitrogen	A-10879
3	Anti-rabbit HRP	Cell Signaling	7074
4	Anti-mouse HRP	Sigma	A-4416
5	β-actin	Sigma	A-5316
6	ERK1/2	Santacruz	Sc-93
7	γH2AX	Millipore	05-636
8	H3S10P	Abcam	Ab5176
9	H3S10P	Millipore	Cc-200583
10	H3K9Ac	Abcam	Ab-4441
11	H3K14Ac	Abcam	Ab-52946
12	H3K56Ac	Abcam	Ab-76307
13	H3	Upstate	05-499
14	H4	Millipore	07-108
15	H3S28 P	Abcam	Ab-5169
16	JNK	Santacruz	Sc-571
17	MSK-1	Santacruz	Sc-25417
18	MKP-1	Santacruz	Sc-370
19	p-MSK1	Abcam	Ab-32190
20	pERK	Cell Signaling	4370
21	pJNK	Cell Signaling	4668
22	pP38	Cell Signaling	4511
23	P38	Santacruz	Sc-728
24	Recombinant H3.1	NEB	M2503S
25	Recombinant H3.2	NEB	M2506S
26	Recombinanat H3.3	NEB	M2507S

Biochemical used in the study

S. No.	Chemical name	Company
1	Acrylamide	Sigma
2	Agarose	USB
3	Ammonium persulfate	USB
4	Acetic Acid	Qualigens
5	Aprotinin	Sigma
6	Amido Black	Sigma
7	Ammonia	Qualigens
8	Bovine Serum Albumin fraction V	Roche-Sigma
9	Bradford reagent	Biorad
10	β-mercapethanol	Sigma
11	Commassie brilliant blue R-250	USB
12	Calcium chloride	SD fine
13	Cysteamine hydrochloride	Sigma
14	Disodium Hydrogen Phosphate	Qualigens
15	Dihydrogen Sodium phosphate	SD fine
16	Dimethyl Sulphoxide	Qualigens
17	EDTA	Sigma
18	EtBr	Sigma
19	ECL detection reagent	Millipore
20	Formaldehyde	Qualigenes
21	Femto	Pierce
22	Glycerol	Merck
23	Glycine	Sigma
24	H89	Millipore
25	Hydrochloric Acid	Qualigens
26	Leupeptin	Sigma
27	Magnesium Chloride	Qualigens
28	Methanol	Merck

29	MNase	USB
30	N-N Methylene Bis-Acrylamide	Sigma, Amresco
31	Nonidet P-40	Sigma
32	Potassium Acetate	SD fine
33	PMSF	Sigma
34	Potassium Chloride	Glaxo
35	Pepstatin A	Sigma
36	Protamine Sulfate	Sigma
37	Potassium Acetate	SD fine
38	PVDF membrane	Millipore
39	Paraformaldehyde	Sigma
40	Riboflavin 5 phosphate	Sigma
41	RNase A	Amresco
42	Sanguinarine	Sigma
43	Silver nitrate	Qualigens, SD fine
44	Sodium Chloride	Qualigens
45	Sodium Orthovandate	Sigma
46	Sodium Lauryl sarcosine	Sigma
47	Sodium Citrate	Merck
48	Sodium Deoxycholate	BDH
49	Sodium Bicarbonate	SD fine
50	Sodium Hydroxide	SD fine
51	Sulphuric Acid	Qualigens
52	Spermine	USB
53	Spermindine	USB
54	SDS	Sigma
55	Sucrose	Sigma
56	Tween-20	Sigma
57	Triton X-100	Sigma
58	Tris	Sigma
59	Trypsin	Sigma
60	TEMED	Sigma
61	Urea	Sigma

3.1. Cell Culture

The different cell lines were cultured in their respective media as shown below:

Table 3.1: List of cell lines

Cell line	Origin	Culture Medium
WRL68	Human embryonic liver immortalized	MEM
HepG2	Human hepatocarcinoma	RPMI 1640
MCF7	Breast adenocarcinoma	DMEM
U87	Glioblastoma multiforme	DMEM
A549	Lung carcinoma	DMEM
A2780	Ovarian carcinoma	DMEM
U2OS	Osteosarcoma	DMEM

The medium was supplemented with 10% FBS, 100U/ml penicillin, 100mg/ml streptomycin, 2mM L-glutamine and 1X non-essential amino acids. These cells were allowed to grow at 37°C in a humidified atmosphere containing 5% carbon dioxide.

3.2. Trypsinization and sub-culturing

Cell lines were passaged every 4-5 days to maintain their normal morphology and proliferation rate. Medium was removed from culture with a sterile pipette, adhered cells were washed with PBS, pH7.2-7.4 (1.9mM NaH_2PO_4, 8.1mM Na_2HPO_4 and 154mM NaCl) and 1ml trypsin/EDTA (0.25% w/v trypsin, 0.2% EDTA in PBS) solution was added. Cells were incubated at 37°C until cells detached from surface. Detached cells were resuspended in 1 ml complete medium. The viable cells were counted as described below and plated in fresh culture dishes ($\sim$2X 10^4 cells/ml). The number of viable cells was determined by staining with 0.5ml of trypan blue (0.4% w/v in PBS). Cells were counted on haemocytometer and number of cells/ml was calculated as follows:

No. of cells/ml = average number of cells per WBC chamber $\times$ dilution factor (10) $\times 10^4$

3.3. Synchronization of cells in different phases of cell cycle

In order to identify cell cycle specific DNA damage responsive histone marks, cells were enriched in different phases of cell cycle. Above mentioned cell lines were enriched at G0/G1 phase by serum starvation. WRL68 cells were synchronized in S and G2/M phases by double thymidine block followed by release of cells in complete media. For pro-metaphase synchronization, cells were incubated for 18h with complete medium containing 200ng/ml of nocodazole after double thymidine block. Progression of cells through the cell-cycle was monitored by flow cytometry. Detailed protocols of cell cycle synchronization and histone extraction from cell line are described below.

3.3.1. Synchronization of cells in G0/G1 phase

Cells were enriched at G0/G1 phase by serum starvation method. Exponentially growing cells were trypsinized and counted as described earlier and plated (2×10^5 cells per 100mm X 15mm culture dish) in respective media. At 30-40% confluent density, serum containing media was replaced by serum free media and cells were incubated for 72 hrs. After completion of incubation, serum starved G1-enriched cells were washed twice with incomplete media and released with 10% FBS containing media for 4hrs before irradiation. Cell pellet obtained was utilized for further downstream experiments.

3.3.2. Synchronization of cells in S, G2/M and pro-metaphase

Cells were synchronized in S and G2/M phases by double thymidine block method.[120] Cells were plated [2×10^5 cells per culture dish (100mmX15mm)] in complete medium and incubated to achieve ~30-40% confluent density. The medium was replaced with complete media containing 4mM thymidine and incubated for 15hrs under standard conditions. Cells were further washed thrice with PBS and incubated in complete medium under standard conditions for 12hrs. After incubation, medium was replaced with medium

containing 4mM thymidine and incubated for another 15hrs. The cells were again washed thrice with PBS and released for normal cell cycle progression for respective time periods: 4hrs for S-phase and 8-9 hrs for G2/M phase synchronization. For pro-metaphase synchronization, cells were incubated for 18hrs with complete medium containing 200ng/ml of nocodazole after double thymidine block. Cells were collected by trypsinization and the cell pellet was processed for further experiments.

3.4. Inhibitor treatment

Specific inhibitor against MKP-1 and MSK1 enzyme were used to study the role of these enzymes in regulation of H3Ser10 phosphorylation in response to DNA damage. Cells were incubated for 1hr with potent MKP-1 inhibitor, sanguinarine in DMSO (10 µM),[121] and MSK1 inhibitor, H89 in DMSO (20µM) before irradiation.[122] The incubation of cells with MKP-1 inhibitor was continued for 8hrs post-IR, whereas MSK1 inhibitor continued for 24hrs post-IR. The protein lysate and histone isolation were carried out at respective time points for immunoblotting.

3.5. Exposure of cells to DNA damaging agents

3.5.1. Radiation

Bhabhatron-2 (Panacea Medical Technologies Pvt. Ltd. and BARC, India) with Co-60 as a source of ionization radiation (gamma irradiation) and with a dose rate of 140.1 cGy/min within field size of 30×30 cm^2 and Dmax i.e. distance of the specimen from the radiation source of 80cm was used to irradiate the cell lines. Cells enriched in different phases of cell cycle were either exposed to 2.5Gy (clinically relevant dose) or 15Gy (lethal dose) of ionization radiation. Subsequently, cells were placed in a 37°C incubator to allow post-IR repair and recovery and later harvested at the subsequent time intervals.

UV light source was used as another mode of DNA damaging agent with treatment done at 10 J/m2 followed by repair-recovery for 1hr before cell harvesting.

3.5.2. Chemical agents

In order to induce direct and indirect DNA damage other than radiation, cells were treated with cisplatin (sigma, 2µg/ml, 4hr), etoposide (sigma,100µM, 4hr), H_2O_2 (SRL, 500µM, 30min), adriamycin (sigma, 10µg/ml, 4hr), phleomycin (sigma, 60µg/ml, 2hr), bleomycin (sigma, 5µg/ml, 2hr) and neocarzinostatin (sigma, 200ng/ml, 2hr). After, treatment cells were washed with PBS to remove drug and incubated for 1hr for recovery.

3.6. Cell viability assay

3.6.1. Trypan Blue Exclusion Assay

Cells were stained with 0.4% Trypan Blue solution after diluting at 1:1 ratio with the cell suspension. Trypan Blue was sterile filtered before using it in order to get rid of particles in the solution that may interfere with the counting process. Manual counting of viable (unstained cells) and non-viable cells (blue stained cells) were carried out in three independent experiments by haemocytometer and calculated as shown above (section 3.2).

3.6.2. MTT assay

Cell viability was quantified by its ability to reduce tetrazolium salt 3-(4,5-dimethylthiazole-2γ)-2,5-diphenyl tetrasodium bromide (MTT) to colored formazan products (Sigma# m-2128) as per manufacturer's protocol. MTT reagent (5mg/ml in PBS) was added to the cells at $1/10^{th}$ volume of the medium to stain only viable cells and incubated at 37°C for 4hrs. MTT solubilisation buffer (0.01M HCl, 10% SDS) of two fold volume was added to cells, followed by incubation in the dark at 37°C for 24hrs. The absorbance was measured at 570nm with Spectrostar Nano-Biotek, Lab Tech plate

Reader. Cell viability was expressed as the percentage of absorbance obtained in control cultures.

3.7. Cell Survival by Colony formation assay

Cells (n=300) were plated in 60mm tissue culture plates and its survival was measured by colonogenic assay in monolayer after 14 days in triplicate. The cells were incubated for 1hr before irradiation with sanguinarine (10μM) or H89 (20μM) and after PBS washes, cells were incubated in complete culture medium for additional 14 days, with media changes after every 2-3 days. Cells were fixed with 4% paraformaldehyde for 1hr, stained with 0.5% crystal violet (Sigma, 0.5% in 70% ethanol) for 1hr at room temperature, rinsed and air-dried. Surviving colonies with more than 50 cells were counted and images were captured using a high-resolution Nikon D70 camera (Nikon, Tokyo, Japan). The survival data of treated cells were normalized to the plating efficiency of control.

3.8. Cell cycle analysis by FACS

Cells were washed with PBS (twice) and fixed with 70% chilled ethanol. During fixation, ethanol was added drop-wise with vortexing to prepare a single cell suspension. After fixation, cells were stored at -20°C. Cells were further washed twice with PBS and suspended in 500μl of PBS with 0.1% Triton X-100 and 100μg/ml of RNaseA followed by incubation at 37°C for 30mins. After incubation, propidium iodide (sigma, 25μg/ml in PBS) was added followed with incubation at 37°C for 10mins. DNA content analysis was carried out in a FACS Calibur flow cytometer (BD Biosciences, USA). Cell cycle analysis was performed using the Mod-fit software from BD Biosciences.

3.9. DNA damage analysis by comet assay

Comet assay essentially measures the degree of fragmentation of DNA within the cell. The comet assay was performed as described previously.[123] Briefly, 10^3 cells were mixed

with 85µl of pre-incubated low melting agarose at 37°C (0.7% in PBS). The cell-agarose mixture was placed on 1% normal agarose-coated glass slides and covered with a cover slip. The cell-agarose mixture was allowed to solidify for 10min at 4°C. After solidification, cover slip was removed and incubated for 60 min in a chilled lysis buffer (10mM Tris, pH10, 2.5M NaCl, 100mM EDTA pH8.0, 1% Sodium sarcosinate, 1% Triton X-100, 10% DMSO). Subsequently, the lysis buffer was drained and slides were placed on a horizontal gel electrophoresis unit. The chamber was filled with chilled electrophoresis buffer for alkaline comet assay (1mM Na_2EDTA, 300mM NaOH, pH 12.8) and the samples were incubated for 20mins to allow unwinding of the DNA. Electrophoresis was performed at 25V, 300 mA at 4°C for 20mins. After electrophoresis, slides were washed in a neutralization buffer (400mM Tris-Cl pH 7.5) to remove alkali and detergent, and further stained with propidium iodide (sigma, 50µg/ml). DNA of individual cells was viewed under Ziess-Upright fluorescence microscope connected to a CCD camera. The quantitative analysis of DNA breaks were measured using the tail moment with CASP software

3.10. Localization of histone modifications by Immuno-fluorescence microscopy

γH2AX foci formation and its co-localization with other histone marks, H3Ser10P, H3Lys9Ac, H3Lys14Ac, H3Lys56Ac after DNA damage, was done by immuno-fluorescence staining against above mentioned modifications. The adherent cells grown on cover slips were washed twice with PBS, fixed with 4% paraformaldehyde for 20mins, and washed three times with PBS to remove paraformaldehyde before permeabilization. Cells were permeabilized in 0.5% Triton X-100 for 20mins and blocked with 5% BSA containing 0.1% NP-40 in PBS (PBS-N) for 1hr. Cells were incubated with primary antibodies for 90mins in 5% BSA in PBS-N. Further, cells were washed four times with PBS and PBS-N before incubating with Alexa-conjugated secondary antibodies in 5%

BSA in PBS-N for 1hr in dark. Cells were washed again as mentioned above, counter stained with DAPI (0.5µg/ml in PBS) for 20min at room temperature before mounting with Vecta-shield mounting medium (Vector laboratories). Finally, cells were imaged with Ziess510 META Confocal Scanning microscope (Zeiss, Jena, Germany) with 63X magnification of objective lens and numerical aperture of 1.4. Routinely, 0.72µm thick focal planes were processed using the Ziess software (LSM 510 Meta) for final image processing.

Table 3.2: Antibodies used for Immunofluorescence Staining

S. No.	Antibody	Species and supplier	Dilution
1.	γH2AX(primary)	Mouse (Millipore)	1:300
2.	H3S10P (primary)	Rabbit (Abcam)	1:200
3.	H3K9Ac (primary)	Rabbit (Abcam)	1:200
4.	H3K14Ac (primary)	Rabbit (Abcam)	1:200
5.	H3K56Ac (primary)	Rabbit (Abcam)	1:200
6.	Alexa-488 (secondary)	Mouse (Invitrogen)	1:300
7.	Alexa-568 (secondary)	Rabbit (Invitrogen)	1:300

3.11. Extraction of histones from cell lines

Histones were extracted from cell lines at respective recovery time points in order to identify alteration of histone modifications in response to DNA damage.[124] Cells were washed twice with PBS, centrifuged, and the cell pellet was suspended in ice-cold lysis buffer (250mM Sucrose, 50mM Tris-Cl pH7.5, 25mM KCl, 5mM $MgCl_2$, 50mM $NaHSO_3$, 45mM Sodium butyrate, 10mM β-mercaptoethanol, 0.2% Triton X-100, 0.2mM PMSF, 0.15mM Spermine, 0.5mM Spermidine, 2mM EDTA, 10mM Sodium fluoride, 1mM Sodium orthovanadate, 10mM β-glycerophosphate) with freshly added protease and phosphatase inhibitors and incubated for 10mins at 4°C with intermittent shaking. After incubation, cells were centrifuged at 5000 rpm for 15 min at 4°C. The nuclear pellet was

washed twice with lysis buffer to obtain pure nuclear pellet. The purified nuclei were subjected for histone isolation by acid extraction method. 0.2M H_2SO_4 was added drop-wise to nuclear pellet with vigorous vortexing and incubated for 30mins at 4°C. After centrifugation at 16,200 rpm at 4°C, supernatant containing histone protein was precipitated overnight with chilled acetone at -20°C. Histone pellet was washed with chilled acidified acetone (50mM HCl in acetone) followed by washing with chilled acetone. Total histone was dissolved in 0.1% β-mercaptoethanol in H_2O and stored at -20°C.

3.12. Fractionation of total soluble protein and chromatin bound histones

In order to understand role of MAP kinase pathway in regulation of H3Ser10P, total soluble protein and chromatin bound histones were isolated from same population of G1-enriched cells, treated with or without specific inhibitor before IR. Cells were washed with PBS and harvested by trypsinization. The harvested cells were washed twice with chilled PBS, lysed in MKK lysis buffer (10mM Tris-Cl, pH 7.4, 0.27M Sucrose, 1mM EDTA, 1mM EGTA, 1% Triton X-100) containing protease and phosphatase inhibitors (1mM Sodium orthovanadate, 10mM Sodium fluoride, 10mM β-glycerophosphate, 10µg/ml Leupeptin, 10 µg/ml Aprotinin and 1mM PMSF) for 30mins at 4°C. Following hypotonic lysis, cells were centrifuged at 12,500rpm for 20mins at 4°C to separate chromatin fraction and total soluble protein fraction. The pelleted chromatin fraction was processed for histone isolation as discussed above. The total soluble protein fraction was resolved on 10% SDS-PAGE which was further transferred on PVDF membrane after estimation of protein by Lowry's method. The transferred proteins were probed with specific antibodies against downstream kinases of MAP kinase pathway. Histones extracted from chromatin fraction were resolved on 18% SDS-PAGE gels and probed with specific histone antibodies.

3.13. Protein Estimation by Lowry's Method

Histone and total protein concentrations in various samples were determined by Lowry method of protein estimation.[125] Protein standards were prepared containing a range of 2-16µg of Bovine Serum Albumin (BSA, Sigma) and unknown samples were also prepared similarly. The freshly prepared Copper Tartrate Carbonate (CTC- 0.1% $CuSO_4$, 0.2% Sodium potassium tartrate, 10% Na_2CO_3; CTC mixture: CTC, 0.8N NaOH, 10% SDS and D/W in 1:1:1:1 ratio,) mixture was added and vortexed. After incubation for 10mins at RT, 500µl of Folin Ciocalteau reagent (1:6 dilutions with D/W, 0.33N) was added, tubes were vortexed and incubated in dark for 30 min at RT. Absorbance was measured at 750 nm and standard curve was prepared to determine protein concentration.

3.14. Resolution of total soluble protein and histones by PAGE

Polyacrylamide gels are formed by the cross linking monomeric acrylamide with N,N'-methylene bisacrylamide. Cross-linking imparts rigidity and tensile strength and form pores through which the proteins to be separated must pass. The size of these pores decreases as the bisacrylamide: acrylamide ratio increases.

3.14.1. SDS-PAGE of total soluble protein and histones

Histones and total soluble protein lysate were separated on 18% and 10% SDS-PAGE respectively. Increased concentrations of buffers used in this modification provide better separation between the stacked histones and SDS micelles. In brief, glass plate sandwich was assembled using 0.1cm thick spacers. Separating gel solution (17.5% w/v acrylamide, 0.5% bisacrylamide, 0.75M Tris pH8.8, 0.1% w/v SDS, 0.033% w/v APS, 0.66% v/v TEMED) was prepared and poured into the glass plate sandwich and allowed to polymerize. Stacking gel solution (3.8% w/v acrylamide, 0.1% w/v bisacrylamide, 0.125M Tris-Cl pH 6.8, 0.1% w/v SDS, 0.05% w/v APS, 0.1% v/v TEMED) was then

prepared and poured into the glass plate sandwich in similar manner. A 0.1cm thick Teflon comb was inserted and gel was allowed to polymerize. Histone samples to be analyzed were diluted 1:1 (v/v) with 2X SDS sample buffer (0.05M Tris-Cl pH6.8, 20% v/v glycerol, 4% w/v SDS, 2% v/v BME, 0.01% w/v bromophenol blue, BPB) and incubated for 5min in boiling water. Teflon comb was removed, sandwich was attached to the electrophoresis chamber and filled with 2X SDS electrophoresis buffer (0.05M Tris, 0.384M glycine, 0.2% w/v SDS, pH8.3-8.6). Samples were loaded into the wells formed by comb. The gel was run at 20mA of constant current until the BPB tracking dye entered the separating gel and then at 30mA until the BPB dye reached the bottom of the gel. The power supply was then disconnected and gel was subjected to Coomassie staining or western blot analysis.

3.14.2. Coomassie staining

After electrophoresis, gel was transferred to tray containing Coomassie Brilliant Blue R-250 (CBBR) staining solution (0.1% w/v CBBR, 50% methanol and 10% acetic acid in water). The gel was stained for ~3 hrs, transferred to destaining solution (50% methanol and 10% acetic acid in water) with several changes until visulization of protein bands. The gel was either stored or used for second dimensional AUT-PAGE.

3.14.3. Ammoniacal Silver nitrate staining

After electrophoresis of histone protein, the gel was treated with three washes of 50% methanol of 1hr followed by overnight incubation at 4°C. The gel was incubated with ammoniacal silver (2.8ml liquid ammonia in 0.38% sodium hydroxide solution (42 ml) followed by drop-wise addition of 8ml 20% silver nitrate to 200ml with D/W) staining solution for 30 minutes, followed by two washes of 5mins with D/W. The washed gel was incubated with developer (15mg citric acid, 0.15 ml formaldehyde in 100 ml D/W) for the

development of protein bands and the reaction was stopped with destaining solution (50% methanol, 10% acetic acid in D/W).[126]

3.14.4. Two dimensional SDS-AUT gel electrophoresis of core histones

In 2D-SDS-AUT PAGE, the first gel system consisted of 18% SDS-PAGE (as mentioned above) gel for the 1D-electrophoresis followed by 2D on 15% AUT-PAGE. Both systems together offer distinct advantages for rapid, high resolution analysis of core histone variants and their post-translationaly modified isoforms.

Second dimensional AUT-PAGE gel was prepared as described.[127] Glass-plate sandwich was assembled using 0.15cm thick spacers to compensate for swelling of first dimension during gel processing. Separating gel solution (15% w/v acrylamide, 0.1% w/v bis-acrylamide, 1% v/v acetic acid, 0.05M ammonium hydroxide, 8M urea, 0.56% w/v Triton X-100, 0.5% TEMED, 0.0004% w/v flavin mononucleotide) was prepared and poured into glass plate sandwich and was allowed to polymerize in presence of bright light. Stacking gel solution (4% w/v acrylamide, 0.16% w/v bis-acrylamide, 1% v/v acetic acid, 0.05M ammonium hydroxide, 0.5% v/v TEMED and 0.0004% w/v flavin mononucleotide) was poured and polymerized into the glass plate sandwich. The gel was pre-electrophoresed for 2hrs at constant voltage of 200V with electrophoresis buffer (1M acetic acid and 0.1M glycine). The gel was removed from the electrophoresis chamber and was used to set-up the second dimension. Core histone region of the track of interest was cut out from the pre-stained first dimensional SDS-PAGE gel was equilibrated for 60mins in equilibration buffer (1% w/v protamine sulfate, 5% v/v BME, 0.75M potassium acetate pH 4.8, 20% v/v glycerol, 1% cysteamine-HCl and 6M urea). The slice was applied horizontally to the top of second dimensional AUT-PAGE and was sealed using melted sealing buffer (1% w/v agarose, 0.75M potassium acetate pH4, 20% v/v glycerol and 0.001% pyronin Y). The gel was electrophoresed at constant voltage of

100V with electrophoresis buffer (1M acetic acid and 0.1M glycine) till the dye migrated to the bottom of gel. The gel was stained by 'SDS-silver' staining method.

3.14.5. 'SDS-silver' staining of AUT-PAGE

Silver staining of AUT-PAGE gel were carried out as described previously.[128] AUT gel was treated with SDS-buffer system as follows. AUT gel was washed twice in ten volumes of buffer A (0.05M acetic acid, 0.5% w/v SDS) for 30mins each and once with modified buffer of O'Farrell (0.0625M Tris-Cl pH 6.8, 2.3% w/v SDS, 1% BME).[129] The gel was processed for ammoniacal silver staining as per protocol discussed above (section 3.14.3).

3.14.6. Two-dimensional AUT-SDS gel electrophoresis of total histones

In 2D-AUT-SDS-PAGE, the first dimensional gel system was 15% AUT-PAGE followed by 18% SDS-PAGE gel for the second dimensional electrophoresis. The dual gel system together offer distinct advantages for high resolution analysis of histone variants mainly H1 variants and their post-translationally modified isoforms.

The first dimensional AUT-PAGE (15%) gel was prepared as described previously.[127] 20µg of acid extracted histones were incubated with 50µl sample buffer for 5mins at RT followed by addition of 2.5µl of glacial acetic acid and 25µl of methylene blue as a loading dye. The histones were resolved mentioned above. The gel was removed and stained by coomassie staining method. The resolved histone and their variants containing gel lane was cut out from the AUT-PAGE gel and equilibrated for 60min in equilibration buffer O'Farrell (10% glycerol, 5% BME, 2.3% SDS, 62.5mM Tris-Cl pH 6.8). The gel slice was applied horizontally to the top of second dimensional 18% SDS-PAGE and was sealed using melted 1% agarose in equilibration buffer O'Farrell. The gel was run at 20mA of constant current until the BPB tracking dye entered the separating gel and then

at 30mA until the BPB dye reached the bottom of the gel. The gel was processed for ammonical silver staining as per protocol discussed above.

3.15. Western hybridization

Western hybridization was introduced by Towbin et al.[130] The underlying principle is the specificity of antibody-antigen interaction that enables identification of a single protein in the midst of a complex mixture.

3.15.1. Electrophoretic transfer of histones from SDS-PAGE

Alternatively, modified histones and proteins separated by SDS-PAGE were identified by blotting onto an adsorbent porous Polyvinylidene difluoride (PVDF) membrane, which gives a mirror image of the gel. Proteins were transferred at 4°C, employing a constant current of 300mA for 200min. A cassette clamping the gel and membrane tightly together in between the two scotch-brite pads was put in the transfer apparatus containing transfer buffer (0.19 M Glycine, 25 mM Tris base, 0.01% SDS and 20% methanol). A current is applied from electrodes situated at either side of the cassette. The buffer is often chilled to avoid heating effects.

3.15.2. Electrophoretic transfer of histones from AUT-PAGE

In order to observe pattern of reduction of Ser10 phosphorylation within the H3 variants after ionization irradiation of G1 and pro-M enriched cells, total histones were resolved on AUT-PAGE on the basis of their mass, charge and hydrophobicity. To achieve complete transfer of basic proteins from AUT gels to PVDF membrane, gels were submerged in equilibration buffer 1 (0.05M acetic acid, 0.5% w/v SDS; 2×30 minutes) to displace the Triton X-100, followed by a 30mins incubation in a Tris-SDS buffer, equilibration buffer 2 (0.0625M Tris-Cl pH 6.8, 2.3% w/v SDS, 1% BME; 2×15 minutes).The transfer of histones from equilibrated AUT gel to PVDF membrane were

carried out by using alkaline transfer buffer (25 mM CAPS, pH 10, 20% v/v methanol).[131] The alkaline transfer buffers increase the efficiency of transfer of strongly basic proteins. Before transfer the PVDF membrane is hydrated in 100% methanol for 30sec, and then washed in water for 30sec. The AUT gel and PVDF membrane were pre-equilibrated in alkaline transfer buffer for 10mins. Finally, the resolved proteins were transferred to PVDF membrane at constant electric current (300mA) overnight at 4°C. After transfer of histone proteins on PVDF membrane, it was processed for immunoblotting.

Following electroblotting, to check for the transferred proteins the PVDF membrane was stained with Fast green (0.03% in destaining solution). The efficiency of transfer was also checked by staining the transferred-gel with Coomassie blue to detect any residual protein in the gel. Subsequently the membrane was washed with TTBS (20 mM Tris-Cl, 500mM NaCl, 0.1% (v/v) Tween 20, pH 7.4) for ~ 5 min to remove the color of Fast green.

After blocking with 5% non-fat skimmed milk or 5% BSA in TTBS (depending upon the protein), membranes were probed with appropriate primary antibody diluted in 5% or 1% BSA at 4°C overnight. Next day, blots were washed with TTBS (5min X 2 and 10 min X 2) and incubated with 1:8000 dilutions of anti-rabbit or 1:5000 dilution of anti-mouse horse radish peroxidase conjugated-secondary antibodies at RT for 1hr. Membranes were then washed with TTBS (5mins X 2 and 10mins X 2). Immunoreactive bands were then visualized with enhanced chemiluminescence reagent (Millipore) or femto west (Pierce) as per the manufacturer's instructions followed by autoradiography. Further, for loading controls the blots were washed with TTBS (10 min x 2), followed by incubating with 2-3 ml of restore western blot restriping buffer (Thermo Scientific) at 37°C for 10-15 min. The blots were then again rigorously washed with TTBS (10 min X 5), until smells of BME is eliminated from the washing buffer. Blots were then re-probed with appropriate

primary antibody for loading control, β-actin for total cell lysate, histone H3 and H4 for

modified histones and processed as described above.

Table 3.3: List of Antibodies used for Immunoblotting (IB)

S.No.	Antibody	Protein conc. (µg)	Working dilution
1.	γH2AX(primary)	2	1:4000
2.	H3S10P(primary)	2	1:7000
3.	H3K9Ac(primary)	2	1:3000
4.	H3K14Ac (primary)	2	1:3000
5.	H3K56Ac (primary)	2	1:3000
6.	H3 (primary)	2	1:3000
7.	H4 (primary)	2	1:3000
8.	p-ERK 1,2	75	1:2000
9.	p-JNK	75	1:2000
10.	p-p38	75	1:2000
11.	ERK 1,2	50	1:2000
12.	JNK	50	1:2000
13.	p38	50	1:2000
14.	p-MSK1	75	1:2000
15.	MSK1	50	1:2000
16.	β-actin	25	1:5000
17.	Lamin A	50	1:3000

3.16. MNase digestion assay

The organization of chromatin in response to DNA damage was studied by MNase

digestion assay as described previously with slight modification.[132] Purified nuclei (as

described above) from irradiated and non-irradiated G1-enriched WRL68 cells followed

by post-IR incubation for different time periods were subjected to MNase digestion for

analysis of nucleosomal organization. Nuclei containing 2mM $CaCl_2$ were incubated for

0, 2.5, and 5mins with 5U MNase/mg of DNA at 37°C in MNase digestion buffer (15

mM Tris-Cl pH 7.4, 15mM NaCl, 2mM $CaCl_2$, 60mM KCl, 15mM β-ME, 0.5mM

spermidine, 0.15mM spermine, 0.2mM PMSF, protease and phosphatase inhibitors). The digestion was stopped by adding 2X lysis buffer (0.6M NaCl, 20mM EDTA, 20mM Tris-Cl pH 7.5, 1% SDS). MNase digested samples were treated with RNaseA (100µg/ml) for 30 min at 37°C followed by proteinase K (80µg/ml) treatment for 2hrs at 50°C. The samples were extracted with phenol, phenol: chloroform and chloroform followed by ethanol precipitation at -20°C. The precipitated DNA was recovered by centrifugation at 12,500 rpm for 20 min. The DNA pellet was washed, air dried, dissolved in 50µl of TE buffer and concentration was determined by A_{260}/A_{280} absorbance. MNase-digested samples were resolved on 1.8% 1XTAE agarose gel electrophoresis with 0.5ug/ml ethidium bromide. The image was scanned with ImageJ software version 1.43u; Java 1.6.0_10 (32-bit).

3.17. Mono-nucleosomes preparation and Co-immunoprecipitation

3.17.1. Preparation of nuclei

Cells were washed twice with PBS, and the cell pellet was suspended in hypotonic lysis buffer (250mM sucrose, 50mM Tris-Cl, pH 7.5, 25mM KCl, 5mM MgCl2, 0.2mM PMSF, 50mM NaHSO$_3$, 45mM sodium butyrate,10mM β-ME, 0.2% TritonX-100) 10 mins at 4°C and centrifuged at 5000 rpm for 15 min at 4°C. The nuclei pellet was washed twice with lysis buffer.

3.17.2. Purification of mononucleosomes

Purified nuclei from irradiated and non-irradiated G1 enriched WRL68 cells followed by 4hrs post-IR incubation were suspended in MNase digestion buffer containing 2mM CaCl$_2$ and 100U MNase/mg of DNA as described above (section 3.16). The reaction was carried out for 45 minutes at 37°C and digestion was stopped by adding 2X lysis buffer (140 mM NaCl, 20mM EDTA, 20mM Tris-Cl pH 7.5, 1% Triton X-100, 10 µg/ml

Leupeptin, 10 µg/m aprotinin and 1 mM PMSF). MNase-digested samples were layered on 10ml linear glycerol-gradient (10% glycerol gradient buffer at the top and 40% at the bottom) and centrifuged for 16hrs at 27,500 rpm at 4°C in a Beckman SW28 rotor. The mono-nucleosomal ring was carefully collected by capillary under a constant pressure maintained by peristaltic pump and quality of mono-nucleosomes was confirmed on 1.8% TAE-agarose gel. The dialysis was carried out in a 10 KDa cut-off dialysis bag and dialyzed against 100 volume of dialysis buffer (20mM Tris pH 7.5, 1mM EDTA and 0.5mM PMSF) at 4°C for 4hr to concentrate and remove salts from the mono-nucleosomes.

3.17.3. Mononucleosomal Immunoprecipitation Assay

3.17.3.1. Preparing 50% slurry of protein-G sepharose beads

0.5 g protein-G beads were suspended in 50ml immunoprecipitation (IP) buffer (20mM Tris pH 7.5, 1mM EDTA, 140mM NaCl, and 1% Triton X-100) overnight at 4°C. The broken beads were removed by low speed centrifugation and the pelleted beads were washed twice with IP buffer for 2hrs at 4°C. Finally, the beads were resuspended in IP buffer so as to make 50% slurry (i.e. depending on how much the beads have swollen, equal amount of IP buffer was added).

3.17.3.2. Pre-clearing of lysate

Purified mononucleosomes were incubated with 20µl of protein-G beads and IP buffer in a final volume of 0.5ml for 2 h at 4°C with gentle rocking. Cleared lysate was collected as supernatant after a centrifugation at 2000 rpm for 5mins at 4°C.

3.17.3.3. Immunoprecipitation

All steps are carried out at 4°C unless otherwise indicated. The pre-treated protein-G beads (blocked by 5% BSA) were incubated for 4hr at 4°C either with 3µg anti-γH2AX/

anti-H3Ser10P/anti-MKP-1 antibody. Pre-cleared mononucleosomes (25µg) from non-irradiated and irradiated cells were incubated overnight at 4^0C with bead bound antibodies with a final volume of 800µl. Bound and unbound immunoprecipitated complexes were separated by centrifugation at 1500rpm at 4°C. The bound fraction was washed thrice with wash buffer to remove unbound non-specific mononucleosomes. The separated, bound and unbound immunoprecipitated fractions were analyzed by immunoblotting with either γH2AX or H3Ser10P antibodies as discussed above.

3.18. Chromatin fractionation

Chromatin fractionation of cells was carried out as described by Stillman *et al* with few modifications.[133] Approximately 3 million cells were washed in PBS and resuspended in 200µl buffer A (10mM HEPES, pH7.9, 10mM KCl, 1.5mM $MgCl_2$, 0.34M sucrose, 10% glycerol, 1mM DTT, 0.1µg/ml aprotinin, 0.1µg/ml leupeptin, 1mM PMSF). Triton X-100 was added to a final concentration of 0.05% followed by incubation on ice for 10mins. Nuclei were collected by centrifugation at 5000rpm for 10mins. The supernatant was cleared by centrifugation for 20min at 20,000rpm and designated as cytosolic fraction. Nuclei were washed in bufferA twice, and then lysed in buffer B (3mM EDTA, 0.2mM EGTA, 1mM DTT) for 30mins on ice followed by mild sonication at 10 amplitude for 5secs. The insoluble chromatin fraction was collected by centrifugation for 4mins at 2000 rpm. The supernatant was cleared by centrifugation at 20,000rpm for 20mins and designated as nucleosolic fraction. Finally, the chromatin fraction was washed in buffer B twice and the chromatin associated proteins solubilized in SDS-sample buffer (1X) and resolved on 10% gel followed by immunoblotting against indicated antibodies.

3.19. *Insilco* **prediction of MSK1 and MKP-1 interaction with native H3 peptide and its posttranslational modifications (PTM)**

3.19.1. Homology modeling of MKP-1and MSK1 structures

The homology modeling of MKP-1 was carried out due to the unavailability of its crystallographic coordinates. The model of active the C-terminus phosphatase domain of MKP-1 (172–314 aa) was constructed using PDB ID: 3EZZ as a template. The N-terminal crystal structure of MSK1 was available, but to model the phosphorylated Ser376 residue of the flexible loop near the active site, PDB ID: 3A8X was used as a template for homology modeling of MSK1 with amino acid residues from 42–380. Modeling studies were performed using Swiss Model.[134] The modeled structure of MKP-1 and MSK1 were cross-validated using multiple tools such as Procheck,[135] Verify_3D,[136] and Errat[137] using SAVES server (http://nihserver.mbi.ucla.edu/SAVES/).

3.19.2. Refinement of crystal structure of 14-3-3ζ with native H3 peptide and its posttranslational modifications (PTM)

In the crystal structure of histone H3 (PDB ID: 2C1J),[138] acetylation at Lys9 and Lys14 and phosphorylation at Ser10 was generated using Discovery Studio Visualizer version 3.5. A total of seven structures of histone H3 were modeled which encompassed combinations of modifications (Lys9, Ser10, Lys14, Lys9-Ser10, Lys9-Lys14, Ser10-Lys14, and Lys9-Ser10-Lys14). The Haddock server[139] was used to score the refinement of PDB ID: 2C1J as native and the modified 14-3-3ζ and histone H3 complex.

3.19.3. Molecular association of MSK1 with histone H3 and its PTM modified structure

The full-length (1–21 aa) loop structure of histone H3 was used to build the three PTM-modified structure (Lys9, Lys14, Lys9-Lys14). The modeled structure of MSK1 was

docked with native and the three PTM-modified structure of histone H3 using the Haddock server.[139] The active site residues (Lys85, Ile88, Val89, Thr95, Arg102, Gln122, and Leu127) of MSK1 and (Lys9, Ser10, and Lys14) of histone H3 were provided as input parameters for targeted docking to analyze protein-protein interactions, Haddock score, hydrogen bonds, and hydrophobic interactions. The molecular interactions of the docked complexes were analyzed using Ligplot[140] for hydrophobic interactions. Discovery studio visualizer 3.5 was used to identify residues involved in hydrogen bonding between the two proteins and for the diagrammatic illustration of the residues involved in the hydrogen bond formation in the docked complex.

3.19.4. Molecular association of native MKP-1 with histone H3 and its PTM modified structure

The full length (1–21 aa) loop structure of histone H3 from the crystal structure of the Xenopus nucleosome (PDB ID: 1KX5) was used.[97] Histone H3 is 100% conserved between Xenopus and humans. The combination of Lys9, Ser10, and Lys14 modifications was generated by site-specific acetylation and phosphorylation resulting in seven PTM structures of histone H3 (Lys9, Ser10, Lys14, Lys9-Ser10, Lys9-Lys14, Ser10-Lys14, and Lys9-Ser10-Lys14). The modeled structure of MKP-1 was docked with native and seven PTM structures of histone H3 using the Haddock server.[139] The active site residues (His257, Cys258, Gln259, Ala260, Gly261, Ile262, Ser263, and Arg264) of MKP-1 and (Lys9, Ser10, and Lys14) of histone H3 were used as input parameters for docking. The results were analyzed for protein-protein interactions and emphasis was given for weak intermolecular interactions such as hydrogen bonding and hydrophobic interactions.

Chapter 4

Results

4.1. Histone Profiling of WRL68 and HepG2 Cell lines

The global alterations in the epigenetic landscape are a common feature of cancer. To investigate the global differences in histone profile between transformed (HepG2) and untransformed immortalized embryonic liver (WRL68) cell lines, purified histone were resolved on three different gel systems: SDS-PAGE, 2D SDS-AUT and 2D AUT-SDS-PAGE. Total histones resolved on 18% SDS-PAGE followed by silver staining shows H1 variants, H2A, H2B, H3 and H4. Histones H1 shows differential expression of variants in these two cell lines (Fig 4.1A). The differential high mobility band is observed in HepG2 in comparison to WRL68 cells. Differentially expressing H1 variant is identified as H1.0 variant whereas the first two bands of H1-linker histones are H1.2 and H1.4.
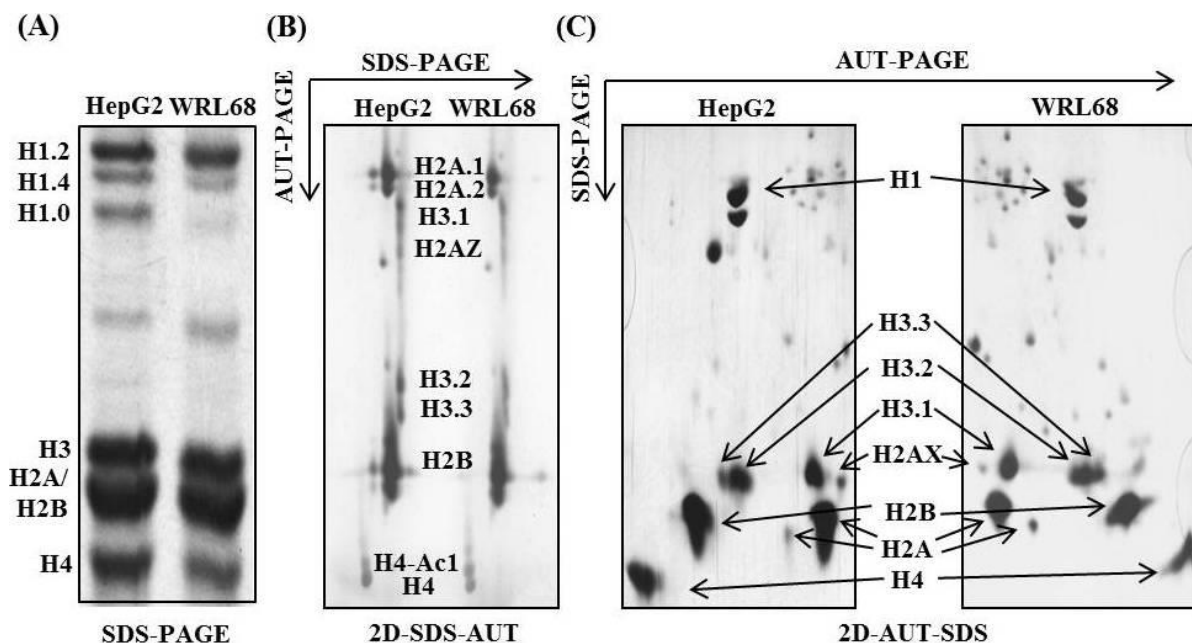
Figure 4.1: Profile of acid extracted histones from WRL68 (untransformed) and HepG2 (transformed) cells. (A) *Total histones resolved on 18% SDS-PAGE followed by ammoniacal silver staining. Total linker histone marked as H1.2, H1.4 and H1.0 region.* **(B)** *SDS-silver staining of core histones resolved on 2D SDS-AUT gel. 20μg of histone from above mentioned cell lines was resolved on 18% SDS-PAGE gel followed by staining and detaining of gel. The resolved core histone region was excised and electrophoresed on second dimensional AUT gel* **(C)** *Total histones resolved on 2D AUT-SDS gel followed by ammoniacal silver staining. 20 μg of histone from above mentioned cell lines was resolved on 15% AUT-PAGE gel. After staining and destaining of gel, the lane was excised and electrophoresed on second dimension 18% SDS-PAGE gel.*

The resolution of core histones on 2D-SDS-AUT-PAGE has not shown any significant difference in the profile of histone variants (Fig 4.1B). This finding is further confirmed by 2D-AUT-SDS-PAGE (Fig 4.1C). Both systems together offer distinct advantages for rapid, high resolution analysis of core histone variants and their post-translationally modified isoforms.

4.2. Cell sensitivity assay at clinically relevant and lethal dose of IR

The two doses of ionizing radiation (IR), clinically relevant dose (2.5Gy) and lethal dose (15Gy) were used to understand the significance of cell cycle phase specific alterations in histone marks in response to DNA damage. HepG2 and WRL68 show more than 50% cell survival on exposure to ionization radiation (Cobalt-60 source) of 2.5Gy and total cell death at 15Gy by MTT assay (Fig 4.2A and B). The cell sensitivity at clinically relevant dose shows that HepG2 cell line is more radiosensitive compared to WRL68. In conclusion, a direct correlation exists between dose of radiation and cell survival.
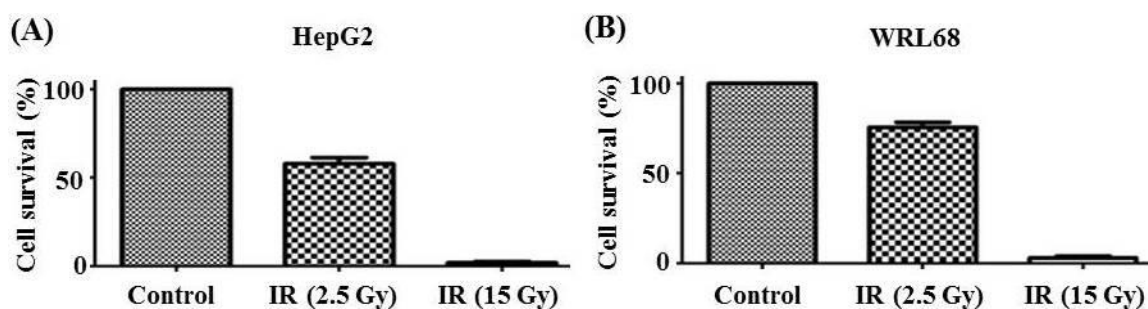
Figure 4.2: MTT assay for cell survival against irradiation dose. (A) *HepG2 cells (n-200) and* **(B)** *WRL68 cells (n-200) were irradiated at indicated IR dose and incubated for 7 days. After 7 days cell viability were detected by the MTT assay and % of cell survival was calculated and plotted against respective IR dose.*

4.3. Time dependent analysis of γH2AX and cell cycle profile following irradiation of G1-enriched cells

One of the well characterized modification on histones after DNA double strand breaks (DSBs) is phosphorylation of the C-terminal tail of histones H2AX (called γH2AX) on the chromatin surrounding the DNA lesion.[43] Time dependent post-IR analysis of γH2AX foci formation and cell cycle analysis were studied following exposure to clinically relevant i.e. 2.5Gy and lethal dose ionization radiation (IR) i.e. 15Gy on G1 enriched transformed liver cells (HepG2) and normal immortalized embryonic liver cells (WRL68). The cells were chased after IR-induced DNA damage with 0, 15min, 30min, 1, 2, 4, 6, 8, 16, 20 and 24hrs to understand 'prime-repair-restore' phases of DNA damage response. γH2AX immunofluorescence studies were carried out at each time point to substantiate DNA damage induced and recovery in response to IR. Immunofluorescence studies suggest that after 2.5Gy irradiation, γH2AX foci formation initiate at 0mins, gradually increases up to 2hrs, stabilized till 4hrs, with gradual decrease after 4hrs in a time-dependent manner and complete recovery of γH2AX foci in 24hrs in both WRL68 and HepG2 cell lines (Fig 4.3A and B). The HepG2 cells show rapid 'priming' i.e. more γH2AX foci formation compared to WRL68 cells as seen at 0min after DNA damage. A dose-dependent increase in γH2AX foci formation is observed at 15Gy dose compared to 2.5Gy dose in prime-repair-recovery phase of DDR in both the cell lines (Fig 4.4A and B). The disappearance of γH2AX foci is delayed (till 8hrs) in WRL68 cells at lethal dose (15Gy) radiation in comparison to clinically relevant dose (2.5Gy) radiation. The delay and intensity of γH2AX foci at lethal dose is more prominent in WRL68 cells as compared to HepG2 cells. Collectively, the γH2AX foci formation suggests that the initiation of DNA damage response, 'prime phase' starts immediately after DNA damage, 'repair phase' ranges from 0min to 8hrs with an overlapping 'recovery phase' starting
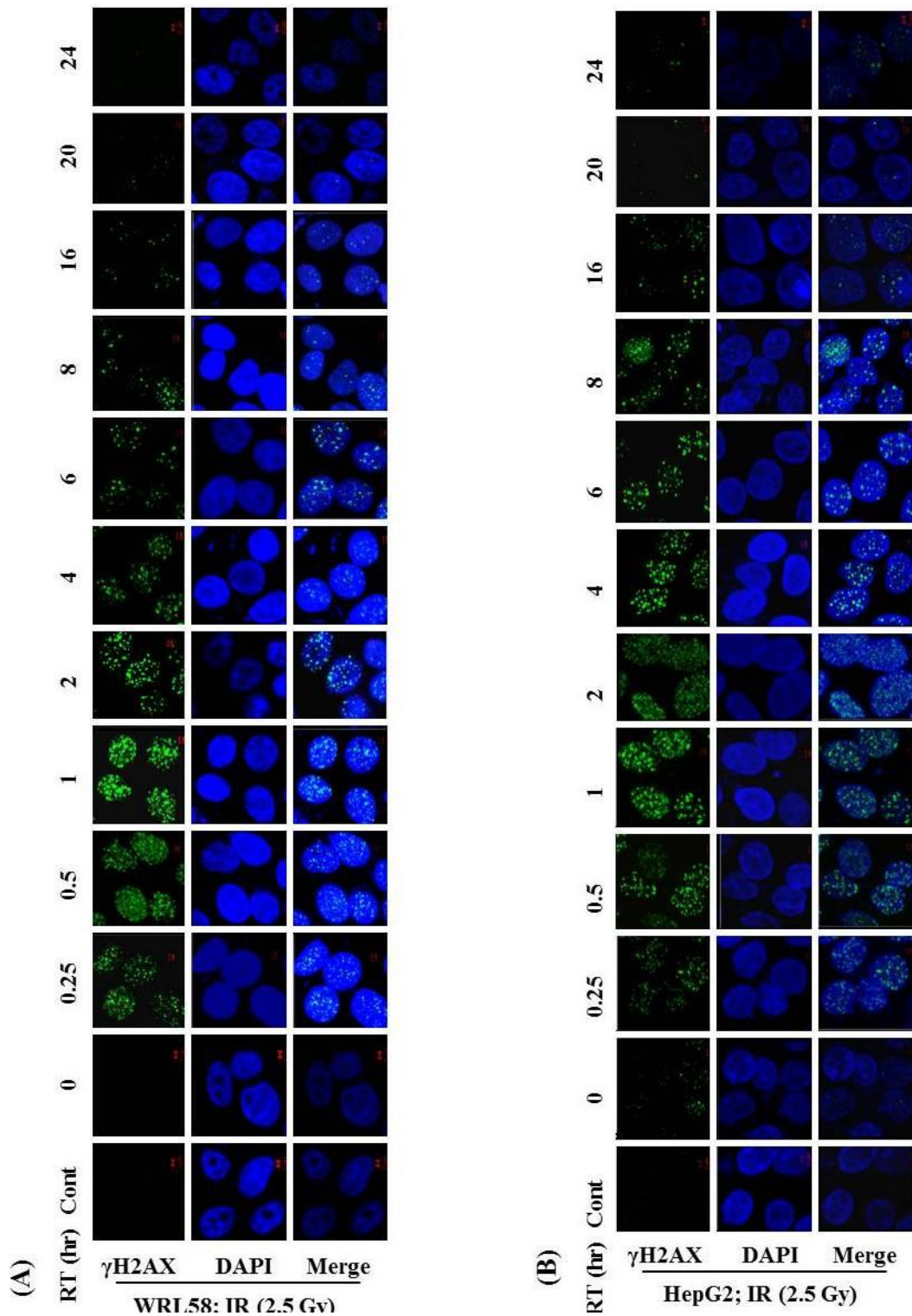
Figure 4.3: Immunofluorescence analysis of time dependent γH2AX foci formation irradiated at 2.5Gy in G1 enriched cells. *Serum starved G1-enriched* **(A)** *WRL68 and* **(B)** *HepG2 cells were released with 10% FBS containing media for 4hrs before irradiation. Both the cells were exposed to 2.5Gy IR dose and incubated for indicated recovery time points (RT) after irradiation. Further both the cells were fixed at indicated time points after irradiation and γH2AX foci formation were analyzed by immunofluorescence staining against γH2AX antibody. These samples were additionally subjected for histone isolation for profiling of site-specific histone modifications (Figure 4.5A) and cell cycle analysis by flow cytometry as shown in appendix (8.1A upper and lower panel). Scale bar, 2μm for IF.*
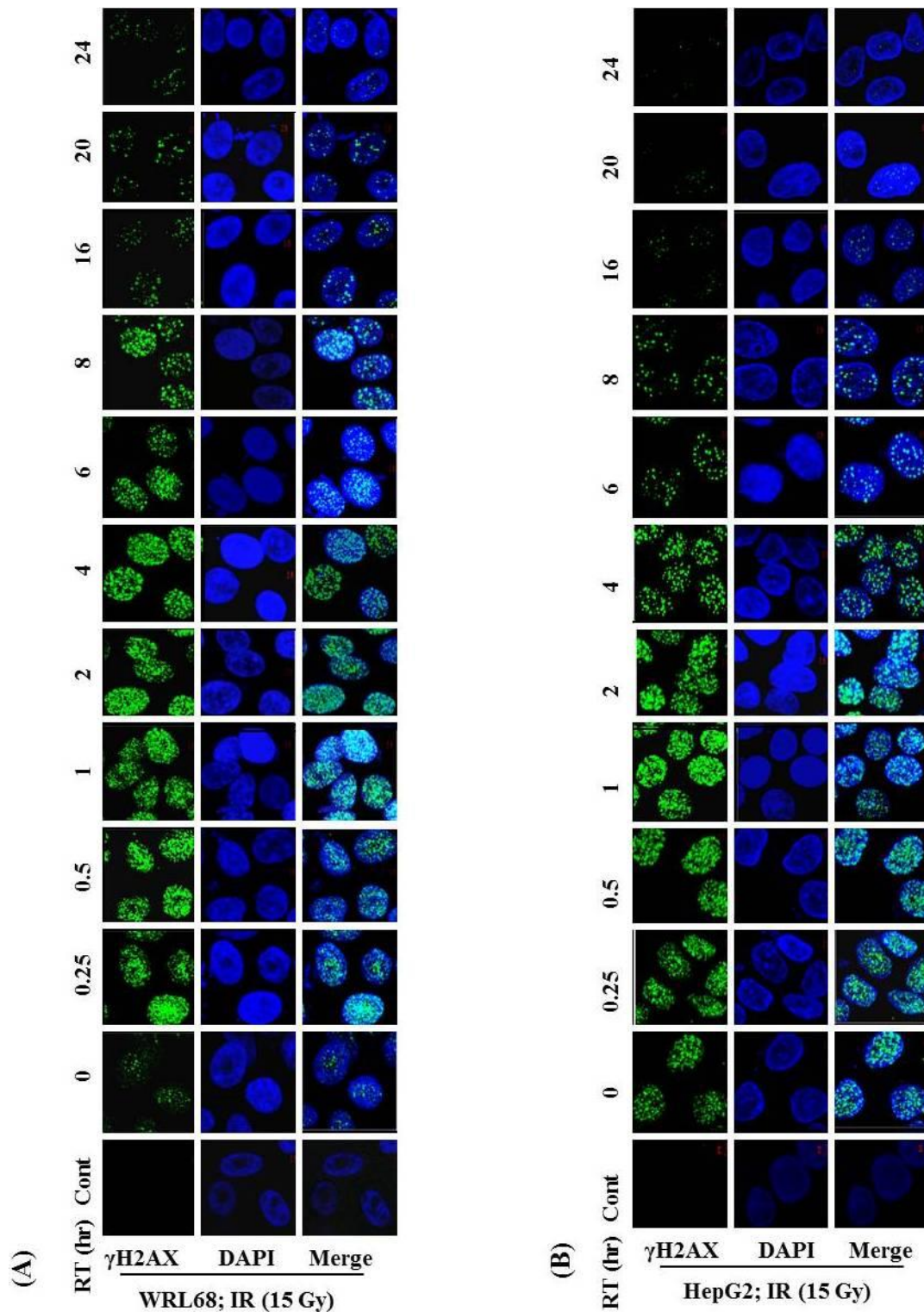
Figure 4.4: Immunofluorescence analysis of time dependent γH2AX foci formation irradiated at 15Gy in G1 enriched cells. *Serum starved G1-enriched* **(A)** *WRL68 and* **(B)** *HepG2 cells were released with 10% FBS containing media for 4hrs before irradiation. Both the cells were exposed to 15Gy IR dose and incubated for indicated recovery time points (RT) after irradiation. Further both the cells were fixed at indicated time points after irradiation and γH2AX foci formation were analyzed by immunofluorescence staining against γH2AX antibody. These samples were additionally subjected for histone isolation for profiling of site-specific histone modifications (Figure 4.5B) and cell cycle analysis by flow cytometry as shown in appendix (A8.1B upper and lower panel). Scale bar, 2μm for IF.*

from 8hr time point. The untransformed WRL68 cells retain higher level of γH2AX in response to lethal dose radiation in 'recovery' phase in comparison to transformed HepG2 cells and are also arrested in G2/M phase of cell cycle (Fig 4.4A, B and A8.1B, upper panel). γH2AX foci becomes undetectable at 24hrs in WRL68 as well as HepG2 in response to either clinically relevant or lethal dose of radiation suggesting complete repair and recovery of cells after damage. Flow cytometry data suggests cells exposed to clinically relevant dose radiation after repair and recovery enters into cell division without any arrest (Appendix A8.1A, upper and lower panel) whereas WRL68 cells exposed to lethal dose radiation enrich in G2/M phase of cell cycle (Appendix A8.1B, upper panel) may be due improper repair resulting into chromosomal aberration and genomic instability further leading to cell death.

4.4. Decrease in phosphorylation of H3Ser10 and its restoration in response to IR induced DNA damage in G1 enriched cells

Phosphorylation of H3Ser10 in G1 phase correlates with chromatin relaxation and gene expression whereas it also correlates with chromosome condensation in mitosis.[141] The phosphorylation status of H3Ser10 in response to DNA damage in mammalian system in specific phase of cell cycle is poorly studied. To delineate H3Ser10P in association with G1-phase of cell cycle and DNA damage phase-specific alteration, post-IR time-dependent western blot analysis was carried out against H3Ser10P and γH2AX. The data shows a gradual decrease in H3Ser10P level in both the cell lines from 0min to 6hrs that coincides with the 'repair' phase of DDR (Fig 4.5A, left and right panel) and (Fig 4.5B, left and right panel). The restoration of H3Ser10 phosphorylation starts at 8hr with a complete recovery at 24hr of post-IR in both the cell line at lethal as well as clinically relevant dose. Further, dose-dependent decrease in H3Ser10P is observed at 15Gy
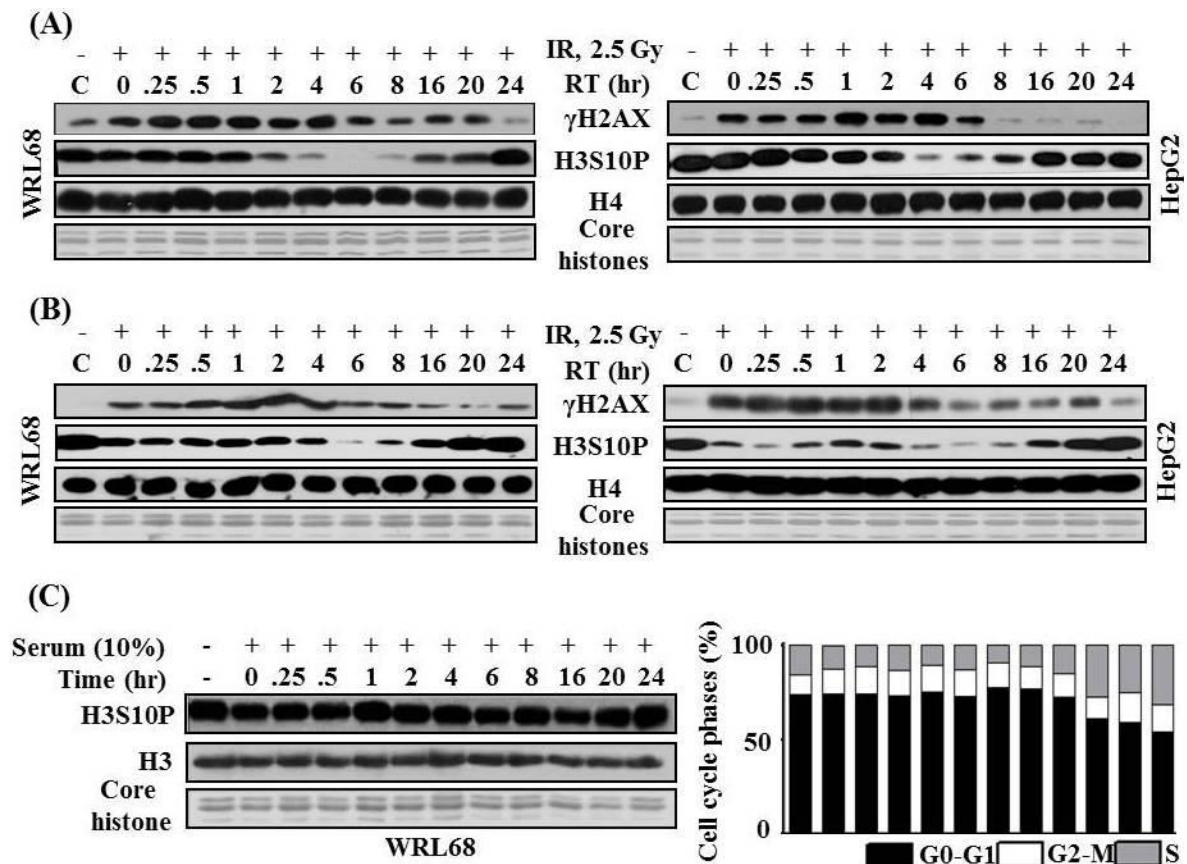
Figure 4.5: H3Ser10P decreases gradually and reversibly upon DNA damage in G1-enriched cells in response to IR. *Serum starved G1-enriched WRL68 and HepG2 cells were released 4hrs before IR irradiation with media containing 10% FBS. Western blotting of acid extracted histones against H3Ser10P, γH2AX and H4 with histones extracted after indicated recovery time points (RT) post-IR from cells irradiated with (**A**) 2.5Gy [left and right panel] (**B**) 15Gy [left and right panel]. In parallel cells were processed for cell cycle distribution by flow cytometry as shown in appendix [A8.1A upper and lower panel] and [A8.1B upper and lower panel], immunofluorescence staining of γH2AX foci formation as shown in [Fig. 4.3A and B] and [Fig. 4.4A and B]. (**C**) Western blotting against H3S10P and H3 with histones from non-irradiated WRL68 cells in normal cell cycle progression after serum starvation release at different time points of incubation (left panel). Histogram data represents percentage of cells in respective phase of cell cycle after serum starvation release (right panel). Control, C – serum released non-irradiated cells. H3Serine10 phosphorylation designated as H3S10P or H3Ser10P.*

(Fig 4.5B, left and right panel) compared to 2.5Gy dose during prime and repair phase of DDR in both the cell lines (Fig 4.5A left and right panel). The level of H3Ser10 phosphorylation after 24hr post-IR is comparable to that of the non-irradiated WRL68 and HepG2 cells. Interestingly, the phosphorylation of H3Ser10 shows an inverse correlation with γH2AX in G1-enriched cells. In coherence with earlier result of retention

of γH2AX foci in time dependent analysis in WRL68 cells, western blot data also shows

delay in decrease of γH2AX.

Histone H3 phosphorylation at Ser10 is shown to begin during prophase, with peak levels

detected during metaphase, followed by a decrease in telophase.[142] Therefore, to validate

reversible reduction of H3Ser10P after IR is concomitant with DNA damage response

and not associated with cell cycle progression, serum starved G1-enriched WRL68 are

released in normal cell cycle progression with 10% serum. Western blot analysis shows

no decrease or restoration of H3Ser10P as observed during DDR in G1 enriched cells

(Fig 4.5C, left pannel). However, the level of H3Ser10P slightly increases due to increase

population of mitotic cells during 20hr and 24hr time points after serum release.
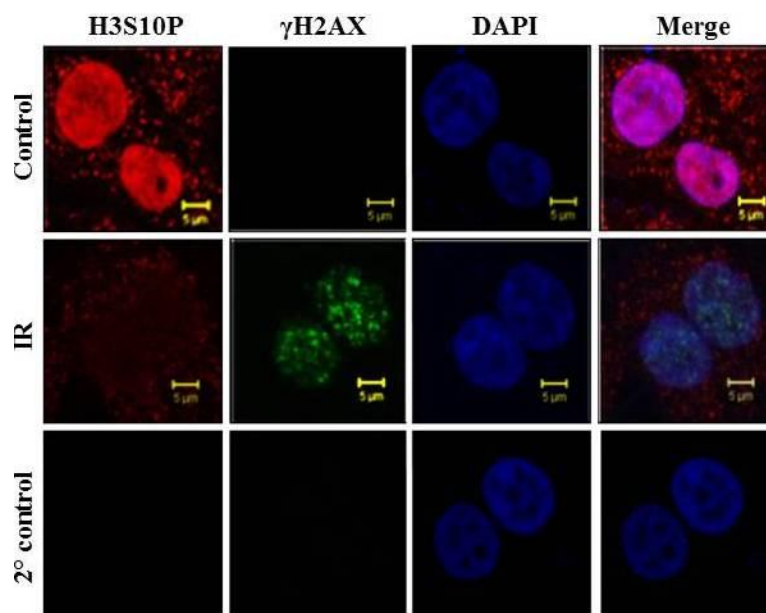
Figure 4.6: Immunofluorescence analysis of H3S10P and γH2AX in G1 enriched cells after DNA damage. *G1-enriched WRL68 cells untreated or treated with 15Gy IR and analysed by immunofluorescence with the indicated antibodies after 1hr of repair time. Induction of DNA damage was visualized by γH2AX foci formation and nucleus by DAPI staining of DNA. 2º Control – secondary negative control, Scale bar, 5μm and H3Serine10 phosphorylation designated as H3S10P or H3Ser10P.*

Further immunofluorescence staining of G1-enriched irradiated cells confirms the loss of

nuclear H3Ser10P and gain of γH2AX compared to non-irradiated cells (Fig 4.6). Thus,

collectively data suggests that a decrease and restoration of H3Ser10P level in parallel with repair and recovery of damaged DNA and is an integral component of DNA damage response in G1 enriched cells.

.

4.5. Decrease of H3 Serine 10 phosphorylation is specific to G1 phase of cell cycle

In mammals, H3Ser10 residue is shown to be phosphorylated with dual functions in G1 and G2/M phases. H3Ser10P is required for chromosome condensation in G2/M phase whereas in G1 it favors active transcription.[143] The untransformed immortalized embryonic liver WRL68 cells are synchronized in three distinct phases of cell cycle, G1, S and pro-M before irradiation with either with 2.5 or 15Gy. Flow cytometry analysis shows that the cells are synchronized in different phase of cell cycle and are cycling to different phases after recovery of DNA damage (Fig 4.7A, lower panel and Appendix A8.2). Western blot data shows that H3Ser10P levels decreases reversibly after irradiation and shows inverse correlation with γH2AX specifically in G1-enriched cells (Fig 4.7A, upper panel), whereas S-phase and pro-M enriched cells doesn't show any detectable change in H3Ser10P level during time points (0, 1 and 4hrs) after ionization irradiation. The alteration of γH2AX levels follows the normal kinetics in all the three phases of cell cycle. The restoration of H3Ser10P levels after 24 hrs of irradiation coincides with the disappearance of universal DNA damage mark i.e. γH2AX specifically in G1 phase of cell cycle.

Western blotting with other mitotic phosphorylation mark, H3Ser28P is carried out to demonstrate specificity of H3Ser10P and whether H3Ser28, being known to be phosphorylated by MAP kinase pathway changes in response to DNA damage. Immunoblotting against H3Ser28P and H3Ser10P with histones purified from cells in different phase of cell cycle (double thymidine block followed by release and chase for different time periods) after 4hr post-irradiation suggests that H3Ser10P decreases
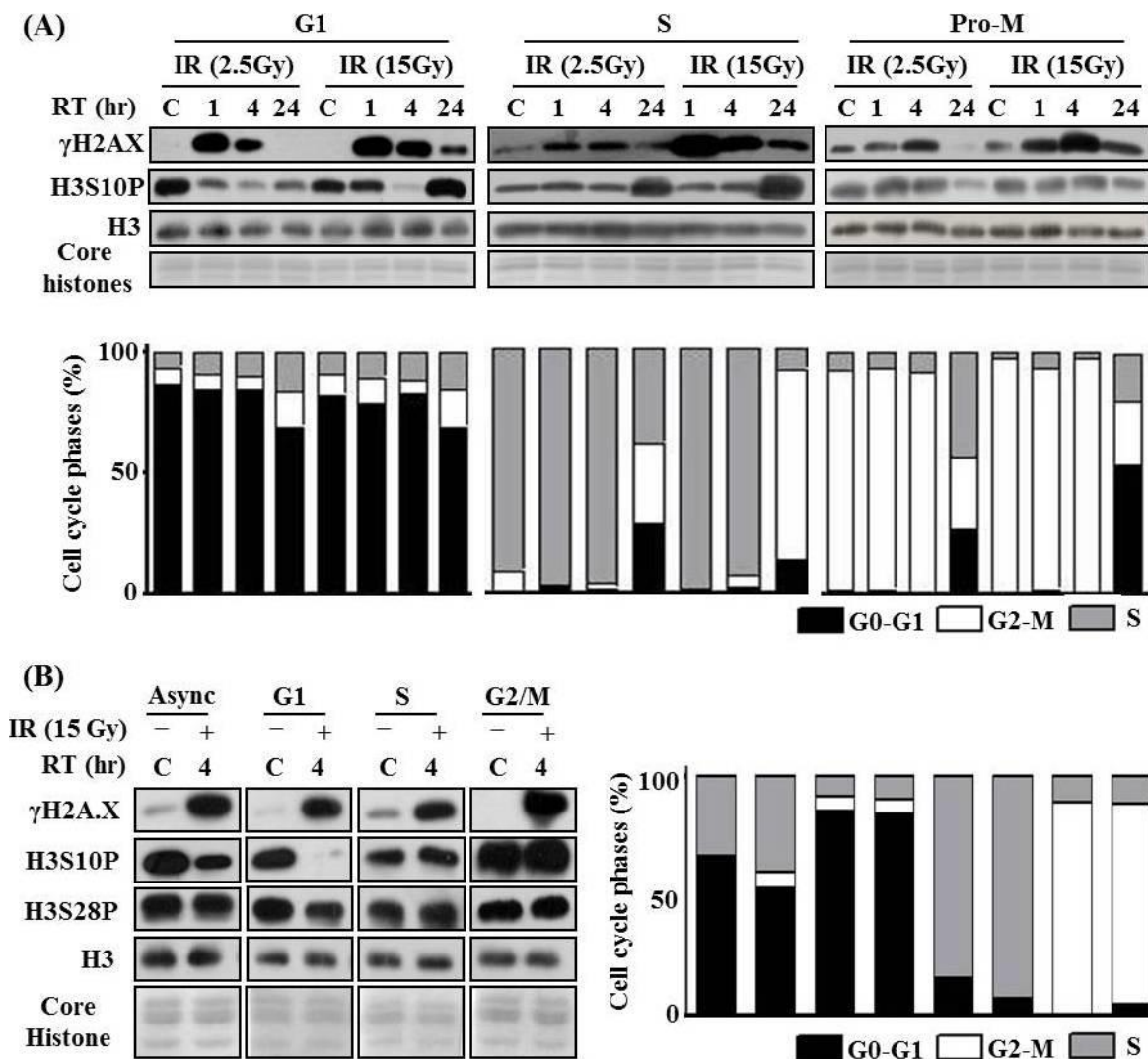
Figure 4.7: H3Ser10 dephosphorylation and phosphorylation upon DNA damage is specific to G1 phase of cell cycle. *WRL68 Cells were enriched in G1, S, G2/M phase of cell cycle with double thymidine block followed by release in complete media for respective time points and pro-M phase with nocodazole (see materials methods in section). (A) Cells enriched in respective phase of cell cycle treated with indicated IR dose and analysed by western blotting of acid extracted histones against H3Ser10P, γH2AX antibodies at indicated recovery time points (RT) after damage (Upper panel). These samples were additionally subjected to flow cytometry analysis for cell cycle distribution as shown in appendix (A8.2). Each histogram data represents percentage of cells in respective phase of cell cycle (A, lower panel). (B) Cells enriched in G1, S and G2/M with similar synchronization condition treated with indicated IR dose and analysed by immunoblotting against H3Ser28P, γH2AX and H3 as loading control (B, left panel). Cell cycle distribution as shown in appendix (A8.3). Histogram data represents percentage of cells in respective phase of cell cycle (A, lower panel) and (B, right panel). H3Serine10 phosphorylation designated as H3S10P or H3Ser10P and H3Serine28 phosphorylation represented as H3S28P or H3Ser28P.*

drastically as compared to H3Ser28P in G1-enriched cells (Fig 4.7B left panel and right

panel, Appendix A8.3). Further, the level of H3Ser10P and H3Ser28P remains unaltered

in S and G2/M enriched cells. Also, the decrease in H3Ser10P is prominent, whereas

H3Ser28P doesn't show decrease after irradiation of asynchronized cells. The data confirms that the decrease in phosphorylation is significant from H3Ser10 but not from H3Ser28 in G1-enriched cells, whereas H3Ser10P and H3Ser28P remains unaltered in S and G2/M enriched cells after DNA damage Thus, collectively data suggests that a decrease and restoration of H3Ser10P level in parallel with repair and recovery of damaged DNA are G1-phase specific.

.

4.6. Decrease of H3 Serine 10 phosphorylation is predominantly from H3.3 variant in G1-enriched cells

In mammals, H3Ser10 residue is highly conserved in H3 variants (H3.1, H3.2 and H3.3) and has been proposed that the modification patterns of each H3 histone variants, H3.1, H3.2 and H3.3 can act as a signature to create different active and repressive chromatin regions in different phases of cell cycle.[144] Flow cytometry analysis of WRL68 cells enriched in G1 and pro-M phase of cell cycle irradiated with IR shows that the majority of growing cells are in G1 (>85%), but also few cells are in S and G2/M phase. Cells treated with nocodazole are arrested in pro-M (>80%) (Fig 4.8A, right panel). Co-immunofluorescence staining with anti-H3Ser10P and anti-γH2AX in G1 or pro-M arrested cells shows the presence of γH2AX foci in both the phases whereas decrease of H3Ser10P is observed only in the G1-enriched cells after IR (Fig 4.8A, left panel). Uniformly distributed staining of nuclear regions is observed in G1 cells. In contrast, the anti-H3Ser10P shows speckled staining of the dense region of the pro-M cells and no enrichment in the outer regions. Immunofluroscence staining of irradiated pro-M phase cells suggests the co-localization of anti-H3Ser10P (red) and anti-γH2AX (green) as depicted by yellow spots in the merged image.

H3Ser10P in G1-enriched cells show significant decrease whereas in pro-M phase cell its

level remains unaltered in response to DNA damage.
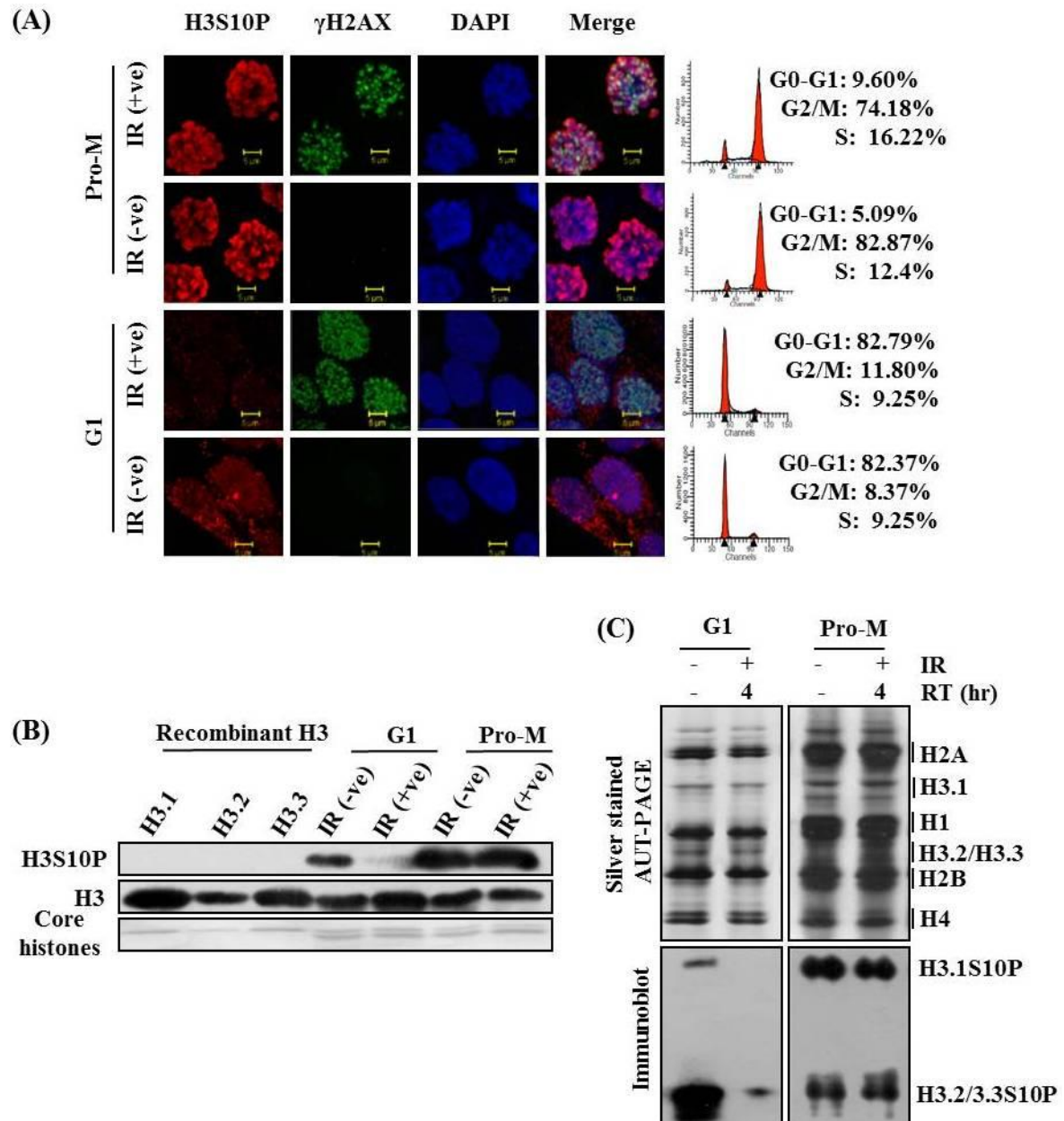
Figure 4.8: H3-variant specific decrease of H3Ser10P upon DNA damage in G1 phase. *G1 and pro-M phase enriched WRL68 cells were released with complete media before either irradiation (15Gy) or non-irradiation.* **(A)** *Cell cycle analysis of G1 and pro-M phase cells with (+IR) i.e. 15Gy or without (-IR) after 4 hrs IR treatment,* **(B)** *Immunofluorescence analysis of H3Ser10 and γH2AX level in G1 and pro-M phase cells with (+IR) or without (-IR) 15Gy IR 1hr post-IR.* **(B)** *Histones from these irradiated G1 and pro-M phase arrested cells and H3-recombinant histones were additionally subjected to western blotting with γH2AX, H3Ser10P and H3 as loading control,* **(C)** *These purified histones were subject to AUT-PAGE followed by silver staining and western blotting with H3Ser10P for cell cycle specific H3-variant analysis. Scale bar, 5μm. RT-recovery time.*

The bacterially expressed H3 variants do not show signal with site-specific anti-H3Ser10P but show signal with H3 antibody confirming the specificity of anti-H3Ser10P (Fig 4.8B). So we asked that whether the decrease in H3Ser10P occurs from a specific H3-variant in G1 phase of cell cycle.

The extracted histones were resolved on AUT-PAGE on basis of mass, charge and hydrophobicity. H3.2 and H3.3 having close hydrophobicity index compared to H3.1 resolved very closely on reverse phase-HPLC column and AUT gel electrophoresis, whereas H3.1 resolved very far from H3.2 and H3.3. Western blotting data shows decrease in phosphorylation of H3Ser10P from all the H3 variants but predominant decrease is observed from H3.3 in G1-enriched cells (Fig 4.8C). However, cells enriched in pro-M phase shows phosphorylation of serine10 at all the variants of H3 without detectable change in phosphorylation status in irradiated cells in comparison to non-irradiated cells. Collectively our data suggests that decrease of phosphorylation is predominantly from H3.3Ser10 and is a G1-specific DNA damage responsive histone mark.

4.7. Reduction of H3Ser10P level is independent of DNA damaging agents and tissue origin in response to DNA damage in G1-enriched cells

Endogenous and exogenous DNA damaging agents induce different types of DNA lesions which activate different repair pathways. These different DNA lesions may also induce different chromatin states and thus raises the possibility of specific modifications might influence the choice of the repair pathway. In order to understand universal nature of H3Ser10P level as a DNA damage responsive mark in response to different DNA lesions, G1 enriched WRL68 cells were treated with various DNA-damaging agents including adriamycin, etoposide, UV, H_2O_2 and cisplatin and histones were extracted after 1hr

recovery and analyzed by immunoblotting with H3Ser10P and γH2AX. Flow cytometry

analysis confirmed the synchronization of cells in G1 phase of cell cycle (Fig 4.9A, lower

panel and appendix A8.4A). Western blot data reveals that there is differential reductions

of H3Ser10P level and increase of γH2AX in response to DNA damage by various

genotoxic agents, and γH2AX and H3Ser10P are reciprocally related (Fig 8.9A). The

reduction of H3Ser10P levels are more pronounced in adriamycin, etoposide and H_2O_2

treated cells as compare to UV and cisplatin treated cells in G1 phase of cell cycle.
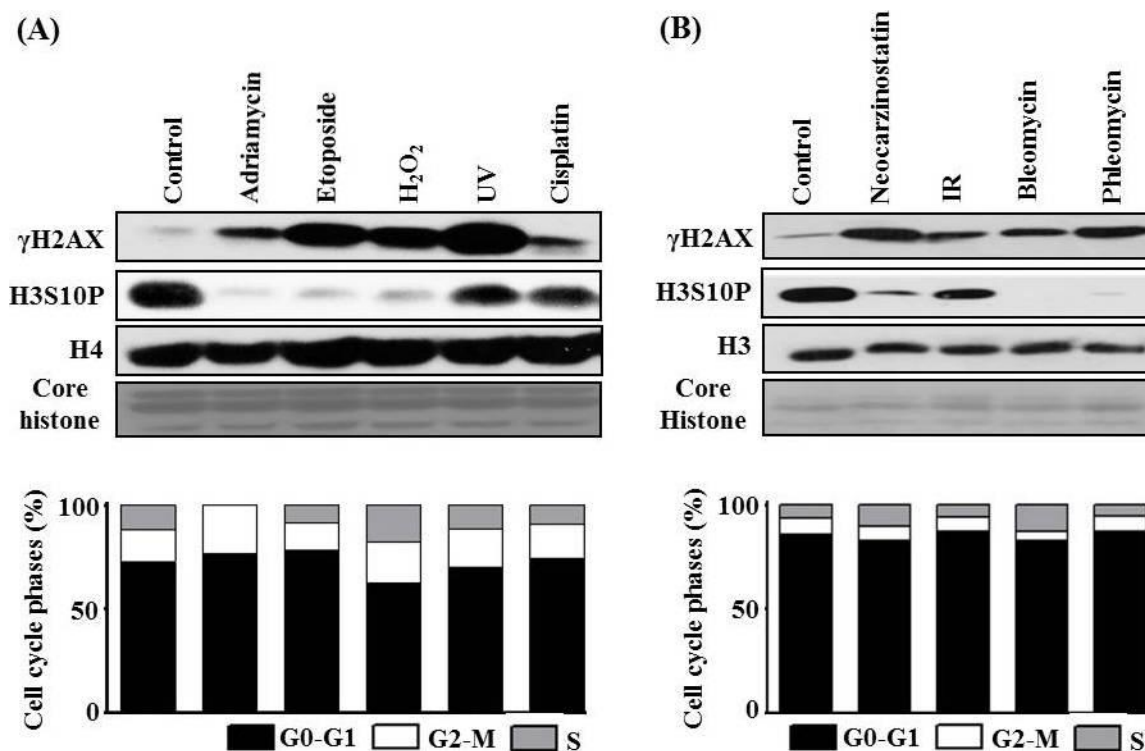
Figure 4.9: H3Ser10 dephosphorylation upon DNA damage with different damaging agents in G1 phase. (A) *G1 enriched WRL68 cells were treated with the indicated DNA-damaging agents (see material and methods for detail. Acid extracted histones after 1hr recovery from treatment were analysed by immunoblotting against anti-H3Ser10P, γH2AX and anti-H4 as loading control to ascertain equal histone loading. These samples were additionally subjected to flow cytometry analysis for cell cycle distribution as shown in appendix (A8.4A). Histogram data represents percentage of cells in respective phase of cell cycle (lower panel).* (B) *G1-enriched WRL68 cells were treated with the indicated radiomimetic drugs and analyzed against H3Ser10P, γH2AX and H3 as loading control. These samples were additionally subjected to flow cytometry analysis for cell cycle distribution as shown in appendix (A8.4B). Histogram data represents percentage of cells in respective phase of cell cycle (lower panel).*

Further radiomimetic drugs, like neocarzinostatin, bleomycin and phleomycin has also

showed differential reduction of H3Ser10P with increase in γH2AX after 1hr recovery

time points in G1-enriched cells (Fig 4.9B). The cell cycle distribution of radiomimetic

treated G1 enriched cells are depicted in (Fig 4.9B, lower panel and appendix A8.4B).

Cells of different tissue origin perform different physiological functions. The response to

ionization radiation and genotoxic agents vary widely in cell lines from different tissue

origin having different genetic and epigenetic background.[145] To investigate reduction of

H3Ser10P level in response to IR induced DNA damage is not specific for normal

immortalized embryonic and transformed liver cells, but universal response against DNA

damage irrespective of cell lines of different tissue origin in G1 phase of cell cycle.

Cancer cell lines (U87, U2OS, MCF7, A2780 and A549) of different tissue origin were

enriched in early G1-phase and histones were isolated after irradiation followed by 1hr

recovery period and immunoblotted against γH2AX and H3Ser10P antibody.
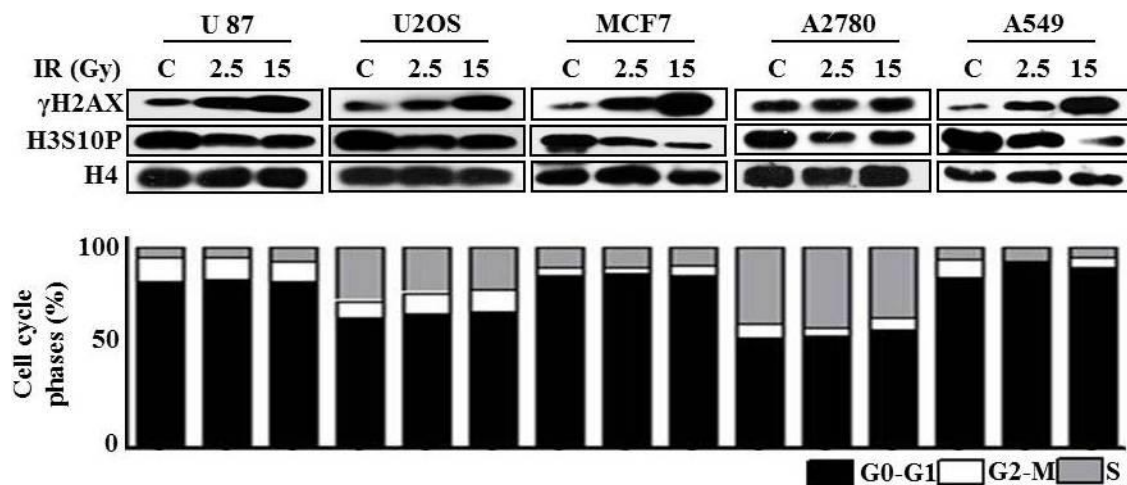
Figure 4.10: Dephosphrylation of H3Ser10 after DNA damage in multiple cell lines. *Cell lines of different tissue origin (U87, U2OS, MCF7, A2780 and A549) enriched in G1 phase were exposed to IR at two different doses 2.5 and 15Gy. Acid extracted histones after 1hr DNA damage recovery were analysed by immunoblotting against anti-H3Ser10P, γH2AX and anti-H4. H4 used as a loading control. Cell cycle distribution of fixed cells from these irradiated cells after 1hr recovery were analysed by flow cytometry and cell cycle distribution shown in appendix (A8.5). Histogram data represents percentage of cells in respective phase of cell cycle (lower panel).*

Flow cytometry data confirms the enrichment of cells in G1 phase (Fig 8.10, lower panel

and appendix A8.5) whereas immunoblot data reveals that prominent reduction of

H3Ser10P is reciprocal to that of γH2AX after DNA damage in these cell lines irrespective of origin of tissue in G1 phase of cell cycle (Fig 8.10, upper pannel). Overall the data suggests that reduction of HSer10P level is a functionally conserved and universal DNA damage responsive mark in G1 phase of cell cycle.

4.8. Decrease in H3Ser10 phosphorylation in G1 cells is associated with de-acetylation of histone marks K9, K14 and K56 on H3

During G1-phase of cell cycle, H3Ser10 phosphorylation associates with transcriptionaly active chromatin. Interestingly, H3Ser10P along with H3Lys14Ac is important for
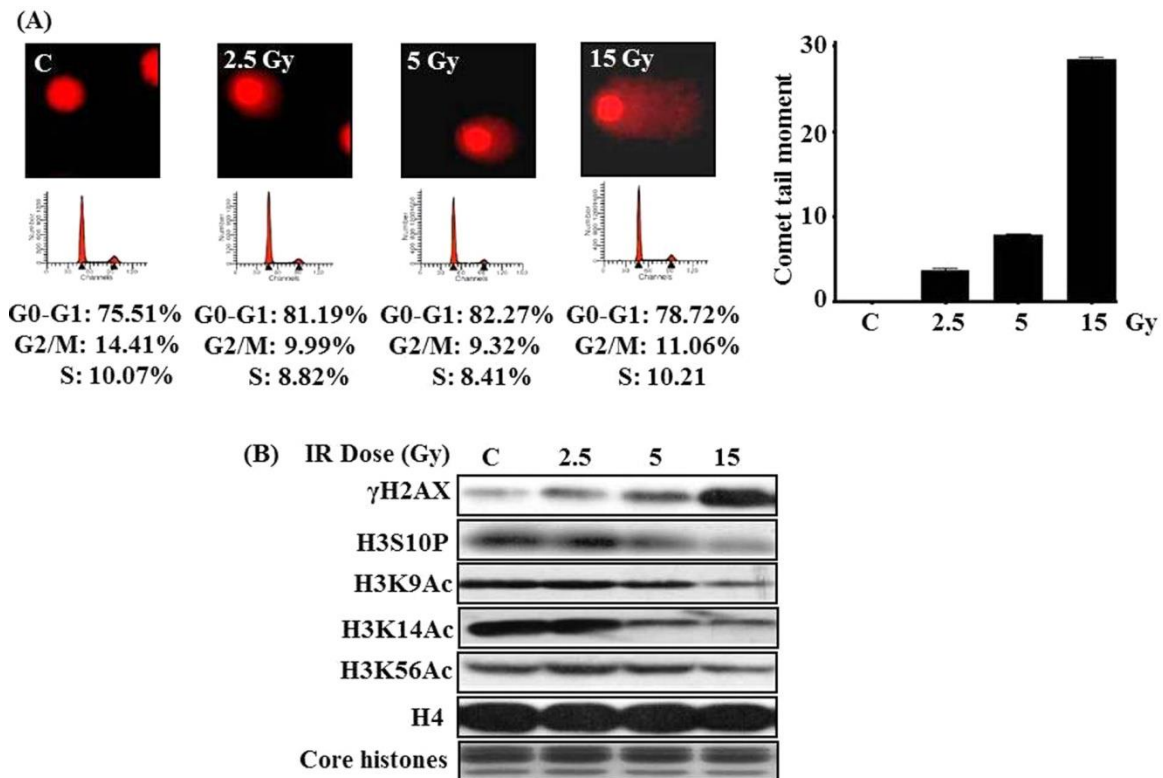
Figure 4.11: Reduction of H3Ser10P and H3 (K9Ac, K14Ac and K56Ac) with increasing IR dose.
*G1-enriched WRL68 cells were exposed to increasing doses (2.5, 5 and 15Gy) of IR and 1hr post-IR treatment following experiments were carried out (**A**) DNA damage analysis by comet tail moment as depicted in representative images of alkaline comet assay (upper left panel), the average tail moment values were determined randomly scoring 50 nuclei per sample (Upper right panel), cell cycle profiling by flow cytometry (lower panel) (**B**) Purified histones from non-irradiated 'C' and with increasing doses of IR were subjected to western blotting with the indicated antibodies after 1hr recovery.*

transcriptional activation mediated through 14-3-3 class of proteins.[146] H3Ser10P also favors recruitment of GCN5 which in turn acetylate H3Lys14 residue.[147] To determine whether decrease in level of H3Ser10P is associated with change in acetylation status of H3Lys9 (K9), Lys14 (K14) and Lys56 (K56), G1-enriched WRL68 cells irradiated with increasing dose (0, 2.5, 5 and 15Gy) of IR. The comet tail moment shows a direct correlation with increasing dose of IR without change in cell cycle profile (Fig 4.11A, upper panel) in G1 enriched cells. The G1-enriched cell cycle distribution analysed by flow cytometry is depicted in (Fig 4.11A lower panel). The dose-dependent analysis of H3Lys9, Lys14 and Lys56 acetylation status reveals a continuous steady decrease in these H3-acetylation marks along with decrease in H3Ser10P and increase in γH2AX (Fig 4.11B).
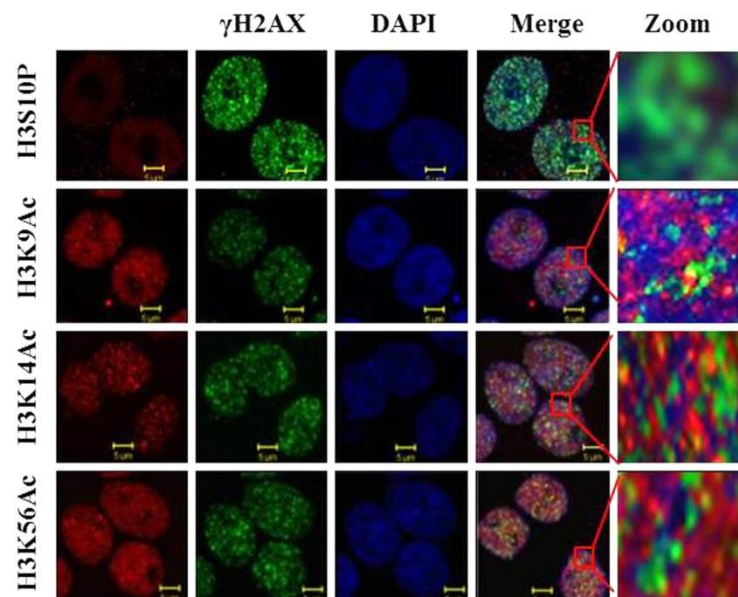
Figure 4.12: Co-localization studies between γH2AX and indicated histone marks after irradiation. *Co-immunofluorescence staining of anti-γH2AX with indicated antibodies after 1hrs irradiation at 15Gy. Nuclei were stained with DAPI. Inset shows a zoomed section of the merged image. Scale bar, 5μm. C – serum released non-irradiated cells.*

The hypoacetylation of H3Lys9 and Lys56 in response to IR is in agreement with earlier reports.[61] The above findings strengthen our view that alteration in these histone modifications is not a cell cycle event but are associated with DNA damage response.

Immunofluorescence studies show spatial localization of γH2AX foci (green) to the sites of DNA damage in IR-treated G1-enriched cells (Fig 4.12). The absence of yellow spots formation and discrete presence of red and green spots separately suggest that gain of γH2AX foci (green) and loss of H3Ser10P, H3Lys9Ac, Lys14Ac and Lys56Ac marks (red) from same damage site. This may favor repressive chromatin state which may facilitate efficient recruitment of repair machinery to DSBs site in G1 phase of cell cycle.

4.9. Phosphorylation of H2AX and de-phosphorylation of H3Ser10 are marks on a same mono-nucleosome.

The chromatin changes in DDR may be facilitated by remodeling and modification of histones mediated through change in electrostatic interactions. The previous data raises a query whether loss of H3Ser10P and gain of γH2AX may occur from the same mono-nucleosomes. To address this, we isolated mono-nucleosomes from G1-enriched WRL68 nuclei before and after 4hr post-IR. The G1 enriched phase of cell cycle was confirmed by flow cytometry (Fig 4.13A), DNA damage by alkaline comet assay (Fig 4.13A) and purity of mononucleosomes was checked on agarose gel (Fig 4.13B). Western blot analysis substantiates the prominent decrease of H3Ser10P, Lys9Ac, Lys14Ac, and Lys56Ac in histones purified from mono-nucleosomes as compared to total nuclear histones (Figure 4.13 C, left and right pannel).

The mono-nucleosomes (MN) are co-immunoprecipitated with either anti-H3Ser10P or anti-γH2AX followed by western blotting against H3Ser10P and γH2AX to confirm co-localization of these marks on same nucleosome. Collectively, the western blot with MN-Co-IP histones in bound and unbound fractions confirms that γH2AX is present on nucleosomes purified from irradiated cells which do not have phosphorylated H3Ser10, whereas, nucleosomes from non-irradiated cells bearing H3Ser10P do not contain

γH2AX (Fig 4.13D). γH2AX-IP with non-irradiated cells shows the presence of γH2AX

in bead-bound fraction but not in the input.
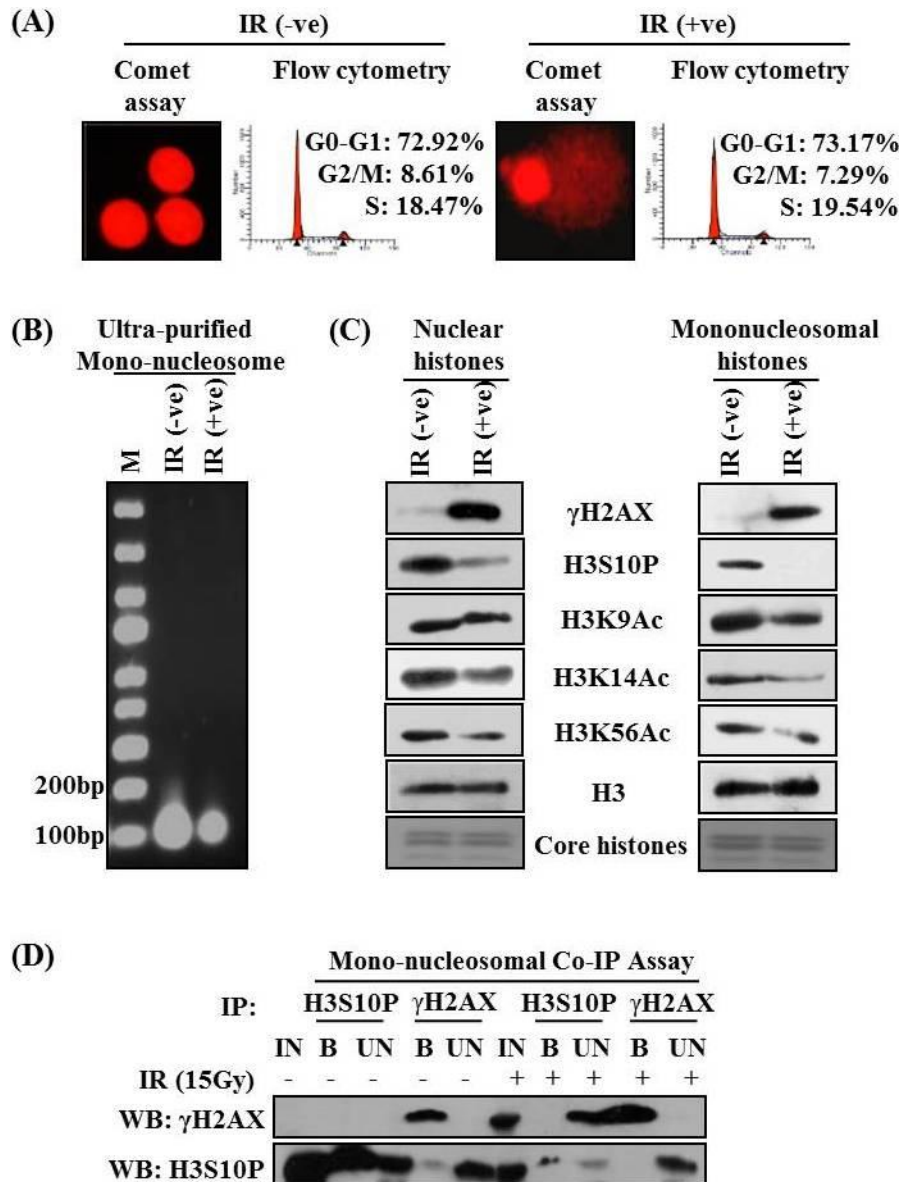
Figure 4.13: Loss of H3S10P and gain of γH2AX from a same mono-nucleosome at DSB site in G1 phase. *WRL68 cells enriched in G1-phase were irradiated at 15Gy (+IR) or non-irradiated (-IR) and allow to repair for 4hrs after irradiation. Purified nuclei from these cells were subjected tocommet assay, cell cycle analysis, histone isolation and mono-nucleosomes preparation for co-IP.* (***A***) *DNA damage analysis by comet tail moment as depicted in representative images of alkaline comet assay and cell cycle profiling by flow cytometry* (***B***) *The purified mono-nucleosome was resolved on 1.8% TAE-agarose gel to check the purity and size of mono-nucleosome.* (***C***) W*estern blotting of histones purified from nuclei and mono-nucleosomes with indicated antibodies.* (***D***) *Co-IP of mono-nucleosomes with γH2AX and H3Ser10P followed by bound [B] and unbound [UB] fractionation. The Input (IN), B and UB fractions from mono-nucleosomal Co-IP were immuno-blotted with anti-H3Ser10P and anti-γH2AX antibody*

This may be due to replication stress and enrichment of γH2AX after IP with γH2AX in bead-bound fraction. This is the first experimental evidence to the best of our knowledge of 'negative cross talk' of the histone marks, 'loss' of H3Ser10P and 'gain' of γH2AX from the same mono-nucleosome at DSB site during DDR in G1 phase.

4.10. Condensation and decondensation of chromatin in 'repair' and 'recovery' phase of DDR in G1-enriched cells.

Previous conflicting reports on asynchronous population of cells have shown that DNA damage is accompanied either by chromatin relaxation or condensation during initial phase of DDR.[27, 40, 148-151] Our data till now have shown decrease of Ser10P, Lys9Ac, Lys14Ac, Lys56Ac on H3 at mono-nucleosomal level in G1 enrich cells in response to IR. The alteration of global chromatin structure is studied by MNase accessibility assay. The data shows increase in appearance of mono-nucleosomes and its multiple with increasing time (0, 2.5 and 5 min) of digestion (Fig 4.14, upper pannel). The densitometric scan of resolved MNase digested chromatin suggests global chromatin compaction at 0 and 4hrs ('repair' phase) post-IR as evident from decrease in intensity of nucleosomes and increase in high MW DNA at 2.5mins digestion in comparison to non-irradiated and 24hr post-IR recovered cells (Fig 4.14, lower pannel).

The restoration of native chromatin organization coincides with 'recovery phase' of DDR. Earlier reports have shown decrease in acetylation of H3Lys9 and Lys56 in repair and increase in recovery phase of DDR.[61] Our data supports that in addition to H3Lys9 and H3Lys56 acetylations, there is also a reversible reduction of H3Ser10P and global condensation of chromatin in 'repair' phase and decondensation in 'recovery' phase after irradiation in G1 cells. This might lead to assembly/disassembly of repair proteins at DNA damage sites.
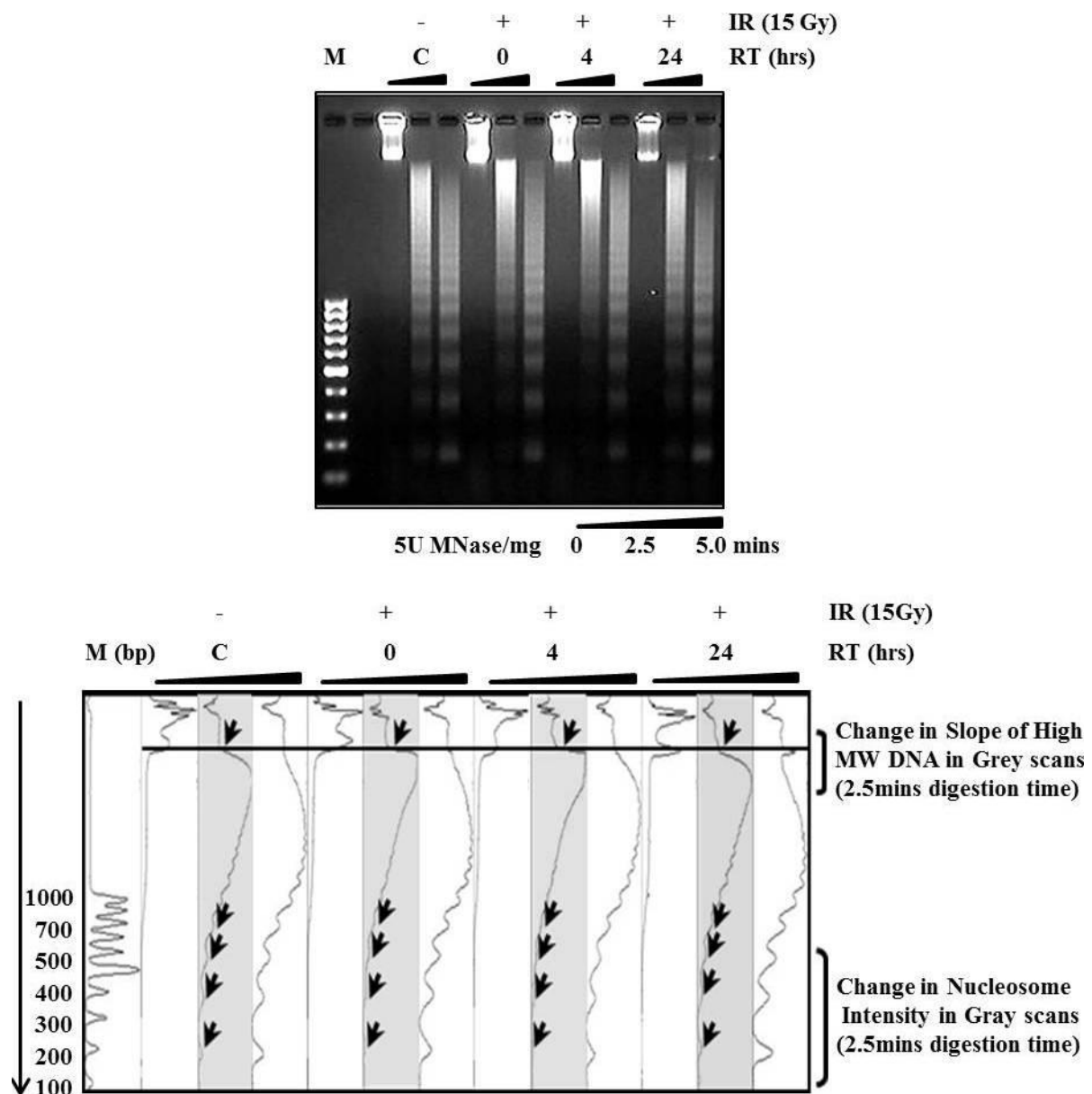
Figure 4.14: Condensation and decondensation of chromatin in 'repair' and 'recovery' phase of DDR in G1-enriched cells. *WRL68 cells enriched in G1-phase were irradiated at 15Gy (+IR) or non-irradiated (-IR) and incubated for indicate time point for recovery (RT) and alteration of chromatin structure were analysed by micrococcal nuclease assay (MNase).MNase (5units/mg of DNA) digested nuclei for 0, 2.5 and 5mins were resolved on 1.8% TAE-agarose gel. The MNase digested gel was scanned and quantified with ImageJ software version 1.43u; Java 1.6.0_10 (32-bit). M- Markers 100bp ladder. C – serum released non-irradiated cells.*

4.11. Phosphorylation status of H3Ser10 in G1 phase cells is correlated with phosphorylation of MAP kinases and their de-phosphorylation by MKP1 in response to irradiation.

Epidermal growth factor (EGF) induces H3Ser10P, which is mediated by RSK-2.[152] In addition, mitogen and stress-activated protein kinases (MSK1) have been shown to

mediate EGF or TPA-induced phosphorylation of H3Ser10.[122] UV-B irradiation induces phosphorylation of histone H3 at serine10 through ERKs and p38 kinases.[108] To check the association of MAP kinase pathway in G1 phase cells with reversible alteration of H3Ser10P during IR induced DDR, we assessed the levels of phospho- (ERK 1/2, JNK, p38 and MSK1) and MKP1 in soluble fractions of cells, and H3Ser10P and γH2AX level in chromatin fraction after IR treatment. Western blot analysis with specific antibodies shows significant decrease in phosphorylation of p38, ERK1/2, JNK and MSK1 whereas increase in MKP1 is at protein level immediately (0min) after IR doses i.e. 2.5 and 15Gy (Fig 4.15A, left and right panel). The increased level of p-p38, p-JNK, p-ERK1/2 and p-MSK1 are restores to its basal level in 'repair' phase (4 and 24hr post-IR treatment). The increased level of MKP-1 protein and p-JNK decrease in 'recovery' phase of lethal dose radiation needs further investigation to understand their significance. In chromatin fraction, H3Ser10P decreases with increase in γH2AX after 0 and 4hr IR treatment and there levels are restored during 'recovery' phase (Fig 4.15B, left and right pannel). MKP-1 is a nuclear protein, encoded by an immediate early gene and capable of inactivating all the three classes of MAPK *in vivo*.[153, 154] Also, MKP-1 is known to be induced by γ-radiation and repressed radiation-induced pro-apoptotic status.[155]

These observations regarding increase of MKP-1 level in response to different stress inducing agents raises the possibility of MKP-1 as a phosphatase mediating decrease of phospho-MAP kinases and H3Ser10P in response to IR induce DNA damage.

To test above possibility G1 enriched WRL68 cells are treated with MKP1 inhibitor, sanguinarine (10µM) for 1hr before IR.[121] Cell cycle profile remains unaltered with or without sanguinarine followed by irradiation (Fig 8.15C, lower panel and appendix A8.6). Western blot analysis with anti-phospho-MAP kinases immediately after irradiation (0min) suggests that the loss of phospho-MAP kinases (p-p38, p-JNK, p-

ERK1/2 and p-MSK1) are inhibited in sanguinarine and IR-treated cells as compare to

only irradiated cells (Fig 8.15C, upper pannel).
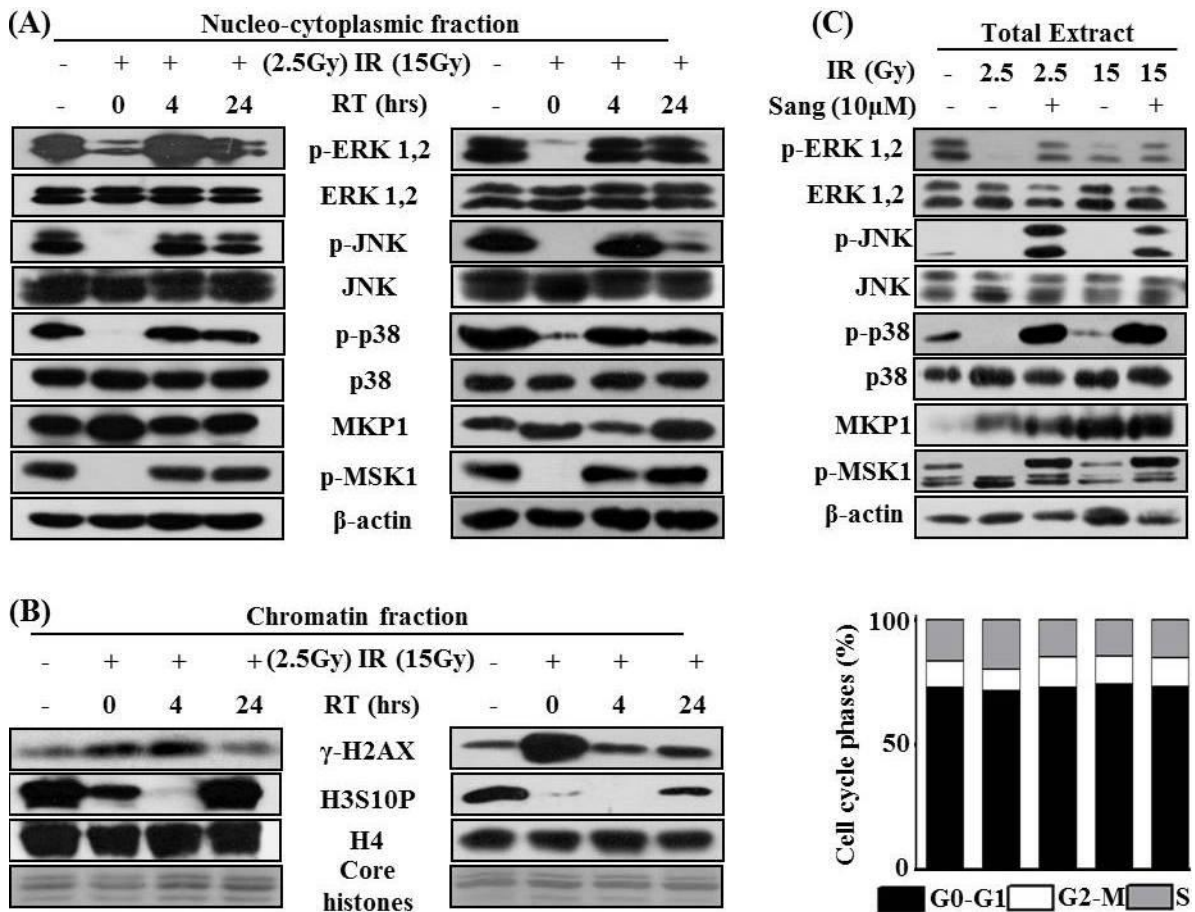
Figure 4.15: Phosphorylation status of H3S10 in G1 phase WRL68 cells is correlated with phosphorylation of MAP kinases and their de-phosphorylation by MKP1 in response to IR. (A) *Purified soluble total proteins were subjected to western blotting with antibodies against indicated site-specific phospho- and total proteins,* **(B)** *Purified chromatin fractions were resolved on 18% SDS-PAGE were immunoblotted against H3Ser10P or γH2AX or H4 as a loading control.* **(C)** *Cells were pretreated with or without 10μM of sanguinarine for 1hr before IR (2.5 and 15Gy). Total lysates were prepared immediately after IR and subjected to western blotting with antibodies against indicated proteins. β-actin was used as an internal control [upper panel]. These samples were additionally subjected to flow cytometry analysis for cell cycle distribution as shown in appendix (A8.6) 'Lower panel' shows cell cycle distribution of above treated and non-treated cells. Sang- Sanguinarine, C – serum released non-irradiated cells. RT- recovery time after DNA damage*

The total proteins of MAP kinases remain unaltered whereas MKP1 protein increases in

dose-dependent manner in response to IR irrespective of sanguinarine treatment. Thus

overall data reveals that dephosphorylation of MAP kinases is mediated through

phosphatase, MKP-1 immediately after IR induce DNA damage in G1-phase cells. This raises the possibility of MKP-1 as a phosphatase for de-phosphorylation of H3Ser10P and inhibition of MAP kinases responsible for phosphorylation of H3Ser10. The delay in dephosphorylation of H3Ser10 in relation to MAP kinase strongly implies role of downstream effectors of MAP kinase pathway in dynamic regulation of H3Ser10P in response to DNA damage.

4.12. *Insilco* prediction of MSK1 and MKP-1 interaction with native H3 peptide and its posttranslational modifications (PTM).

4.12.1. Homology modeling of MKP1 and MSK1 structures.

Homology modeling was carried out for MKP1 and MSK1 by studying their molecular interactions with modified and unmodified H3. MKP1 consists of 367 amino acids with two domains that are separated by a flexible loop region.[156] The C-terminal domain regulates the phosphatase activity of MKP1.[157] To examine the importance of MKP1 protein and its molecular interactions with H3, we conducted modeling studies as the crystal or solution structure of MKP1 was not available. Data from the Protein Data Bank revealed that the C-terminal crystal structure of human MKP2 (PDB ID: 3EZZ) has sequence identity of 85.31% with human MKP1. This structure is used as a template for homology modeling of C-terminal of MKP1 from 172–314 amino acids. The dual specificity protein phosphatase (DUSP) domain is also reported to be located between 180–312 amino acids. The modeled structure of MKP1 is found to have a QMEAN Z-score of −0.693.21.[134] The energy of the MKP1 structure is minimized using Discovery studio 2.5, from an initial potential energy of -5246.07 to -9131.51 kcal/mol by conjugate gradient converging at 1397 steps. The MKP1 structure is also validated using the SAVES server

and show that 0.8% residues are located in the disallowed region of the Ramachandran plot according to Procheck,[135] confirming the correct overall geometry of the MKP1 model. Verfiy_3D[136] show 89.19% residues with average 3D to 1D scores .0.2 by assigning a structural class. The modeled structure of C-terminal of MKP1 (172– 314 aa) and the active site residues (257–264 aa) are shown in red color in (Fig 4.16A) and appendix (A8.7A).

The crystal structure of the N-terminal kinase domain of MSK1 is available (PDB ID: 1VZO 24–345); however, inactive MSK1 requires an association with the phosphorylated loop residue (Ser376) to convert into the active form. Therefore, to model the loop with the N-terminal domain, PDB ID: 3A8X was used as template for homology modeling. 3A8X is the crystal structure of protein kinase C (PKC-iota), which has sequence identity of 62% with the N-terminus of MSK1. The modeled structure of MSK1 has a QMEAN Z-score -1.216.[139]
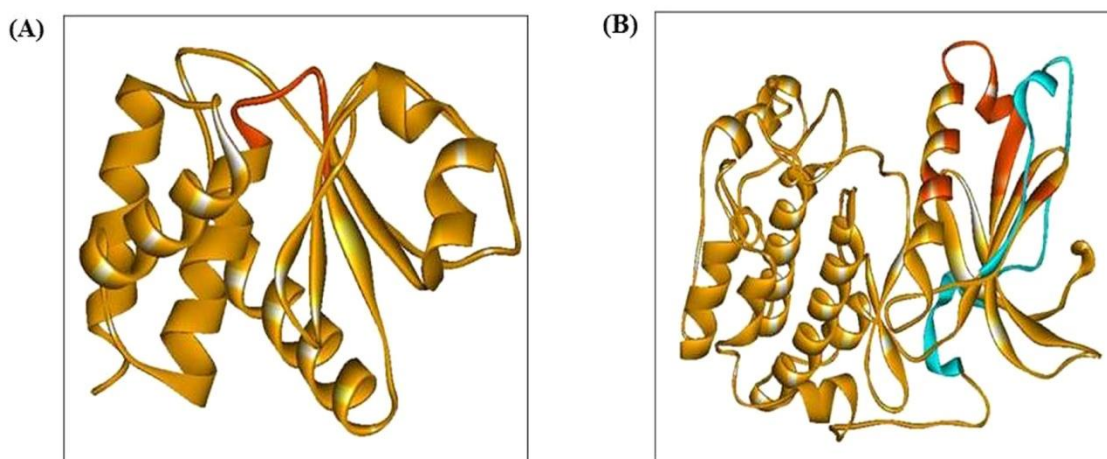
Figure 4.16: Homology modeling of MKP1 and MSK1 structures. *(A) Homology modeled structure of C-terminal phosphatase domain of MKP1 (172–314 aa) is shown in yellow color, while the active site includes His257, Cys258, Gln259, Ala260, Gly261, Ile262, Ser263, and Arg264 residues in orange color. (B) Homology modeled structure of N-terminal kinase domain of MSK1 (42–380 aa) is shown in yellow color. The blue colored region is the flexible loop near the active site. The orange color indicates the active site residues Lys85, Ile88, Val89, Thr95, Arg102, Gln122, and Leu127.*

The modeled structure has four beta-sheets, fifteen alpha-helices, and fifteen loops (Appendix A8.7B). The MSK1 model validated through the SAVES server showed 0.7%

residues are in the disallowed region of the Ramachandran plot according to Procheck,[135]

which confirmed the correct overall geometry. Verfiy_3D[136] show that 88.82% residues

have average 3D to 1D scores of .0.2 by assigning a structural class. The overall quality

of the model is given by the ERRAT score[137] of 95.886 by analyzing the non-bonding

interaction between different atom types.

The modeled structure of MSK1 and MKP-1 with active domains was used for molecular

interaction studies with H3 peptide with either phosphorylation or acetylation at specific

residues, Lys9, Ser10, or Lys14.

4.12.2. Docking of native MSK1 with histone H3 and its PTM modified structure.

The modeled structure of N-terminal domain of MSK1 (42–380 aa) was docked with

native and acetylated histone H3 at Lys9 or Lys14 independently or together (Fig 4.16B

and appendix A8.9). The active site residues (Lys85, Ile88, Val89, Thr95, Arg102,

Gln122, and Leu127) of MSK1 are obtained from the literature.[158] The native histone H3

score highest compared to acetylated Lys9 and Lys14 (Table 4.1).
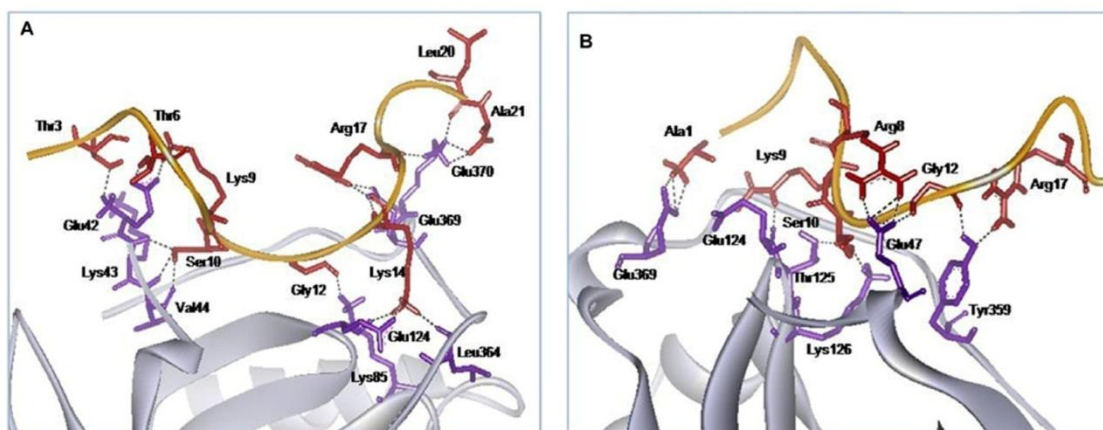
Figure 4.17: Docking of MSK1 with histone H3 and its PTM structure *(A) MSK1 and histone H3 and (B) MSK1 and histone H3Lys9AcLys14Ac. The ribbon diagram of MSK1 (grey) with the residues (violet) and histone H3 peptide (orange) with the residues (red) are involved in the H-bonding interaction and is shown as a dotted black line.*

The bound state is stabilized by an intramolecular interaction. In native histone H3, the

salt-bridge interaction was observed between Lys14 of H3 with Glu124 of MSK1 (Fig

Table 4.1: Docking of native MSK1 with histone H3 and its PTM modified structure

Docked complexes	HADDOCK score	Interacting residues	
		H-bonds	**Hydrophobic**
MSK1 H3	-92.1 +/- 7.8	**Ser10**: *Lys43, Val44* **Gly12**: *Lys85* **Lys14**: *Glu124, Leu364, Glu369* **Arg17**: *Lys370* **Leu20**: *Lys370* **Ala21**: *Lys370*	**Gly12:** *Thr123* **Gly13:** *Glu369* **Lys14:** *Glu369*
MSK1 H3_K9	-47.4 +/- 9.0	**Ala1:** *Glu369* **Arg8:** *Glu47* **Lys9**: *Glu124* **Ser10**: *Thr125, Lys126* **Gly12**: *Glu47* **Arg17**: *Tyr359*	**Lys9**: *Glu124* **Ser10**: *Lys126* **Thr11**: *Glu47, Tyr359*
MSK1 H3_K14	-64.0 +/- 6.5	**Ala1:** *Ser367, Glu369* **Thr3***: Glu124* **Lys9***: Glu124, Glu369* **Ser10***: Lys85, Glu369* **Arg17***: Lys43, Glu47* **Lys18***: Glu47, Ile69*	**Arg2:** *Pro365* **Gly13:** *Glu42*
MSK1 H3_K9-K14	-50.2 +/- 10.2	**Ala1:** *Glu369* **Arg8:** *Glu47* **Lys9:** *Glu124* **Ser10:** *Thr125, Lys126* **Gly12:** *Glu47* **Arg17:** *Tyr359*	**Arg2**: *Pro365* **Ser10**: *Thr123* **Thr11:** *Tyr359*

*Bold alphabets are for Histone H3 and italics are for binding partners.

4.17A and appendix A8.10), but when histone H3 was acetylated at either position, Lys9 forms a salt-bridge with Glu124 (Fig. 4.17B and Appendix A8.10). Histone H3 acetylation at Lys14 favored an interaction with MSK1 with a Haddock score of -64.0 compared to a -47.4 score for Lys9 (Table 4.1). Haddock scores for the interaction of MSK1 with H3Ser10PLys9Ac and H3Ser10PLys14Ac clearly suggest that acetylation is not a prerequisite for phosphorylation of H3Ser10P by MSK1.

4.13. Docking of native MKP1 with histone H3 and its PTM structure

Previous studies by us and other groups have shown that in interphase cells, H3Ser10P is associated with acetylation of H3Lys9 and Lys14, which may favour gene transcription. The homology model structure of the C-terminal phosphatase domain of MKP-11 (172–314 aa) is used for docking with the loop crystal structure of H3 peptide (1–21 aa) using the Haddock server (Fig. 4.16A and Appendix A8.9). The active site amino acid, Cys258, and nearby residue important for the formation of the active site (His257, Cys258, Gln259, Ala260, Gly261, Ile262, Ser263, and Arg264) for MKP-11 are obtained from UniProt ID: P28562. These residues are used for targeted docking native and modified histone H3 peptides.
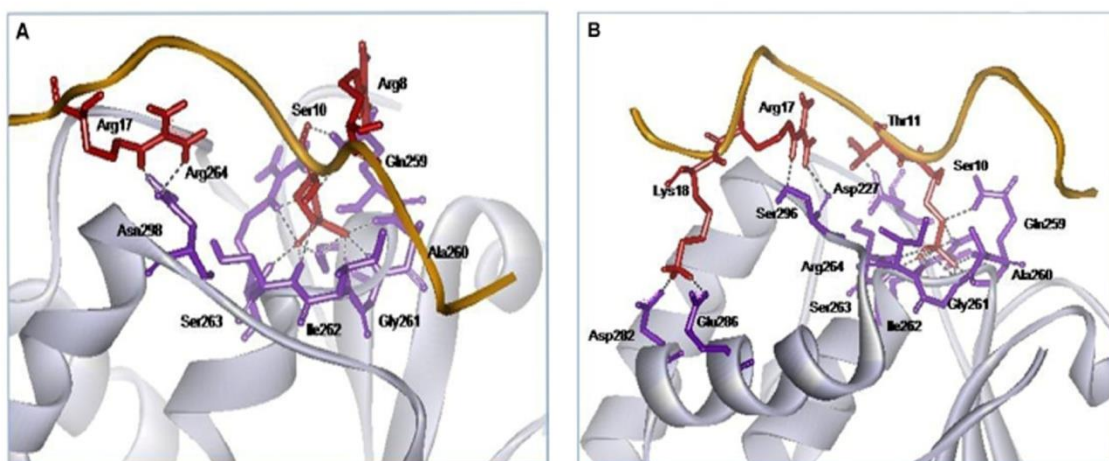
Figure 4.18: Docking of MKP1 with histone H3 and its PTM structure. *(A) MKP1 and histone H3Ser10 and (B) MKP1 and histone H3Lys9AcSer10PLys14Ac. The ribbon diagram of MKP1 (grey) with the residues (violet) and histone H3 peptide (orange) with the residues (red) are involved in the H-bonding interaction and is shown as a dotted black line.*

Haddock scores from all eight complexes suggest that the complex of MKP-11 and H3Lys9AcSer10PLys14Ac show the strongest binding compared to the complex containing the native histone H3 and MKP1 (Table 4.2, Fig. 4.18A, B and Appendix 8.11).

Table 4.2: Docking of native MKP-1 with histone H3 and its PTM modified structure

Docked complexes	HADDOCK score	Interacting residues	
		H-bonds	**Hydrophobic**
MKP1 H3	-61.8 +/- 6.8	**Arg8:** *Gln259* **Thr11**: *Asp227* **Lys14**: *Asn228* **Arg17**: *Asp227, Asn228* **Ala21**: *His229*	**Ser10**: *Ala260* **Lys14**: *Asn228*
MKP1 H3_S10	-90.3 +/- 3.8	**Arg8:** *Gln259* **Ser10**: *Cys258, Gln259, Ala260, Gly261, Ile262, Ser263, Arg264* **Arg17**: *Asn298*	**Thr3**: *Ile294* **Lys9**: *Ser296*
MKP1 H3_K9-S10	-121.6 +/- 16.4	**Lys9**:*Gln259* **Thr11**: *Asp227* **Ser10**: *Cys258, Gln259, Ala260, Gly261,Ile262, Ser263, Arg264*	**Gly13:** *Phe299* **Lys14**: *Phe299* **Lys18**: *Phe299*
MKP1 H3_S10-K14	-122.6 +/- 17.7	**Thr3:** *Arg292* **Thr11:** *Asp227, Asn298* **Arg17:** *Ser296, Pro297* **Lys18:** *Asp282, Glu286* **Ser10**: *Cys258, Gln259, Ala260, Gly261, Ile262, Ser263, Arg264*	**Lys9**: *Ser185* **Lys14**: *Phe299*
MKP1 H3_K9-S10-K14	-138.6 +/- 12.1	**Thr11:** *Asp227* **Ser10**: *Gln259, Ala260, Gly261, Ile262, Ser263, Arg264* **Arg17**: *Ser296, Pro297* **Lys18**: *Asp282, Glu286*	**Lys9**: *Ile262, Ala260* **Gly13**: *Phe299* **Lys14**: *Phe299, Asn298* **Lys18**: *Phe285*
MKP1 H3_K9	-56.8 +/- 6.9	**Ala1:** *Ser296* **Thr3**: *Asp227* **Lys9**: *Gly261* **Ser10**: *Arg292* **Lys14**: *Tyr187* **Lys18**: *His213*	**Lys4:** *Asp227* **Lys9**: *Ala260, Ile262* **Gly13:** *Tyr187*
MKP1 H3_K14	-67.8 +/- 6.3	**Ala1:** *Asn209, Glu226* **Thr3**: *Ser185, Tyr187* **Arg8**: *Asp227, Gln259* **Lys9**: *Gln259* **Ser10**: *Asp227*	**Lys4**:*Try187* **Lys9**: *Ala260* **Thr11**: *Asp227*
MKP1 H3_K9-K14	-61.9 +/- 4.4	**Ala1:** *Ser296* **Thr3**: *Arg264* **Lys9**: *Gly261, Ile262* **Lys14**: *Tyr187* **Lys18**: *Ser190, His213*	**Lys9**: *Gln259, Ile262, Ser263* **Arg17**: *Tyr187*

*Bold alphabets are for Histone H3 and italics are for binding partners.

However, when either Lys9 or Lys14 acetylation is added with Ser10, the Haddock score increases from -90.3 to around -122. The residues involved in the interaction with phosphorylated Ser10 are mostly from active site (Gln259, Ala260, Gly261, Ile262, Ser263, Arg264) of MKP1 observed in all the complexes. Our molecular modeling suggests that the acetylation protects the phosphorylation at H3Ser10 from being removed by phosphatase and the acetylation of the H3 tail favors active chromatin organization, which may facilitates gene transcription.

4.14. MKP-1 associates with chromatin in response to DNA damage.

Our *insilco* data highlighted the possible interaction of MKP-1 with site-specific phosphorylation (H3Ser10P) and acetylation (H3Lys9 and H3Lys14) of H3.[159] Earlier studies from Kinney *et al* have demonstrated that MKP-1 interacts with H3 in VEGF-treated endothelial cells.[113] These reports raises the possible role of MKP-1 in the dephosphorylation of H3Ser10P in response to DNA damage. To investigate the localization of MKP-1 in G1-enriched cells, total soluble (SF) and chromatin (CF) fractions were prepared from control and irradiated cells followed for 2 and 24hrs after DNA damage and immunoblotted with specific antibodies. The cell cycle distribution in G1 enriched cells before irradiation and after the irradiation as depicted in (Fig 4.19A). The data reveal that MKP-1 is predominant in chromatin fraction compared to soluble fraction after 2hr of irradiation (Fig 4.19B, left and right panel). Further, β-actin is reported to interact with chromatin along with INO.80 complex.[160] The western blot experiment with β-actin confirms the recruitment of β-actin at chromatin and it also gradually increases in chromatin fraction in response to DNA damage. Interestingly, after DNA damage is repaired i.e. 24hr, the level of MKP-1 decreases in chromatin fraction with increase in soluble fraction. The data suggests that decrease in H3Ser10P in response to DNA damage may be due to the recruitment of MKP-1 on the chromatin.

Further, to investigate the recruitment of MKP-1 at the DNA damage site after 2hr of irradiation, mononucleosomes from control and irradiated G1-enriched cells were immunoprecipated with MKP-1 antibody followed by immunoblot against γH2AX. The G1 enriched phase of cell cycle was confirmed by flow cytometry (Fig 4.20A) and purity of mononucleosomes was checked on agarose gel (Fig 4.20B). Immunoprecipitated mononucleosome against MKP-1 and immunoblotted with γH2AX shows recruitment of MKP-1 at γH2AX bearing mononucleosomes after irradiation (Fig 4.20C).
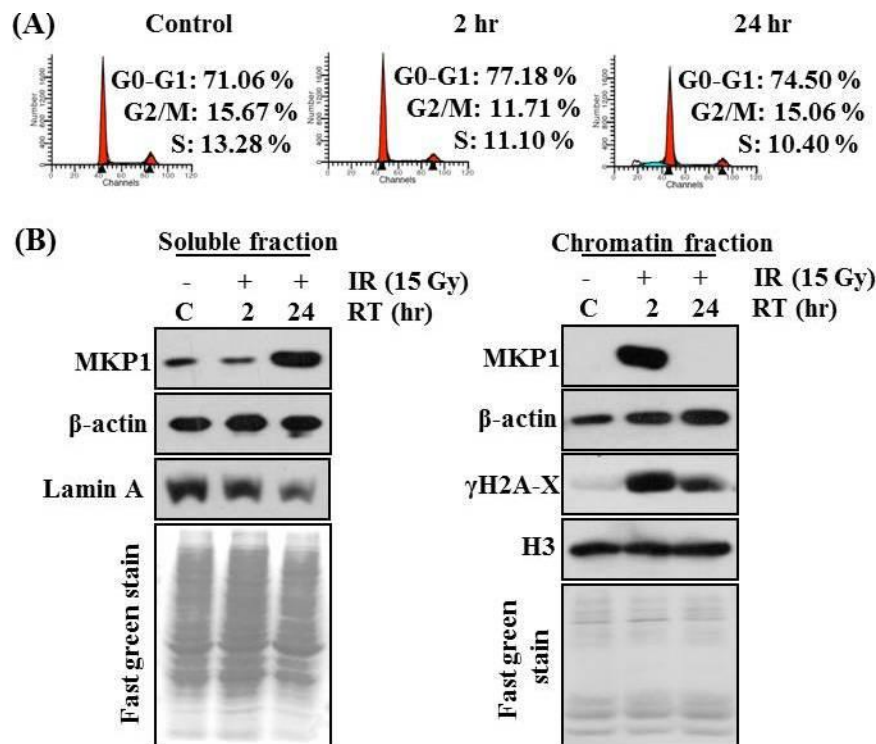
Figure 4.19 MKP1 associates with chromatin in response to DNA damage: *(A) G1 enriched cells were either non-irradiated or irradiated with 15Gy of IR. (A) Cell cycle distribution analysed by flow cytometry. Two hours later, cells were fractionated as described in Materials and methods. (B) Soluble fractions (SF) were resolved on 10% whereas chromatin fractions (CF) were separated on 18% SDS-PAGE. Immunoblot was carried out against indicated antibodies. Protein transferred onto membrane was stained with fast green as a control. RT- recovery time after DNA damage*

The above data have shown presence of γH2AX and dephosphorylation of H3Ser10P on the same mononucleosome. Collectively, the data demonstrates MKP-1 as a potential phosphatase for H3Ser10P at DNA damage site.
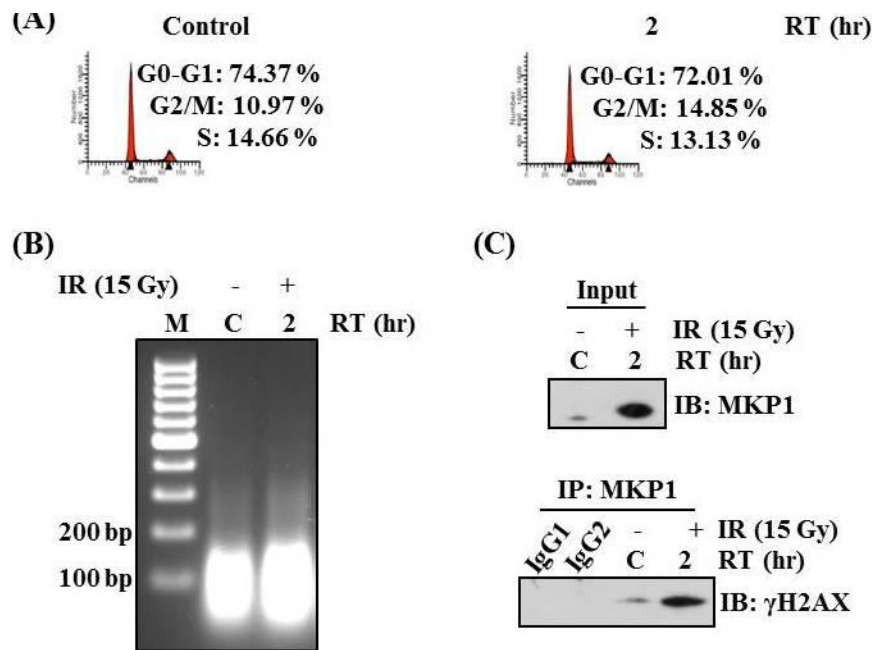
Figure 4.20: MKP1 interaction with mononucleosome bearing γH2AX after irradiation: (A) *WRL68 cells enriched in G1 phase were either non-irradiated or irradiated with 15Gy of IR and cell cycle profiling by flow cytometry. (**B**) The purified mono-nucleosome was resolved on 1.8% TAE-agarose gel to check the purity and size of mono-nucleosome. (**C**) The mononucleosomes prepared from cells as mentioned above were immunoprecipitated against MKP1 antibody and immunoblotted against γH2AX. RT-recovery time after DNA damage*

4.15. Reversible phosphorylation of H3Ser10 is mediated through dynamic balance between MKP-1 and MSK1 in G1 phase.

Kinney *et al* have shown DUSP1/MKP1 mediated dephosphorylation of H3Ser10 after stimulation of endothelial cells and down regulation of its own expression favoring H3Ser10P.[113] To investigate a link between immediate early gene, MKP1 and H3Ser10 dephosphorylation after irradiation, G1-enriched cells were treated with specific MKP-1 inhibitor, sanguinarine (10μM) for 1hr before irradiation. Western blot analysis against H3Ser10P suggests complete inhibition of H3Ser10 dephosphorylation in sanguinarine-treated irradiated cells whereas untreated irradiated cells show decrease of H3Ser10P (Fig 4.21A, upper panel). The cell cycle distribution at each time points as depicted in (Fig 4.21A, lower panels and appendix A8.12A). Cells treated with sanguinarine before

irradiation shows retention of γH2AX and phosphorylation of H3Ser10 during 'recovery'

phase of DDR. The presence of phosphorylated H3Ser10 may hamper repair of damaged

DNA as evident from retention of γH2AX level even in 'recovery' phase of DDR i.e.

24hr post-IR. Our immunofluorescence data also corroborates the above finding of

phosphorylation status of H3Ser10 and γH2AX foci (Fig 4.22, middle panel). The co-

localization of γH2AX foci (green) and H3Ser10P (red) is observed as 'yellow spots' in

sanguinarine-treated and irradiated G1 enriched cells (Fig 4.22, middle panel).
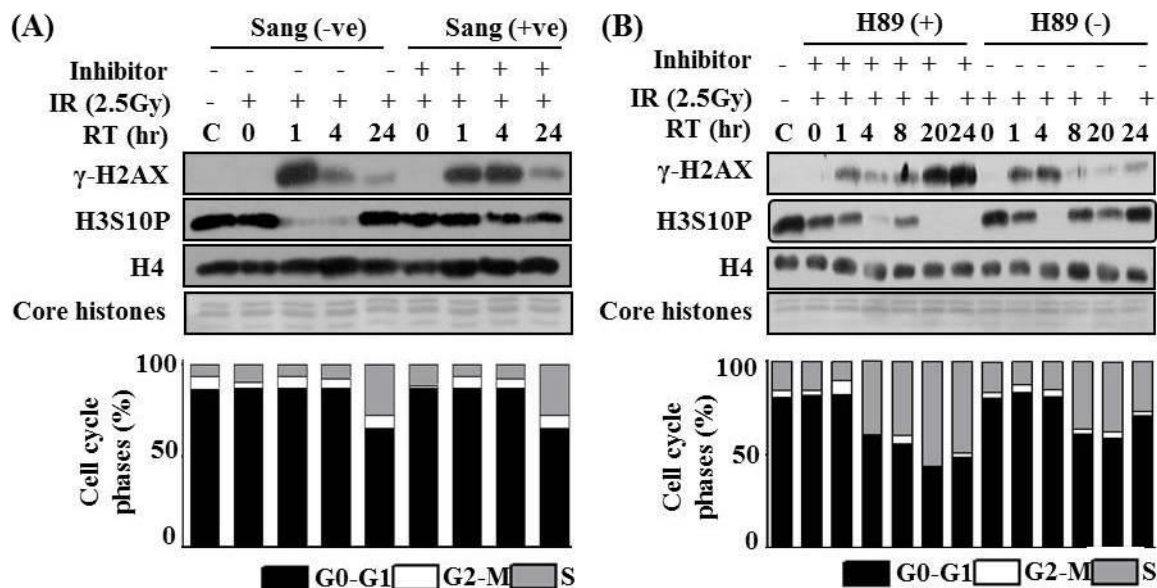
Figure 4.21: Reversible phosphorylation of H3S10 is mediated through dynamic balance between MKP1 and MSK1 in G1 phase. *G1-enriched WRL68 cells were untreated or pre-treated with inhibitor independently i.e. (A) Sanguinarine (10μM) or (B) H89 (20μM) for 1hr before 2.5Gy IR treatment. Histones were purified after indicated repair time points and subjected to western blotting with antibodies against indicated histone marks. H4 is used as equal loading control. The cell cycle distribution were determined by flow cytometry as shown in appendix (A16 upper panel and lower panel). Histogram data represents percentage of cells in respective phase of cell cycle (4.21A lower and 4.21B lower panel). RT-Recovery time after DNA damage*

Collectively, our data demonstrate MKP-1 as a phosphatase for dephosphorylation of

H3Ser10P in response to IR in G1-phase cells. The cells with double negative mutant of

MKP-1 have been also shown reduced colonogenic survival in response to IR.[161] To

90
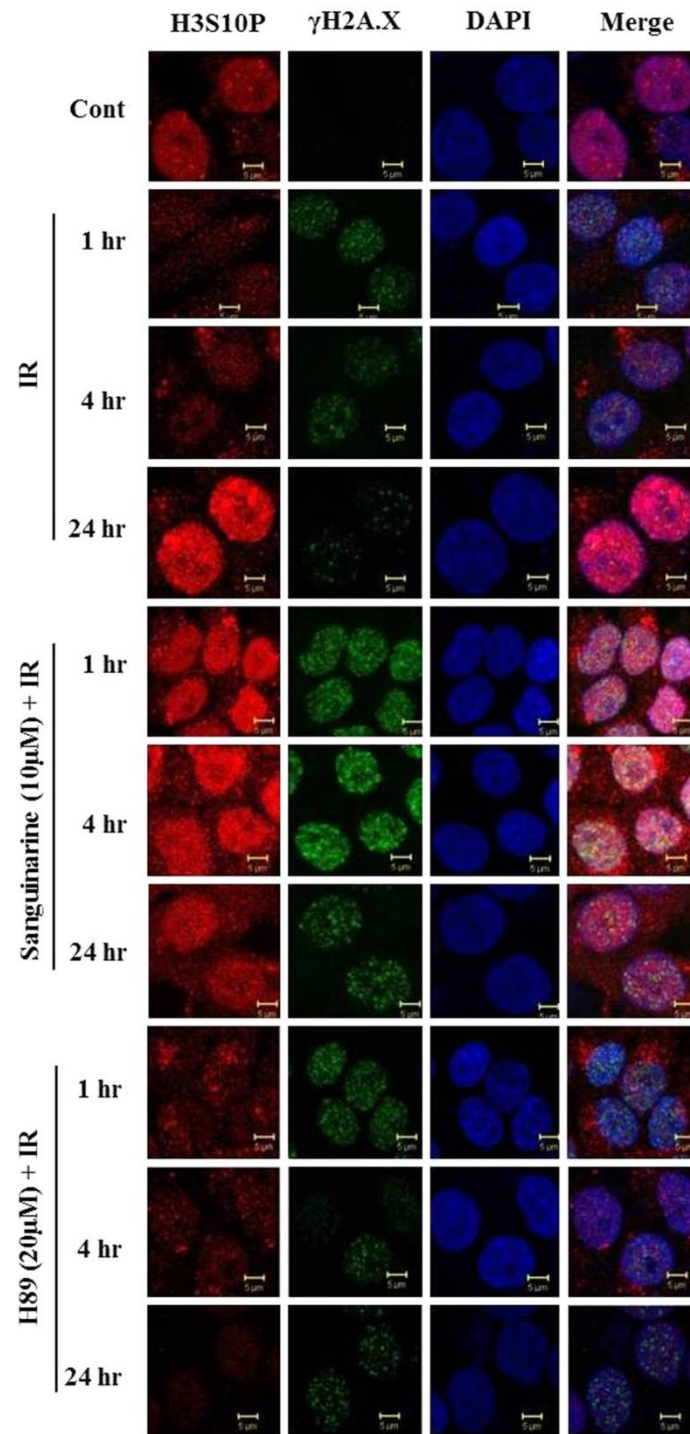
Figure 4.22: Immunoflourescence staining of H3Ser10P and γH2AX after MKP1 and MSK1 inhibition during DDR. *G1-enriched WRL68 cells were untreated or pre-treated with inhibitor i.e. sanguinarine (10µM) or H89 (20µM) for 1hr before 2.5Gy IR treatment. The cells were fixed after indicated time points (RT) and processed for immunofluorescence staining with γH2AX (green) and H3Ser10P (red). DNA in nuclei was counterstained by DAPI. Control+IR [left panel], sanguinarine+IR [middle panel] and H89+IR [right panel].*

identify the possible role of MSK1 as a downstream kinase of the MAP kinases pathway

responsible for mediating IR-induced restoration of H3Ser10 phosphorylation in

'recovery' phase, the G1-enriched cells were treated with a specific nucleosomal kinase inhibitor of MSK1, H89 1hr before irradiation [50]. Western blot with anti-H3Ser10P shows decrease in phosphorylation of H3Ser10 in 'repair' phase (1 to 8hr) in H89-treated as well as untreated cells. However, in 'recovery' phase (20 to 24hr), restoration of H3Ser10P is inhibited in irradiated H89-treated cells in comparison to untreated irradiated cells (Fig 4.21B, upper and lower panel). This demonstrates MSK1 as downstream kinase for phosphorylation of H3Ser10 during recovery phase of DNA damage response in G1-phase. In parallel, western with γH2AX antibody shows normal kinetics of γH2AX in untreated irradiated cells.

In contrast, level of γH2AX shows a significant increase and retention of γH2AX foci in recovery phase of H89-treated irradiated cells (Fig 4.22, lower panel). The data suggests that in recovery phase H3Ser10P restoration is inhibited and coincided with increase in γH2AX in H89-treated irradiated cells. Our immunofluorescence data is in coherence with the above finding of phosphorylation status of H3Ser10 and γH2AX foci (Fig 4.22). Collectively these data revealed that the reversible change in H3Ser10P is under tight regulation of downstream effector of MAP kinase pathway i.e. MKP-1 phosphatase and MSK1 kinase during IR-induced DDR in G1 phase of cell cycle.

4.16. Inhibition of MKP1 and MSK1 promotes radiation-induced cell death.

MKP-1 is known to be induced by γ-radiation and over expression of MKP-1 represses radiation-induced pro-apoptotic status in cells.[161] Further, studies suggest MKP-1 over expressing human DU145 prostate cancer cells are resistant to Fas ligand-induced mitochondrial perturbations and cellular apoptosis.[155, 162] The abrogation of MKP-1 activity increases radiosensitivity and the down-regulation of MKP-1 is also known to sensitize cancer cells to radiotherapy.[161, 163] Our studies have shown that the

phosphorylation of H3Ser10 and H2AX is abrogated after inhibition of MKP-1 and

MSK1 in response to DNA damage. Further, localization of MKP1 at the site of DNA

damage suggested that MKP-1 have a functional role in DNA repair. Consistent with

these observations we asked whether blocking of MKP-1 and MSK-1 promotes radiation-

induced cell death.
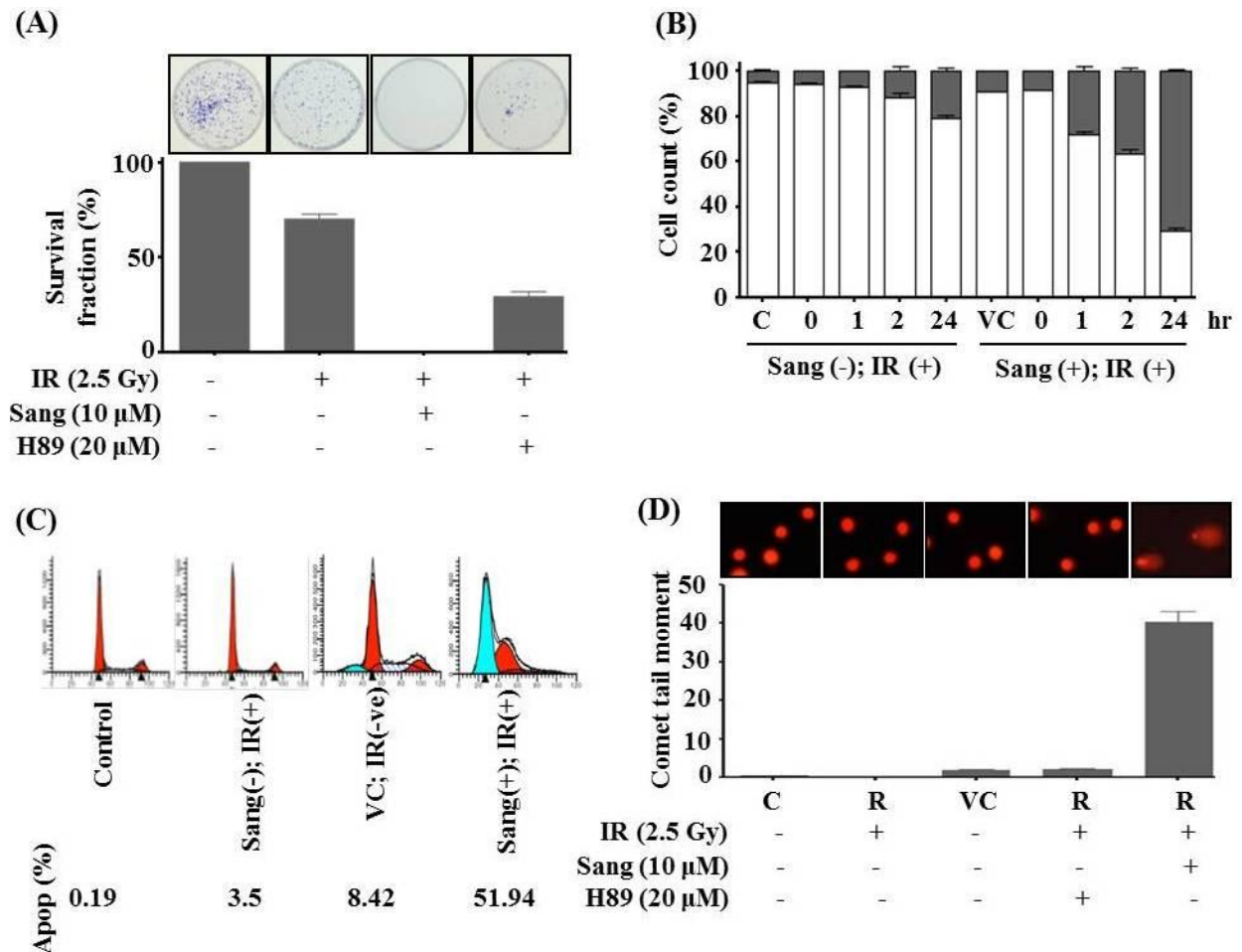
Figure 4.23: Inhibition of MKP1 and MSK1 activity promotes radiation-induced apoptosis. *WRL68 cells were pre-treated with MKP1 (Sanguinarine, 10μM) and/or MSK-1 inhibitors (H89, 20μM) and irradiated with 2.5 Gy IR. The cells were incubated for indicated time periods for recovery (RT) and processed independently for colony formation, cell viability, cell cycle analysis and comet assay. (A) Colony formation assay: Cells (n=300) were treated with specific inhibitors, irradiated, washed, incubated for 14 days to allow colonies formation, fixed and stained with crystal violet (upper panel). The survival fraction was calculated as the colony formation efficiency of the treated cells compared with control (lower panel). (B) Cell Viability assay: Cells after irradiation at respective indicated time points (0, 1, 4 and 24 hr after DNA damage) were stained with trypan blue, and dead and viable cells were counted by haemocytometer from three independent experiments. (C) Flow cytometry analysis for Sub-G0 apoptotic population after recovery for 24h after irradiation. (D) Comet Assay: Total of fifty nuclei from were analysed by CASP software for assessment of DNA damage by comet tail moment. Data for above experiments were pooled from three independent experiments and average value was represented as bars graph. C-Control, VC- Vehicle control and R- Recovery time after irradiation.*

The colony formation assay shows total cell death in cells treated with sanguinarine before IR (Fig 4.23A). However, the cells treated with MSK1 inhibitor, H89 shows significant decrease in colony number compared to only IR treated cells. The data strengthens the earlier finding that inhibition of dephosphorylation of H3Ser10P by MKP-1 inhibitor in response to IR may be important for the DNA repair process and the integrity of the genome. Further, inhibiting the restoration of H3Ser10P by MSK1 inhibitor, H89 hampers the dephosphorylation of γH2AX and may be affecting the recovery of native chromatin state which result in poor cell survival. The cell viability studies by trypan blue staining shows that the cells treated with MKP-1 inhibitor followed by irradiation induce more than 50% cell death compared to IR-treated cells after 24hrs of recovery (Fig 4.23B). Further, flow cytometry data of cells treated with MKP-1 inhibitor before irradiation shows increase of sub-G1 apoptotic (Sub-G1 fraction) population as compare to only irradiated and control cells (Fig 4.23C). The comet tail moment of cells pre-treated with MKP-1 inhibitors and irradiated with IR show heavy DNA damage suggesting impaired recovery compared to control and MSK1 inhibitor treated cells after 24hr recovery time point (Fig 4.23D). Collectively, the data suggest that the inhibition of dephosphorylation of H3Ser10P in response of DNA damage affects the DNA repair mechanism and induces cell death.

Chapter 5

Discussion

The covalent histone modifications undergo dynamic alterations throughout the cell cycle and thus regulate distinct chromatin state and functions in specific phase of cell cycle.[91, 92] Activation of the DNA damage response (DDR) following the detection of DNA breaks leads to cell cycle arrest and DNA repair which occurs in close context of chromatin structure to ensure genome integrity and cell survival. Recent reports demonstrate that alteration in chromatin structure are primarily mediated through damage responsive 'histone marks' to facilitate effective DNA damage response. Thus, these histone marks not only undergo dynamic alteration in context of DNA damage, but also changes dynamically during cell cycle progression. The phosphorylation of H3Ser10 is associated with dual activities during progression of cell cycle, induce chromatin condensation in mitosis and thus play a key role in chromosome segregation, whereas in interphase, favours chromatin relaxation which activate gene transcription.[143] Previous studies have shown ambiguous result of increase or decrease of H3Ser10P in response to DNA damage[105-108] which may be due to the use of different (a) doses of radiation, (b) time for histone marks analysis after damage, (c) extract preparation and damage treatment, (d) asynchronous population of cells, and (e) DNA damaging agents. Therefore, damage induced alterations in histone mark, H3Ser10P and its regulation need scientific clarity.

In this study we have demonstrated that dephosphorylation of H3Ser10 is mediated through MKP1 and chromatin condensation in 'repair phase' whereas restoration of phosphorylation is favoured by MSK1 with chromatin relaxation in 'recovery phase' of DDR in response to clinically-relevant and high-dose of IR in G1 phase of cell cycle. The reduction of H3Ser10P occurs during the 'prime' and 'repair phase' of DNA damage response but its basal level is restored during 'recovery phase' and also shows inverse correlation with kinetics of γH2AX level. The level of γH2AX is induced immediately, whereas H3Ser10P is gradually dephosphorylated from the chromatin in response to

DNA damage. γH2AX attains maximum level within 30mins whereas complete dephosphorylation of H3Ser10 takes ~6hrs after induction of DSB by irradiation. Therefore, the data suggests that the decrease of H3Ser10 dephosphorylation may be initiated by increase of Ser139 phosphorylation (γH2AX). The reversible reduction of H3Ser10 is inversely correlated with γH2AX level in both untransformed (WRL68) and transformed (HepG2) cells at both the doses of IR during DDR. The untransformed liver cells at lethal dose take longer period to repair their damaged DNA in comparison to transformed cells as evident by retention of γH2AX and G2/M phase arrest. The global profiling of histone modifications in tumour samples or transformed cell lines has shown hyper acetylation of H4Lys5 and H4Lys8, hypoacetylation of H4Lys12 and H4Lys16, and loss of H4Lys20me3 and H3Lys9me3.[164] These alterations in histone marks are also known to induce distinct chromatin landscape which may affect the efficient DNA damage response in transformed cells. The basal level of pre-existing histone marks, H4Lys16Ac, H3Lys9me3 and H4Lys20me3 in normal cells are also reported to play an important role in 'prime and repair' phase of DDR.[54] Therefore, the differential behaviour of DNA repair in untransformed cells and transformed cells may be due to efficient repair of damaged DNA with proper histone marks in cell cycle phase arrest to prevent chromosomal aberration in untransformed cells, whereas tumour cells have altered histone marks that may change the chromatin structure and thereby acquire genetic aberrations during tumour progression leading to compromised checkpoint which facilitates faster cell cycle progression in tumour cells.[165, 166] The level of H3Ser10P is known to change in between different phases of cell cycle with highest level in mitosis. The serum starved cells are released with serum containing media and are allowed to cycle in different phases. The decrease in H3Ser10P observed in response to DNA damage is not observed in non-irradiated cycling cells. The non-irradiated cells entered in

either S or G2/M phase of cell cycle at ~20-24 hrs resulting in gradual increase of H3Ser10P. The change in histone modifications will play a critical role and may be directly associated with repair of damaged DNA and change in chromatin state when they alter at and around flanking region of DSBs or on the same nucleosome bearing γH2AX. Our studies have revealed for the first time that dephosphorylation of H3Ser10P occur at the same mononucleosomes bearing γH2AX signifying the alteration of cell cycle specific histone marks during DDR. Also, this establishes that reversible reduction of H3Ser10P in 'repair and recovery phase' are associated within the flanking region of DSBs and supports our notion that H3Ser10P is an integral component for maintaining genomic stability in G1 phase cells.

We have demonstrated that dephosphorylation of H3Ser10P level is a G1-specific universal DNA damage responsive histone mark in cell lines of different tissue origin and in response to different DNA damaging agents. The response to radiation and genotoxic agents vary widely in cell lines from different tissue origin may be due to different genetic and epigenetic background.[145] The level of reduction in H3Ser10P with induction in γH2AX is more prominent in MCF7 and A549 compared to U87, U2OS and A2780 in response to IR. The differential alteration in the γH2AX level induction and H3Ser10P may be due to the differences in radio-sensitivity of these cell lines. The differential level of alteration at chromatin and DNA damage induced by different DNA damaging agents, adriamycin and etoposide induce DSB, cisplatin forms 1, 2-intrastand d(CpG) adducts, whereas UV induce thymine-thymine dimer formation and H_2O_2 induce single strand break may be responsible for differential γH2AX induction and H3Ser10P reduction. The differential alteration of chromatin states is evident from non-uniform appearance of γH2AX level in response to various damaging agents. Earlier reports have shown γH2AX as an indicator of cellular sensitivity after radiotherapy and chemotherapy.[167-169] In

addition, H2BS14 is also reported to be rapidly phosphorylated at sites of DNA double-strand breaks and accumulated in to irradiation-induced foci.[53] Our studies have shown that irradiation of G1-phase cells induce phosphorylation of H2AX and dephosphorylation H3Ser10P, whereas G2/M and S-phase cells have phosphorylated H3S10 as well as H2AX. Earlier reports suggest that the G2/M cells are being more sensitive to IR-induced cell death compared to G1 cells. It is therefore tempting to speculate that the H3S10 phosphorylation may be the critical step for cell fate that functions downstream of MAPK pathways in response to irradiation. The future experiments will be able to support or refute this intriguing concept. The G1-specific loss of H3Ser10P during different phases of cell cycle may be due to differential chromatin organisation and neighbouring histone marks in response to IR induce DNA damage. H3Ser10P is tightly regulated by its neighboring histone marks which are different in different phase of cell cycle. Mitotic H3Ser10 phosphorylation induce association of HP1 to H3 methylated at Lys9, ejecting HP1 protein from chromatin and recruiting cohesion protein that further induces rearrangement of chromatin to higher order structure in heterochromatin. In contrast, phosphorylation of H3Ser10 occurs in interphase cells is restricted to significantly smaller fractions of nucleosomes and tightly linked with acetylation of H3Lys9 and H3Lys14 on the same H3 tails favouring open chromatin organisation for the activation of transcription. The phosphorylation of H3Ser28 along with H3Ser10 is also related to transcriptional activities during interphase and increases predominantly in chromosomes during early mitosis and coincides with the initiation of mitotic chromosomes condensation.[170-172] The H3Ser10P decreases drastically compared to H3Ser28P in G1-enriched cells in response to IR. The level of H3Ser28P like H3Ser10P remains unaltered in S and G2/M enriched cells. In asynchronous population of cells the H3Ser10P decreases prominently whereas H3Ser28P doesn't show detectable

reduction after irradiation. *In-silico* docking studies have shown that dual acetylation on H3Lys9 and H3Lys14, flanking H3Ser10P is a prerequisite condition for phosphatase MKP-1 to interact and mediate dephosphorylation of H3Ser10P after irradiation. Whereas, H3Ser28 is not flanked by dual acetylation sites and this may be the probable reason for its differential dephosphorylation in response to irradiation. The neighboring combinations of histone marks of H3Ser10P and Ser28P may facilitate recruitment of erasers proteins in response to DNA damage in G1 phase of cell cycle which needs further scientific investigation. The level of H3Ser10P doesn't change in 'repair phase' of S and pro-M synchronized cells in coherence with increase of γH2AX in response to IR induced DNA damage. However, in 'recovery phase' (24hr post-IR) of S and pro-M synchronized cells, the cells repair their damaged DNA, cycle to G2/M and G1 phases, and therefore shows an increase and decrease in level of H3Ser10P, respectively. This experimental evidence raises the importance of cell cycle synchronization and time of analysis after DNA damage for evaluation of specific alteration of histones marks in response to DNA damage and their association with specific phase of cell cycle.

Further, we have also demonstrated that the specific loss of serine10 phosphorylation is predominantly from H3.3 variant after DNA damage in G1-enriched cells but the cells arrested in pro-M phase show presence of Ser10P at all the variants of H3 which remain unaltered in response to DNA damage. Earlier study has suggested decrease in H3Ser10P is due to change in mitotic population of cells, a cell cycle phase where this PTM is most abundant [36]. Our studies of serine 10 on H3 variant profiling in cell cycle phases, G1 and pro-M phase clearly shows presence of cell cycle specific H3 variants in both the phases and specific loss of serine 10 phosphorylation occur predominantly from H3.3 in G1 phase. Previous report suggests that there is enrichment in acetylation of the histones variants H3.3 as compared with the replicative histone H3.1 and 3.2. Majority of

modifications present on H3.3 represent a transcriptionaly active region of the chromatin.[144] Interestingly, comparisons of the H3.1 and H3.2 PTMs in mammals have shown that H3.2 is enriched in modification associated with transcriptional repression whereas H3.1 carries both active and repressive marks. Also, H3.3 variant is reported to be predominantly present in transcriptionaly active chromatin in G1-phase of cell cycle.[173] These findings strongly suggests that reduction of Ser10P level is predominantly from H3.3 variant and specific to G1 phase cells in response to DNA damage and not due to reduction in proportion of mitotic cells after post-irradiation. Further, recent reports revealed that transcription inhibition and its restoration are achieved at 2hr and 24hr post-IR, respectively and recovery of H3.3 at damage sites is mediated by HIRA chaperone to restore active transcription post-recovery.[174] In concert with our data, it is tempting to speculate that predominant loss of H3.3Ser10P after 2hr of DNA damage and chromatin condensation may be associated with inhibition of transcription at damage sites whereas restoration of H3.3Ser10P after 24hr of recovery may restore open chromatin organisation and active transcription. It will be interesting to explore association between initial loss and restoration of transcription and reversible decrease in DNA damage responsive marks, H3Ser10P, H3Lys9Ac, H3Lys14Ac and H3Lys56Ac in response to DNA damage.

Histone PTMs are known to regulate the DDR by the dynamic cross-talk with other modifications, recruitment of proteins at sites of DNA damage and alteration in chromatin structure. The pre-existence of H3Ser10P and acetylated neighbouring lysine (Lys9, Lys14 and Lys56) residues induce repulsive force between intra- and inter-nucleosomal interactions on chromatin fibre and favouring relaxed chromatin state thus facilitating active transcription.[114, 175, 176] The acetylation on H3Lys56 alone is sufficient to cause a 7-fold increase in DNA breathing on the nucleosome.[98] Previous studies suggest that there

is reversible reduction of H3Lys56Ac and H3Lys9Ac in response to DNA damage.[60, 61, 101-103] Further, HDAC1 and HDAC2 are recruited to promote hypo-acetylation of H3Lys56 which facilitates efficient DSB repair particularly NHEJ.[62] Thus reduction of phosphorylation from H3Ser10 with induction of γH2AX along with hypo-acetylation of H3 at Lys9, Lys14 and Lys56 will minimizes the repulsive force on nucleosomes and may induce compact chromatin state in 'repair phase' of DDR in G1 phase of the cell cycle as demonstrated by MNase digestion assay. Previous studies on asynchronous population of cells have suggested that DNA damage is accompanied by chromatin relaxation during initial phase of the repair process.[40, 148] But conflicting reports have shown repressive chromatin organization and direct evidence is the accumulation of heterochromatin protein HP1 variants at DSB sites.[27, 150] The compact chromatin could influence DNA repair efficiency by upsurge of repair proteins in the surrounding area of the DSB, favouring tethering of damage DNA molecule and decreases the chances of aberrant DNA repair. The similar mode of chromatin organization has also been proposed for increase in γH2AX which modulates NHEJ and protects genomic integrity.[177] Also, the inhibition or delay in transcription due to de-phosphorylation of H3Ser10 will prevent transcription from interfering with DNA repair process. Therefore, we propose initial remodelling of chromatin in 'repair phase' may be essential for maintaining the condensed state of chromatin for efficient repair of DNA damage. Since affinity of GCN5 increases for H3 when Ser10 of H3 get phosphorylated as compare to H3 but recent studies demonstrate that HDAC1 and HDAC2 get recruited to damage site and mediate reduction of H3Lys56Ac and H4Lys16Ac. In agreement with our observation about reduction of H3Ser10P at damage sites immediately after DNA damage may be responsible for recruitment of HDAC1 and 2 which need further scientific investigation. After DNA damage gets repaired, the decrease of γH2AX phosphorylation, increase of

H3Ser10P may favour open chromatin organization in 'recovery phase' and facilitate active transcription in G1 phase of cell cycle.

The contribution of H3Ser10P to chromatin dynamics and defining the precise functions during DDR cannot be easily determined by genetic manipulation. The multiple copies of histone H3 genes and their homomorphous variants makes it difficult to study effect of different modifications individually or in combination by generating mutants. Therefore, specific inhibitor against modifiers becomes the better alternative to understand regulation of H3Ser10 phosphorylation in DDR. Our results show that the MAP kinases (ERK1/2, JNK, p38 and MSK1) phosphorylation status decreases with increase in the level of MKP1 immediately after IR in G1phase of cell cycle. Further our inhibitor studies against MKP1 demonstrate that dephosphorylation p-ERK1/2, p-p38, p-JNK and p-MSK1 are mediated by MKP1 in response to DNA damage. Also, MKP-1 is known to be induced by γ-radiation and repressed radiation-induced pro-apoptotic status.[155] [53]. Ataxia Telangiectasia Mutated (ATM) down-regulates phospho-ERK1/2 via activation of MKP1 in response to radiation[161] whereas induction of MKP-1 by H_2O_2 correlates with inactivation of JNK and p38 activity. Over expression of MKP-1 increases cell resistance to H_2O_2-induced death.[178] Previous studies suggest that H3Ser10P and its neighbouring modified residues influence its interaction with 'writer', 'reader' and 'eraser' proteins. *In silico* studies suggested that the complex of MKP1 and H3Lys9Ac, Ser10P, Lys14Ac has the strongest binding affinity compared to other combination of modification or native histone H3. The residues involved in the interaction with phosphorylated Ser10 are mostly from active site of MKP1. Interestingly, cysteine256 (Cys256) which is an active site residue of MKP-1 shows H-bond interaction with phosphorylated S10 residue of H3. Thus, MKP-1 has a domain to interact with H3Ser10P and it neighbouring acetylated H3K9 and H3K14 residues which increases the binding affinity. These observation

corroborates with the experimental evidences that G1-enriched cells has pre-existing H3Lys9Ac, H3Ser10P and H3Lys14Ac which act as a prerequisite condition, for recruitment of MKP-1 to mediate selectively dephosphorylation of H3Ser10P after DNA damage. Further, our *in silico* docking studies between MSK1 and different combination of site-specific histone H3 modifications on Lys9, Ser10, and Lys14 suggests that MSK1 interacts more strongly with native H3 than H3 acetylated at Lys9 and Lys14. Our present studies are in agreement with earlier reports of reversible reduction of H3Lys9Ac, Lys14Ac, and Lys56Ac in response to DNA damage.[61, 103] Thus, overall the data supports that acetylation is not a prerequisite for phosphorylation of H3Ser10 by MSK1 during recovery phase of DNA damage.

In agreement with earlier reports and our data also suggest that MKP1 is highly inducible by IR-radiation and localizes at γH2AX bearing nucleosomes which may be responsible for dephosphorylation of H3Ser10P from the same mononucleosome at DNA damage site. The immediate increase in level of MKP1 is due to stability of protein mediated by post-translational modifications but not due to transcriptional activation of gene.[161] The specific inhibitor of MKP1 or MSK1 alters the dynamic phosphorylation of H3Ser10 with accumulation of γH2AX after IR-induced DNA damage in G1-enriched cells. It is tempting to speculate in consent with our results that the incomplete restoration of H3Ser10P affects the restoration of native chromatin state. Our result suggests that γH2AX foci accumulated in sanguinarine-treated irradiated cells in 'repair phase' and H89-treated irradiated cells in 'recovery phase' of DDR as compare to untreated irradiated cells which may be due to reactivation of ATM mediated through altered chromatin organization.[179] Our functional studies have shown total cell death with increase in sub-G1 population in sanguinarine and irradiated cells as compared to only irradiated cells. The maintenance of phosphorylation on H3Ser10 by MKP-1 inhibitor,

sanguinarine and persistence of γH2AX in G1-enriched cells during DDR likely reflect the clustering of damaged chromatin regions that contain complex DNA damages involving multiple lesions that are refractory to repair. These DNA damages can be carried over a few cell divisions, which may induce multiple errors and accumulation of chromosomal aberrations finally leading to cell death. Further, earlier studies have shown that after completion of DNA repair, either γH2AX is replaced with H2AX or dephosphorylation of γH2AX by PP4.[180, 181] It will be interesting to understand whether along with phosphorylation and dephosphorylation of chromatin bound H3Ser10 by MSK1 and MKP-1, respectively other mechanisms like replacement with parental H3 are playing a role in its recruitment during DDR. The study supports that DNA strand breaks causes change in nucleosomal organization mediated through histone marks in 'prime and repair' phase if not restored in 'recovery' phase will affect the repair mechanism and genomic surveillance. Further our studies point to an involvement of downstream effector phosphatase and kinase of MAP kinase pathway in regulation of DNA damage responsive histone marks H3Ser10P in response to DNA damage in G1 phase of cell cycle and further add up to epigenetic experimental evidences for MAP kinase pathway response against ionization irradiation induced genotoxic stress.

DNA damage and inability to faithfully segregate chromosome to two daughter cells – leading to aneuploidy is a wide spread phenomenon in solid tumors that is thought to promote tumour progression. The recurrent mutation in H3F3A in paediatric and young adult glioblastoma multiforme, which encodes the replication-independent histone H3 variant H3.3 led to amino acid substitutions at two critical positions within the histone tail (Lys27Meth, Gly34Arg/Gly34Val) involved in key regulatory post-translational modifications and is associated with disease pathogenesis.[182] The present study suggests that distinct predominant reversible histone mark, H3.3Ser10P is associated with DNA

damage response in G1-phase of cell cycle and plays a critical role in chromatin organization which facilitates maintenance of genomic stability and may promote differential sensitivity against radiation in cell cycle-specific manner. Also, recent reports have shown that H3Ser10 phosphorylation mediates deregulation of RNA polymerase III genes resulting in cell proliferation and transformation.[183] Previous studies demonstrate that reduction of H3Lys56Ac and H4Lys16Ac which is mediated by HDAC1 and 2 at damage sites promote non-homologous end joining repair system which is predominant in G1 phase of cell cycle and further deregulation of these histone marks results in impaired DNA repair process.[62] Further, histone deacetylases like HDAC1, HDAC2 and phosphatase, MKP-1 are also known to over-express in many cancer.[162, 184] Multiple HDAC inhibitors, like vorinostat, valproic acid are under clinical evaluation as a potential therapeutic agent for cancer.[185] The present study has shown that blocking the reversible reduction of H3Ser10P by MKP-1 inhibitor, sanguinarine impair DNA repair processes in G1 phase cells and results in poor survival of cells in response to irradiation. Thus, the study raises the possibility of combining radiotherapy with combinatorial modulation of H3S10P and histone acetylation with specific inhibitors to target the cancer cells in G1-phase and may serve as a promising target for cancer therapy.

Chapter 6

Summary & Conclusions

Chromatin acts as a natural hindrance in 'prime, repair and recovery' phase of DNA-damage response. The complex array of histone modifications/variants alters the overall charge and conformation of chromatin which helps in recruitment of factors at damage site to facilitate repair, and thus in maintaining genomic integrity in response to DNA damaging agents. Histone modifications in regulation of transcription are well studied but recent studies are unraveling role of histone marks in the DDR. These DNA damage responsive histone marks not only undergo alteration in response to DNA damage but also are known to be altered during cell cycle to facilitate distinct chromatin states and function in specific phase of cell cycle. Histone mark, H3Ser10 phosphorylation is highly dynamic and plays a dual role in different phases of cell cycle, maintaining relaxed chromatin state for active transcription in interphase and condensed chromatin state for segregation in mitosis. Previous studies have shown ambiguous result of increase or decrease of H3Ser10P in response to DNA damage in asynchronous population of cells. Therefore, damage induced alterations in H3Ser10P mark and its regulation in specific phase of cell cycle needs scientific clarity. Therefore, our study delineated the alteration of H3Ser10P and its regulation in G1-phase of cell cycle in response to DNA damage in human cells.

The salient findings of the work done are:

- The phosphorylation of H3Ser10 decreases in 'prime-repair' phase of DDR and is restored in 'recovery' phase in response to IR induced DNA damage in G1 enriched cells.

- The phosphorylation of H2AX at Ser139 (γH2AX) is inversely correlated with decrease of H3Ser10P in response DNA damage in G1 enriched cells.

- The reversible reduction of H3Ser10P after IR is concomitant with DNA damage response and not associated with cell cycle progression.

- The profiling of H3Ser10P in cells enriched in different phases of cell cycle, G1, S, G2/M and pro-M established that change in H3Ser10P is only associated with G1 phase of cell cycle in response to IR induced DNA damage.

- The reduction of H3Ser10P level is independent of cell lines of different tissue origin and DNA damaging agents suggesting H3Ser10P is a universal phenomenon and potential DNA damage responsive histone mark for G1 phase cells.

- The decrease of H3Ser10 phosphorylation is predominantly from H3.3 variant in G1-enriched cells.

- The reversible reduction in H3Ser10P in G1-enriched cells is associated with deacetylation of histone marks Lys9, Lys14 and Lys56 on H3.

- The phosphorylation of H2AX (γH2AX) and dephosphorylation of H3Ser10 occurs from same mono-nucleosome in response to DNA damage.

- The changes in histone modifications are associated with condensation and decondensation of chromatin in 'prime-repair' and 'recovery' phase of DDR in G1-enriched cells.

- The phosphorylation status of H3Ser10 in G1 phase cells is correlated with phosphorylation of MAP kinases and their de-phosphorylation by MKP1 in response to irradiation.

- The MKP-1 interacts with highest affinity to H3 modified at Lys9Ac, Ser10P, Lys14Ac compared to native histone H3 and therefore, acetylation of Lys9 and Lys14 is the pre-requisite for dephosphorylation of H3Ser10 as shown by *insilco* studies.

- *Insilco* studies have shown that MSK1 interacts with native histone H3 with highest binding affinity and acetylation of Lys9 and Lys14 is not the pre-requisite for phosphorylation of H3 at Ser10.

- The MKP-1 interacts with the mononucleosomes bearing γH2AX in response to DNA damage.

- The reversible phosphorylation of H3Ser10 is mediated through dynamic balance between MKP-1 and MSK1 activity during DDR during G1 phase cells.

- The inhibition of MKP-1 and MSK1 activities by specific inhibitors promotes radiation-induced cell death.

Dynamic change in G1-specific DNA-damage responsive histone mark, H3Ser10 phosphorylation
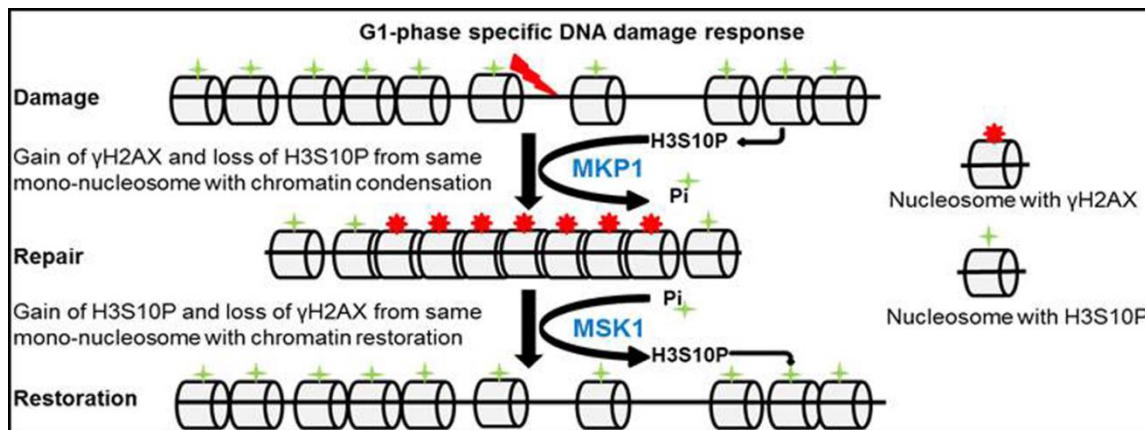
To summaries, H3Ser10P decreases from the γH2AX bearing mono-nucleosomes in response to IR induced DNA damage and inversely correlated with the level of γH2AX in 'prime-repair' phase with restoration in 'recovery' phase of DDR specifically from G1-enriched cells. The reversible reduction of H3Ser10P is regulated by opposing activities of phosphatase, MKP-1 and kinase, MSK1 of the MAP kinase pathway in response to DNA damage. The present work has shown that reversible reduction of histone mark,

H3Ser10P is required for efficient repair of DNA damage and blocking the activity of MKP-1 increases the sensitivity against radiation and induces cell death. Further, histone deacetylases like HDAC1, HDAC2 and phosphatase, MKP-1 are known to over-express in many cancers. Thus, the study proposes that the combinatorial modulation of histone phosphorylation and acetylation marks with specific inhibitors may targets the radio-resistant cancer cells.

Chapter 7

Bibliography

1.   Holliday R. The inheritance of epigenetic defects. Science 1987; 238:163-70.
2.   Holliday R. Epigenetics: an overview. Developmental genetics 1994; 15:453-7.
3.   Sawan C, Vaissiere T, Murr R, Herceg Z. Epigenetic drivers and genetic passengers on the road to cancer. Mutation research 2008; 642:1-13.
4.   Goldberg AD, Allis CD, Bernstein E. Epigenetics: a landscape takes shape. Cell 2007; 128:635-8.
5.   Watson JD. Celebrating the genetic jubilee: a conversation with James D. Watson. Interviewed by John Rennie. Scientific American 2003; 288:66-9.
6.   Kornberg RD. Chromatin structure: a repeating unit of histones and DNA. Science 1974; 184:868-71.
7.   Luger K, Mader AW, Richmond RK, Sargent DF, Richmond TJ. Crystal structure of the nucleosome core particle at 2.8 A resolution. Nature 1997; 389:251-60.
8.   Allfrey VG, Faulkner R, Mirsky AE. Acetylation and Methylation of Histones and Their Possible Role in the Regulation of Rna Synthesis. Proceedings of the National Academy of Sciences of the United States of America 1964; 51:786-94.
9.   Turner BM. Cellular memory and the histone code. Cell 2002; 111:285-91.
10. Dawson MA, Kouzarides T. Cancer epigenetics: from mechanism to therapy. Cell 2012; 150:12-27.
11. Tropberger P, Schneider R. Going global: novel histone modifications in the globular domain of H3. Epigenetics : official journal of the DNA Methylation Society 2010; 5:112-7.
12. Santos-Rosa H, Kirmizis A, Nelson C, Bartke T, Saksouk N, Cote J, et al. Histone H3 tail clipping regulates gene expression. Nature structural & molecular biology 2009; 16:17-22.
13. Strahl BD, Allis CD. The language of covalent histone modifications. Nature 2000; 403:41-5.
14. Jenuwein T, Allis CD. Translating the histone code. Science 2001; 293:1074-80.
15. Zlatanova J, Thakar A. H2A.Z: view from the top. Structure 2008; 16:166-79.
16. Altaf M, Auger A, Covic M, Cote J. Connection between histone H2A variants and chromatin remodeling complexes. Biochemistry and cell biology = Biochimie et biologie cellulaire 2009; 87:35-50.
17. Stiff T, O'Driscoll M, Rief N, Iwabuchi K, Lobrich M, Jeggo PA. ATM and DNA-PK function redundantly to phosphorylate H2AX after exposure to ionizing radiation. Cancer research 2004; 64:2390-6.
18. Costanzi C, Pehrson JR. MACROH2A2, a new member of the MARCOH2A core histone family. The Journal of biological chemistry 2001; 276:21776-84.
19. Perche PY, Vourc'h C, Konecny L, Souchier C, Robert-Nicoud M, Dimitrov S, et al. Higher concentrations of histone macroH2A in the Barr body are correlated with higher nucleosome density. Current biology : CB 2000; 10:1531-4.
20. Hake SB, Garcia BA, Duncan EM, Kauer M, Dellaire G, Shabanowitz J, et al. Expression patterns and post-translational modifications associated with mammalian histone H3 variants. The Journal of biological chemistry 2006; 281:559-68.

21. Sarma K, Reinberg D. Histone variants meet their match. Nature reviews Molecular cell biology 2005; 6:139-49.

22. Hanahan D, Weinberg RA. Hallmarks of cancer: the next generation. Cell 2011; 144:646-74.

23. Rouse J, Jackson SP. Interfaces between the detection, signaling, and repair of DNA damage. Science 2002; 297:547-51.

24. Jackson SP, Bartek J. The DNA-damage response in human biology and disease. Nature 2009; 461:1071-8.

25. Smerdon MJ. DNA repair and the role of chromatin structure. Current opinion in cell biology 1991; 3:422-8.

26. Deem AK, Li X, Tyler JK. Epigenetic regulation of genomic integrity. Chromosoma 2012; 121:131-51.

27. Luijsterburg MS, Dinant C, Lans H, Stap J, Wiernasz E, Lagerwerf S, et al. Heterochromatin protein 1 is recruited to various types of DNA damage. The Journal of cell biology 2009; 185:577-86.

28. Soria G, Polo SE, Almouzni G. Prime, repair, restore: the active role of chromatin in the DNA damage response. Molecular cell 2012; 46:722-34.

29. Ljungman M. The DNA damage response--repair or despair? Environmental and molecular mutagenesis 2010; 51:879-89.

30. Bartek J, Lukas J. DNA damage checkpoints: from initiation to recovery or adaptation. Current opinion in cell biology 2007; 19:238-45.

31. Shiloh Y. ATM and related protein kinases: safeguarding genome integrity. Nature reviews Cancer 2003; 3:155-68.

32. Zhou BB, Elledge SJ. The DNA damage response: putting checkpoints in perspective. Nature 2000; 408:433-9.

33. Riley T, Sontag E, Chen P, Levine A. Transcriptional control of human p53-regulated genes. Nature reviews Molecular cell biology 2008; 9:402-12.

34. Kastan MB, Bartek J. Cell-cycle checkpoints and cancer. Nature 2004; 432:316-23.

35. Takahashi K, Kaneko I. Changes in nuclease sensitivity of mammalian cells after irradiation with 60Co gamma-rays. International journal of radiation biology and related studies in physics, chemistry, and medicine 1985; 48:389-95.

36. Shim EY, Hong SJ, Oum JH, Yanez Y, Zhang Y, Lee SE. RSC mobilizes nucleosomes to improve accessibility of repair machinery to the damaged chromatin. Molecular and cellular biology 2007; 27:1602-13.

37. Kruhlak MJ, Celeste A, Dellaire G, Fernandez-Capetillo O, Muller WG, McNally JG, et al. Changes in chromatin structure and mobility in living cells at sites of DNA double-strand breaks. The Journal of cell biology 2006; 172:823-34.

38. Tsukuda T, Fleming AB, Nickoloff JA, Osley MA. Chromatin remodelling at a DNA double-strand break site in Saccharomyces cerevisiae. Nature 2005; 438:379-83.

39. Goodarzi AA, Jeggo P, Lobrich M. The influence of heterochromatin on DNA double strand break repair: Getting the strong, silent type to relax. DNA repair 2010; 9:1273-82.

40.   Ziv Y, Bielopolski D, Galanty Y, Lukas C, Taya Y, Schultz DC, et al. Chromatin relaxation in response to DNA double-strand breaks is modulated by a novel ATM- and KAP-1 dependent pathway. Nature cell biology 2006; 8:870-6.

41.   Goodarzi AA, Noon AT, Deckbar D, Ziv Y, Shiloh Y, Lobrich M, et al. ATM signaling facilitates repair of DNA double-strand breaks associated with heterochromatin. Molecular cell 2008; 31:167-77.

42.   Berkovich E, Monnat RJ, Jr., Kastan MB. Roles of ATM and NBS1 in chromatin structure modulation and DNA double-strand break repair. Nature cell biology 2007; 9:683-90.

43.   Rogakou EP, Pilch DR, Orr AH, Ivanova VS, Bonner WM. DNA double-stranded breaks induce histone H2AX phosphorylation on serine 139. The Journal of biological chemistry 1998; 273:5858-68.

44.   Rogakou EP, Boon C, Redon C, Bonner WM. Megabase chromatin domains involved in DNA double-strand breaks in vivo. The Journal of cell biology 1999; 146:905-16.

45.   Chanoux RA, Yin B, Urtishak KA, Asare A, Bassing CH, Brown EJ. ATR and H2AX cooperate in maintaining genome stability under replication stress. The Journal of biological chemistry 2009; 284:5994-6003.

46.   Celeste A, Petersen S, Romanienko PJ, Fernandez-Capetillo O, Chen HT, Sedelnikova OA, et al. Genomic instability in mice lacking histone H2AX. Science 2002; 296:922-7.

47.   Bassing CH, Alt FW. H2AX may function as an anchor to hold broken chromosomal DNA ends in close proximity. Cell Cycle 2004; 3:149-53.

48.   Xiao A, Li H, Shechter D, Ahn SH, Fabrizio LA, Erdjument-Bromage H, et al. WSTF regulates the H2A.X DNA damage response via a novel tyrosine kinase activity. Nature 2009; 457:57-62.

49.   Cook PJ, Ju BG, Telese F, Wang X, Glass CK, Rosenfeld MG. Tyrosine dephosphorylation of H2AX modulates apoptosis and survival decisions. Nature 2009; 458:591-6.

50.   Ahn SH, Cheung WL, Hsu JY, Diaz RL, Smith MM, Allis CD. Sterile 20 kinase phosphorylates histone H2B at serine 10 during hydrogen peroxide-induced apoptosis in S. cerevisiae. Cell 2005; 120:25-36.

51.   Cheung WL, Turner FB, Krishnamoorthy T, Wolner B, Ahn SH, Foley M, et al. Phosphorylation of histone H4 serine 1 during DNA damage requires casein kinase II in S. cerevisiae. Current biology : CB 2005; 15:656-60.

52.   Utley RT, Lacoste N, Jobin-Robitaille O, Allard S, Cote J. Regulation of NuA4 histone acetyltransferase activity in transcription and DNA repair by phosphorylation of histone H4. Molecular and cellular biology 2005; 25:8179-90.

53.   Fernandez-Capetillo O, Allis CD, Nussenzweig A. Phosphorylation of histone H2B at DNA double-strand breaks. The Journal of experimental medicine 2004; 199:1671-7.

54.   Hunt CR, Ramnarain D, Horikoshi N, Iyengar P, Pandita RK, Shay JW, et al. Histone modifications and DNA double-strand break repair after exposure to ionizing radiations. Radiation research 2013; 179:383-92.

55. Kumar R, Horikoshi N, Singh M, Gupta A, Misra HS, Albuquerque K, et al. Chromatin modifications and the DNA damage response to ionizing radiation. Frontiers in oncology 2012; 2:214.

56. Murr R, Loizou JI, Yang YG, Cuenin C, Li H, Wang ZQ, et al. Histone acetylation by Trrap-Tip60 modulates loading of repair proteins and repair of DNA double-strand breaks. Nature cell biology 2006; 8:91-9.

57. Taipale M, Rea S, Richter K, Vilar A, Lichter P, Imhof A, et al. hMOF histone acetyltransferase is required for histone H4 lysine 16 acetylation in mammalian cells. Molecular and cellular biology 2005; 25:6798-810.

58. Sharma GG, So S, Gupta A, Kumar R, Cayrou C, Avvakumov N, et al. MOF and histone H4 acetylation at lysine 16 are critical for DNA damage response and double-strand break repair. Molecular and cellular biology 2010; 30:3582-95.

59. Fraga MF, Ballestar E, Villar-Garea A, Boix-Chornet M, Espada J, Schotta G, et al. Loss of acetylation at Lys16 and trimethylation at Lys20 of histone H4 is a common hallmark of human cancer. Nature genetics 2005; 37:391-400.

60. Das C, Lucia MS, Hansen KC, Tyler JK. CBP/p300-mediated acetylation of histone H3 on lysine 56. Nature 2009; 459:113-7.

61. Tjeertes JV, Miller KM, Jackson SP. Screen for DNA-damage-responsive histone modifications identifies H3K9Ac and H3K56Ac in human cells. The EMBO journal 2009; 28:1878-89.

62. Miller KM, Tjeertes JV, Coates J, Legube G, Polo SE, Britton S, et al. Human HDAC1 and HDAC2 function in the DNA-damage response to promote DNA nonhomologous end-joining. Nature structural & molecular biology 2010; 17:1144-51.

63. Chen CC, Carson JJ, Feser J, Tamburini B, Zabaronick S, Linger J, et al. Acetylated lysine 56 on histone H3 drives chromatin assembly after repair and signals for the completion of repair. Cell 2008; 134:231-43.

64. Huyen Y, Zgheib O, Ditullio RA, Jr., Gorgoulis VG, Zacharatos P, Petty TJ, et al. Methylated lysine 79 of histone H3 targets 53BP1 to DNA double-strand breaks. Nature 2004; 432:406-11.

65. Botuyan MV, Lee J, Ward IM, Kim JE, Thompson JR, Chen J, et al. Structural basis for the methylation state-specific recognition of histone H4-K20 by 53BP1 and Crb2 in DNA repair. Cell 2006; 127:1361-73.

66. Pei H, Zhang L, Luo K, Qin Y, Chesi M, Fei F, et al. MMSET regulates histone H4K20 methylation and 53BP1 accumulation at DNA damage sites. Nature 2011; 470:124-8.

67. Ayoub N, Jeyasekharan AD, Bernal JA, Venkitaraman AR. HP1-beta mobilization promotes chromatin changes that initiate the DNA damage response. Nature 2008; 453:682-6.

68. Sun Y, Jiang X, Xu Y, Ayrapetov MK, Moreau LA, Whetstine JR, et al. Histone H3 methylation links DNA damage detection to activation of the tumour suppressor Tip60. Nature cell biology 2009; 11:1376-82.

69.   Ikura T, Tashiro S, Kakino A, Shima H, Jacob N, Amunugama R, et al. DNA damage-dependent acetylation and ubiquitination of H2AX enhances chromatin dynamics. Molecular and cellular biology 2007; 27:7028-40.

70.   Stewart GS, Panier S, Townsend K, Al-Hakim AK, Kolas NK, Miller ES, et al. The RIDDLE syndrome protein mediates a ubiquitin-dependent signaling cascade at sites of DNA damage. Cell 2009; 136:420-34.

71.   Bergink S, Salomons FA, Hoogstraten D, Groothuis TA, de Waard H, Wu J, et al. DNA damage triggers nucleotide excision repair-dependent monoubiquitylation of histone H2A. Genes & development 2006; 20:1343-52.

72.   Ismail IH, Andrin C, McDonald D, Hendzel MJ. BMI1-mediated histone ubiquitylation promotes DNA double-strand break repair. The Journal of cell biology 2010; 191:45-60.

73.   Moyal L, Lerenthal Y, Gana-Weisz M, Mass G, So S, Wang SY, et al. Requirement of ATM-dependent monoubiquitylation of histone H2B for timely repair of DNA double-strand breaks. Molecular cell 2011; 41:529-42.

74.   Dery U, Masson JY. Twists and turns in the function of DNA damage signaling and repair proteins by post-translational modifications. DNA repair 2007; 6:561-77.

75.   San Filippo J, Sung P, Klein H. Mechanism of eukaryotic homologous recombination. Annual review of biochemistry 2008; 77:229-57.

76.   Beucher A, Birraux J, Tchouandong L, Barton O, Shibata A, Conrad S, et al. ATM and Artemis promote homologous recombination of radiation-induced DNA double-strand breaks in G2. The EMBO journal 2009; 28:3413-27.

77.   Lieber MR. The mechanism of human nonhomologous DNA end joining. The Journal of biological chemistry 2008; 283:1-5.

78.   Williamson EA, Wray JW, Bansal P, Hromas R. Overview for the histone codes for DNA repair. Progress in molecular biology and translational science 2012; 110:207-27.

79.   Faucher D, Wellinger RJ. Methylated H3K4, a transcription-associated histone modification, is involved in the DNA damage response pathway. PLoS genetics 2010; 6.

80.   Ogiwara H, Ui A, Otsuka A, Satoh H, Yokomi I, Nakajima S, et al. Histone acetylation by CBP and p300 at double-strand break sites facilitates SWI/SNF chromatin remodeling and the recruitment of non-homologous end joining factors. Oncogene 2011; 30:2135-46.

81.   Williams RS, Williams JS, Tainer JA. Mre11-Rad50-Nbs1 is a keystone complex connecting DNA repair machinery, double-strand break signaling, and the chromatin template. Biochemistry and cell biology = Biochimie et biologie cellulaire 2007; 85:509-20.

82.   Tamburini BA, Tyler JK. Localized histone acetylation and deacetylation triggered by the homologous recombination pathway of double-strand DNA repair. Molecular and cellular biology 2005; 25:4903-13.

83.   Oishi H, Kitagawa H, Wada O, Takezawa S, Tora L, Kouzu-Fujita M, et al. An hGCN5/TRRAP histone acetyltransferase complex co-activates BRCA1

transactivation function through histone modification. The Journal of biological chemistry 2006; 281:20-6.

84. Hanks SK, Rodriguez LV, Rao PN. Relationship between histone phosphorylation and premature chromosome condensation. Experimental cell research 1983; 148:293-302.

85. Sharma GG, Hwang KK, Pandita RK, Gupta A, Dhar S, Parenteau J, et al. Human heterochromatin protein 1 isoforms HP1(Hsalpha) and HP1(Hsbeta) interfere with hTERT-telomere interactions and correlate with changes in cell growth and response to ionizing radiation. Molecular and cellular biology 2003; 23:8363-76.

86. Aucott R, Bullwinkel J, Yu Y, Shi W, Billur M, Brown JP, et al. HP1-beta is required for development of the cerebral neocortex and neuromuscular junctions. The Journal of cell biology 2008; 183:597-606.

87. Downs JA, Nussenzweig MC, Nussenzweig A. Chromatin dynamics and the preservation of genetic information. Nature 2007; 447:951-8.

88. Sanders SL, Portoso M, Mata J, Bahler J, Allshire RC, Kouzarides T. Methylation of histone H4 lysine 20 controls recruitment of Crb2 to sites of DNA damage. Cell 2004; 119:603-14.

89. Gupta A, Sharma GG, Young CS, Agarwal M, Smith ER, Paull TT, et al. Involvement of human MOF in ATM function. Molecular and cellular biology 2005; 25:5292-305.

90. Pederson T. Chromatin structure and the cell cycle. Proceedings of the National Academy of Sciences of the United States of America 1972; 69:2224-8.

91. Kouzarides T. Chromatin modifications and their function. Cell 2007; 128:693-705.

92. Bonenfant D, Towbin H, Coulot M, Schindler P, Mueller DR, van Oostrum J. Analysis of dynamic changes in post-translational modifications of human histones during cell cycle by mass spectrometry. Molecular & cellular proteomics : MCP 2007; 6:1917-32.

93. Lennox RW, Oshima RG, Cohen LH. The H1 histones and their interphase phosphorylated states in differentiated and undifferentiated cell lines derived from murine teratocarcinomas. The Journal of biological chemistry 1982; 257:5183-9.

94. Talasz H, Helliger W, Puschendorf B, Lindner H. In vivo phosphorylation of histone H1 variants during the cell cycle. Biochemistry 1996; 35:1761-7.

95. Crosio C, Fimia GM, Loury R, Kimura M, Okano Y, Zhou H, et al. Mitotic phosphorylation of histone H3: spatio-temporal regulation by mammalian Aurora kinases. Molecular and cellular biology 2002; 22:874-85.

96. Shogren-Knaak M, Ishii H, Sun JM, Pazin MJ, Davie JR, Peterson CL. Histone H4-K16 acetylation controls chromatin structure and protein interactions. Science 2006; 311:844-7.

97. Davey CA, Sargent DF, Luger K, Maeder AW, Richmond TJ. Solvent mediated interactions in the structure of the nucleosome core particle at 1.9 a resolution. Journal of molecular biology 2002; 319:1097-113.

98. Neumann H, Hancock SM, Buning R, Routh A, Chapman L, Somers J, et al. A method for genetically installing site-specific acetylation in recombinant histones defines the effects of H3 K56 acetylation. Molecular cell 2009; 36:153-63.

99. Helleday T, Petermann E, Lundin C, Hodgson B, Sharma RA. DNA repair pathways as targets for cancer therapy. Nature reviews Cancer 2008; 8:193-204.

100. Guo R, Chen J, Mitchell DL, Johnson DG. GCN5 and E2F1 stimulate nucleotide excision repair by promoting H3K9 acetylation at sites of damage. Nucleic acids research 2011; 39:1390-7.

101. Yuan J, Pu M, Zhang Z, Lou Z. Histone H3-K56 acetylation is important for genomic stability in mammals. Cell Cycle 2009; 8:1747-53.

102. Vempati RK, Jayani RS, Notani D, Sengupta A, Galande S, Haldar D. p300-mediated acetylation of histone H3 lysine 56 functions in DNA damage response in mammals. The Journal of biological chemistry 2010; 285:28553-64.

103. Battu A, Ray A, Wani AA. ASF1A and ATM regulate H3K56-mediated cell-cycle checkpoint recovery in response to UV irradiation. Nucleic acids research 2011; 39:7931-45.

104. Huen MS, Grant R, Manke I, Minn K, Yu X, Yaffe MB, et al. RNF8 transduces the DNA-damage signal via histone ubiquitylation and checkpoint protein assembly. Cell 2007; 131:901-14.

105. Ozawa K. Reduction of phosphorylated histone H3 serine 10 and serine 28 cell cycle marker intensities after DNA damage. Cytometry Part A : the journal of the International Society for Analytical Cytology 2008; 73:517-27.

106. Monaco L, Kolthur-Seetharam U, Loury R, Murcia JM, de Murcia G, Sassone-Corsi P. Inhibition of Aurora-B kinase activity by poly(ADP-ribosyl)ation in response to DNA damage. Proceedings of the National Academy of Sciences of the United States of America 2005; 102:14244-8.

107. Tang X, Hui ZG, Cui XL, Garg R, Kastan MB, Xu B. A novel ATM-dependent pathway regulates protein phosphatase 1 in response to DNA damage. Molecular and cellular biology 2008; 28:2559-66.

108. Zhong SP, Ma WY, Dong Z. ERKs and p38 kinases mediate ultraviolet B-induced phosphorylation of histone H3 at serine 10. The Journal of biological chemistry 2000; 275:20980-4.

109. Sanz-Garcia M, Monsalve DM, Sevilla A, Lazo PA. Vaccinia-related kinase 1 (VRK1) is an upstream nucleosomal kinase required for the assembly of 53BP1 foci in response to ionizing radiation-induced DNA damage. The Journal of biological chemistry 2012; 287:23757-68.

110. Park CH, Kim KT. Apoptotic phosphorylation of histone H3 on Ser-10 by protein kinase Cdelta. PloS one 2012; 7:e44307.

111. Corpet A, Almouzni G. A histone code for the DNA damage response in mammalian cells? The EMBO journal 2009; 28:1828-30.

112. Healy S, Khan P, He S, Davie JR. Histone H3 phosphorylation, immediate-early gene expression, and the nucleosomal response: a historical perspective. Biochemistry and cell biology = Biochimie et biologie cellulaire 2012; 90:39-54.

113.   Kinney CM, Chandrasekharan UM, Yang L, Shen J, Kinter M, McDermott MS, et al. Histone H3 as a novel substrate for MAP kinase phosphatase-1. American journal of physiology Cell physiology 2009; 296:C242-9.

114.   Agalioti T, Chen G, Thanos D. Deciphering the transcriptional histone acetylation code for a human gene. Cell 2002; 111:381-92.

115.   Cheung P, Tanner KG, Cheung WL, Sassone-Corsi P, Denu JM, Allis CD. Synergistic coupling of histone H3 phosphorylation and acetylation in response to epidermal growth factor stimulation. Molecular cell 2000; 5:905-15.

116.   Demidov D, Hesse S, Tewes A, Rutten T, Fuchs J, Ashtiyani RK, et al. Aurora1 phosphorylation activity on histone H3 and its cross-talk with other post-translational histone modifications in Arabidopsis. The Plant journal : for cell and molecular biology 2009; 59:221-30.

117.   Hendzel MJ, Wei Y, Mancini MA, Van Hooser A, Ranalli T, Brinkley BR, et al. Mitosis-specific phosphorylation of histone H3 initiates primarily within pericentromeric heterochromatin during G2 and spreads in an ordered fashion coincident with mitotic chromosome condensation. Chromosoma 1997; 106:348-60.

118.   Prigent C, Dimitrov S. Phosphorylation of serine 10 in histone H3, what for? Journal of cell science 2003; 116:3677-85.

119.   Wei Y, Yu L, Bowen J, Gorovsky MA, Allis CD. Phosphorylation of histone H3 is required for proper chromosome condensation and segregation. Cell 1999; 97:99-109.

120.   Ma HT, Poon RY. Synchronization of HeLa cells. Methods in molecular biology 2011; 761:151-61.

121.   Vogt A, Tamewitz A, Skoko J, Sikorski RP, Giuliano KA, Lazo JS. The benzo[c]phenanthridine alkaloid, sanguinarine, is a selective, cell-active inhibitor of mitogen-activated protein kinase phosphatase-1. The Journal of biological chemistry 2005; 280:19078-86.

122.   Thomson S, Clayton AL, Hazzalin CA, Rose S, Barratt MJ, Mahadevan LC. The nucleosomal response associated with immediate-early gene induction is mediated via alternative MAP kinase cascades: MSK1 as a potential histone H3/HMG-14 kinase. The EMBO journal 1999; 18:4779-93.

123.   Singh NP, McCoy MT, Tice RR, Schneider EL. A simple technique for quantitation of low levels of DNA damage in individual cells. Experimental cell research 1988; 175:184-91.

124.   Bonenfant D, Coulot M, Towbin H, Schindler P, van Oostrum J. Characterization of histone H2A and H2B variants and their post-translational modifications by mass spectrometry. Molecular & cellular proteomics : MCP 2006; 5:541-52.

125.   Peterson GL. A simplification of the protein assay method of Lowry et al. which is more generally applicable. Analytical biochemistry 1977; 83:346-56.

126.   Wray W, Boulikas T, Wray VP, Hancock R. Silver staining of proteins in polyacrylamide gels. Analytical biochemistry 1981; 118:197-203.

127. Davie JR. Two-dimensional gel systems for rapid histone analysis for use in minislab polyacrylamide gel electrophoresis. Analytical biochemistry 1982; 120:276-81.

128. Pramod KS, Bharat K, Sanjay G. Mass spectrometry-compatible silver staining of histones resolved on acetic acid-urea-Triton PAGE. Proteomics 2009; 9:2589-92.

129. O'Farrell PH. High resolution two-dimensional electrophoresis of proteins. The Journal of biological chemistry 1975; 250:4007-21.

130. Towbin H, Staehelin T, Gordon J. Electrophoretic transfer of proteins from polyacrylamide gels to nitrocellulose sheets: procedure and some applications. Proceedings of the National Academy of Sciences of the United States of America 1979; 76:4350-4.

131. Delcuve GP, Davie JR. Western blotting and immunochemical detection of histones electrophoretically resolved on acid-urea-triton- and sodium dodecyl sulfate-polyacrylamide gels. Analytical biochemistry 1992; 200:339-41.

132. Jeong S, Stein A. Micrococcal nuclease digestion of nuclei reveals extended nucleosome ladders having anomalous DNA lengths for chromatin assembled on non-replicating plasmids in transfected cells. Nucleic acids research 1994; 22:370-5.

133. Mendez J, Stillman B. Chromatin association of human origin recognition complex, cdc6, and minichromosome maintenance proteins during the cell cycle: assembly of prereplication complexes in late mitosis. Molecular and cellular biology 2000; 20:8602-12.

134. Arnold K, Bordoli L, Kopp J, Schwede T. The SWISS-MODEL workspace: a web-based environment for protein structure homology modelling. Bioinformatics 2006; 22:195-201.

135. Laskowski RA, Rullmannn JA, MacArthur MW, Kaptein R, Thornton JM. AQUA and PROCHECK-NMR: programs for checking the quality of protein structures solved by NMR. Journal of biomolecular NMR 1996; 8:477-86.

136. Luthy R, Bowie JU, Eisenberg D. Assessment of protein models with three-dimensional profiles. Nature 1992; 356:83-5.

137. Colovos C, Yeates TO. Verification of protein structures: patterns of nonbonded atomic interactions. Protein science : a publication of the Protein Society 1993; 2:1511-9.

138. Macdonald N, Welburn JP, Noble ME, Nguyen A, Yaffe MB, Clynes D, et al. Molecular basis for the recognition of phosphorylated and phosphoacetylated histone h3 by 14-3-3. Molecular cell 2005; 20:199-211.

139. Dominguez C, Boelens R, Bonvin AM. HADDOCK: a protein-protein docking approach based on biochemical or biophysical information. Journal of the American Chemical Society 2003; 125:1731-7.

140. Wallace AC, Laskowski RA, Thornton JM. LIGPLOT: a program to generate schematic diagrams of protein-ligand interactions. Protein engineering 1995; 8:127-34.

141. Sawicka A, Seiser C. Histone H3 phosphorylation - a versatile chromatin modification for different occasions. Biochimie 2012; 94:2193-201.

142. Gurley LR, D'Anna JA, Barham SS, Deaven LL, Tobey RA. Histone phosphorylation and chromatin structure during mitosis in Chinese hamster cells. European journal of biochemistry / FEBS 1978; 84:1-15.

143. Nowak SJ, Corces VG. Phosphorylation of histone H3: a balancing act between chromosome condensation and transcriptional activation. Trends in genetics : TIG 2004; 20:214-20.

144. Hake SB, Allis CD. Histone H3 variants and their potential role in indexing mammalian genomes: the "H3 barcode hypothesis". Proceedings of the National Academy of Sciences of the United States of America 2006; 103:6428-35.

145. Amundson SA, Bittner M, Meltzer P, Trent J, Fornace AJ, Jr. Physiological function as regulation of large transcriptional programs: the cellular response to genotoxic stress. Comparative biochemistry and physiology Part B, Biochemistry & molecular biology 2001; 129:703-10.

146. Winter S, Simboeck E, Fischle W, Zupkovitz G, Dohnal I, Mechtler K, et al. 14-3-3 proteins recognize a histone code at histone H3 and are required for transcriptional activation. The EMBO journal 2008; 27:88-99.

147. Lo WS, Trievel RC, Rojas JR, Duggan L, Hsu JY, Allis CD, et al. Phosphorylation of serine 10 in histone H3 is functionally linked in vitro and in vivo to Gcn5-mediated acetylation at lysine 14. Molecular cell 2000; 5:917-26.

148. Carrier F, Georgel PT, Pourquier P, Blake M, Kontny HU, Antinore MJ, et al. Gadd45, a p53-responsive stress protein, modifies DNA accessibility on damaged chromatin. Molecular and cellular biology 1999; 19:1673-85.

149. Goodarzi AA, Kurka T, Jeggo PA. KAP-1 phosphorylation regulates CHD3 nucleosome remodeling during the DNA double-strand break response. Nature structural & molecular biology 2011; 18:831-9.

150. Baldeyron C, Soria G, Roche D, Cook AJ, Almouzni G. HP1alpha recruitment to DNA damage by p150CAF-1 promotes homologous recombination repair. The Journal of cell biology 2011; 193:81-95.

151. Hamilton C, Hayward RL, Gilbert N. Global chromatin fibre compaction in response to DNA damage. Biochemical and biophysical research communications 2011; 414:820-5.

152. Sassone-Corsi P, Mizzen CA, Cheung P, Crosio C, Monaco L, Jacquot S, et al. Requirement of Rsk-2 for epidermal growth factor-activated phosphorylation of histone H3. Science 1999; 285:886-91.

153. Chu Y, Solski PA, Khosravi-Far R, Der CJ, Kelly K. The mitogen-activated protein kinase phosphatases PAC1, MKP-1, and MKP-2 have unique substrate specificities and reduced activity in vivo toward the ERK2 sevenmaker mutation. The Journal of biological chemistry 1996; 271:6497-501.

154. Groom LA, Sneddon AA, Alessi DR, Dowd S, Keyse SM. Differential regulation of the MAP, SAP and RK/p38 kinases by Pyst1, a novel cytosolic dual-specificity phosphatase. The EMBO journal 1996; 15:3621-32.

155. Wang Z, Cao N, Nantajit D, Fan M, Liu Y, Li JJ. Mitogen-activated protein kinase phosphatase-1 represses c-Jun NH2-terminal kinase-mediated apoptosis via NF-kappaB regulation. The Journal of biological chemistry 2008; 283:21011-23.

156. Boutros T, Chevet E, Metrakos P. Mitogen-activated protein (MAP) kinase/MAP kinase phosphatase regulation: roles in cell growth, death, and cancer. Pharmacological reviews 2008; 60:261-310.

157. Hutter D, Chen P, Li J, Barnes J, Liu Y. The carboxyl-terminal domains of MKP-1 and MKP-2 have inhibitory effects on their phosphatase activity. Molecular and cellular biochemistry 2002; 233:107-17.

158. Smith KJ, Carter PS, Bridges A, Horrocks P, Lewis C, Pettman G, et al. The structure of MSK1 reveals a novel autoinhibitory conformation for a dual kinase protein. Structure 2004; 12:1067-77.

159. Sharma AK, Mansukh A, Varma A, Gadewal N, Gupta S. Molecular Modeling of Differentially Phosphorylated Serine 10 and Acetylated lysine 9/14 of Histone H3 Regulates their Interactions with 14-3-3zeta, MSK1, and MKP1. Bioinformatics and biology insights 2013; 7:271-88.

160. Zheng B, Han M, Bernier M, Wen JK. Nuclear actin and actin-binding proteins in the regulation of transcription and gene expression. The FEBS journal 2009; 276:2669-85.

161. Nyati MK, Feng FY, Maheshwari D, Varambally S, Zielske SP, Ahsan A, et al. Ataxia telangiectasia mutated down-regulates phospho-extracellular signal-regulated kinase 1/2 via activation of MKP-1 in response to radiation. Cancer research 2006; 66:11554-9.

162. Srikanth S, Franklin CC, Duke RC, Kraft RS. Human DU145 prostate cancer cells overexpressing mitogen-activated protein kinase phosphatase-1 are resistant to Fas ligand-induced mitochondrial perturbations and cellular apoptosis. Molecular and cellular biochemistry 1999; 199:169-78.

163. Koukourakis MI, Giatromanolaki A, Sheldon H, Buffa FM, Kouklakis G, Ragoussis I, et al. Phase I/II trial of bevacizumab and radiotherapy for locally advanced inoperable colorectal cancer: vasculature-independent radiosensitizing effect of bevacizumab. Clinical cancer research : an official journal of the American Association for Cancer Research 2009; 15:7069-76.

164. Chervona Y, Costa M. Histone modifications and cancer: biomarkers of prognosis? American journal of cancer research 2012; 2:589-97.

165. Bartkova J, Horejsi Z, Koed K, Kramer A, Tort F, Zieger K, et al. DNA damage response as a candidate anti-cancer barrier in early human tumorigenesis. Nature 2005; 434:864-70.

166. Gorgoulis VG, Vassiliou LV, Karakaidos P, Zacharatos P, Kotsinas A, Liloglou T, et al. Activation of the DNA damage checkpoint and genomic instability in human precancerous lesions. Nature 2005; 434:907-13.

167. Olive PL, Banath JP. Phosphorylation of histone H2AX as a measure of radiosensitivity. International journal of radiation oncology, biology, physics 2004; 58:331-5.

168. Clingen PH, Wu JY, Miller J, Mistry N, Chin F, Wynne P, et al. Histone H2AX phosphorylation as a molecular pharmacological marker for DNA interstrand crosslink cancer chemotherapy. Biochemical pharmacology 2008; 76:19-27.

169. Huang X, Okafuji M, Traganos F, Luther E, Holden E, Darzynkiewicz Z. Assessment of histone H2AX phosphorylation induced by DNA topoisomerase I and II inhibitors topotecan and mitoxantrone and by the DNA cross-linking agent cisplatin. Cytometry Part A : the journal of the International Society for Analytical Cytology 2004; 58:99-110.

170. Cerutti H, Casas-Mollano JA. Histone H3 phosphorylation: universal code or lineage specific dialects? Epigenetics : official journal of the DNA Methylation Society 2009; 4:71-5.

171. Goto H, Yasui Y, Nigg EA, Inagaki M. Aurora-B phosphorylates Histone H3 at serine28 with regard to the mitotic chromosome condensation. Genes to cells : devoted to molecular & cellular mechanisms 2002; 7:11-7.

172. Goto H, Tomono Y, Ajiro K, Kosako H, Fujita M, Sakurai M, et al. Identification of a novel phosphorylation site on histone H3 coupled with mitotic chromosome condensation. The Journal of biological chemistry 1999; 274:25543-9.

173. Ahmad K, Henikoff S. The histone variant H3.3 marks active chromatin by replication-independent nucleosome assembly. Molecular cell 2002; 9:1191-200.

174. Adam S, Polo SE, Almouzni G. Transcription Recovery after DNA Damage Requires Chromatin Priming by the H3.3 Histone Chaperone HIRA. Cell 2013; 155:94-106.

175. Nishida H, Suzuki T, Kondo S, Miura H, Fujimura Y, Hayashizaki Y. Histone H3 acetylated at lysine 9 in promoter is associated with low nucleosome density in the vicinity of transcription start site in human cell. Chromosome research : an international journal on the molecular, supramolecular and evolutionary aspects of chromosome biology 2006; 14:203-11.

176. Xie W, Song C, Young NL, Sperling AS, Xu F, Sridharan R, et al. Histone h3 lysine 56 acetylation is linked to the core transcriptional network in human embryonic stem cells. Molecular cell 2009; 33:417-27.

177. Fernandez-Capetillo O, Nussenzweig A. Linking histone deacetylation with the repair of DNA breaks. Proceedings of the National Academy of Sciences of the United States of America 2004; 101:1427-8.

178. Zhou JY, Liu Y, Wu GS. The role of mitogen-activated protein kinase phosphatase-1 in oxidative damage-induced cell death. Cancer research 2006; 66:4888-94.

179. Bakkenist CJ, Kastan MB. DNA damage activates ATM through intermolecular autophosphorylation and dimer dissociation. Nature 2003; 421:499-506.

180. Heo K, Kim H, Choi SH, Choi J, Kim K, Gu J, et al. FACT-mediated exchange of histone variant H2AX regulated by phosphorylation of H2AX and ADP-ribosylation of Spt16. Molecular cell 2008; 30:86-97.

181. Nakada S, Chen GI, Gingras AC, Durocher D. PP4 is a gamma H2AX phosphatase required for recovery from the DNA damage checkpoint. EMBO reports 2008; 9:1019-26.

182. Schwartzentruber J, Korshunov A, Liu XY, Jones DT, Pfaff E, Jacob K, et al. Driver mutations in histone H3.3 and chromatin remodelling genes in paediatric glioblastoma. Nature 2012; 482:226-31.

183. Zhong Q, Shi G, Zhang Q, Zhang Y, Levy D, Zhong S. Role of phosphorylated histone H3 serine 10 in DEN-induced deregulation of Pol III genes and cell proliferation and transformation. Carcinogenesis 2013.

184. Glozak MA, Seto E. Histone deacetylases and cancer. Oncogene 2007; 26:5420-32.

185. Camphausen K, Tofilon PJ. Inhibition of histone deacetylation: a strategy for tumor radiosensitization. Journal of clinical oncology : official journal of the American Society of Clinical Oncology 2007; 25:4051-6.

Chapter 8

Appendix

Appendix A 8.1 (A): Cell cycle distribution in G1 enriched population as depicted in Figure (Fig 4.3 and 4.5 A). Serum starved G1-enriched WRL68 and HepG2 cells were released 4hrs before 2.5 Gy IR irradiation with media containing 10% FBS. After indicated recovery time points cell cycle distribution were analysed by flow cytometer.

	C	0	0.25	0.50	1	2 Time (hrs)
G0-G1%:	81.78	83.37	83.19	80.93	82.42	81.13
G2/M%:	11.51	10.10	09.97	10.57	10.60	12.84
S%:	06.72	06.53	06.84	08.50	06.97	06.03

	4	6	8	16	20	24 Time (hrs)
G0-G1%:	71.95	74.82	68.40	58.18	64.93	69.06
G2/M%:	21.66	18.50	22.51	20.63	18.43	14.06
S%:	06.39	06.62	09.10	21.18	16.65	16.88

WRL68; IR (2.5 Gy)

	C	0	0.25	0.50	1	2 Time (hrs)
G0-G1%:	75.52	78.48	73.10	81.14	80.11	79.50
G2/M%:	06.31	12.27	10.36	08.87	08.79	09.23
S%:	18.17	09.25	16.54	09.99	11.09	11.27

	4	6	8	16	20	24 Time (hrs)
G0-G1%:	77.63	75.29	67.53	53.93	44.23	51.30
G2/M%:	08.15	06.09	05.22	11.74	24.85	24.17
S%:	14.22	18.62	27.25	34.33	30.51	24.53

HepG2 ; IR (2.5 Gy)
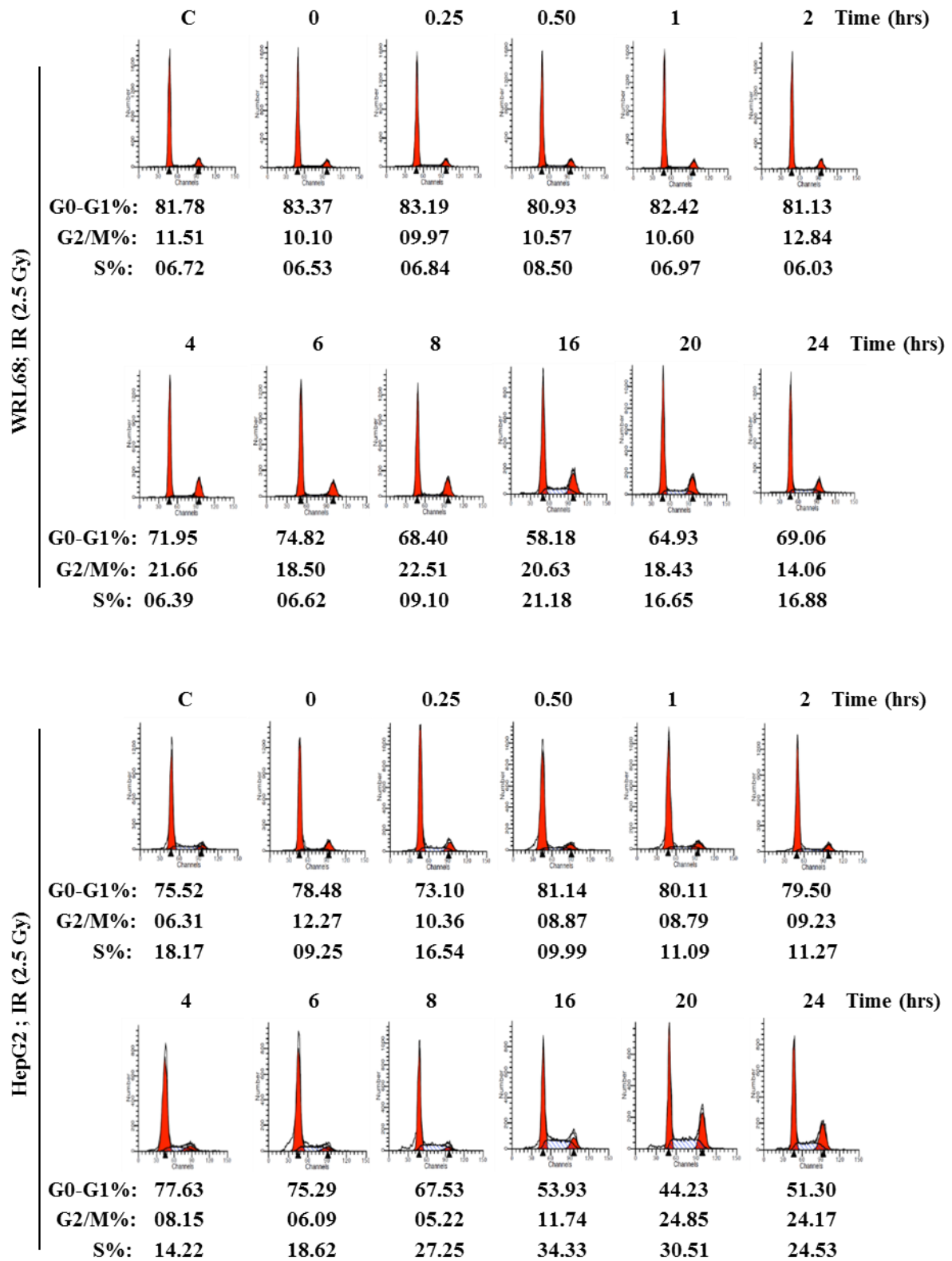
Appendix A8.1 (B): Cell cycle distribution in G1 enriched population as depicted in Figure (Fig 4.4 and 4.5 B). Serum starved G1-enriched WRL68 and HepG2 cells were released 4hrs before 2.5 Gy IR irradiation with media containing 10% FBS. After indicated recovery time point's cell cycle distribution were analysed by flow cytometer.

WRL68; IR (15 Gy)	C	0	0.25	0.50	1	2 Time (hrs)
G0-G1%:	83.60	80.69	78.18	77.04	74.02	79.44
G2/M%:	08.60	10.35	10.03	10.51	18.00	09.76
S%:	07.80	08.96	11.79	12.54	07.98	10.81

	4	6	8	16	20	24 Time (hrs)
G0-G1%:	76.13	74.93	68.18	52.63	40.02	45.04
G2/M%:	13.06	11.09	15.94	24.25	45.38	42.92
S%:	10.81	13.98	15.89	23.12	14.61	12.05

HepG2; IR (15 Gy)	C	0	0.25	0.50	1	2 Time (hrs)
G0-G1%:	71.17	70.08	77.54	79.23	73.85	74.43
G2/M%:	13.84	12.80	12.57	10.06	10.16	11.05
S%:	14.99	17.11	09.90	10.72	15.99	14.52

	4	6	8	16	20	24 Time (hrs)
G0-G1%:	73.46	70.00	67.53	77.64	81.48	73.60
G2/M%:	07.74	07.29	05.22	14.72	13.56	12.20
S%:	18.80	22.71	27.25	07.64	04.95	14.20

124
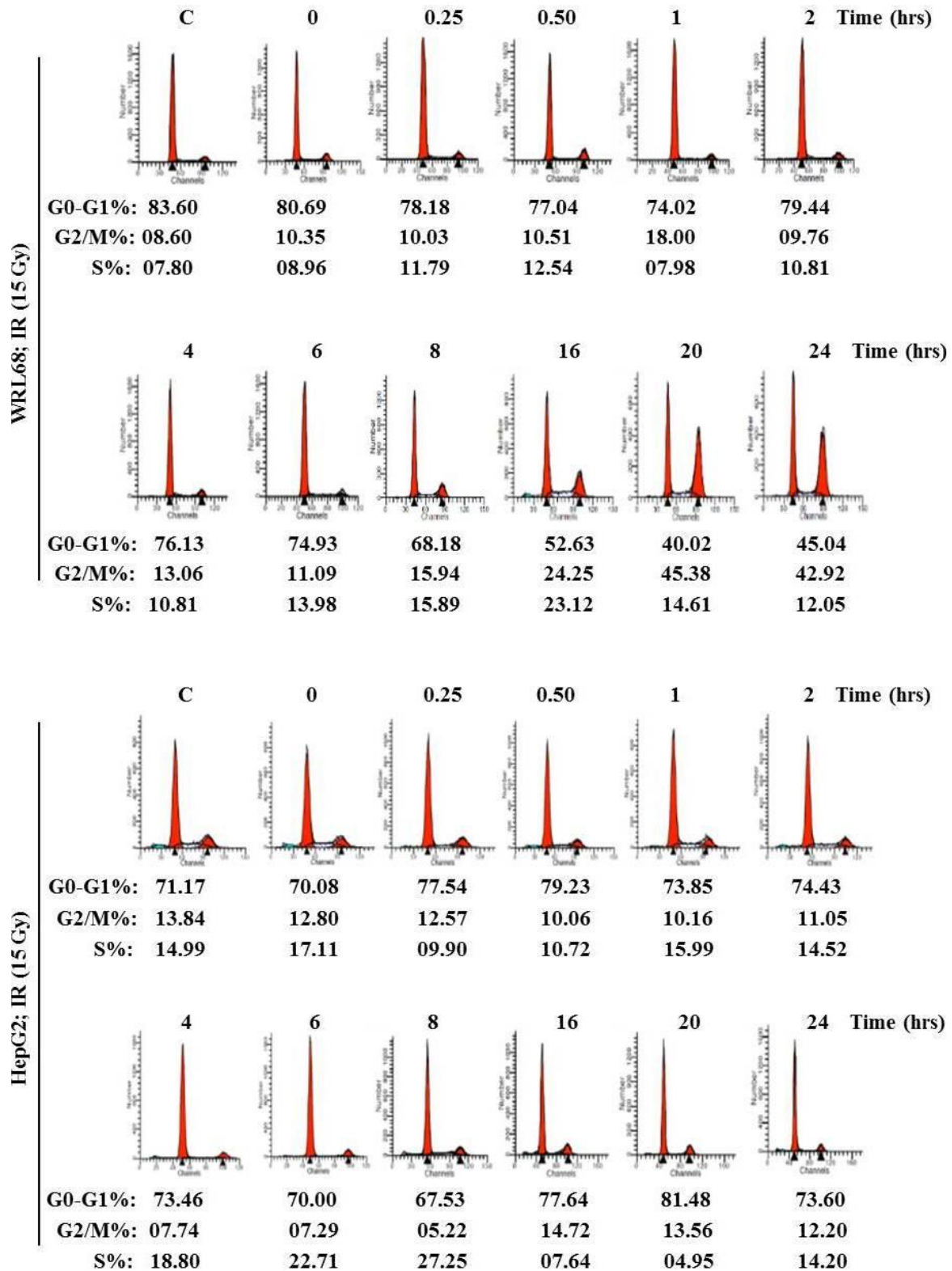
Appendix A 8.2: Cell cycle distribution G1, S and Pro-M phase arrested cells as depicted in (Fig 4.7 A). WRL68 Cells were enriched in G1, S phase of cell cycle with double thymidine block followed by release in complete media for respective time points and pro-M phase with nocodazole. Cell cycle distribution analysed by flow cytometry.

(A)

G1 arrest; IR (2.5 Gy)

	C	1	4	24
G0-G1%:	86.88	84.08	84.25	69.18
G2/M%:	06.98	06.71	05.96	14.33
S%:	06.14	09.22	09.79	16.49

G1 arrest; IR (15 Gy)

	C	1	4	24
G0-G1%:	82.37	78.72	82.79	69.25
G2/M%:	08.47	11.06	05.41	14.99
S%:	09.25	10.21	11.80	15.76

(B)

S arrest; IR (2.5 Gy)

	C	1	4	24
G0-G1%:	00.32	03.05	04.23	28.29
G2/M%:	08.74	00.00	02.41	33.26
S%:	90.95	96.95	95.77	38.45

S arrest; IR (15 Gy)

	1	4	24
G0-G1%:	01.30	01.99	13.34
G2/M%:	00.00	05.38	78.41
S%:	98.70	92.63	08.25

(C)

S arrest; IR (2.5 Gy)

	C	1	4	24
G0-G1%:	01.63	01.86	00.00	26.77
G2/M%:	91.12	91.46	91.64	29.86
S%:	07.26	06.68	08.36	43.37

Pro-M arrest; IR (15 Gy)

	C	1	4	24
G0-G1%:	00.44	01.86	00.38	53.37
G2/M%:	96.74	91.46	96.76	25.95
S%:	02.82	06.68	02.85	20.18

Time (hrs)

125

Appendix A 8.3: Cell cycle distribution G1, S and G2/M phase arrested cells as depicted in (Fig 4.7 B). WRL68 Cells were enriched in G1, S phase of cell cycle with double thymidine block followed by release in complete media for respective time points. Cell cycle distribution analysed by flow cytometry.

	Asynchronous		G1 phase enriched	
	C	IR (15 Gy)	C	IR (15 Gy)
G0-G1%:	65.41	53.13	85.28	84.22
G2/M%:	01.24	06.51	05.82	05.64
S%:	33.34	40.36	08.89	10.14
	S phase enrished		G2/M phase enriched	
	C	IR (15 Gy)	C	IR (15 Gy)
G0-G1%:	15.66	07.22	00.71	04.92
G2/M%:	00.00	00.00	88.47	83.38
S%:	84.34	92.78	10.81	11.70
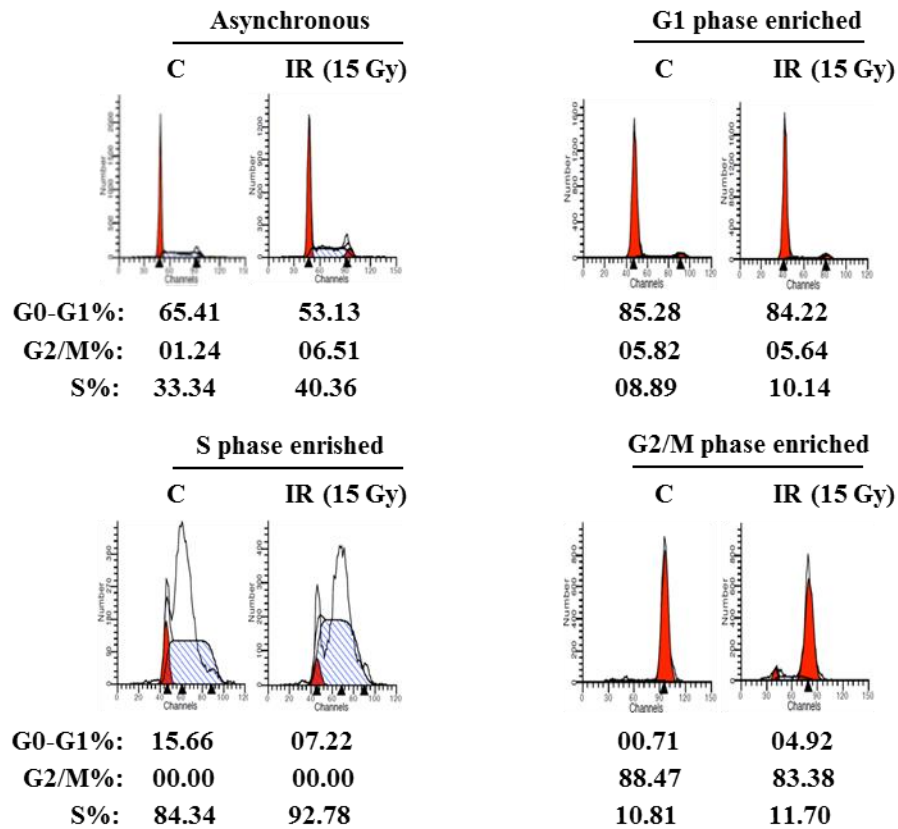
Appendix A 8.4 (A): Cell cycle distribution in G1 enriched population as depicted in Figure (Fig 4.9 A). G1 enriched WRL68 cells were treated with the indicated DNA-damaging agents. After 1hr recovery cell cycle distribution analysed by flow cytometry.

	C	Adriamycin	Etoposide	H_2O_2	UV	Cisplatin
G0-G1%:	72.75	76.72	78.41	62.57	70.22	74.61
G2/M%:	15.35	23.19	13.27	19.79	18.32	16.35
S%:	11.90	00.09	08.32	17.63	11.46	09.03
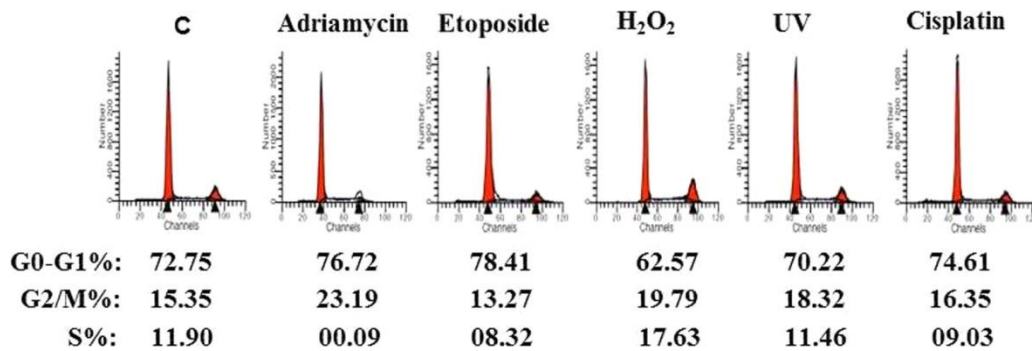
Appendix A 8.4 (B): Cell cycle distribution in G1 enriched population as depicted in Figure (Fig 4.9 B). G1 enriched WRL68 cells were treated with the indicated DNA-damaging agents. After 1hr recovery cell cycle distribution analysed by flow cytometry.

	C	Neocarzastatin	IR (15 Gy)	Bleomycin	Phleomycin
G0-G1%:	85.60	82.73	87.34	82.94	87.29
G2/M%:	07.95	06.83	06.87	04.21	07.18
S%:	06.45	10.44	05.79	12.84	05.53

127
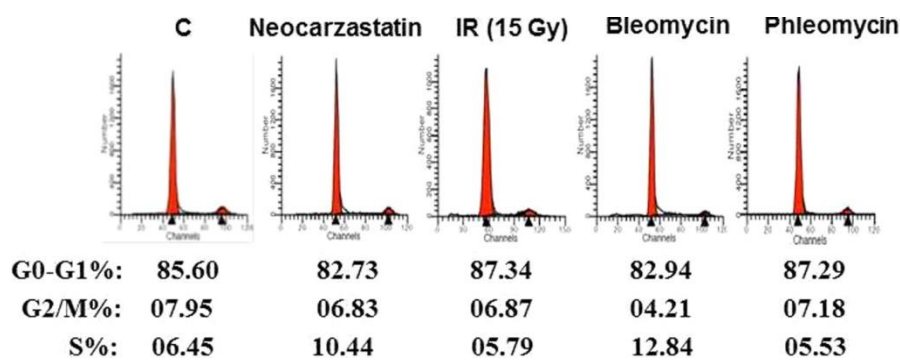
Appendix A8.5: Cell cycle distribution in G1 enriched population of multiple cell lines as depicted in Figure (Fig 4.10). Cell lines of different tissue origin (U87, U2OS, MCF7, A2780 and A549) enriched in G1 phase were exposed to IR at two different doses 2.5 and 15Gy. After 1hr recovery cell cycle distribution analysed by flow cytometry.

	C	2.5	15 (Gy)
U 87			
G0-G1%:	83.13	83.89	83.03
G2/M%:	12.07	10.89	10.02
S%:	04.80	05.21	06.95
U 2OS			
G0-G1%:	64.61	67.08	67.80
G2/M%:	08.93	10.43	11.08
S%:	26.46	22.48	21.18
MCF 7			
G0-G1%:	88.39	86.75	86.27
G2/M%:	03.91	03.48	04.66
S%:	09.71	09.77	09.07
A 2780			
G0-G1%:	55.41	55.56	59.46
G2/M%:	06.90	04.79	05.96
S%:	37.69	39.65	34.64
A 549			
G0-G1%:	85.13	93.10	86.64
G2/M%:	09.03	00.00	05.83
S%:	05.84	06.90	04.63

128
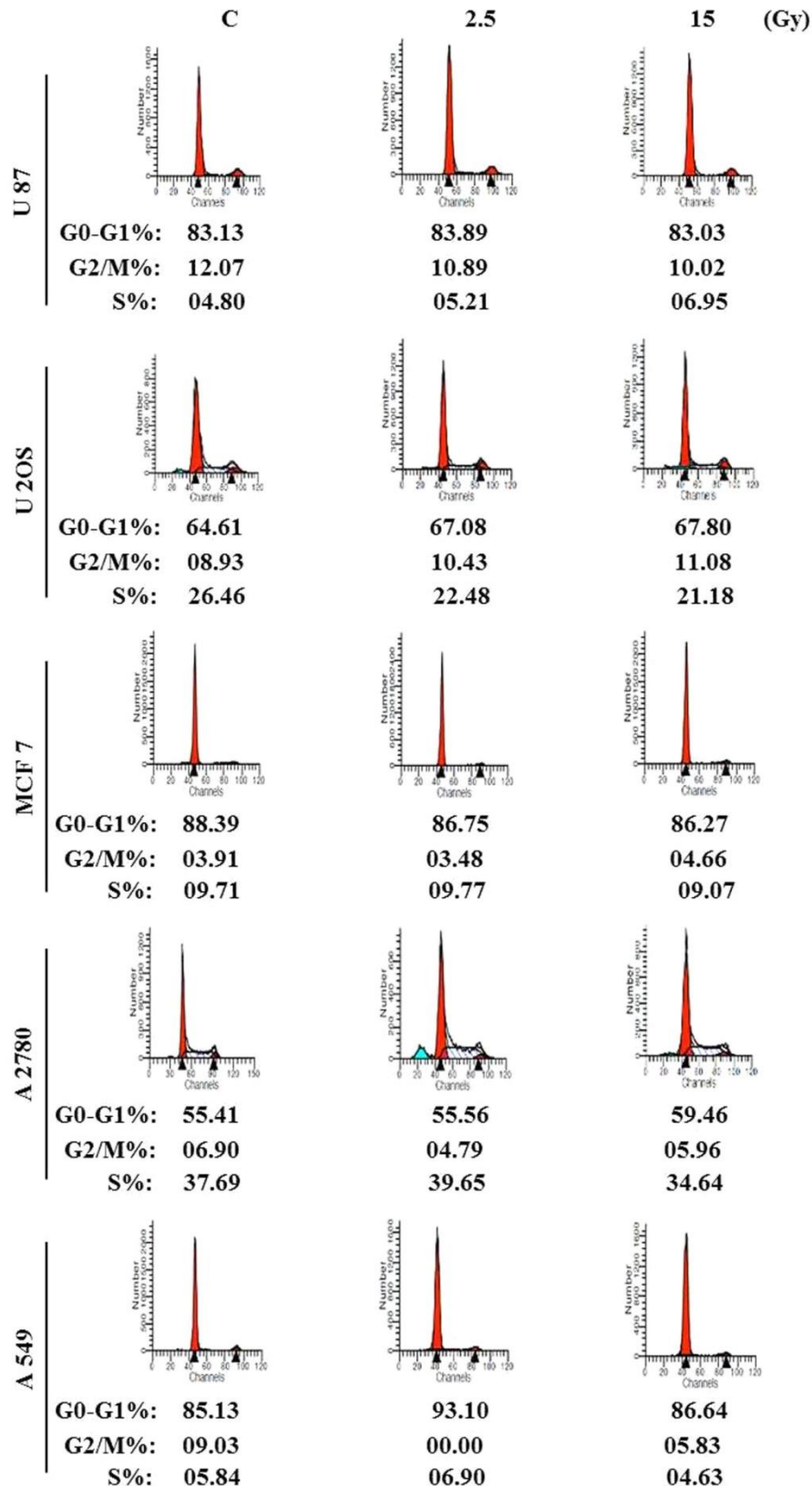
Appendix A8.6:Cell cycle distribution in G1 enriched population as depicted in Figure (Fig 4.15 C). G1 enriched cells were pre-treated with or without 10μM of sanguinarine for 1hr before IR (2.5 and 15Gy). Cell cycle distribution analysed by flow cytometry.

	IR (-), Sang (+)	IR (2.5Gy), Sang (-)	IR(2.5Gy), Sang (+)	IR (15Gy), Sang (-)	IR (15Gy), Sang (+)
G0-G1%:	73.17	71.64	73.18	74.50	73.47
G2/M%:	10.32	08.56	12.13	11.24	11.64
S:	16.51	19.80	14.69	14.25	14.89
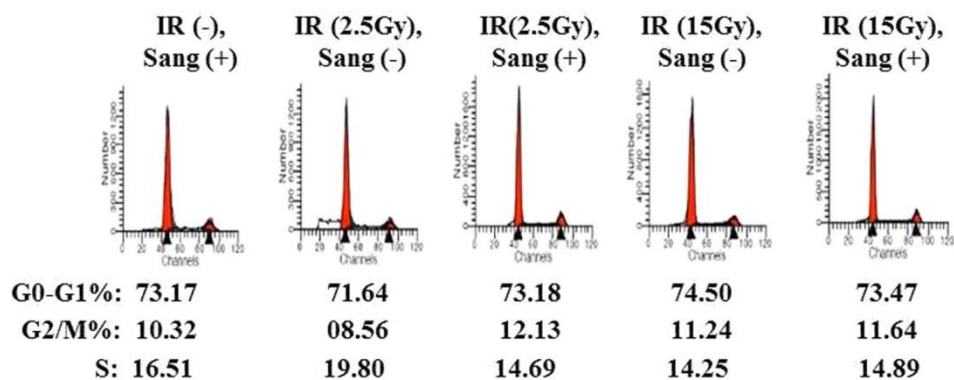
Appendix A8.7: Line diagram for the secondary structures of MKP1 and MSK1(A) C-terminal phosphatase domain of MKP1 (172–314 aa) and (B) N-terminal kinase domain of MSK1 (42–380 aa).

(A) Secondary structure of C-terminal phosphatase domain of MKP-1 (172-314)

GGPVEILPFLYLGSAYHASRKDMLDALGITALINVSANCPNHFEGHYQYKSIPVEDNHK

ADISSWFNEAIDFIDSIKNAGGRVFVHCQAGISRSATICLAYLMRTNRVKLDEAFEFVKQ

RRSIISPNFSFMGQLLQFESQVLA

(B) Secondary structure of N-terminal kinase domain of MSK1 (42-380)

EKVGIENFELLKVLGTGAYGKVFLVRKISGHDTGKLYAMKVLKKATIVQKAKTTEHTR

TERQVLEHIRQSPFLVTLHYAFQTETKLHLILDYINGGELFTHLSQRERFTEHEVQIYVG

EIVLALEHLHKLGIIYRDIKLENILLDSNGHVVLTDFGLSKEFVADETERAYSFCGTIEYM

APDIVRGGDSGHDKAVDWWSLGVLMYELLTGASPFTVDGEKNSQAEISRRILKSEPPYP

QEMSALAKDLIQRLLMKDPKKRLGCGPRDADEIKEHLFFQKINWDDLAAKKVPAPFKP

VIRDELDVSNFAEEFTEMDPTYSPAALPQSSEKLFQGYSFVAP

Key:
Loop:
Beta sheet:
Alpha helix:

Appendix A8.8:Histone H3 peptide from PDB: 2C1J was modified by phosphorylation of Ser10 and acetylation of Lys9 and Lys14. (**A**) Native histone H3, (**B**) H3Lys9Ac, (C) H3Ser10P, (**D**) H3Lys14Ac, (E) H3Lys9AcSer10P, (**F**) H3Ser10PLys14Ac, (**G**) H3Lys9AcLys14Ac, and (**H**) H3Lys9AcSer10PLys14Ac.
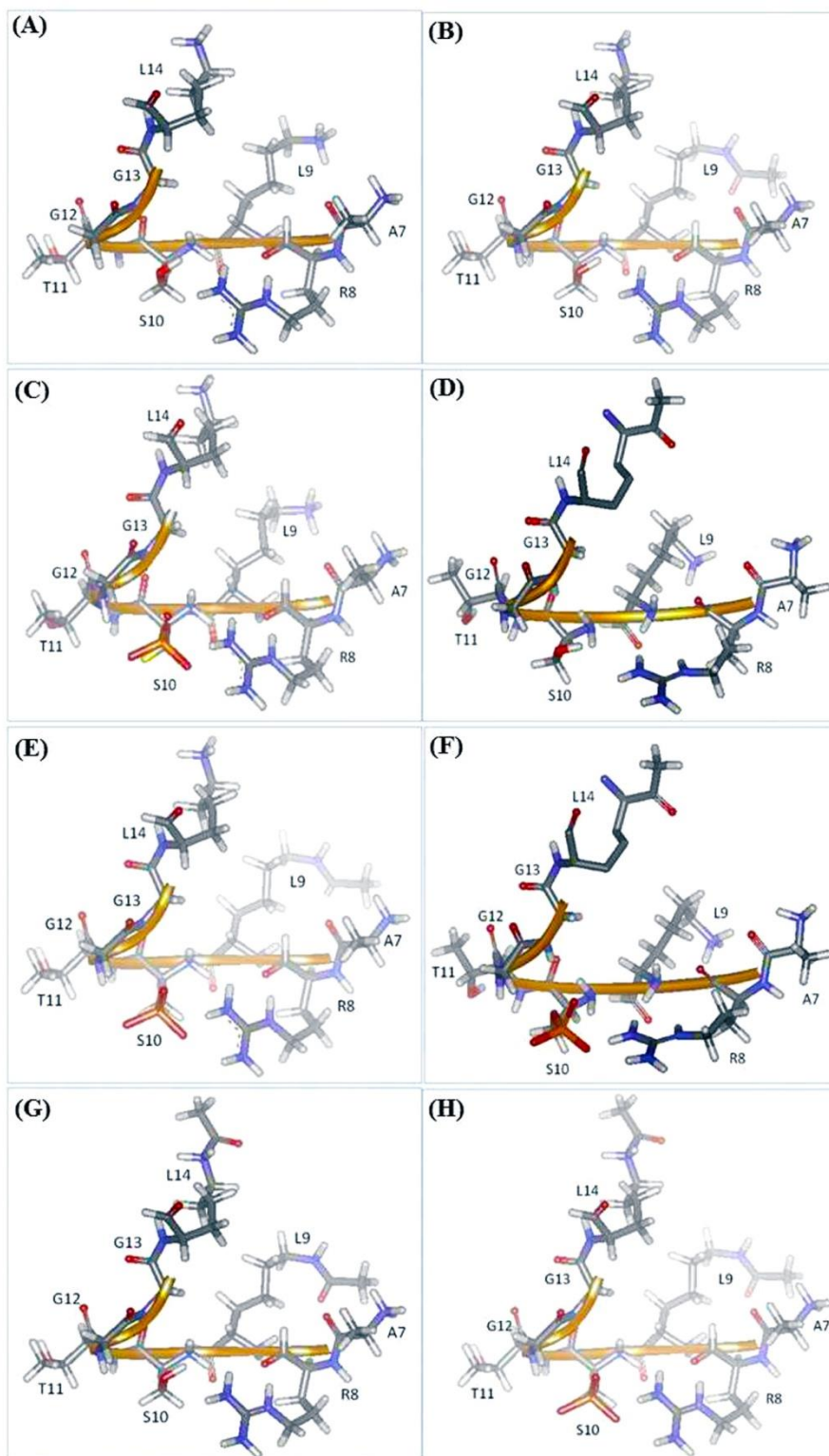
Appendix A8.9:Full-length loop structure of histone H3 peptide from PDB: 1KX5 was modified by phosphorylation of Ser10 and acetylation of Lys9 and Lys14. (A) Native histone H3, (B) H3Lys9Ac, (C) H3Ser10P, (D) H3Lys14Ac, (E) H3Lys9AcSer10P, (F) H3Ser10PLys14Ac, (G) H3Lys9AcLys14Ac, and (H) H3Lys9AcSer10PLys14Ac.

132

Appendix A8.10: The Ligplot of the MSK1 and histone H3 docked complexes to analyze hydrophobic interactions. (A) Native MSK1/H3 (B) MSK/H3Lys9Ac, (C) MSK1/H3Lys14Ac, and (D) MKP1/H3Lys9AcLys14Ac.
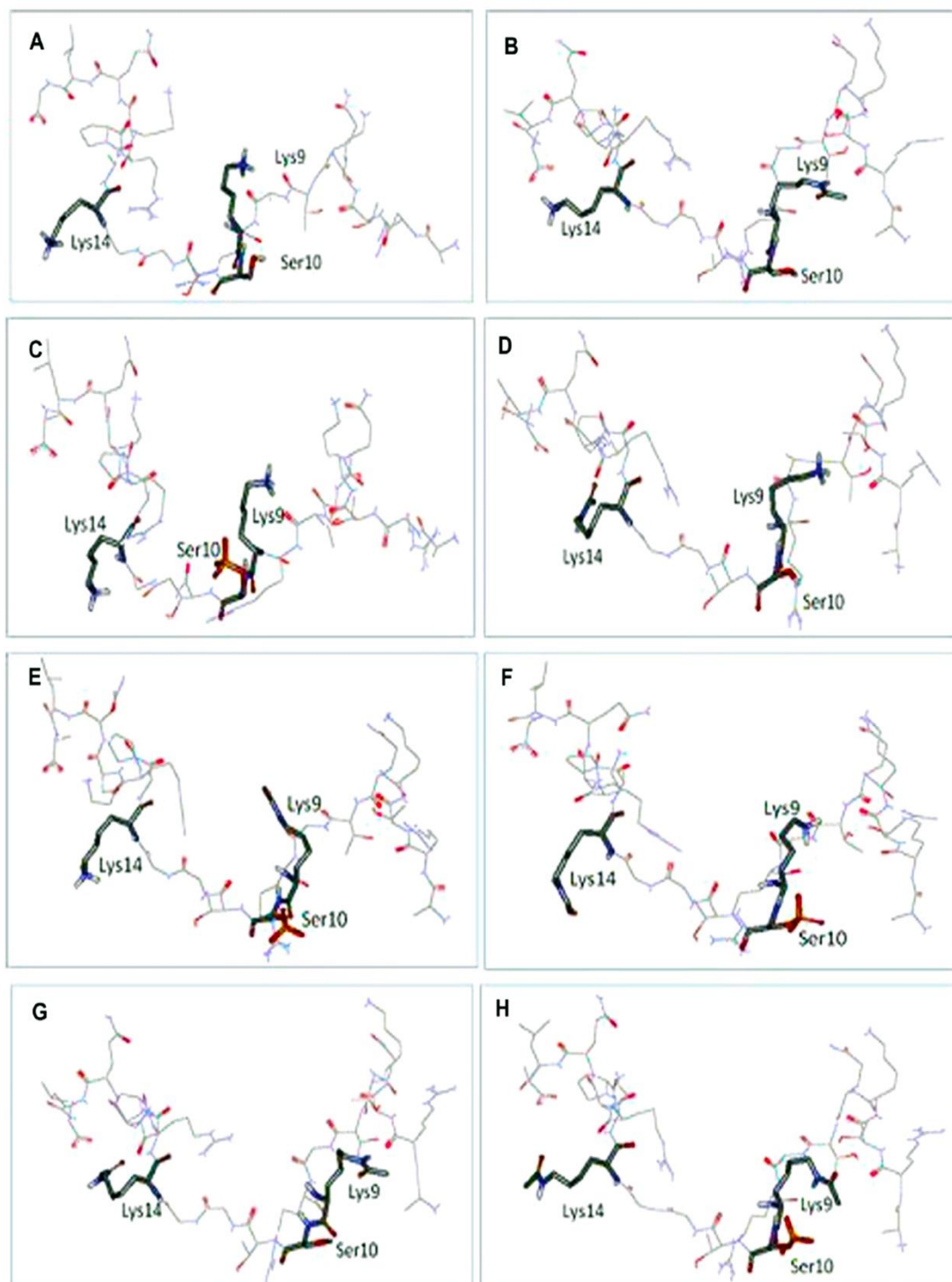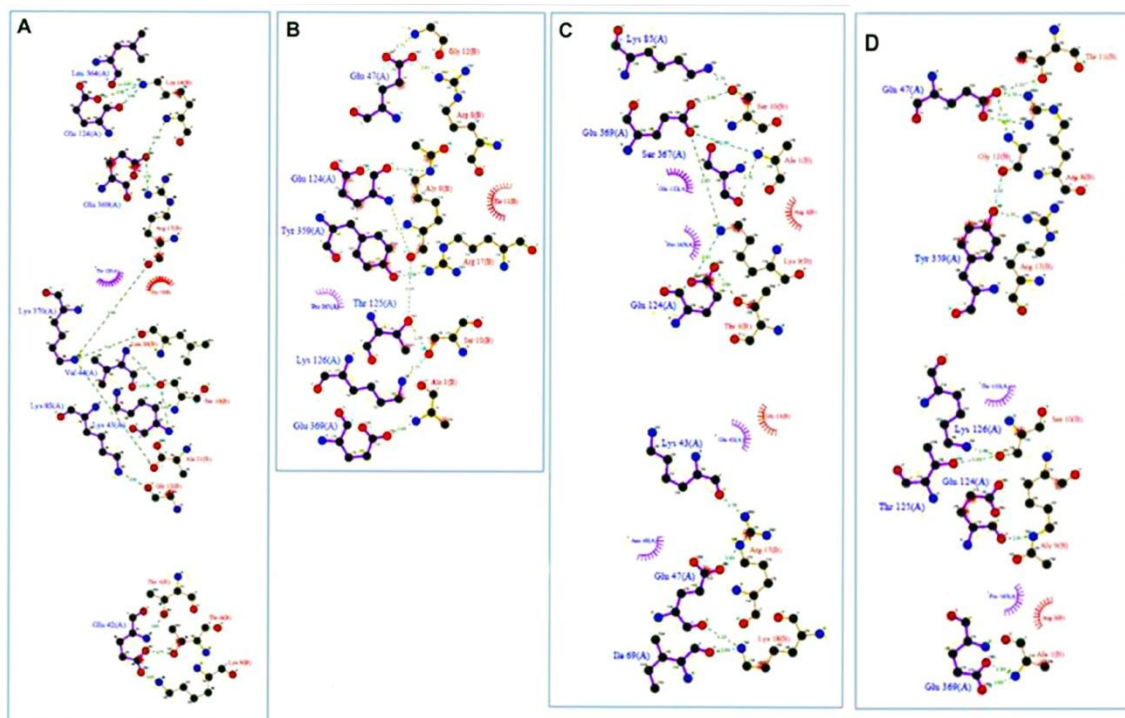
Appendix A8.11: Ligplot of the MKP1 and histone H3 docked complexes to analyze hydrophobic interactions. (A) Native MKP1/H3 (B) MKP1/H3Lys9Ac, (C) MKP1/H3Ser10P, (D) MKP1/H3Lys14Ac, (E) MKP1/H3Lys9AcSer10P, (F) MKP1/H3Ser10PLys14Ac, (G) MKP1/H3Lys9AcLys14Ac, and (H) MKP1/H3Lys9AcSer10PLys14Ac.
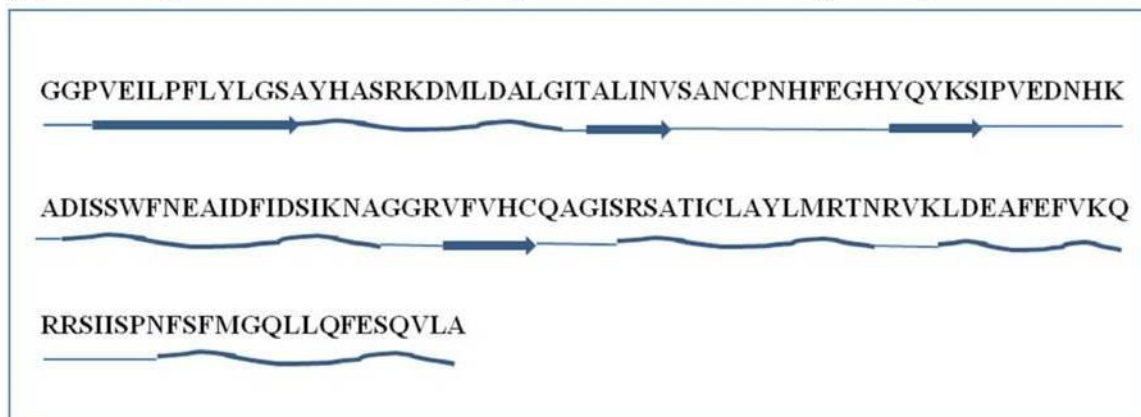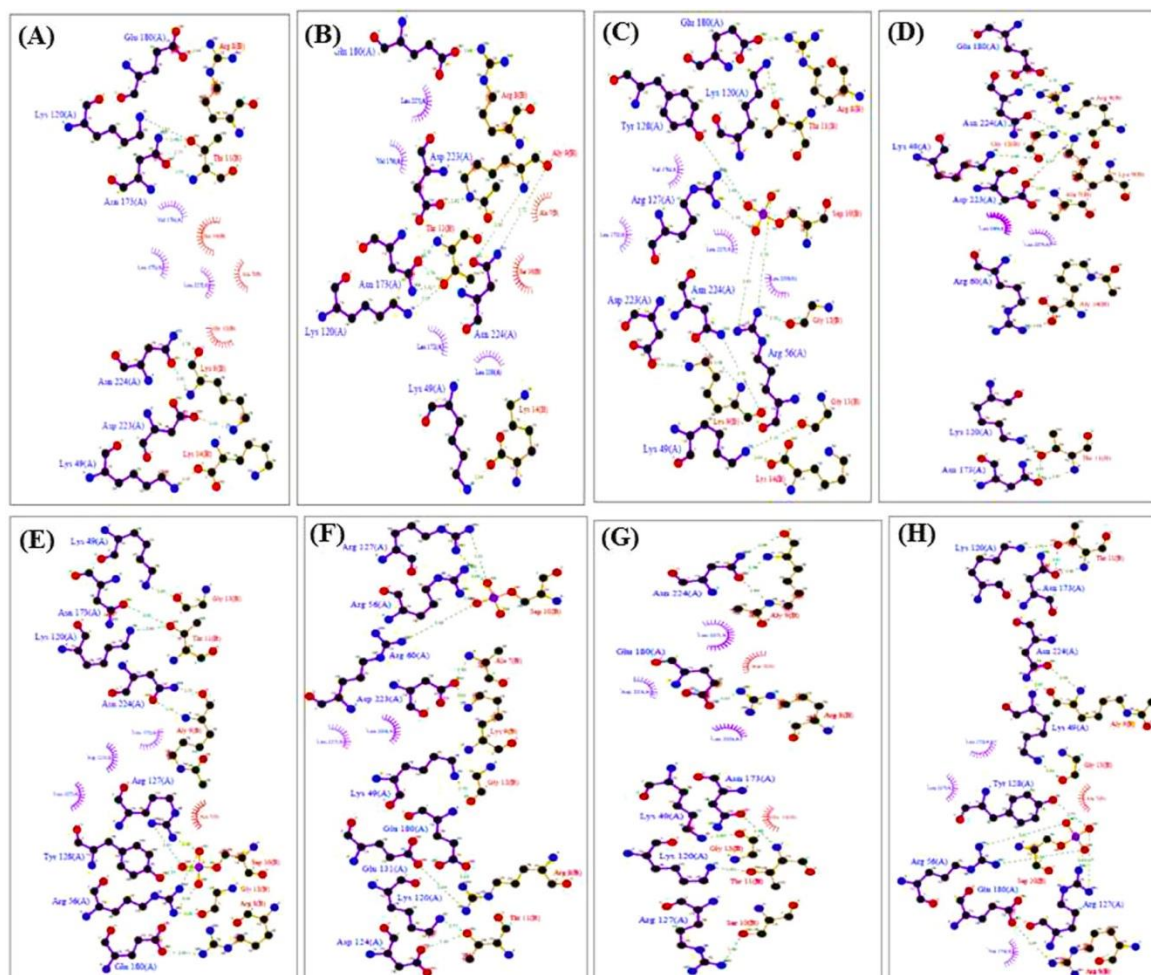
Appendix A8.12: Cell cycle distribution in G1 enriched population as depicted in Figure (8.21). G1-enriched WRL68 cells were untreated or pre-treated with inhibitor independently i.e. (A) Sanguinarine (10µM) or (B) H89 (20µM) for 1hr before 2.5Gy IR treatment. Cell cycle distribution analysed by flow cytometry at indicated time points after irradiation.

Sang (-ve); IR (2.5 Gy)

	C	0	1	4	24
G0-G1%:	86.90	87.10	87.27	87.15	65.32
G2/M%:	06.56	03.23	06.30	05.57	06.75
S%:	06.55	09.68	06.43	07.28	27.93

Sang (+ve); IR (2.5 Gy)

	0	1	4	24
G0-G1%:	87.03	87.27	87.15	65.32
G2/M%:	01.73	06.30	05.57	06.75
S%:	11.25	06.43	07.28	27.93

Time (hr)

H89 (+ve); IR (2.5 Gy)

	C	0	1	4	8	20	24
G0-G1%:	80.57	81.78	82.13	59.77	55.55	43.53	48.62
G2/M%:	03.90	02.77	07.51	00.94	04.79	00.26	02.26
S%:	15.54	15.45	10.35	39.40	39.66	56.21	49.12

H89 (-ve); IR (2.5 Gy)

	0	1	4	8	20	24
G0-G1%:	80.12	83.44	80.82	61.10	58.86	01.01
G2/M%:	03.26	04.11	04.19	02.64	03.34	02.21
S%:	16.32	12.45	14.99	36.26	37.39	26.78

Time (hr)

List of Instruments

Instruments	Model	Company
Spectrophotometer	UV – 160 A, UV – 240	Shimadzu, Japan
	U – 2001	Hitachi, Japan
	Biophotometer 6131	Eppendorf, Germany
Centrifuges		
High – speed	Rota 4-R, Superspin R -V FA	Plasto Crafts, India
	Sorvall RC5C, Sorvall RC – 5C plus	DuPont, USA
Ultracentrifuge	Sorvall Ultra 80;	DuPont, USA
	Centrikon T – 1065	Kontron, USA
Tabletop ultracentrifuge	TL – 100, Optima TLX	Beckman, USA
Microfuge	Spinwin	Tarsons, India
Speedvac concentrator	SVC 1000, AES 1000	Savant, USA
Upright microscope	Axioimager.Z1	Zeiss, Germany
	Eclipse 50i	Nikon, Japan
Confocal microscope	LSM 510 Meta	Zeiss, Germany
X-ray film developing machine	Optimax	Protec, Germany
pH meter	APX 175E	Ingold, Germany
Vertical electrophoresis assembly	Monokin, Minikin, Macrokin	Techno Source, India
Electroblot transfer assembly	Technoblot	Techno Source, India
	Trans – Blot Cell	Bio – Rad, USA
Power packs	Gativaan	Techno Source, India;
	Power pac 2000	Bio – Rad, USA
ELISA reader	Spectra Max 190	Molecular Devices, USA

Chapter 9

Publications

Publication from the Thesis:

1. **Ajit K Sharma**, Abhilasha Mansukh, Ashok Varma, Nikhil Gadewal and Sanjay Gupta   Molecular modeling of differentially phosphorylated Serine 10 and acetylated lysine 9/14 of histone H3 regulates their interactions with 14-3-3ζ, MSK1 and MKP1. *Bioinformatics and Biology Insights.* 2013:7 271–288

2. **Ajit K. Sharma**, Tejkiran Sagwekar, Shafqat A. Khan, Saikat Bhattacharyya and Sanjay Gupta* Dynamic alteration in H3 Serine10 phosphorylation is G1-phase specific during IR-induced DNA damage response in human cells (Under Review).

3. **Ajit Kumar Sharma**, Shafqat A Khan, Divya V Reddy, Tejkiran Sagwekar, Sanjay Gupta**.** MKP1 phosphatase mediate dephosphorylation of H3Serine10P during ionization radiation induced DNA damage response in G1 phase of cell cycle. (Under Review).

Other Publications:

1. Khare SP, **Sharma A K**, Deodhar KK, Gupta S .Overexpression of histone variant H2A.1 and cellular transformation is related in N-nitrosodiethylamine-induced sequential hepatocarcinogenesis. *Exp Biol Med* (Maywood), 2011; 236(1):30-5.

2. Rhea Mohan, **Ajit K. Sharma**, Sanjay Gupta, C. S. Ramaa. Design, synthesis, and biological evaluation of novel 2, 4-thiazolidinedione derivatives as histone deacetylase inhibitors targeting liver cancer cell line. *Med. Chem. Research*, March 2011, pp, 1-10.

3. Shafqat A Khan, Monica Tyagi, **Ajit K Sharma**, Savio G Barreto, Bhawna Sirohi, Mukta Ramadwar, Shailesh V Shrikhande, Sanjay Gupta. β-actin expression in gastric cancer: cell type specificity and correlation with clinicopathological parameters. World Journal of Gastroenterology (In Press)

Bioinformatics and Biology Insights

ORIGINAL RESEARCH

Molecular Modeling of Differentially Phosphorylated Serine 10 and Acetylated lysine 9/14 of Histone H3 Regulates their Interactions with 14-3-3ζ, MSK1, and MKP1

Ajit K. Sharma[1,#], Abhilasha Mansukh[2,#], Ashok Varma[2], Nikhil Gadewal[2,*] and Sanjay Gupta[1,*]

[1]Gupta Laboratory, [2]Bioinformatics Centre, Cancer Research Institute, Advanced Centre for Treatment Research and Education in Cancer, Tata Memorial Centre, Kharghar, Navi Mumbai 410210, MH, India. [#]These authors contributed equally to this work. *Corresponding authors email: sgupta@actrec.gov.in; ngadewal@actrec.gov.in

Abstract: Histone modifications occur in precise patterns, with several modifications known to affect the binding of proteins. These interactions affect the chromatin structure, gene regulation, and cell cycle events. The dual modifications on the H3 tail, serine10 phosphorylation, and lysine14 acetylation (H3Ser10PLys14Ac) are reported to be crucial for interaction with 14-3-3ζ. However, the mechanism by which H3Ser10P along with neighboring site-specific acetylation(s) is targeted by its regulatory proteins, including kinase and phosphatase, is not fully understood. We carried out molecular modeling studies to understand the interaction of 14-3-3ζ, and its regulatory proteins, mitogen-activated protein kinase phosphatase-1 (MKP1), and mitogen- and stress-activated protein kinase-1 (MSK1) with phosphorylated H3Ser10 alone or in combination with acetylated H3Lys9 and Lys14. In silico molecular association studies suggested that acetylated Lys14 and phosphorylated Ser10 of H3 shows the highest binding affinity towards 14-3-3ζ. In addition, acetylation of H3Lys9 along with Ser10PLys14Ac favors the interaction of the phosphatase, MKP1, for dephosphorylation of H3Ser10P. Further, MAP kinase, MSK1 phosphorylates the unmodified H3Ser10 containing N-terminal tail with maximum affinity compared to the N-terminal tail with H3Lys9AcLys14Ac. The data clearly suggest that opposing enzymatic activity of MSK1 and MKP1 corroborates with non-acetylated and acetylated, H3Lys9Lys14, respectively. Our in silico data highlights that site-specific phosphorylation (H3Ser10P) and acetylation (H3Lys9 and H3Lys14) of H3 are essential for the interaction with their regulatory proteins (MKP1, MSK1, and 14-3-3ζ) and plays a major role in the regulation of chromatin structure.

Keywords: modeling, histone H3 modifications, 14-3-3ζ, MSK1, MKP1

Introduction

Histones undergo different posttranslational modifications such as lysine acetylation, lysine and arginine methylation, serine and threonine phosphorylation, sumoylation, ADP-ribosylation, and ubiquitination.[1] These modifications are read by the binding partner 'readers' at the level of a distinct or multiple modifications. The binding of partners to histones facilitate chromatin organization to control gene expression and perform particular biological functions in specific phases of the cell cycle.[2–4]

Phosphorylation at serine10 on histone H3 (H3Ser10P) is linked with two different events, including transcriptional activation in G1-phase and chromatin condensation in G2/M-phase of the cell cycle.[5] Literature suggests that the phospho-specific domain containing protein, 14-3-3ζ, an isoform of 14-3-3 family interacts, with H3Ser10P.[6] The crystal structure of 14-3-3ζ with H3Ser10P peptide (PDB: 2C1N) indicates that it is stabilized by intermolecular hydrogen bonding interactions.[6] The side chains of the 14-3-3ζ residues Lys120, Asn224, and Asn173 interact with the backbone carbonyl and amide groups of the H3 peptide. Phosphorylated H3Ser10 is neutralized by a basic pocket formed by 14-3-3ζ with the highly basic amino acids Lys49, Arg127, Arg56, and the side chain amide nitrogen of Asn173. It has also been shown that 14-3-3ζ proteins bind to 'writers' and 'erasers' of histone modification, such as histone acetyltransferase (HAT) and histone deacetylases (HDAC) and help in mediating transcriptional activation of specific subset of mammalian genes and DNA replication mediated through acetylation on Lys9 and Lys14.[7–9] Further, the crystal structure of 14-3-3ζ interaction with H3Lys9AcSer10P peptide (PDB: 2C1J) showed hydrogen bonding interactions of Ser10P with triad Arg56, Arg127 and Tyr128 and Lys9Ac with Asn224.[6] Earlier studies have also linked H3Ser10P to Lys14Ac on the same histone tail, and it has been shown that H3Ser10PLys14Ac is important for binding of 14-3-3ζ with high affinity compared to H3Ser10P alone.[9,10] The bromodomain-containing proteins are known to interact with acetylated histones;[11] 14-3-3ζ does not contain a bromodomain, suggesting that its molecular interaction is specific to the phosphoserine residue. Therefore, whether dual acetylation marks at the chromatin, H3Lys9, or H3Lys14 is important for stabilizations

and protection of the phosphorylated H3Ser10 during transcriptional activation of immediate early genes in interphase of the cell cycle remains an enigma.

The phosphorylation of H3Ser10 on the promoter of immediate early genes in response to epidermal growth factor (EGF) is mediated through mitogen- and stress-activated kinase1 (MSK1), whereas dephosphorylation of H3Ser10P occurs by mitogen-activated protein kinase phosphatase 1 (MKP1) in response to vascular endothelial growth factor (VEGF).[12,13] MKP1 is also known to be overexpressed in many human tumors.[14,15] Thus, MKP1 is a reasonable target for the treatment of cancer, but the search for inhibitors has been difficult because of the non-availability of structural information for MKP1. MKP1 is a 367-amino acid protein consisting of two domains, inactive N-terminal rhodanase domain and active C-terminal phosphatase domain, separated by a flexible loop region containing six proline residues.[16] MSK1, a kinase that phosphorylates H3Ser10, is an 802-amino acid protein with a serine/threonine nuclear kinase domain and acts downstream of both ERK and p38 MAPKs.[17,18] MSK1 contains two kinase domains separated by a flexible loop segment. The crystal structure of the MSK1 N-terminal domain is available (PDB ID: 1VZO 24-345); however, inactive MSK1 requires the association of an activation loop residue (Ser376) phosphorylation for conversion into the active form.[19]

Inducible site-specific H3 phosphoacetylation (H3Ser10PLys9AcLys14Ac) is a tightly regulated process that occurs on the nucleosomes, which is well-established in the literature.[12] It is not clear whether such dynamic chromatin markers, phosphorylation, and acetylation on H3 tails, are required independently or in concert with one another for their interaction with 14-3-3ζ and MKP1. Additionally, whether acetylation is a pre-requisite for MSK1-mediated phosphorylation of H3Ser10 is not known. The investigation of interactions between H3Ser10P along with Lys9 and Lys14 modification(s) and their binding partner, 14-3-3ζ, has been carried out using biochemical methods. The existing biochemical experiments from different labs on different cell lines in response to different inducible agents support and contradict both hypotheses.[6,9] The theoretical efforts to delineate the cross-talk and understand the molecular association of phosphorylated H3 or acetylated H3 singly or in different combinations (H3Ser10PLys9AcLys14Ac)

with 'writers' and 'erasers' have been limited. The three-dimensional structures of MKP1 and MSK1 also remains unknown, which are essential for understanding their conformation, active regions, interaction sites, and binding domains with other proteins. To study the molecular interactions of histone H3 with its binding partner, the expert interface of Haddock docking server was used. Haddock is an information-driven flexible docking approach, where active sites residues are provided for docking.[20] To ascertain the role of each modified residues of histone H3, different combination of modified residue complexes were built and docked. The Haddock score of docked protein complex is a weighted sum of intermolecular electrostatic, van der Waals, desolvation, and buried surface area terms.

Molecular modeling studies suggest that the differential modification(s), Lys9Ac, Ser10P, and Lys14Ac at the N-terminal tail of histone H3 regulates its interaction with 14-3-3ζ, MSK1, and MKP1. In agreement with an earlier study, our in silico results also suggest that dual phospho-acetylation of H3Ser10-PLys14Ac favors the interaction with 14-3-3ζ. The MKP1 interaction with N-terminal tail of H3 showed a strong preference for Ser10PLys14AcLys9Ac modifications over Ser10P alone. The interphase-specific H3 kinase, MSK1 phosphorylates H3Ser10 with the highest binding affinity when Lys9Lys14 are non-acetylated. Our in silico studies demonstrate that differential phospho-acetylation on the N-terminal tail of H3 is highly dynamic and regulates its reversible interaction(s) with binding partners, MSK1 and MKP1.

Methods
Homology modeling of MKP1 and MSK1 structures

We conducted homology modeling due to the unavailability of crystallographic coordinates of MKP1. The model of active the C-terminus phosphatase domain of MKP1 (172–314 aa) was constructed using PDB ID: 3EZZ as a template. The N-terminal crystal structure of MSK1 is available, but to model the phosphorylated Ser376 residue of the flexible loop near the active site, PDB ID: 3A8X was used as a template for homology modeling of MSK1 with amino acid residues from 42–380. Modeling studies were performed using Swiss Model.[21] The modeled structure of

MKP1 and MSK1 were cross-validated using multiple tools such as Procheck,[22] Verify_3D,[23] and Errat[24] using SAVES server (http://nihserver.mbi.ucla.edu/SAVES/). The cross-validated modeled structures of MKP1 and MSK1 are shown as Figure 1 and secondary structures for both are depicted in Supplementary Figure S1.

Refinement of crystal structure of 14-3-3ζ with native H3 peptide and its posttranslational modifications (PTM)

In the crystal structure of histone H3 (PDB ID: 2C1J),[6] acetylation at Lys9 and Lys14 and phosphorylation at Ser10 was generated using Discovery Studio Visualizer version 3.5. A total of seven structures of histone H3 were modeled which encompassed combinations of modifications [Lys9, Ser10, Lys14, Lys9-Ser10, Lys9-Lys14, Ser10-Lys14, and Lys9-Ser10-Lys14] (Supplementary Fig. S2). The Haddock server[20] was used to score the refinement of PDB ID: 2C1J as native and the modified 14-3-3ζ and histone H3 complex. The Haddock scores of the complexes are tabulated in Table 1 and Figure 2.

Molecular association of MSK1 with histone H3 and its PTM modified structure

The full-length (1–21 aa) loop structure of histone H3 was used to build the three PTM-modified structure [Lys9, Lys14, Lys9-Lys14]. The modeled structure of MSK1 was docked with native and the three PTM-modified structure of histone H3 using the Haddock
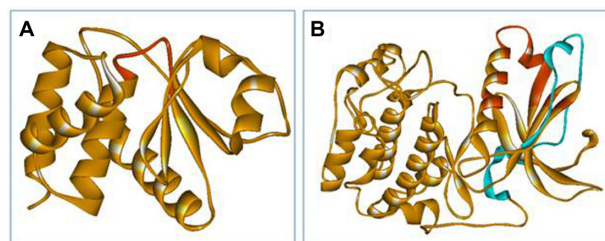
Figure 1. Homology modeling of MKP1 and MSK1 structures (**A**) Homology modeled structure of C-terminal phosphatase domain of MKP1 (172–314 aa) is shown in yellow color, while the active site includes His257, Cys258, Gln259, Ala260, Gly261, Ile262, Ser263, and Arg264 residues in orange color. (**B**) Homology modeled structure of N-terminal kinase domain of MSK1 (42–380 aa) is shown in yellow color. The blue colored region is the flexible loop near the active site. The orange color indicates the active site residues Lys85, Ile88, Val89, Thr95, Arg102, Gln122, and Leu127.

Table 1. 14-3-3ζ with histone H3 PDB complex and its PTM structure.

PDB complexes	HADDOCK score	Interacting residues	
		H-bonds	**Hydrophobic**
14-3-3ζ H3	−40.3 ± 2.1	**Arg8:** *Glu180* **Lys9:** *Asp223, Asn224* **Thr11:** *Lys120, Asn173* **Lys14:** *Lys49*	**Ala7:** *Leu227* **Ser10:** *Leu172* **Gly12:** *Lys49*
14-3-3ζ H3Ser10P	−62.4 ± 5.3	**Arg8:** *Glu131, Glu180* **Lys9:** *Asp223, Asn224* **Ser10:** *Arg56, Arg127, Tyr128* **Thr11:** *Lys120, Asn173* **Gly12:** *Arg56* **Lys14:** *Lys49*	**Arg8:** *Leu227* **Lys9:** *Leu220* **Ser10:** *Leu172,* *Val176*
14-3-3ζ H3Ser10PLys9Ac	−46.5 ± 2.6	**Arg8:** *Glu180* **Lys9:** *Asn224* **Ser10:** *Arg56, Arg127, Tyr128* **Thr11:** *Lys120, Asn173* **Gly13:** *Lys49*	**Ala7:** *Leu227* **Lys9:** *Asp223* **Ser10:** *Leu172*
14-3-3ζ H3Ser10PLys14Ac	−119.7 ± 2.5	**Ala7:** *Asp223* **Arg8:** *Glu131, Glu180* **Lys9:** *Asp223, Asn224* **Ser10:** *Arg56, Arg60, Arg127* **Thr11:** *Lys120* **Gly12:** *Lys49*	**Ala7:** *Leu227, Leu220* **Lys9:** *Leu220* **Thr11:** *Lys120*
14-3-3ζ H3Lys9AcSer10PLys14Ac	−54.0 ± 6.8	**Arg8:** *Glu180* **Lys9:** *Asn224* **Ser10:** *Arg56, Arg127, Tyr128* **Thr11:** *Asn173, Lys120* **Gly13:** *Lys49*	**Ala7:** *Leu227* **Arg8:** *Val176* **Ser10:** *Leu172*
14-3-3ζ H3Lys9Ac	−29.0 ± 4.5	**Arg8:** *Glu180* **Lys9:** *Asn224* **Thr11:** *Lys120, Asn173* **Lys14:** *Lys49*	**Ala7:** *Leu227, Val176* **Lys9:** *Asp223* **Ser10:** *Asn173*
14-3-3ζ H3Lys14Ac	−98.9 ± 2.4	**Ala7:** *Asp223* **Arg8:** *Glu180* **Lys9:** *Asp223, Asn224* **Thr11:** *Asn173, Lys120* **Gly12:** *Lys49* **Lys14:** *Arg60*	**Ala7:** *Leu227* **Lys9:** *Leu220* **Arg8:** *Glu180* **Gly12:** *Lys49*
14-3-3ζ H3Lys9AcLys14Ac	−43.0 ± 1.8	**Arg8:** *Glu180* **Lys9:** *Asn224* **Ser10:** *Arg127* **Thr11:** *Lys120, Asn173* **Gly13:** *Lys49*	**Lys9:** *Leu220, Leu227* **Arg8:** *Asp223* **Gly12:** *Lys49*

Note: Bold letters indicate histone H3 and italics indicate binding partners.

server (Fig. 1B and Supplementary Fig. S3).[20] The active site residues (Lys85, Ile88, Val89, Thr95, Arg102, Gln122, and Leu127) of MSK1 and (Lys9, Ser10, and Lys14) of histone H3 were provided as input parameters for targeted docking. The protein-protein interactions, Haddock score, hydrogen bonds, and hydrophobic interactions are tabulated in Table 2 and Figure 3.

The molecular interactions of the docked complexes were analyzed using Ligplot[25] for hydrophobic interactions (Supplementary Fig. S4). Discovery studio visualizer 3.5 was used to identify residues involved in hydrogen bonding between the two proteins and for the diagrammatic illustration of the residues involved in the hydrogen bond formation in the docked complex.
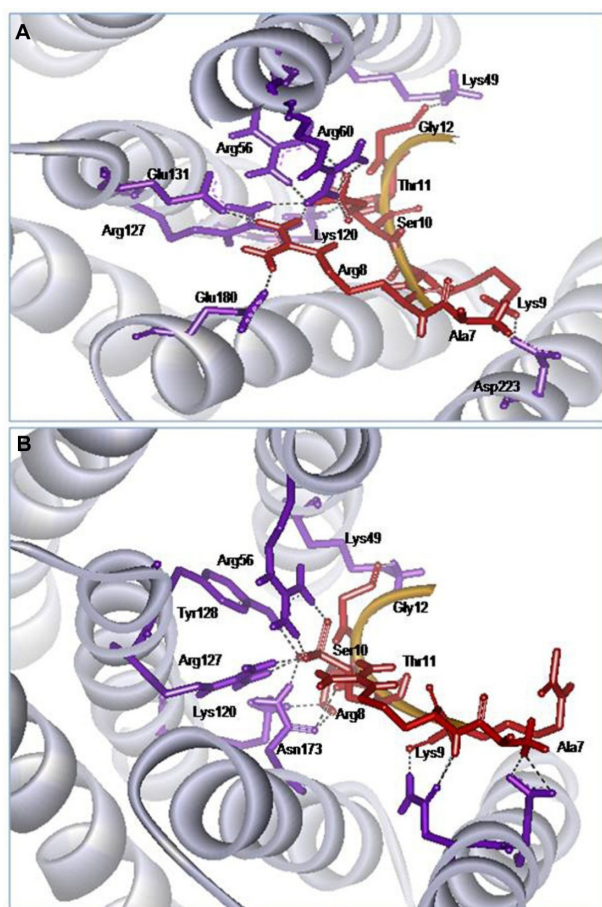
Figure 2. Docking of 14-3-3-ζ with histone H3 and its PTM structure (**A**) 14-3-3ζ and histone H3Ser10PLys14Ac (**B**) 14-3-3ζ and histone H3Lys9AcSer10PLys14Ac. The ribbon diagram of 14-3-3ζ (grey) with the residues (violet) and histone H3 peptide (orange) with the residues (red) are involved in H-bonding interaction and are shown as a dotted black line.

Molecular association of native MKP1 with histone H3 and its PTM modified structure

The full length (1–21 aa) loop structure of histone H3 from the crystal structure of the Xenopus nucleosome (PDB ID: 1KX5) was used.[26] Histone H3 is 100% conserved between Xenopus and humans. The combination of Lys9, Ser10, and Lys14 modifications was generated by site-specific acetylation and phosphorylation resulting in seven PTM structures of histone H3 [Lys9, Ser10, Lys14, Lys9-Ser10, Lys9-Lys14, Ser10-Lys14, and Lys9-Ser10-Lys14]. The modeled structure of MKP1 was docked with native and seven PTM structures of histone H3 using the Haddock server (Fig. 1A and Supplementary Fig. S3).[20] The active site residues (His257, Cys258, Gln259,

Ala260, Gly261, Ile262, Ser263, and Arg264) of MKP1 and (Lys9, Ser10, and Lys14) of histone H3 were used as input parameters for docking. The Haddock scores of the complexes are tabulated in Table 3 and Figure 4. The results were analyzed for protein-protein interactions and emphasis was given for weak intermolecular interactions such as hydrogen bonding and hydrophobic interactions.

Results and Discussion

Histone H3 phosphorylation is involved in the transcriptional activation of genes in interphase cells. The phosphorylation of histone H3Ser10 is known to facilitate acetylation of Lys9 and Lys14. Cross-talk between site-specific phosphorylation and acetylation of the H3 tail regulates this process, but whether this occurs singly or in combination is not clearly understood. We have investigated in silico interactions between the regulatory proteins MKP1, MSK1, and 14-3-3ζ and different combination of site-specific histone H3 modifications on Lys9, Ser10, and Lys14.

Homology modeling of MKP1 and MSK1 structures

Homology modeling was carried out for MKP1 and MSK1 by studying their molecular interactions with modified and unmodified H3.

Modeling of MKP1 structure

MKP1 consists of 367 amino acids with two domains that are separated by a flexible loop region. Truncated MKP1 with a deleted N-terminal rhodanase domain showed evidence of better phosphatase activity than its full-length counterparts, both in vivo and in vitro.[27] However, C-terminal truncations could neither change substrate affinity nor substrate-dependent catalytic activation. These studies clearly suggest that the C-terminal domain regulates the phosphatase activity of MKP1.[28] To examine the importance of MKP1 protein and its molecular interactions with other proteins, we built conducted modeling studies as the crystal or solution structure of MKP1 was not available. Data from the Protein Data Bank revealed that the C-terminal crystal structure of human MKP2 (PDB ID: 3EZZ) has sequence identity of 85.31% with human MKP1. Therefore, this structure was used

Table 2. Docking of native MSK1 with histone H3 and its PTM structure.

Docked complexes	HADDOCK score	Interacting residues	
		H-bonds	**Hydrophobic**
MSK1 H3	−92.1 ± 7.8	**Ser10:** *Lys43, Val44* **Gly12:** *Lys85* **Lys14:** *Glu124, Leu364, Glu369* **Arg17:** *Lys370* **Leu20:** *Lys370* **Ala21:** *Lys370*	**Gly12:** *Thr123* **Gly13:** *Glu369* **Lys14:** *Glu369*
MSK1 H3Lys9Ac	−47.4 ± 9.0	**Ala1:** *Glu369* **Arg8:** *Glu47* **Lys9:** *Glu124* **Ser10:** *Thr125, Lys126* **Gly12:** *Glu47* **Arg17:** *Tyr359*	**Lys9:** *Glu124* **Ser10:** *Lys126* **Thr11:** *Glu47, Tyr359*
MSK1 H3Lys14Ac	−64.0 ± 6.5	**Ala1:** *Ser367, Glu369* **Thr3:** *Glu124* **Lys9:** *Glu124, Glu369* **Ser10:** *Lys85, Glu369* **Arg17:** *Lys43, Glu47* **Lys18:** *Glu47, Ile69*	**Arg2:** *Pro365* **Gly13:** *Glu42*
MSK1 H3Lys9AcLys14Ac	−50.2 ± 10.2	**Ala1:** *Glu369* **Arg8:** *Glu47* **Lys9:** *Glu124* **Ser10:** *Thr125, Lys126* **Gly12:** *Glu47* **Arg17:** *Tyr359*	**Arg2:** *Pro365* **Ser10:** *Thr123* **Thr11:** *Tyr359*

Note: *Bold letters indicate histone H3 and italics indicate binding partners.

as a template for homology modeling of C-terminal of MKP1 from 172–314 amino acids. The dual specificity protein phosphatase (DUSP) domain is also reported to be located between 180–312 amino acids. The modeled structure of MKP1 was found to have a QMEAN Z-score of −0.693.[21] The energy of the MKP1 structure was minimized using Discovery studio 2.5, from an initial potential energy of −5246.07 to −9131.51 kcal/mol by conjugate gradient converging at 1397 steps. The MKP1 structure was later validated using the SAVES server and showed that 0.8% residues were located in the disallowed region of the Ramachandran plot according to Procheck,[22] confirming the correct overall geometry of the MKP1 model. Verfiy_3D[23] showed 89.19% residues with average 3D to 1D scores >0.2 by assigning a structural class. The modeled structure of C-terminal of MKP1 (172– 314 aa) and the active site residues (257–264 aa) are shown in red color in Figure 1A and Supplementary Figure S1A. The modeled structure has four beta-sheets, five alpha-helices, and seven loops. The overall quality of the model is given by

ERRAT score[24] of 98.519 by analyzing the non-binding interaction between different atom types.

Modeling of MSK1 structure

Earlier studies showed that the C-terminal (CTD) and N-terminal domains (NTD) of MSK1 are structurally distinct kinases. NTD MSK1 belongs to the AGC kinase family and is characterized by a kinase domain followed by a hydrophobic motif region with phosphorylation sites.[17] The crystal structure of the N-terminal kinase domain of MSK1 is available (PDB ID: 1VZO 24–345); however, inactive MSK1 requires an association with the phosphorylated loop residue (Ser376) to convert into the active form. Therefore, to model the loop with the N-terminal domain, PDB ID: 3A8X was used as template for homology modeling. 3A8X is the crystal structure of protein kinase C (PKC-iota), which has sequence identity of 62% with the N-terminus of MSK1. The modeled structure of MSK1 has a QMEAN Z-score −1.216.[20] The modeled structure of N-terminal of MSK1 (42–380 aa) with the active site residues (Lys85, Ile88, Val89, Thr95, Arg102,
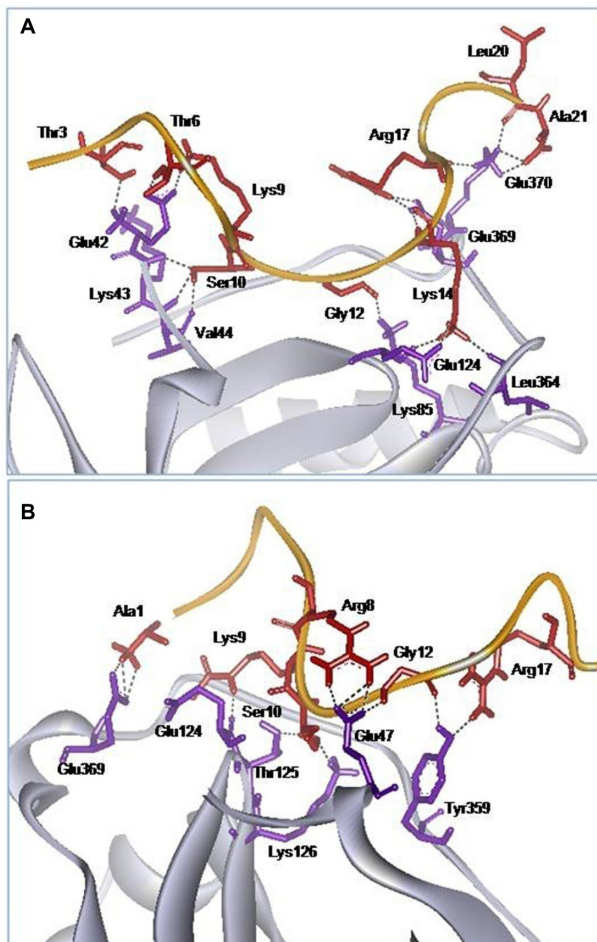
Figure 3. Docking of MSK1 with histone H3 and its PTM structure (**A**) MSK1 and histone H3 and (**B**) MSK1 and histone H3Lys9AcLys14Ac. The ribbon diagram of MSK1 (grey) with the residues (violet) and histone H3 peptide (orange) with the residues (red) are involved in the H-bonding interaction and is shown as a dotted black line.

Gln122, and Leu127) are highlighted in red color, while the cyan color indicates the loop (345–380 aa) in Figure 1B. The modeled structure was energy minimized by Discovery studio 2.5 from an initial potential energy of −11978.41 to −22806.55 kcal/mol by conjugate gradient, which converged at 1348 steps. The modeled structure has four beta-sheets, fifteen alpha-helices, and fifteen loops (Supplementary Fig. S1B). The MSK1 model validated through the SAVES server showed 0.7% residues are in the disallowed region of the Ramachandran plot according to Procheck,[22] which confirmed the correct overall geometry. Verfiy_3D[23] showed that 88.82% residues have average 3D to 1D scores of >0.2 by assigning a structural class. The overall quality of the model was given by the ERRAT score[24] of 95.886 by analyzing the non-bonding interaction between different atom types.

The modeled structures of MSK1 and MKP1 with active domains will be used for molecular interaction studies with H3 peptide with either phosphorylation or acetylation at specific residues, Lys9, Ser10, or Lys14.

Interaction of crystal structure of 14-3-3ζ with native H3 peptide and its PTM modified structures

Phosphorylation of histone H3 at Ser10 has been implicated in transcriptional activation of immediate early genes in organisms ranging from yeast to humans in interphase.[29] Mahadevan et al demonstrated that 14-3-3ζ interacts with H3 only when phosphorylated at Ser10.[6] Additionally, recruitment of 14-3-3ζ has been observed at the promoters of transcriptionally active genes, *c-fos* and *c-jun*.[6] The activation of HDAC1 gene transcription and binding of 14-3-3ζ at its promoter have been shown to be directly correlated with phosphorylation of H3Ser10.[9] 14-3-3ζ has also been shown to play a crucial role in the transcription of the mammalian FOSL1 gene by binding of the histone acetyltransferase, MOF.[30] The study also suggested that H3Lys9Ac is involved in recruitment of MOF, but supportive evidence and how 14-3-3ζ mediates the crosstalk between H3Ser10 phosphorylation and Lys9 acetylation during transcription are not available.

The interaction of 14-3-3ζ with phosphorylated proteins occurs through the two most favorable binding motifs.[31] The phosphorylated peptide of H3 forms a conserved primary interaction with Arg56, Arg127, and Tyr128 residues of 14-3-3ζ. Since the crystal structure of 14-3-3ζ bound to an H3 peptide was available (PDB ID: 2C1J), the complex was subjected to the refinement mode of the Haddock server to score the interactions (Table 1 and Supplementary Fig. S4.1). The complex in which H3 is modified at Ser10 and Lys14 showed a high Haddock score, while the complex with acetylation at Lys9 showed the lowest Haddock score. In all the complexes with a phosphorylated Ser10, a conserved interaction with triad Arg56, Arg127, and Tyr128 was observed (Fig. 2). Our docking studies also support earlier studies of the molecular interaction between the phosphopeptide-interacting motif and the Arg–Arg–Tyr triad of 14-3-3ζ.[32]

Our in silico data suggest that 14-3-3ζ interacts more strongly with H3Ser10P than with H3Lys9AcSer10P,

Table 3. Docking of native MKP1 with histone H3 and its PTM structure.

Docked complexes	HADDOCK score	Interacting residues	
		H-bonds	**Hydrophobic**
MKP1 H3	−61.8 ± 6.8	**Arg8:** *Gln259* **Thr11:** *Asp227* **Lys14:** *Asn228* **Arg17:** *Asp227, Asn228* **Ala21:** *His229*	**Ser10:** *Ala260* **Lys14:** *Asn228*
MKP1 H3Ser10P	−90.3 ± 3.8	**Arg8:** *Gln259* **Ser10:** *Cys258, Gln259, Ala260, Gly261, Ile262, Ser263, Arg264* **Arg17:** *Asn298*	**Thr3:** *Ile294* **Lys9:** *Ser296*
MKP1 H3Lys9AcSer10P	−121.6 ± 16.4	**Lys9:** *Gln259* **Thr11:** *Asp227* **Ser10:** *Cys258, Gln259, Ala260, Gly261, Ile262, Ser263, Arg264*	**Gly13:** *Phe299* **Lys14:** *Phe299* **Lys18:** *Phe299*
MKP1 H3Ser10PLys14Ac	−122.6 ± 17.7	**Thr3:** *Arg292* **Thr11:** *Asp227, Asn298* **Arg17:** *Ser296, Pro297* **Lys18:** *Asp282, Glu286* **Ser10:** *Cys258, Gln259, Ala260, Gly261, Ile262, Ser263, Arg264*	**Lys9:** *Ser185* **Lys14:** *Phe299*
MKP1 H3Lys9AcSer10PLys14Ac	−138.6 ± 12.1	**Thr11:** *Asp227* **Ser10:** *Gln259, Ala260, Gly261, Ile262, Ser263, Arg264* **Arg17:** *Ser296, Pro297* **Lys18:** *Asp282, Glu286*	**Lys9:** *Ile262, Ala260* **Gly13:** *Phe299* **Lys14:** *Phe299, Asn298* **Lys18:** *Phe285*
MKP1 H3Lys9Ac	−56.8 ± 6.9	**Ala1:** *Ser296* **Thr3:** *Asp227* **Lys9:** *Gly261* **Ser10:** *Arg292* **Lys14:** *Tyr187* **Lys18:** *His213*	**Lys4:** *Asp227* **Lys9:** *Ala260, Ile262* **Gly13:** *Tyr187*
MKP1 H3Lys14Ac	−67.8 ± 6.3	**Ala1:** *Asn209, Glu226* **Thr3:** *Ser185, Tyr187* **Arg8:** *Asp227, Gln259* **Lys9:** *Gln259* **Ser10:** *Asp227*	**Lys4:** *Try187* **Lys9:** *Ala260* **Thr11:** *Asp227*
MKP1 H3Lys9AcLys14Ac	−61.9 ± 4.4	**Ala1:** *Ser296* **Thr3:** *Arg264* **Lys9:** *Gly261, Ile262* **Lys14:** *Tyr187* **Lys18:** *Ser190, His213*	**Lys9:** *Gln259, Ile262, Ser263* **Arg17:** *Tyr187*

Note: *Bold letters indicate histone H3 and italics indicate binding partners.

which contradicts previous experimental results.[9,33] A possible reason for the lower binding affinity of H3Lys9AcSer10P with 14-3-3ζ is the change in the salt bridge and H-bonding between the two proteins (Supplementary Fig. S4.1 and S4.1e). The acetylation at Lys9 and Lys14 alters the specificity of interaction of the phosphorylated peptide. Specifically, acetylation of Lys9 confers a negative charge, which prevents salt-bridge formation with Asp223 observed in all the complexes. Acetylated Lys9 prefers hydrogen

bonding with Asn224 rather than Asp223. However, non-acetylated Lys9 forms salt-bridge interaction with Asp223 and the hydrogen bond with Asn224. This suggests that the non-acetylated peptide at Lys9 may bind with higher affinity to 14-3-3ζ compared to the peptide with an acetylated Lys9. In the crystal structure, the side-chain of Lys14 pointing away from 14-3-3ζ thus limits a direct interaction. To compare the individual role of acetylation at Lys9 and Lys14, the complex with only Lys14 acetylated yielded −98.9
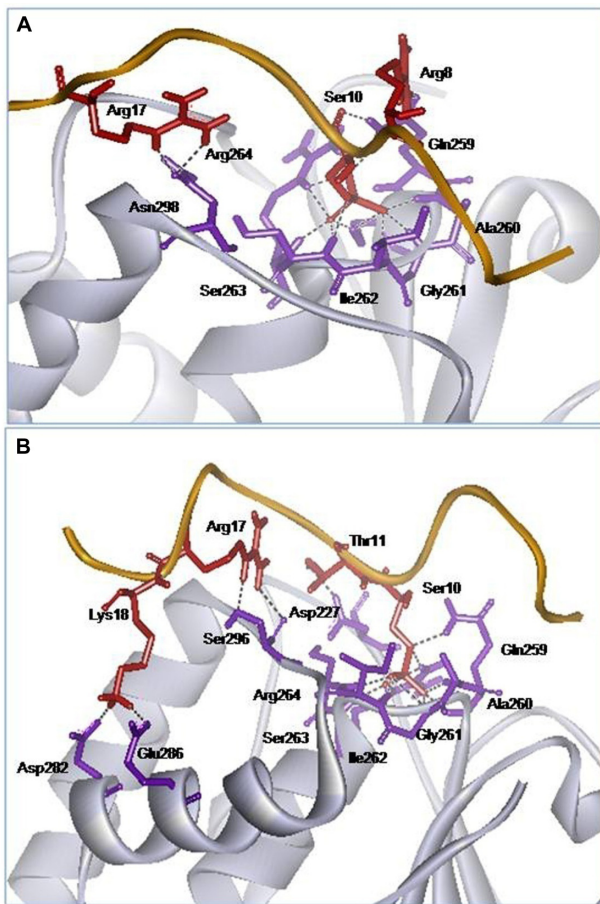
Figure 4. Docking of MKP1 with histone H3 and its PTM structure (**A**) MKP1 and histone H3Ser10 and (**B**) MKP1 and histone H3Lys9Ac-Ser10PLys14Ac. The ribbon diagram of MKP1 (grey) with the residues (violet) and histone H3 peptide (orange) with the residues (red) are involved in the H-bonding interaction and is shown as a dotted black line.

Haddock score as compared to −29.0 score from only Lys9 acetylated complex. To study the effect of Lys9 and Lys14 acetylation in combination with Ser10 phosphorylation, the complex with Ser10 and Lys14 modification yielded highest score −119.7 as compared to −46.5 for the complex with Ser10 and Lys9 modification (Table 1).

The complex with all modifications yielded a lower score compared to the 14-3-3ζ H3Ser10PLys14Ac complex, indicating that Lys9 acetylation decreases the binding affinity while Lys14 acetylation increase the binding affinity of the phosphorylated peptide. In this scenario, lysine acetylation may function as an 'auxiliary modification' that supports the relatively weak interaction of 14-3-3ζ with H3Ser10P. Modified crystal structure (PDB ID: 2C1J) studies of the 14-3-3ζ interaction with the H3 peptide containing phosphorylated Ser10 and acetylated Lys9 and

Lys14 suggested no major alterations in the interactions compared to in 14-3-3ζ and H3 phosphopeptide complexes (Fig. 2). However, our in silico studies suggest that acetylation of Lys9 residue decreases the binding affinity. The alterations in hydrogen bonding and salt bridge formation due to introduction of acetyl groups resulting in charge neutralization may contribute to the decreased molecular interaction of 14-3-3ζ with the H3 phosphoacetylated peptide.

The dual acetylation of Lys9 and Lys14 along with Ser10 phosphorylation allows one-step higher level of mechanism for controlling gene regulation. The dual modification will result in different combinations and provide different interaction sites for different interacting partners on the basis of charge or domain and may respond to distinct signaling pathways. In contrast, a previous study indicated no significant effect of dual H3Lys9/Lys14 acetylation on this interaction.[6] Our data clearly indicates a modulation of the 14-3-3ζ and histone H3 interaction by dual acetylation at Lys9 and Lys14 (Fig. 2B). This decreased binding affinity of 14-3-3ζ with acetylation at Lys9 may result because the positive effect of single acetylation is neutralized by the dual acetylation or due to the close proximity of H3Ser10P with Lys9, which may affect the interaction of the phospho-domain of 14-3-3ζ. The dual acetylation and phosphorylation may also modulate 14-3-3ζ interactions with other regulatory proteins such as HATs, HDACs, and phosphatases, among others.

Docking of native MSK1 with histone H3 and its PTM modified structure

The dephosphorylation and phosphorylation of H3Ser10P in response to different stress-inducing agents such as oxidative stress and UV irradiation is a highly dynamic and reversible.[34,35] MSK1 belongs to a family of protein kinases that contain two active domains in one polypeptide chain.[36] In the dual domain protein kinase MSK1, the N-terminal kinase has been shown to be phosphorylated by exogenous substrates, while the C-terminal kinase and the linker region act to regulate activity of the N-terminal kinase.[19]

The modeled structure of N-terminal domain of MSK1 (42–380 aa) was docked with native and acetylated histone H3 at Lys9 or Lys14 independently or together (Fig. 1B and Supplementary Fig. S3). The active site residues (Lys85, Ile88, Val89, Thr95,

Arg102, Gln122, and Leu127) of MSK1 were obtained from the literature.[36] The native histone H3 scored highest compared to acetylated Lys9 and Lys14 (Table 2). The bound state is stabilized by an intra-molecular interaction. In native histone H3, the salt-bridge interaction was observed between Lys14 of H3 with Glu124 of MSK1, but when histone H3 was acetylated at either position, Lys9 forms a salt-bridge with Glu124 (Fig. 3 and Supplementary Fig. S4.2). Histone H3 acetylation at Lys14 favored an interaction with MSK1 with a Haddock score of −64.0 compared to a −47.4 score for Lys9 (Table 2). Haddock scores for the interaction of MSK1 with H3Ser10PLys9Ac and H3Ser10PLys14Ac clearly suggest that acetylation is not a prerequisite for phosphorylation of H3Ser10P by MSK1. The phosphoserine Cα-Cβ bond is free to rotate. Thus, for an extended peptide that binds along the groove, two orientations are possible, differing by a two-fold rotation around the Cα-Cβ bond. There-fore, the phosphorylated H3 tails may change their conformation to favor the interaction with 14-3-3ζ. Since the amino-acid composition of histone H3 sur-rounding Ser10 does not match that of the high-affin-ity 14-3-3ζ binding motifs, the postulated modulation of binding may only be relevant for a specific subset of 14-3-3ζ-associated proteins with initial low-affin-ity binding to interact with other histone modifying enzymes such as HATs. Previous experimental results have suggested that the interaction of 14-3-3ζ with the phosphorylated H3Ser10 favors the interaction of HATs responsible for acetylation of Lys14.[12] Col-lectively, the phosphorylation of Ser10 by MSK1 followed by low affinity interaction of 14-3-3ζ and acetylation of Lys14 by HAT stabilizes the binding of 14-3-3ζ to differentially modified H3 in interphase cells to interact with other proteins.

Docking of native MKP1 with histone H3 and its PTM structure

MKP1 is considered as a regulator which controls the access and recruitment of the transcriptional machin-ery to the promoter of targeted genes by dephospho-rylating H3 on Ser10 after stimulation of endothelial cells by VEGF or thrombin.[13] Previous studies by us and other groups have shown that in interphase cells, H3Ser10P is associated with acetylation of H3Lys9 and Lys14, which may favor gene transcription. This suggests that the interaction of MKP1 with H3Ser10P

will be in the neutralized positive charge surrounding due to Lys9 and Lys14 acetylation. However, the role of H3Lys9 and Lys14 acetylation in the dephospho-rylation of H3Ser10 has been the subject of debate. These modifications are known to occur in response to the same stimuli, in the same tissue, and on the same histone tails.[12] In silico studies were carried out to understand the effect of neighboring acetylation on H3Lys9 and H3Lys14 on the dephosphorylation of H3Ser10P by MKP1.

The homology model structure of the C-terminal phosphatase domain of MKP1 (172–314 aa) was used for docking with the loop crystal structure of H3 peptide (1–21 aa) using the Haddock server (Fig. 1A and Supplementary Fig. S3). The active site amino acid, Cys258, and nearby residue important for the formation of the active site (His257, Cys258, Gln259, Ala260, Gly261, Ile262, Ser263, and Arg264) for MKP1 were obtained from UniProt ID: P28562. These residues were used for targeted docking native and modified histone H3 peptides. Haddock scores from all eight complexes suggested that the complex of MKP1 and H3Lys9AcSer10PLys14Ac showed the strongest binding compared to the complex con-taining the native histone H3 and MKP1 (Table 3, Supplementary Fig. S4.3 and Fig. 4). The Ser10 mod-ification of histone H3 increased the binding affinity from −61.8 to −90.3 with MKP1. However, when either Lys9 or Lys14 acetylation was added with Ser10, the Haddock score increased from −90.3 to around −122. The residues involved in the interaction with phos-phorylated Ser10 are mostly from active site (Gln259, Ala260, Gly261, Ile262, Ser263, Arg264) of MKP1 observed in all the complexes. Based on this observa-tion, acetylation at Lys9 or Lys14 may favor the inter-action between Ser10 with MKP1. The modification of H3 at all the three locations (Lys9, Ser10, Lys14) further increased the hydrophobic interactions lead-ing to form a stable and high-affinity interaction with MKP1 (Supplementary Fig. S4.3).

Our molecular modeling and previous studies sug-gest that the phosphorylation of H3Ser10 by MSK1 favors the recruitment of 14-3-3ζ, which in turn recruits HATs and acetylates H3Lys9 and H3Lys14. Acetylation protects the phosphorylation at H3Ser10 from being removed by phosphatase and the acetylation of the H3 tail favors active chromatin organization, which facili-tates gene transcription. The level of MKP1 is known

to increase in response to stress-inducing agents such as oxidative stress.[15] Based on our in silico results, we hypothesize that the enhanced level of MKP1 may favor concentration-dependent binding and replacement of 14-3-3ζ from H3Ser10PLys14Ac. The increased binding of MKP1 dephosphorylates H3Ser10P. The dephosphorylation of H3Ser10 favors deacetylation of H3Lys9/Lys14, which favors condensation of chromatin structure. Thus, these studies suggest that different proteins targeted to different PTMs can regulate chromatin structure and gene expression. However, our in silico findings can be validated by in vitro assays such as isothermal titration calorimetry and peptide pull-down coupled with mass spectroscopy to understand the interaction of proteins with no specific interacting domains for different types of posttranslational modifications.

Summary

The combinations of different modifications on histone tails alter the interaction of histone proteins with DNA and effector proteins. Histone H3Ser10 phosphorylation along with acetylation on neighboring lysine residues, Lys9 and Lys14, are highly dynamic modifications that regulate their interactions with other functional proteins in interphase cells to favor transcriptional activation. In silico studies revealed that phosphorylation is the prime event with interaction of 14-3-3ζ followed by acetylation of Lys9 and Lys14 on the H3 tail. MKP1 dephosphorylates H3Ser10P in response to stress, but Lys9 and Lys14 acetylation favors the interaction of MKP1 with H3, whereas acetylation of Lys9 and Lys14 do not favor phosphorylation of H3Ser10 by MSK1. These data suggest that these dual modifications have implications for accessibility and further protein-protein interactions in response to different stimuli.

Author Contributions

Conceived and designed the experiments: SG, NG, AKS, AM. Analyzed the data: SG, NG, AKS, AM. Wrote the first draft of the manuscript: SG, NG. Contributed to the writing of the manuscript: AKS, AV. Agree with manuscript results and conclusions: SG, NG, AV, AKS, AM. Jointly developed the structure and arguments for the paper: SG, NG, AV. Made critical revisions and approved final version: SG, NG, AKS. All authors reviewed and approved of the final manuscript.

Competing Interests

Author(s) disclose no potential conflicts of interest.

Disclosures and Ethics

As a requirement of publication the authors have provided signed confirmation of their compliance with ethical and legal obligations including but not limited to compliance with ICMJE authorship and competing interests guidelines, that the article is neither under consideration for publication nor published elsewhere, of their compliance with legal and ethical guidelines concerning human and animal research participants (if applicable), and that permission has been obtained for reproduction of any copyrighted material. This article was subject to blind, independent, expert peer review. The reviewers reported no competing interests.
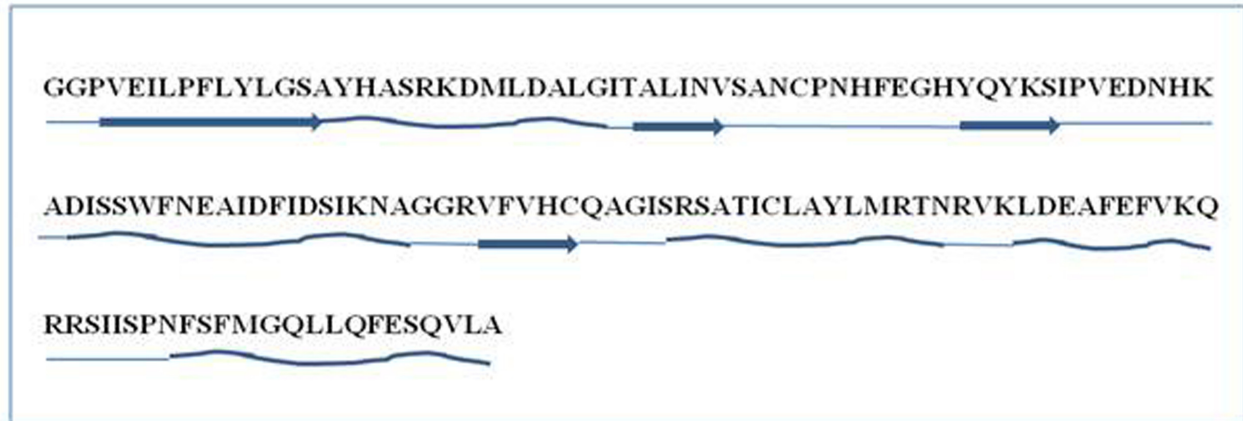
References

1. Strahl BD, Allis CD. The language of covalent histone modifications. *Nature*. 2000;403(6765):41–5.
2. Cohen I, Poręba E, Kamieniarz K, Schneider R. Histone modifiers in cancer: friends or foes? *Genes Cancer*. 2011;2(6):631–47.
3. Yun M, Wu J, Workman JL, Li B. Readers of histone modifications. *Cell Res*. 2011;21(4):564–78.
4. Bannister AJ, Kouzarides T. Regulation of chromatin by histone modifications. *Cell Res*. 2011;21(3):381–95.
5. Nowak SJ, Corces VG. Phosphorylation of histone H3: a balancing act between chromosome condensation and transcriptional activation. *Trends Genet*. 2004;20(4):214–20.
6. Macdonald N, Welburn JP, Noble ME, et al. Molecular basis for the recognition of phosphorylated and phosphoacetylated histone h3 by 14-3-3. *Mol Cell*. 2005;20(2):199–211.
7. Lottersberger F, Panza A, Lucchini G, Longhese MP. Functional and physical interactions between yeast 14-3-3 proteins, acetyltransferases, and deacetylases in response to DNA replication perturbations. *Mol Cell Biol*. 2007;27(9):3266–81.
8. Wang AH, Kruhlak MJ, Wu J, et al. Regulation of histone deacetylase 4 by binding of 14-3-3 proteins. *Mol Cell Biol*. 2000;20(18):6904–12.
9. Winter S, Simboeck E, Fischle W, et al. 14-3-3 proteins recognize a histone code at histone H3 and are required for transcriptional activation. *EMBO J*. 2008;27(1):88–99.
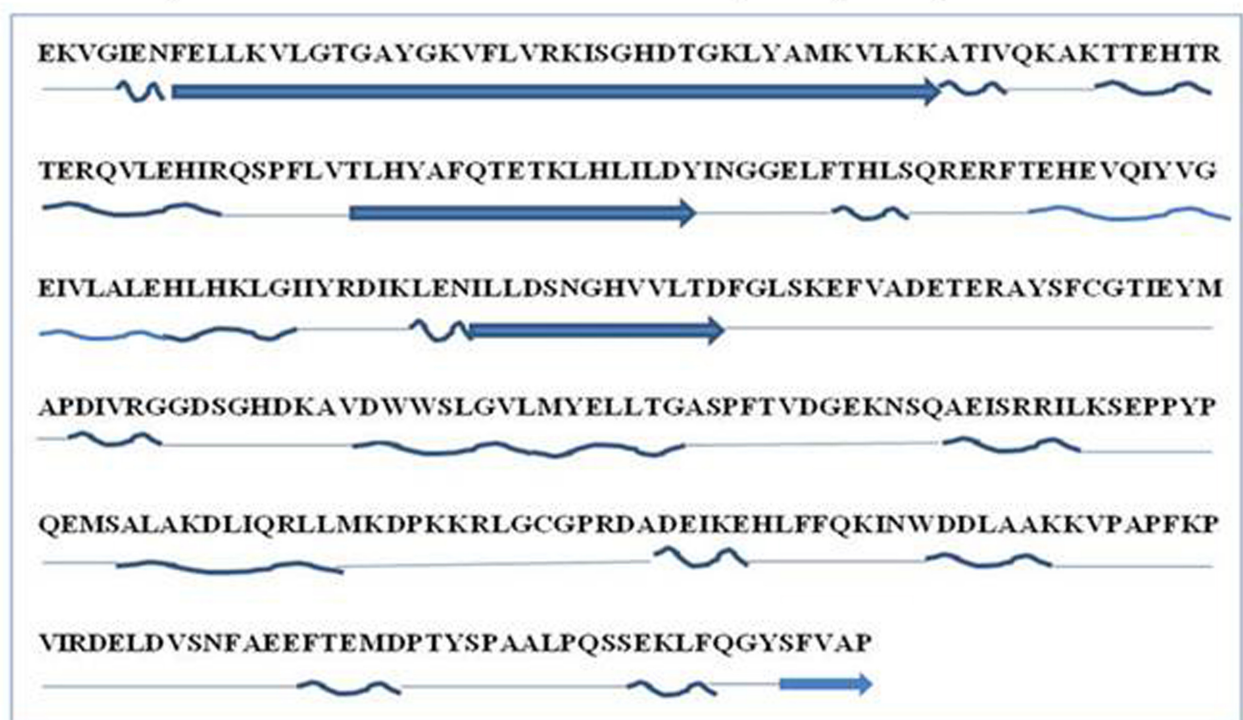
10. Walter W, Clynes D, Tang Y, Marmorstein R, Mellor J, Berger SL. 14-3-3 interaction with histone H3 involves a dual modification pattern of phosphoacetylation. *Mol Cell Biol*. 2008;28(8):2840–9.

11. Kanno T, Kanno Y, Siegel RM, Jang MK, Lenardo MJ, Ozato K. Selective recognition of acetylated histones by bromodomain proteins visualized in living cells. *Mol Cell*. 2004;13(1):33–43.

12. Cheung P, Tanner KG, Cheung WL, Sassone-Corsi P, Denu JM, Allis CD. Synergistic coupling of histone H3 phosphorylation and acetylation in response to epidermal growth factor stimulation. *Mol Cell*. 2000;5(6): 905–15.

13. Kinney CM, Chandrasekharan UM, Yang L, et al. Histone H3 as a novel substrate for MAP kinase phosphatase-1. *Am J Physiol, Cell Physiol*. 2009;296(2):C242–9.

14. Wang HY, Cheng Z, Malbon CC. Overexpression of mitogen-activated protein kinase phosphatases MKP1, MKP2 in human breast cancer. *Cancer Lett*. 2003;191(2):229–37.

15. Srikanth S, Franklin CC, Duke RC, Kraft RS. Human DU145 prostate cancer cells overexpressing mitogen-activated protein kinase phosphatase-1 are resistant to Fas ligand-induced mitochondrial perturbations and cellular apoptosis. *Mol Cell Biochem*. 1999;199(1–2):169–78.

16. Owens DM, Keyse SM. Differential regulation of MAP kinase signalling by dual-specificity protein phosphatases. *Oncogene*. 2007;26(22):3203–13.

17. Deak M, Clifton AD, Lucocq LM, Alessi DR. Mitogen- and stress-activated protein kinase-1 (MSK1) is directly activated by MAPK and SAPK2/p38, and may mediate activation of CREB. *EMBO J*. 1998;17(15):4426–41.

18. Kim HG, Lee KW, Cho YY, et al. Mitogen- and stress-activated kinase 1-mediated histone H3 phosphorylation is crucial for cell transformation. *Cancer Res*. 2008;68(7):2538–47.

19. McCoy CE, Campbell DG, Deak M, Bloomberg GB, Arthur JS. MSK1 activity is controlled by multiple phosphorylation sites. *Biochem J*. 2005; 387(Pt 2):507–17.

20. Dominguez C, Boelens R, Bonvin AM. HADDOCK: a protein-protein docking approach based on biochemical or biophysical information. *J Am Chem Soc*. 2003;125(7):1731–7.

21. Arnold K, Bordoli L, Kopp J, Schwede T. The SWISS-MODEL workspace: a web-based environment for protein structure homology modelling. *Bioinformatics*. 2006;22(2):195–201.

22. Laskowski RA, Rullmannn JA, MacArthur MW, Kaptein R, Thornton JM. AQUA and PROCHECK-NMR: programs for checking the quality of protein structures solved by NMR. *J Biomol NMR*. 1996;8(4):477–86.

23. Lüthy R, Bowie JU, Eisenberg D. Assessment of protein models with three-dimensional profiles. *Nature*. 1992;356(6364):83–5.

24. Colovos C, Yeates TO. Verification of protein structures: patterns of non-bonded atomic interactions. *Protein Sci*. 1993;2(9):1511–9.

25. Wallace AC, Laskowski RA, Thornton JM. LIGPLOT: a program to generate schematic diagrams of protein-ligand interactions. *Protein Eng*. 1995;8(2):127–34.

26. Davey CA, Sargent DF, Luger K, Maeder AW, Richmond TJ. Solvent mediated interactions in the structure of the nucleosome core particle at 1.9 a resolution. *J Mol Biol*. 2002;319(5):1097–113.

27. Boutros T, Chevet E, Metrakos P. Mitogen-activated protein (MAP) kinase/MAP kinase phosphatase regulation: roles in cell growth, death, and cancer. *Pharmacol Rev*. 2008;60(3):261–310.

28. Hutter D, Chen P, Li J, Barnes J, Liu Y. The carboxyl-terminal domains of MKP-1 and MKP-2 have inhibitory effects on their phosphatase activity. *Molecular and Cellular Biochemistry*. 2002;233(1–2):107–17.

29. Cerutti H, Casas-Mollano JA. Histone H3 phosphorylation: universal code or lineage specific dialects? *Epigenetics*. 2009;4(2):71–5.

30. Zippo A, Serafini R, Rocchigiani M, Pennacchini S, Krepelova A, Oliviero S. Histone crosstalk between H3S10ph and H4K16ac generates a histone code that mediates transcription elongation. *Cell*. 2009;138(6): 1122–36.

31. Rittinger K, Budman J, Xu J, et al. Structural analysis of 14-3-3 phosphopeptide complexes identifies a dual role for the nuclear export signal of 14-3-3 in ligand binding. *Mol Cell*. 1999;4(2):153–66.

32. Yang X, Lee WH, Sobott F, et al. Structural basis for protein-protein interactions in the 14-3-3 protein family. *Proc Natl Acad Sci U S A*. 2006; 103(46):17237–42.

33. Winter S, Fischle W, Seiser C. Modulation of 14-3-3 interaction with phosphorylated histone H3 by combinatorial modification patterns. *Cell Cycle*. 2008;7(10):1336–42.

34. Ozawa K. Reduction of phosphorylated histone H3 serine 10 and serine 28 cell cycle marker intensities after DNA damage. *Cytometry A*. 2008;73(6):517–27.

35. Zhong SP, Ma WY, Dong Z. ERKs and p38 kinases mediate ultraviolet B-induced phosphorylation of histone H3 at serine 10. *J Biol Chem*. 2000;275(28):20980–4.

36. Smith KJ, Carter PS, Bridges A, et al. The structure of MSK1 reveals a novel autoinhibitory conformation for a dual kinase protein. *Structure*. 2004;12(6):1067–77.

Supplementary Figures

a. Secondary structure of C-terminal phosphatase domain of MKP1 (172-314)

GGPVEILPFLYLGSAYHASRKDMLDALGITALINVSANCPNHFEGHYQYKSIPVEDNHK

ADISSWFNEAIDFIDSIKNAGGRVFVHCQAGISRSATICLAYLMRTNRVKLDEAFEFVKQ

RRSIISPNFSFMGQLLQFESQVLA

b. Secondary structure of N-terminal kinase domain of MSK1 (42-380)

EKVGIENFELLKVLGTGAYGKVFLVRKISGHDTGKLYAMKVLKKATIVQKAKTTEHTR

TERQVLEHIRQSPFLVTLHYAFQTETKLHLILDYINGGELFTHLSQRERFTEHEVQIYVG

EIVLALEHLHKLGIIYRDIKLENILLDSNGHVVLTDFGLSKEFVADETERAYSFCGTIEYM

APDIVRGGDSGHDKAVDWWSLGVLMYELLTGASPFTVDGEKNSQAEISRRILKSEPPYP

QEMSALAKDLIQRLLMKDPKKRLGCGPRDADEIKEHLFFQKINWDDLAAKKVPAPFKP

VIRDELDVSNFAEEFTEMDPTYSPAALPQSSEKLFQGYSFVAP

Key:
Loop: ——————
Beta sheet: ➤
Alpha helix: ∿

Figure S1. Line diagram for the secondary structures (**A**) C-terminal phosphatase domain of MKP1 (172–314 aa) and (**B**) N-terminal kinase domain of MSK1 (42–380 aa).
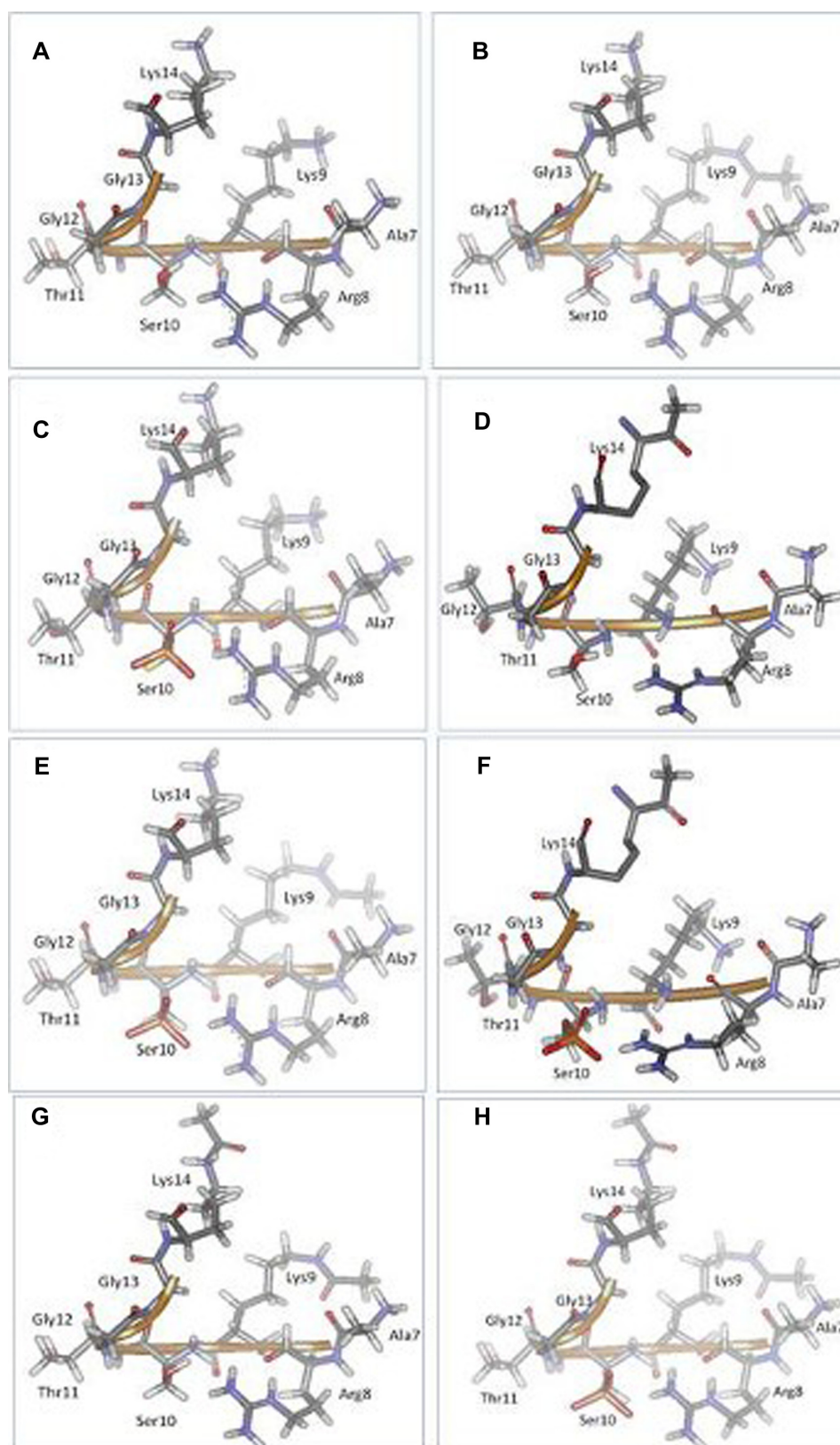
Figure S2. Histone H3 peptide from PDB: 2C1J was modified by phosphorylation of Ser10 and acetylation of Lys9 and Lys14. (**A**) Native histone H3, (**B**) H3Lys9Ac, (**C**) H3Ser10P, (**D**) H3Lys14Ac, (**E**) H3Lys9AcSer10P, (**F**) H3Ser10PLys14Ac, (**G**) H3Lys9AcLys14Ac, and (**H**) H3Lys9AcSer10PLys14Ac.
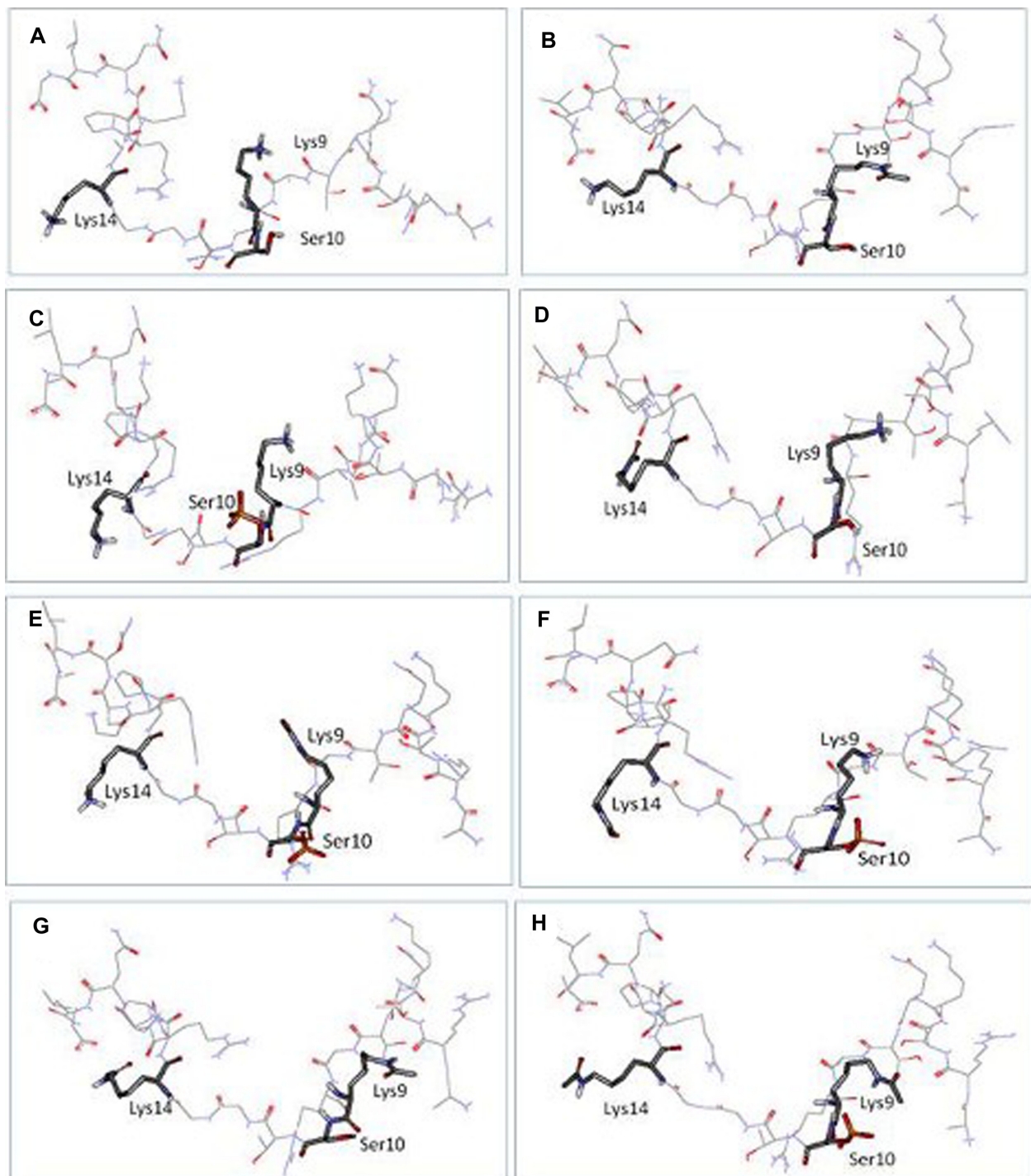
Figure S3. Full-length loop structure of histone H3 peptide from PDB: 1KX5 was modified by phosphorylation of Ser10 and acetylation of Lys9 and Lys14. (**A**) Native histone H3, (**B**) H3Lys9Ac, (**C**) H3Ser10P, (**D**) H3Lys14Ac, (**E**) H3Lys9AcSer10P, (**F**) H3Ser10PLys14Ac, (**G**) H3Lys9AcLys14Ac, and (**H**) H3Lys9AcSer10PLys14Ac.
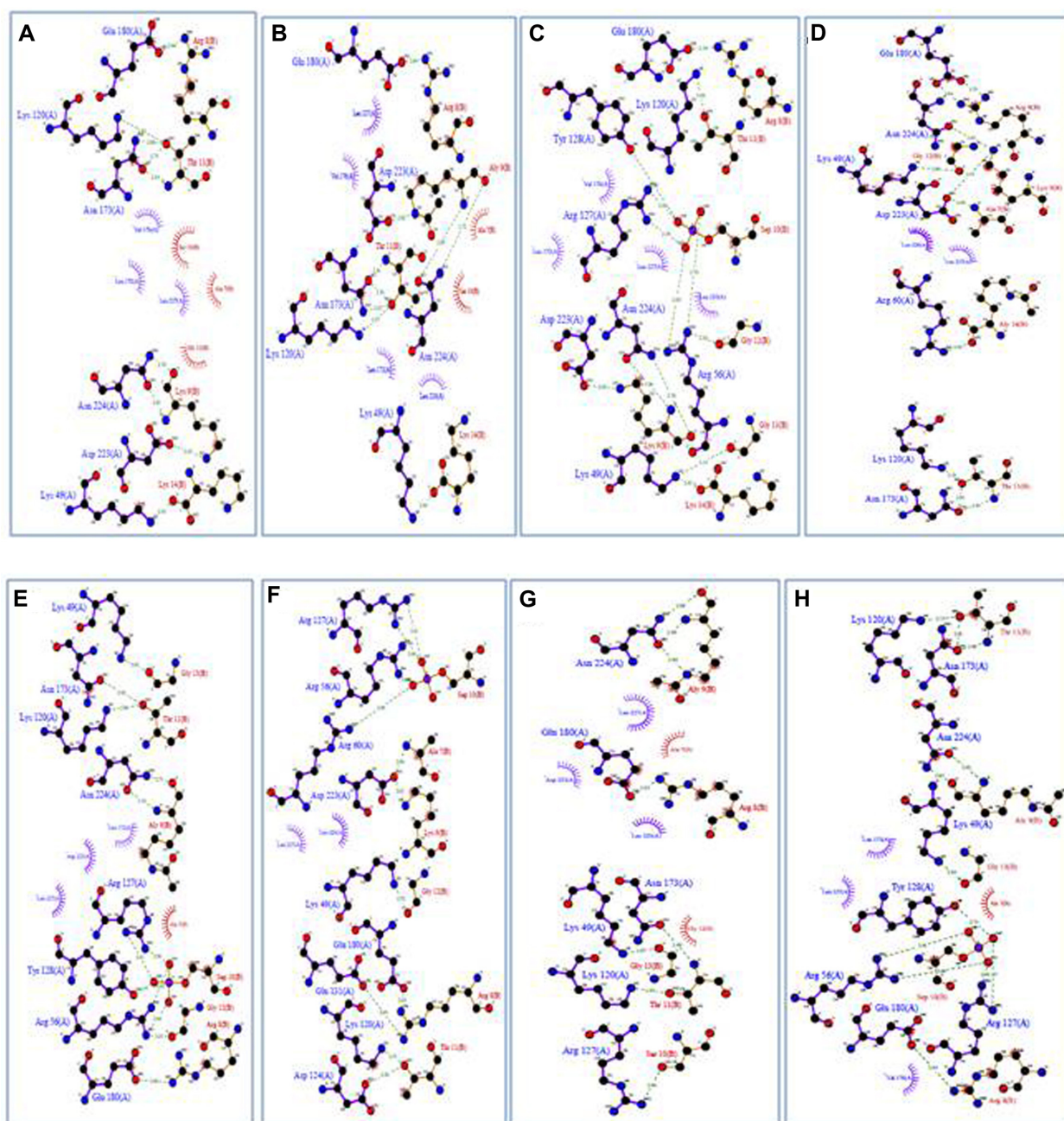
Figure S4.1. The Ligplot of the 14-3-3ζ and histone H3 docked complexes to analyzehydrophobic interactions. (**A**) Native 14-3-3ζ/H3, (**B**) 14-3-3ζ/H3Lys9Ac, (**C**) 14-3-3ζ/H3Ser10P, (**D**) 14-3-3ζ/H3Lys14Ac, (**E**) 14-3-3ζ/H3Lys9AcSer10P, (**F**) 14-3-3ζ/H3Ser10PLys14Ac, (**G**) 14-3-3ζ/H3Lys9AcLys14Ac, and (**H**) 14-3-3ζ/H3Lys9AcSer10PLys14Ac.
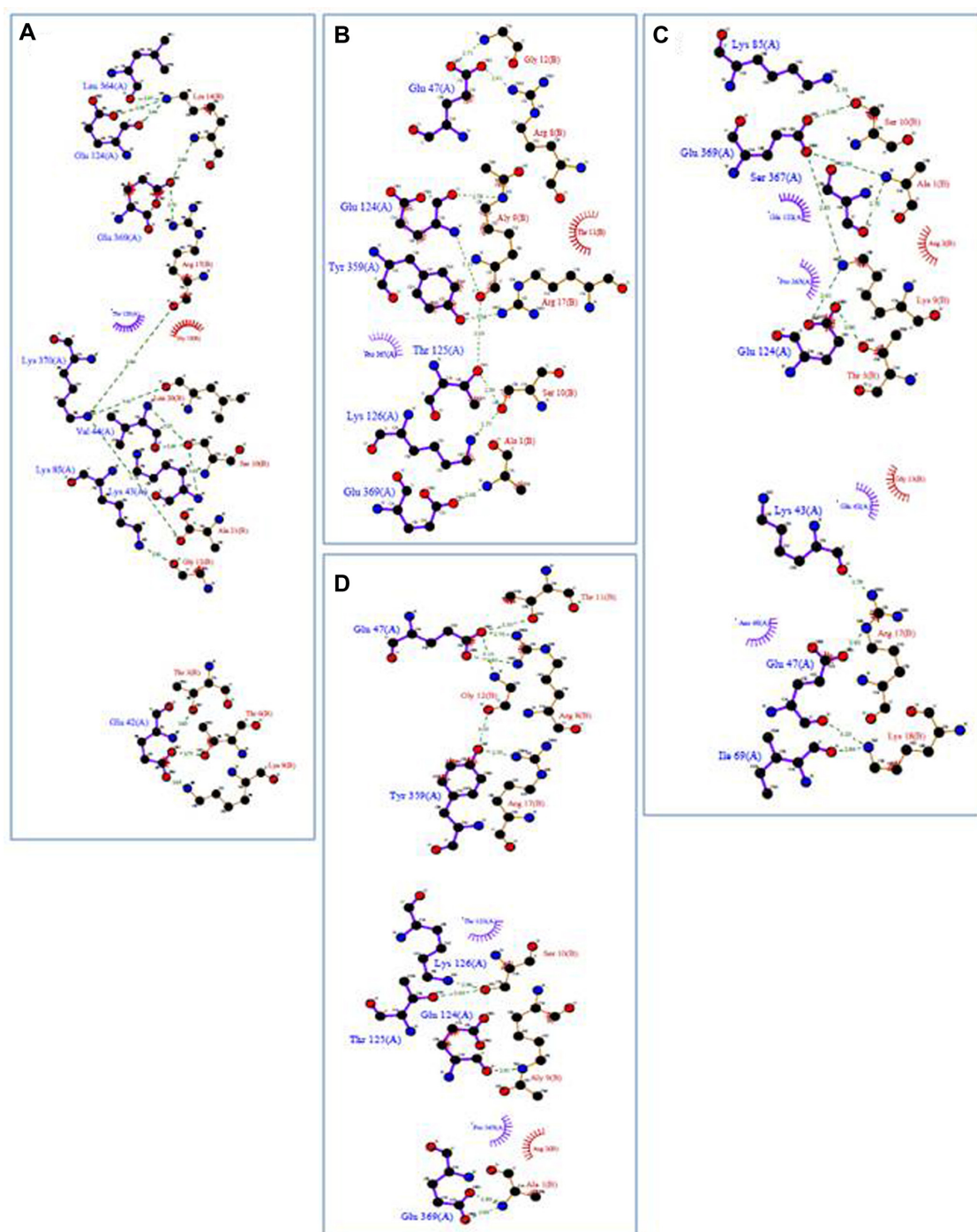
Figure S4.2. The Ligplot of the MSK1 and histone H3 docked complexes to analyze hydrophobic interactions. (**A**) Native MSK1/H3 (**B**) MSK/H3Lys9Ac, (**C**) MSK1/H3Lys14Ac, and (**D**) MKP1/H3Lys9AcLys14Ac.
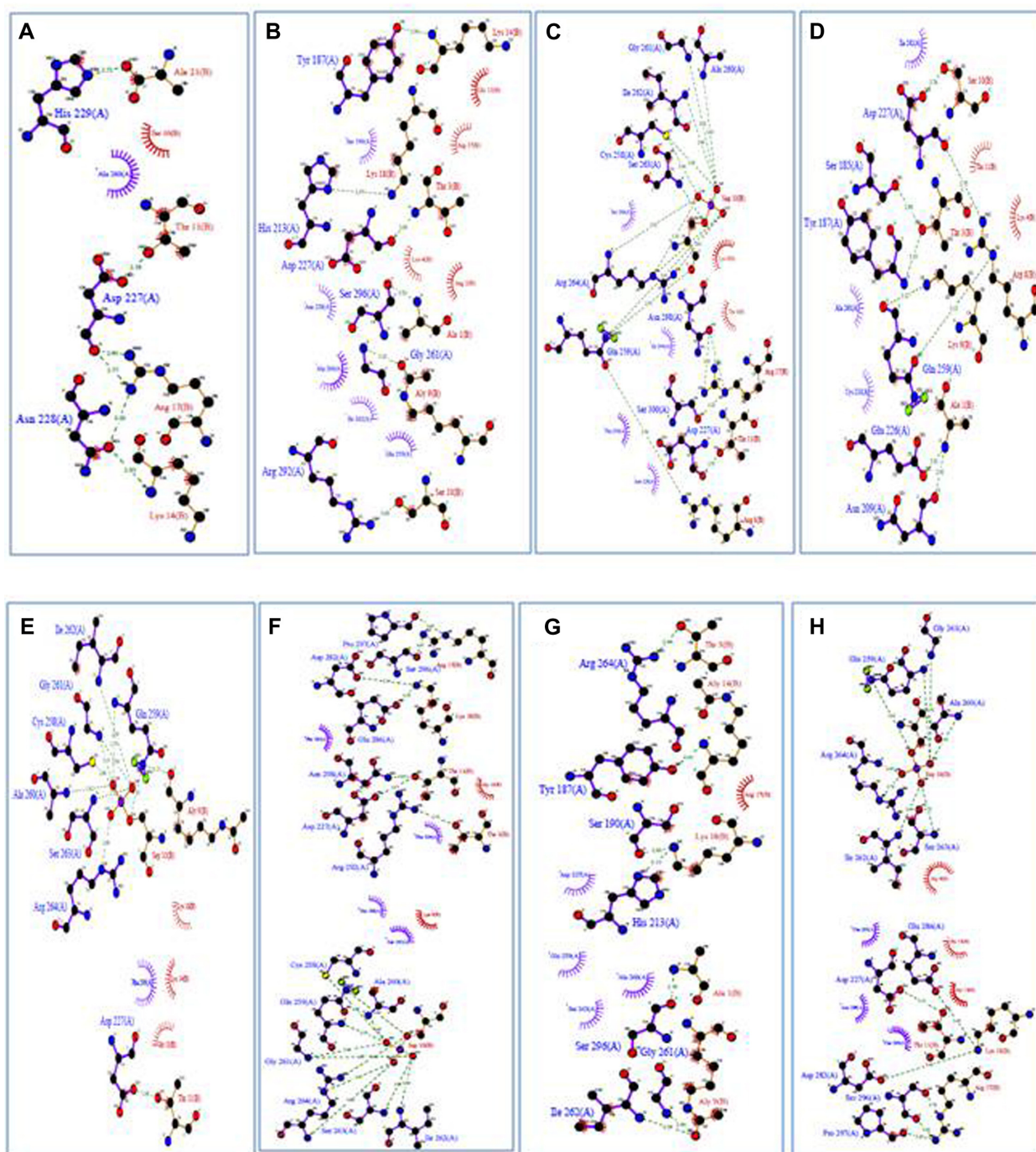
Figure S4.3. Ligplot of the MKP1 and histone H3 docked complexes to analyze hydrophobic interactions. (**A**) Native MKP1/H3 (**B**) MKP1/H3Lys9Ac, (**C**) MKP1/H3Ser10P, (**D**) MKP1/H3Lys14Ac, (**E**) MKP1/H3Lys9AcSer10P, (**F**) MKP1/H3Ser10PLys14Ac, (**G**) MKP1/H3Lys9AcLys14Ac, and (**H**) MKP1/H3Lys9AcSer10PLys14Ac.